INTERNATIONAL DOCTORAL
SCHOOL OF THE USC

Rebeca
Martínez Borrajo

PhD Thesis

Improving Osteoarthritis Therapy through the design of Intra-articular Drug Delivery Systems engineered with Artificial Intelligence Tools.

Santiago de Compostela, 2024

Doctoral Programme in Drug Research and Development

ESCOLA DE DOUTORAMENTO
INTERNACIONAL DA USC

DOCTORAL THESIS

IMPROVING OSTEOARTHRITIS THERAPY THROUGH THE DESIGN OF INTRA-ARTICULAR DRUG DELIVERY SYSTEMS ENGINEERED WITH ARTIFICIAL INTELLIGENCE TOOLS

Rebeca Martínez Borrajo

Supervisor/s: Patricia Díaz Rodríguez and Mariana Landín Pérez

Tutor: Mariana Landín Pérez

PHD PROGRAMME IN DRUG RESEARCH AND DEVELOPMENT

SANTIAGO DE COMPOSTELA

2024

USC
UNIVERSIDADE
DE SANTIAGO
DE COMPOSTELA

LIST OF PUBLICATIONS

Engineering mannose-functionalized nanostructured lipid carriers by sequential design using hybrid artificial intelligence tools. **Rebeca Martinez-Borrajo**, Patricia Diaz-Rodriguez, and Mariana Landin. Drug Delivery and Translational Research, *2024*. DOI: 10.1007/s13346-024-01603-z. (Published in May 2024).

Rationalized design to explore the full potential of PLGA microspheres as drug delivery systems. **Rebeca Martinez-Borrajo**, Patricia Diaz-Rodriguez, and Mariana Landin. Drug Delivery, *2023*. DOI:10.1080/10717544.2023.2219864 (Published in June 2023).

USC
UNIVERSIDADE DE SANTIAGO DE COMPOSTELA

USC
UNIVERSIDADE
DE SANTIAGO
DE COMPOSTELA

"Nadie dijo que sería fácil,
solo prometieron que valdría la pena"

Anónimo

USC
UNIVERSIDADE
DE SANTIAGO
DE COMPOSTELA

USC
UNIVERSIDADE
DE SANTIAGO
DE COMPOSTELA

ACKNOWLEDMENTS

Parece que fue ayer cuando empecé este apasionante viaje. Hoy, después de mucho esfuerzo y dedicación, llego al final de esta etapa, una etapa llena de retos y aprendizajes y, sobre todo, llena de buenos momentos gracias a todas las personas que han estado a mi lado en todo este proceso. Sin todo su apoyo, llegar hasta aquí no habría sido posible.

En primer lugar, me gustaría darles las gracias a mis directoras, Patricia Díaz Rodríguez y Mariana Landín Pérez. Gracias por darme la oportunidad de formarme con vosotras y descubrirme este apasionante mundo de la investigación. Gracias por vuestra orientación, buenos consejos e implicación a lo largo de todo este proceso. Gracias por darme no solo las herramientas necesarias para la realización de este trabajo, sino también por transmitirme vuestro cariño y paciencia durante todos estos años.

Gracias a todos los integrantes del proyecto NeoGiANT. Formar parte de este proyecto ha sido una experiencia muy enriquecedora para mí. Estoy muy agradecida de haber compartido este camino con todos vosotros. Mención especial a Lara, mi compañera de laboratorio con la que compartí esta etapa de aprendizaje, demostrándome siempre su apoyo y colaboración a lo largo de todo el proyecto. En ti encontré la amistad y espero que por muchos años. Gracias por todos los momentos compartidos dentro y fuera del laboratorio. Trabajar juntas en el desarrollo de formulaciones de uso veterinario no solo ha sido para mí un desafío profesional, sino también una oportunidad de crecimiento personal.

También me gustaría agradecer a todos los miembros del grupo I+D Farma con los que compartí tantos momentos en el laboratorio a lo largo de todo este proceso. Quisiera también extender mi agradecimiento a aquellos miembros que, aunque ya no forman parte del equipo, coincidieron conmigo en algún momento durante este proceso. Me gustaría agradecer especialmente a Helena, Lorena, Luís, Carlos, María, Patricia y Lucía. Gracias por vuestro apoyo y por todos los buenos momentos vividos tanto dentro como fuera del laboratorio.

También me gustaría dar las gracias a Carmen Évora y Araceli Delgado por acogerme en la Universidad de La Laguna durante mi primera estancia. Agradezco sinceramente a todos los compañeros de ambos grupos de investigación, especialmente a Erik, María, Amor y Edu, por su hospitalidad y por todos los buenos momentos compartidos fuera y dentro del laboratorio. Vuestra cálida bienvenida y la oportunidad de explorar Tenerife con personas como vosotros hicieron de mi tiempo allí una experiencia inolvidable.

I would also like to thank Pieter de Beule for the warm welcome in his research group (Medical Devices) at the INL during my stay in Braga. Thank you for giving me the opportunity to be part of this group even though we did not know each other. Thanks for teaching me the more physical part of this work. It was a very enriching period, both

personally and professionally. Thanks to the IACOBUS programme for giving me the opportunity to do my internship at the INL.

I would also like to thank Adelaide for her good advice. Susana, Hedieh, Diogo, Fábio, and Rafa for the good times we shared together. Thank you for being my friends there and for continuing this friendship despite the distance.

À minha querida Lina, por me ter mostrado Portugal e todos os seus encantos. Muito obrigada pela tua amizade, por me apoiares nas minhas decisões, por todas essas viagens que fizemos juntas e por todas as que ainda estão para vir.

A Raquel, Conchi, Marce y Carlos. Gracias por pasar de ser mis compañeros de alemán a unos buenos amigos con los que poder desconectar del laboratorio y con los que compartí tan buenos momentos durante todos estos años. Esa buena amistad que ni la pandemia fue capaz de debilitar.

A Sandra, por esas cenas, noches de impro, tardes de paseos o de cafés y, sobre todo, por esta amistad y apoyo durante este proceso.

Finalmente, pero no menos importante, me gustaría expresar mi profundo agradecimiento a mi familia y amigos. A mis amigos, los de siempre, por todos los buenos momentos compartidos juntos a lo largo de todos estos años, por vuestra comprensión y apoyo y por estar siempre ahí para celebrar juntos todos nuestros logros y alegrías. A Álex por apoyarme en todas mis decisiones y por compartir conmigo ese amor por la química. Por nuestros intercambios de ideas, descubrimientos y momentos de aprendizaje juntos, así como por todos los buenos momentos compartidos. A Ana y a Juanjo por su amistad incondicional y por ser parte de este viaje.

A toda mi familia, los que están y los que ya no están. Gracias por hacer este largo camino mucho más sencillo con todo vuestro apoyo.

Gracias a mis padres, Paula y Manuel y gracias a mi hermano Manuel. A vosotros os debo un agradecimiento sin límites. Sin vuestro apoyo incondicional, cariño y paciencia, nada de esto habría sido posible. Gracias por contribuir a convertirme en la persona que soy hoy. Este trabajo os lo dedico a vosotros.

USC
UNIVERSIDADE DE SANTIAGO DE COMPOSTELA

TABLE OF CONTENT

USC
UNIVERSIDADE
DE SANTIAGO
DE COMPOSTELA

USC
UNIVERSIDADE
DE SANTIAGO
DE COMPOSTELA

CONTENTS

CONTENTS ..... **I**
LIST OF ABBREVIATIONS ..... **IV**
SUMMARY ..... **VII**
RESUMO ..... **XV**
1 INTRODUCTION **1**
1.1 Osteoarthritis 3
1.2 Intraarticular treatments currently used in clinic 5
1.2.1 Immediate release IA formulations: solutions and dispersions of therapeutic molecules 5
1.2.2 Controlled drug delivery systems for IA injection 8
1.3 Intraarticular treatments under clinical trials 11
1.3.1 Immediate release IA formulations: solutions and dispersions of therapeutic molecules 11
1.3.2 Controlled drug delivery systems for IA injection 15
1.4 Systems currently under development 15
1.4.1 Nanometric particles 16
1.4.2 Micrometric particles 18
1.4.3 Hydrogels 19
1.5 Artificial intelligence tools in drug delivery systems development 19
1.5.1 Nanometric particles designed by artificial intelligence tools. 20
1.5.2 Micrometric particles designed by artificial intelligence tools 22
2 OBJECTIVES **25**
3 MATERIALS AND METHODS **29**
3.1 Functionalized indomethacin-loaded nanostructured lipid carriers 31
3.1.1 Materials 31
3.1.2 Selection of NLCs components 31
3.1.3 Experimental design 33
3.1.4 NLCs modelling and optimization 34
3.1.5 Mannose-labelling 37
3.1.6 NLCs functionalization with mannose 37
3.1.7 NLCs characterization 38
3.1.8 *In vitro* cell studies 39
3.1.9 Statistical analysis 42
3.2 Lipid-polymer hybrid nanoparticles loaded with IL-4 to modulate macrophage phenotype. 43
3.2.1 Materials 43

USC UNIVERSIDADE DE SANTIAGO DE COMPOSTELA

3.2.2 Experimental design 44
3.2.3 LPNPs modelling 45
3.2.5 LPNPs characterization 46
3.2.6 Fluorescence cross-correlation spectroscopy 47
3.2.7 *In vitro* cell studies 48
3.2.8 Statistical analysis 51
3.3 Design and evaluation of senolytic loaded microspheres 52
3.3.1 Materials 52
3.3.2 Experimental design 52
3.3.3 Microspheres modelling 53
3.3.4 Preparation of microspheres for intra-articular delivery 55
3.3.5 Microspheres characterization 55
3.3.6 *In vitro* cell studies 56
3.3.7 *In vivo* studies 58
3.3.8 Statistical analysis 59
4 RESULTS AND DISCUSSION 61
4.1 Functionalized indomethacin-loaded nanostructured lipid carriers 63
4.1.1 Liquid lipid and solid lipid selection 63
4.1.2 NLCs design and optimization 65
4.1.3 NLCs functionalization of the optimized formulation 72
4.1.4 Deep characterization of optimized formulations 77
4.1.5 Cell proliferation and internalization studies 79
4.1.6 Anti-inflammatory activity 84
4.2 Lipid-polymer hybrid nanoparticles loaded with IL-4 to modulate macrophage phenotype 87
4.2.1 Effect of the studied variables on hybrid nanoparticles properties 88
4.2.2 Characterization of the obtained IL-4-LPNPs 90
4.2.3 Fluorescence cross-correlation spectroscopy 91
4.2.4 Cell viability 94
4.2.5 Cell uptake 95
4.2.6 Anti-inflammatory activity 97
4.3 Design and evaluation of senolytic loaded microspheres 100
4.3.1 Effect of the studied variables on microspheres properties 100
4.3.2 Evaluation of microsphere formulations for intra-articular delivery 105
4.3.3 Characterization of the obtained microspheres 107
4.3.4 Senescent cells viability 109
4.3.5 Senolytic activity and autophagy induction 111

4.3.6 *In vivo* therapeutic effects of microspheres 113
5 CONCLUSIONS 117
6 REFERENCES 121
ANNEXES 145
ANNEX 1 147
ANNEX 2 152
ANNEX 3 153
APPENDICES. RIGHTS AND PERMISSIONS 161
Appendix I: Conflict of interest 163
Appendix II: List of publications included in this thesis and permissions 164
Appendix III: Images, tables, and figures. 166
CHECKLISTS AND PERMISSIONS 167

USC
UNIVERSIDADE DE SANTIAGO DE COMPOSTELA

LIST OF ABBREVIATIONS

^{1}H-NMR	Proton nuclear magnetic resonance spectroscopy analysis
2AA	2-aminobenzoic acid or anthranilic acid
ANOVA	Analysis of variance
AAV	Adeno-associated virus
ACS	Autologous conditioned serum
ADAMTS5	Disintegrin metalloproteinase with thrombospondin motifs 5
AE	Association efficiency
AI	Artificial Intelligence
ANGPTL3	Angiopoietin-like 3
ANN	Artificial neural networks
APCs	Antigen-presenting cells
APS	Autologous protein solution
ASMOD	Adaptive Spline Modelling of Data
AV	Adenovirus
BALB/3T3	Murine fibroblasts
BMDCs	Bone marrow-derived dendritic cells
BoNT-A	Botulinum toxin-A
BSA	Bovine Serum Albumin
BV	Baculovirus
CCK-8	Cell Counting Kit-8
CMC	Carboxymethyl cellulose
CPM	Counts per molecule
D_2O	Deuterated water
DAPI	4′,6-diamidino-2-phenylindole
DCM	Dichloromethane
DDS	Drug delivery systems
DiD'	1,1'-Dioctadecyl-3,3,3',3'-Tetramethylindodicarbocyanine, 4-Chlorobenzenesulfonate Salt
DL	Drug loading
DLS	Dynamic light scattering
DMEM	Dulbecco's Modified Eagle Medium
DMOAD	Disease modifying osteoarthritis drug
DNA	Deoxyribonucleic acid
DOPE-ATTO 488	1,2-Dioleoyl-sn-glycero-3-phosphoethanolamine labelled with Atto 488
DPBS	Dulbecco's Phosphate-Buffered Saline
DPSS	Diode-pumped solid-state
DSC	Differential scanning calorimetry
DSPE-PEG2000	1,2-distearoyl-sn-glycero-3-phosphoethanolamine-N-[amino(polyethylene glycol)-2000] (ammonium salt)
DSPE-PEG-NH_2	1,2-Distearoyl-sn-Glycero-3-Phosphoethanolamine-polyethylene glycol-amine
ECM	Extracellular matrix
EE	Encapsulation efficiency
EGF	Epidermal growth factor
ELISA	Enzyme-linked immunosorbent assay
EMA	European Medicines Agency

USC UNIVERSIDADE DE SANTIAGO DE COMPOSTELA

EU	European Union
FBS	Fetal Bovine Serum
FCCS	Fuorescence cross-correlation spectroscopy
FDA	Food and Drug Administration
FN	Fenofibrate
GA	Genetic Algorithms
GRAS	Generally recognized as safe
HA	Hyaluronic acid
HC-adenovirus	Helper-dependent adenovirus
IA	Intra-articular
IAIC	Intra-articular corticosteroids injections
IFN-β	Interferon-beta
IFN-γ	Interferon-gamma
IGF-1	Insulin-like growth factor-1
IL-1	Interleukin-1
IL-10	Interleukin-10
IL-13	Interleukin-13
IL-1RA	Interleukin-1 receptor antagonist
IL-4	Interleukin-4
IND	Indomethacin
L:G ratio	Lactide:glycolide ratio
LC3	Light chain 3
LL	Liquid lipids
LPNPs	Lipid-polymer nanoparticles
LPS	Lipopolysaccharide
LV	Lentivirus
MAN	Mannose
MCL	Medial collateral ligament
miRNA	Micro ribonucleic acid
MMP13	Matrix metalloproteinase-13
MMPs	Matrix metalloproteinases
MMTL	Medial meniscotibial ligament
MPs	Microparticles
mRNA	Messenger ribonucleic acid
MSCs	Mesenchymal stem cells
MWCO	Molecular weight cut-off
NA	Numerical aperture
NFκB	Nuclear factor κB
NLCs	Nanostructured lipid carriers
NPs	Nanoparticles
NSAIDs	Non steroidal anti-inflammatory drugs
OA	Osteoarthritis
OACs	Primary human osteoarthritic chondrocytes
OARSI	Osteoarthritis Research Society International
PBS	Phosphate Buffered Saline
PCL	Poly-caprolactone

USC UNIVERSIDADE DE SANTIAGO DE COMPOSTELA

PDGF	Platelet-derived growth factor
PDI	Polydispersity index
PEG	Polyethylene glycol
PLA	Poly-lactic acid
PLGA	Poly-lactic-co-glycolic acid
PMA	Phorbol 12-myristate 13-acetate
PNIPAM	Poly(N-isopropylacrylamide)
PPARα	peroxisome proliferator activated receptor alpha
PRGF	Plasma rich in growth factors
PRP	Platelet rich plasma
PVA	Polyvinyl alcohol
rAAV	Recombinant adeno-associated viral vector
RAW 264.7	Murine macrophages
RPMI 1640	Roswell Park Memorial Institute 1640 Medium
RT	Room temperature
RTX	Resiniferatoxin
RV	Retrovirus
SA	Octadecylamine or Stearylamine
SASP	Senescence-associated secretory phenotype
SD	Standard deviation
SDS	Sodium dodecyl sulphate
SEM	Scanning Electron Microscopy
sIL-1RII	Soluble interleukin-1 receptor type II
siRNA	Short interfering RNA
SL	Solid lipids
SLNs	Solid lipid nanoparticles
SRM	Structural Risk Minimization
sTNF-RI	Tumour necrosis factor receptor type I
sTNF-RII	Tumour necrosis factor receptor type II
TEM	Transmission Electron Microscopy
TGF-β	Transforming growth factor beta
THP-1	Human monocytes
TNF-α	Tumor necrosis factor-alpha
VEGF	Vascular endothelial growth factor
ZP	Zeta potential

USC UNIVERSIDADE DE SANTIAGO DE COMPOSTELA

SUMMARY

Osteoarthritis (OA) is a multifaceted degenerative joint disorder primarily characterized by the progressive breakdown of cartilage, alterations in synovial fluid composition, and subchondral bone remodelling. It affects mainly weight-bearing joints such as hips and knees, impacting approximately 7% of the population, with a growing incidence associated to the aging of the population and lifestyle factors.

The triggering factors of OA are still not fully understood but is believed to be associated to traumas, abnormal mechanical loads, and ageing. In this scenario, synovial joint cells such as fibroblasts and macrophages exert a chronic pro-catabolic and pro-inflammatory role secreting soluble inflammatory mediators that primes the pathological degradative cascade instauration. Moreover, under these stimuli, chondrocytes start depicting diminished proliferation and turnover. These changes contribute to synovitis, cartilage angiogenesis, subchondral bone sclerosis, and osteophyte formation, ultimately leading to joint function deterioration, swelling, stiffness and pain.

Current OA treatments focus on relieving these symptoms and improving joint function. These therapies include: non-pharmacological approaches such as exercise, weight management, and physical therapy; pharmacological interventions as analgesics, corticosteroids and non-steroidal anti-inflammatory drugs (NSAIDs); and surgical interventions. However, all these treatments fail to avoid the progression of the joint damage.

With these challenges in mind, there is a pressing need for therapies that halt the advancement of OA leading to the so-called disease modifying OA drugs (DMOADs). In this context, the development of intra-articular (IA) formulations emerges as a viable solution, providing enhanced local bioavailability and reduced systemic adverse effects.

IA treatments currently in clinic, under clinical trials or under development encompass various therapeutic approaches, including immediate release formulations and controlled drug delivery systems (DDS).

Immediate release IA formulations consist of solutions and dispersions of therapeutic molecules. Different approaches can be currently found in clinic, including the use of anti-inflammatory drugs that act by reducing inflammation, suppressing the synthesis of inflammatory mediators, or autologous blood products that contain high concentrations of growth factors and anti-inflammatory cytokines to control the expression of inflammatory mediators, reduce pain, and promote tissue regeneration. However, their efficacy varies among individuals, and some concerns have been raised about potential articular cartilage damage. Additionally, several immediate release IA formulations are under clinical trials to analyse the efficacy, safety, synergic effect, or superiority between different therapeutic strategies or to other administration routes such as the oral

USC UNIVERSIDADE DE SANTIAGO

route. These therapies include therapeutic molecules such as anti-inflammatory drugs or analgesics and new therapies such as the use of senolytic drugs or the gene therapy.

Due to the limited retention time that these immediate release injections exhibit, several DDS have emerged with the aim of overcoming the rapid clearance of free therapeutic molecules from the joint cavity. These innovative approaches offer the potential for sustained drug release directly on the affected joint, potentially improving therapeutic outcomes. Some of these DDS that are currently in clinic or under clinical trials include the use of micrometric particles (MPs) such as Zilretta®, nanometric particles (NPs) such as Lipotalon® or TLC599, and hydrogels such as Cingal® and Condrotide®Plus. However, these systems are designed to provide only OA pain relief.

In recent years, there has been growing interest in developing DMOADs that target underlying disease mechanisms and modify disease progression. These include agents aimed at reducing inflammation, preserving cartilage integrity, and promoting tissue repair. Additionally, advancements in drug delivery technologies, such as MPs, NPs, and hydrogels, hold promise for enhancing OA treatments efficacy by ensuring drug stability, prolonging drug release, and minimizing systemic side effects.

However, the development of new DDS is a complex task as many variables are involved in their production process. Artificial intelligence (AI) tools offer promising solutions by establishing patterns from complex databases. Moreover, these tools can optimize the formulation composition and procedures to obtain systems with desirable characteristics by identifying critical variables and their impact on the DDS final properties, facilitating an efficient and thoroughly DDS development process.

The integration of AI tools in the development of DDS for OA, holds significant promise, offering tailored solutions to meet specific requirements. AI techniques enable a deeper understanding of formulation processes while optimizing DDS designs. This innovative approach opens up new avenues for enhancing the precision and effectiveness of OA treatments through AI-assisted design of IA DDS-based injections.

Despite advances in treatment options, there is still a significant unmet need for disease modifying therapies that can halt or slow OA progression. Emerging research in regenerative medicine, tissue engineering, and drug delivery fields, can provide further knowledge for developing novel systems to prevent or reduce structural damage in OA with long-term patients benefits.

Taking this into account, the aim of this thesis is the design, development, and optimization of innovative DDS that could act as DMOADs following three different strategies.

USC UNIVERSIDADE DE SANTIAGO DE COMPOSTELA

The first strategy is aimed at designing, developing, and characterizing nanostructured lipid carriers (NLCs) loaded with an anti-inflammatory drug and able to be specifically internalized by pro-inflammatory cells. Mannosylation has emerged as a valuable tool for increasing the ability of NPs to be recognized and internalized by antigen-presenting cells (APCs) such as macrophages. Nevertheless, the design and development of functionalized NLCs is a complex task that entails the optimization of numerous variables and steps, making the process challenging and time-consuming. In this work, hybrid AI technologies were used to help in the design of mannosylated drug loaded NLCs following a sequential design. This approach allows to obtain models that get trained on the different fabrication steps leading to intermediate optimized formulations. NLCs were prepared by hot shear homogenization process and indomethacin (IND), an anti-inflammatory drug currently used by oral administration in OA management, was selected as a cargo.

Artificial neural networks combined with fuzzy logic or genetic algorithms were employed to understand the particle formation processes and optimize the combinations of variables for the different steps in the functionalization process. Mannose was chemically modified to allow, for the first time in the development of mannosylated NPs, functionalization efficiency quantification and optimization. Additionally, the optimal formulation underwent further physicochemical characterization to assess drug leakage, morphological structure, and thermal properties. An *in silico* docking analysis was also performed to better understand the affinity and interaction between the drug and the excipients. Moreover, cell viability studies, as well as uptake studies were performed to study the cytocompatibility of the developed systems and internalization in macrophages presenting a pro-inflammatory phenotype. Cell uptake studies were also conducted in murine fibroblasts to study the specificity of the developed NLCs to be taken up by stimulated macrophages. In addition, as these DDS were designed to control inflammation, the secretion of pro-inflammatory cytokines was also determined.

The proposed sequential methodology has enabled the design of a robust procedure for obtaining stable mannosylated and drug loaded NLCs with a uniform particle size distribution, small particle size (< 100 nm), and a substantial positive zeta potential (> 20 mV) that confer adequate characteristics to be endocytosed by APCs. The correct mannose labelling was confirmed by a ^{1}H-NMR analysis. The incorporation of mannose on the surfaces of these DDS following the established protocols achieved higher than 85% of functionalization efficiency. Moreover, the *in silico* studies demonstrated a high affinity between the drug and the functionalization linker employed to attach the mannose, which was then confirmed by thermal analysis. The high affinity between both components, provided specific properties to the NLCs, such as reduced particle size and slow drug leaking compared to those systems prepared without the mannose coating

USC DE COMPOSTELA

and, therefore, without the functionalization linker. The performed drug release studies showed adequate drug permanence within developed NLCs.

Additionally, a specific and efficient uptake by macrophages was observed. As expected, the developed systems exhibit non-toxic features and show an intracellular distribution compatible with a receptor-mediated endocytosis internalization pathway, owing to their high affinity for the mannose receptors (CD206) present on the membrane of APCs. This feature was acquired thanks to their mannose coating. Furthermore, the developed drug loaded systems were able to reduce the secretion of pro-inflammatory cytokines as TNF-α or IL-8, while increasing the secretion of the anti-inflammatory cytokine IL-4. This latter outcome may be attributed to the NLCs interaction with the CD206 receptor resulting in a beneficial anti-inflammatory effect.

Therefore, the developed NLCs not only enhanced their recognition and internalization by macrophages but also were able to modulate the inflammatory response, thus stopping the pathology degradative cycle at the inflammation point and facilitating the OA treatment.

The second strategy is focused on the design, development, and characterization of lipid-polymer nanoparticles (LPNPs) loaded with IL-4 to modulate macrophage phenotype. IL-4 was chosen based on its immunomodulatory capacity. LPNPs have emerged as new delivery systems that combine the properties of polymeric and lipid NPs in terms of stability and functionalization capacity. Therefore, they were selected as DDS to encapsulate the selected immunomodulatory protein. These systems were composed of a polymeric core where the therapeutic molecule was encapsulated, and a pegylated lipid corona including reactive groups at the terminal polyethylene glycol chain that provides steric stability and enables efficient surface functionalization.

AI tools were employed to determine the best LPNPs composition able to obtain stable NPs. LPNPs were prepared, in a first step, employing bovine serum albumin (BSA) as the only cargo following a modified nanoprecipitation method. The obtained models were then employed to design LPNPs loaded with the immunomodulatory protein with the composition that leads to the best LPNPs attributes. Moreover, the core-shell structure of these systems, as well as the surface coating, were characterized, employing fluorescence cross-correlation spectroscopy (FCCS), a very sensitive technique that studies molecular dynamics. To the best of our knowledge, this is the first time FCCS was used to characterize LPNPs. To this end, the nanoparticle components were fluorescently labelled. The lipid shell was labelled by the hydrophobic insertion of ATTO488-DOPE, mannose was labelled following the formation of a Schiff base through the Maillard reaction with ATTO488-NH_2, and the polymeric core was stained by the incorporation of DiD´ to the polymeric dispersion during LPNPs synthesis. This

USC DE SANTIAGO DE COMPOSTELA

technique allows to determine the colocalization of the fluorophores, thus corroborating the LPNPs structure.

Furthermore, *in vitro* cell studies were performed to assess cell viability and uptake by pro-inflammatory macrophages. Confocal microscopy was employed to image cell cytoplasm and early endosomes, previously labelled. To ensure IL-4 stability, thereby preserving its immunomodulatory capacity, these LPNPs should avoid the lysosomal degradation. The activity and immunomodulatory capacity were assessed by analysing the secretion of pro-inflammatory and anti-inflammatory cytokines after the treatment of pro-inflammatory macrophages with the developed protein-loaded systems.

Results showed that the obtained IL-4 loaded LPNPs exhibit small and uniform particle size distributions (< 200 nm) as well as a negative zeta potential (≈ - 20 mV) that confer them, together with the pegylated lipid layer, colloidal stability avoiding the formation of aggregates during storage. Moreover, a high association efficiency (≈ 99.0%) was achieved, not observing protein leaking within the studied period, meaning the encapsulated protein remains within the developed systems at least 24 hours. Furthermore, a high functionalization efficiency, was achieved improving those previously observed for NLCs. This effect could be attributed to a higher availability of the functional groups to react with mannose thanks to the polyethylene glycol linker. Therefore, the developed systems exhibit adequate characteristics to be taken up by macrophages.

The FCCS studies showed a high cross-correlation function between fluorescently labelled species, confirming the core-shell structure, as well as the mannose coating. The structure of the fluorescently labelled mannose was again confirmed by a ^{1}H-NMR analysis. The confirmation of the LPNPs structure is essential to better understand their interaction with cells. Thus, this technique serves as a potent tool to characterize complex structures as functionalized LPNPs.

Regarding the *in vitro* cell evaluation using IL-4 loaded LPNPs, the developed systems led to an enhanced proliferation or metabolic activity in both, macrophages and fibroblasts. The increased metabolic activity observed was primarily attributed to the delivery of IL-4, a pro-regenerative and anti-inflammatory molecule. Moreover, confocal images revealed that both, mannose-functionalized, and non-functionalized formulations were highly internalized. However, LPNPs were observed within early endosomes. Interestingly, more mannose-functionalized formulations were co-localized in early endosomes than non-functionalized ones, indicating that those with the mannose coating were taken up by receptor mediated endocytosis. Nevertheless, the anionic polymeric core would allow LPNPs to escape from the late endosome by changing their surface charge in response to the pH change as the endosome vesicle matures. Besides,

USC
DE SANTIAGO
DE COMPOSTELA

the LPNPs escape from the late endosomes was confirmed with the immunomodulatory effect shown by the developed systems. The treatment of pro-inflammatory macrophages with the developed LPNPs led to a significant increase in the secretion of IL-10, while a significant reduction of IL-8 was observed. Interestingly, the enhancement of IL-10 secretion was more pronounced for IL-4 formulations than previously reported for the protein alone indicating a possible beneficial effect of the mannose and IL-4 combination.

These findings point out the LPNPs loaded with IL-4 avoids protein degradation, while providing a macrophage phenotype modulation to an anti-inflammatory one and, therefore, their suitability as a DMOAD.

The last strategy aimed at designing polymeric microspheres loaded with a senolytic drug to restore cartilage damage and tissue homeostasis. Fenofibrate was selected as the cargo due to its senolytic activity, which may decrease cartilage degradation by modulating senescence and autophagy, thus being considered a novel disease modifying therapeutic molecule.

Despite polymeric microspheres are widely used as DDS, the lack of a general procedure for producing microspheres of predictable characteristics makes their development relegated to test-error approaches.

In this work, polymeric microspheres were prepared through a single emulsion-solvent evaporation process. The relationship between the variables involved in the preparation process and the quality parameters of the polymeric microspheres were established by AI tools using a single low molecular weight polymer. The obtained model was validated, and microspheres with the desired characteristics were successfully prepared and thoroughly characterized. Moreover, these systems were intended to remain within the joint cavity for a more prolonged period compared to the previously developed NPs exerting their release at the extracellular level. To achieve a more sustained drug release profile a polymer with higher molecular weight and lower degradation rate was incorporated to the initial one in the microspheres formulation.

Furthermore, the effect of the developed microspheres on cell viability, cell senescence (irreversible cell division arrest), and autophagy induction, a cellular recycling process, were studied using primary human osteoarthritic chondrocytes. Additionally, murine fibroblasts were employed to demonstrate the specific senolytic effect of the selected drug.

Moreover, the therapeutic activity of the fenofibrate loaded microspheres was also studied *in vivo*. To this end, a surgically induced OA mice model was employed, and microspheres were IA injected at two fenofibrate doses 1 and 10 µg.

USC
UNIVERSIDADE
DE SANTIAGO
DE COMPOSTELA

The used AI tools were able to generate models of high predictability (> 85%) for the microsphere's properties. Moreover, the obtained set of linguistic rules, *IF-THEN* rules, allowed to dictate general guidelines to better select the polymeric microspheres formulation parameters following the single emulsion-solvent evaporation process.

Following the obtained rules, microspheres with the desired characteristics were obtained validating the model. The developed drug loaded microspheres showed small and uniform particle sizes (≈ 30 μm), adequate to be IA administered. Moreover, high drug loadings (1%) and encapsulation efficiencies (≈ 100%) were achieved. Moreover, the fenofibrate release profile was studied for formulations containing two polymeric compositions: 1) a low molecular weight and fast degrading polymer or 2) a blend of a low molecular weight and fast degrading polymer with a high molecular weight and slow degradation profile polymer. The results showed a significant reduction in the release constant for the formulation that includes the polymers mixture (375.99 ± 52.46 and 210.56 ± 7.85 $day^{-1/2}$, respectively), which can be related with the rate of polymer degradation. In both cases, the fenofibrate release profile was extended for up to three months. These results demonstrate the suitability of the developed microspheres as fenofibrate delivery systems.

Viability assays were conducted on senescent chondrocytes to assess the impact of the developed microspheres or free drug. A notable reduction in cell viability was observed following treatment with both, the microspheres and the free drug associated to the senolytic activity of the drug. Additionally, to evaluate whether the drug could induce a non-specific decrease in cell viability, and, therefore, toxicity, viability studies were conducted on fibroblasts. The data obtained confirmed the specific senolytic effect of fenofibrate. Thus, the developed fenofibrate-loaded microspheres could exert a specific senolytic effect in senescent cells without exhibiting toxicity to healthy cells.

The capacity of the drug-loaded microspheres in decreasing the number of senescent cells was also assessed in primary osteoarthritic chondrocytes. A cell senescence reduction was observed after the treatment with the drug loaded microspheres compared to the free drug regardless of their polymeric composition. The ability of the designed microspheres to increase autophagy of osteoarthritic chondrocytes was also evaluated. Although no significant differences in autophagy induction were observed compared to the free drug, the obtained results showed the developed microspheres are adequate for fenofibrate delivery.

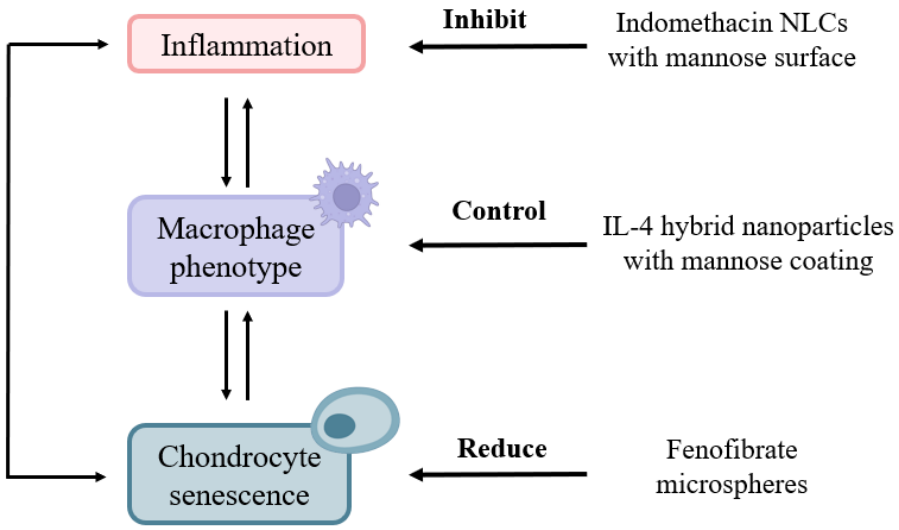
The formulation depicting a more sustained drug release was selected to be tested in a *in vivo* model of OA. Results showed a significant cartilage morphology improvement after the treatment with the drug loaded microspheres at both tested doses.

USC UNIVERSIDADE DE SANTIAGO DE COMPOSTELA

The obtained results demonstrate the usefulness of AI tools to design microspheres with desired physicochemical properties for IA administration. Moreover, the polymeric composition can be tailored to achieve more prolonged drug release profiles. The decrease in OA-type changes in the articular cartilage of OA mice after microspheres administration demonstrated the potential of these formulations as DMOADs.

The promising results achieved in this thesis, highlights the important role of AI tools in the design, development, and optimization of DDS. Furthermore, the developed DDS were not only able to successfully encapsulate the selected therapeutic molecules, but also improve their therapeutic activity. These systems demonstrated potential as DMOADs, targeting the two main hallmarks of OA: inflammation and cartilage degradation. This approach is achieved following three independent but closely related strategies (**Graphical abstract**); inflammation control, macrophage phenotype modulation and chondrocyte senescence reduction, reversing disease progression. Therefore, either individually or used in combination these DDS depict high potential in the management of OA.

Graphical abstract



USC UNIVERSIDADE DE SANTIAGO DE COMPOSTELA

RESUMO

A artrose é un trastorno articular dexenerativo polifactorial caracterizado principalmente pola degradación progresiva da cartilaxe, alteracións na composición do líquido sinovial e remodelación do óso subcondral. Afecta principalmente ás articulacións que soportan peso, como as cadeiras e os xeonllos, e afecta aproximadamente ao 7% da poboación, cunha incidencia crecente debido ao envellecemento da poboación e a factores relacionados co estilo de vida.

Os factores causantes da OA aínda non se coñecen de todo, pero creese que están asociados a traumatismos, cargas mecánicas anormais e envellecemento. Neste escenario, as células da articulación sinovial, como os fibroblastos e os macrófagos, exercen un papel pro-catabólico e pro-inflamatorio crónico segregando mediadores inflamatorios solubles que conducen á instauración do ciclo patolóxico degradativo. Ademais, baixo estes estímulos, os condrocitos empezan a mostrar unha proliferación e un recambio diminuídos. Estes cambios contribúen á sinovitis, a anxioxénese da cartilaxe, a esclerose do óso subcondral e a formación de osteofitos, o que en última instancia conduce á deterioración da función articular, a inflamación, a rixidez e a dor.

Os tratamentos actuais da OA céntranse en aliviar estes síntomas e mellorar a función articular. Inclúen enfoques non farmacolóxicos como o exercicio, o control do peso e a fisioterapia, intervencións farmacolóxicas como analxésicos, corticosteroides e antiinflamatorios non esteroideos (AINEs) e intervencións cirúrxicas. Con todo, todos estes tratamentos non conseguen evitar a progresión do dano articular.

Ante estes desafíos, existe unha necesidade imperiosa de terapias que deteñan o avance da enfermidade, o que da lugar aos denominados fármacos modificadores da enfermidade da artrose (DMOADs, polas súas siglas en inglés). Neste contexto, o desenvolvemento de formulacións de administración intraarticular emerxe como unha solución viable, proporcionando unha maior biodispoñibilidade local á vez que se reducen os efectos adversos sistémicos.

Os tratamentos intraarticulares actualmente en clínica, en fase de ensaio clínico ou en desenvolvemento abarcan varios enfoques terapéuticos, incluídas as formulacións de liberación inmediata e os sistemas de liberación controlada de fármacos (DDS, polas súas siglas en inglés).

As formulacións intraarticulares de liberación inmediata consisten en solucións e dispersións de moléculas terapéuticas. Na actualidade pódense atopar diferentes enfoques na clínica, incluído o uso de fármacos antiinflamatorios que actúan reducindo a inflamación, suprimindo a síntese de mediadores inflamatorios, ou produtos sanguíneos autólogos que conteñen altas concentracións de factores de crecemento e citoquinas antiinflamatorias para controlar a expresión de mediadores inflamatorios,

USC UNIVERSIDADE DE SANTIAGO

reducir a dor e promover a rexeneración tisular. Con todo, a súa eficacia varía dunha persoa a outra, e existe certa preocupación polos posibles danos na cartilaxe articular. Ademais, estanse a realizarse ensaios clínicos con varias formulacións intraarticulares de liberación inmediata para analizar a eficacia, a seguridade, o efecto sinérxico ou a superioridade entre diferentes estratexias ou respecto a outras vías de administración, como a vía oral. Estas terapias inclúen moléculas terapéuticas como antiinflamatorios ou analxésicos e novas terapias como o uso de fármacos senolíticos ou a terapia xénica.

Debido ao limitado tempo de retención que presentan estas inxeccións de liberación inmediata, xurdiron varios DDS co obxectivo de superar a rápida eliminación das moléculas terapéuticas libres da cavidade articular. Estes enfoques innovadores ofrecen a posibilidade dunha liberación sostida do fármaco directamente na articulación afectada, mellorando potencialmente os resultados terapéuticos. Algúns destes DDS que se atopan actualmente na clínica ou en fase de ensaio clínico inclúen o uso de partículas micrométricas (MPs) como Zilretta®, partículas nanométricas (NPs) como Lipotalon® ou TLC599, e hidroxeles como Cingal® e Condrotide®Plus. Con todo, estes sistemas están deseñados para proporcionar únicamente alivio da dor na OA.

Nos últimos anos, creceu o interese por desenvolver DMOADs que actúen sobre os mecanismos subxacentes da enfermidade e modifiquen a súa progresión. Entre eles atópanse os destinados a reducir a inflamación, preservar a integridade da cartilaxe e promover a reparación tisular. Ademais, os avances nas tecnoloxías de administración de fármacos, como as NPs, os polímeros multiproteicos e os hidroxeles, son prometedores para mellorar a eficacia dos tratamentos da artrose ao garantir a estabilidade do fármaco, prolongar a súa liberación e minimizar os efectos secundarios sistémicos.

Con todo, o desenvolvemento de novos DDS é unha tarefa complexa, xa que no seu proceso de produción interveñen moitas variables. As ferramentas de intelixencia artificial ofrecen solucións prometedoras ao establecer patróns a partir de bases de datos complexas. Ademais, estas ferramentas poden optimizar a composición da formulación e os procedementos para obter sistemas con características desexables mediante a identificación de variables críticas e o seu impacto nas propiedades finais dos DDS, facilitando un proceso de desenvolvemento de DDS eficiente e exhaustivo.

A integración de ferramentas de intelixencia artificial no desenvolvemento de DDS para a artrose é moi prometedora, xa que ofrece solucións a medida para satisfacer requisitos específicos. As técnicas de intelixencia artificial permiten unha comprensión máis profunda dos procesos de formulación á vez que optimizan os deseños dos DDS. Este enfoque innovador abre novas vías para mellorar a precisión e a eficacia dos tratamentos

USC UNIVERSIDADE DE SANTIAGO DE COMPOSTELA

da artrose mediante o deseño asistido por ferramentas de intelixencia artificial de inxeccións baseadas en DDS para administración intraarticular.

A pesar dos avances nas opcións de tratamento, segue existindo unha importante necesidade non cuberta de terapias modificadoras da enfermidade que poidan deter ou retardar a progresión desta patoloxía. A investigación emerxente nos campos da medicina rexenerativa, a enxeñería de tecidos e a administración de fármacos é prometedora para o desenvolvemento de novos sistemas que permitan previr ou reducir o dano estrutural na artrose, á vez que proporcionan beneficios a longo prazo aos doentes.

Tendo isto en conta, o obxectivo desta tese é o deseño, desenvolvemento e optimización de DDS innovadores que poidan actuar como DMOADs seguindo tres estratexias diferentes.

A primeira estratexia está dirixida ao deseño, desenvolvemento e caracterización de portadores lipídicos nanoestructurados (NLCs, polas súas siglas en inglés) cargados cun fármaco antiinflamatorio e capaces de ser internalizados especificamente por células proinflamatorias. A manosilación revelouse como unha valiosa ferramenta para aumentar a capacidade dos NLCs de ser recoñecidos e internalizados por células presentadoras de antíxenos (APCs, polas súas siglas en inglés) como os macrófagos. Con todo, o deseño e desenvolvemento de NLCs funcionalizadas é unha tarefa complexa que conleva a optimización de numerosas variables e pasos, convertíndose nun proceso lento e desafiante. Neste traballo, empregáronse tecnoloxías híbridas de intelixencia artificial para axudar no deseño de NLCs cargadas con fármacos e recubertos en superficie con manosa seguindo un deseño secuencial. Este enfoque permite obter modelos que se adestran nos diferentes pasos de fabricación, dando lugar a formulacións intermedias optimizadas. As NLCs preparáronse mediante un proceso de homoxeneización por cizallamento en quente e seleccionouse como fármaco a indometacina (IND), un antiinflamatorio empregado actualmente por vía oral no tratamento da artrose.

Empregáronse redes neuronais artificiais combinadas con lóxica difusa ou algoritmos xenéticos para comprender os procesos de formación de partículas e optimizar as combinacións de variables para os distintos pasos do proceso de funcionalización. A manosa modificouse químicamente para permitir, por primeira vez no desenvolvemento de NPs manosiladas, a cuantificación e optimización da eficiencia da funcionalización. Ademais, a formulación óptima someteuse a unha caracterización fisicoquímica adicional para avaliar a perda do fármaco, a estrutura morfolóxica e as propiedades térmicas. Tamén se realizou unha análise *in silico* para comprender mellor a afinidade e a interacción entre o fármaco e os excipientes. Ademais, realizáronse estudos de

USC DE SANTIAGO DE COMPOSTELA

viabilidade celular, así como estudos de captación para estudar a citocompatibilidade dos sistemas desenvolvidos e a internalización en macrófagos que presentan un fenotipo proinflamatorio. Realizáronse tamén estudos de captación celular empregando fibroblastos murinos para estudar a especificidade dos NLCs desenvolvidos para ser captados por macrófagos estimulados. Ademais, dado que estes DDS deseñáronse para controlar a inflamación, tamén se determinou a secreción de citoquinas proinflamatorias nos devanditos macrófagos.

A metodoloxía secuencial proposta permitiu o deseño dun procedemento robusto para a obtención de NLCs estables, manosilados e cargados de fármaco cunha distribución uniforme do tamaño de partícula, un tamaño de partícula pequeno (< 100 nm), e un potencial zeta positivo (> 20 mV) que confiren características adecuadas para ser endocitadas por APCs.

A correcta marcaxe da manosa confirmouse mediante unha análise de ^{1}H-NMR. A incorporación de manosa nas superficies destes DDS seguindo os protocolos establecidos alcanzou unha eficiencia de funcionalización superior ao 85%. Ademais, os estudos *in silico* demostraron unha alta afinidade entre o fármaco e a molécula de funcionalización empregada para unir covalentemente a manosa, o que se confirmou posteriormente mediante análise térmica. A alta afinidade entre ambos compoñentes, proporcionou propiedades específicas ás NLCs, tales como a redución do tamaño de partícula e a redución da perda do fármaco en comparación con aqueles sistemas preparados sen o recubrimento de manosa e, por tanto, sen a molécula de funcionalización. Os estudos de liberación de fármaco realizados mostraron unha adecuada permanencia do fármaco dentro das NLCs desenvolvidas.

Ademais, observouse unha captación específica e eficiente por parte dos macrófagos. Como era de esperar, os sistemas desenvolvidos presentan características non tóxicas e mostran unha distribución intracelular compatible ca vía de internalización por endocitosis mediada por receptor, debido á súa alta afinidade polos receptores de manosa (CD206) presentes na membrana das APCs. Esta característica adquiriuse grazas ao seu recubrimento de manosa. Ademais, os sistemas cargados con fármacos desenvolvidos foron capaces de reducir a secreción de citocinas proinflamatorias como o TNF-α ou a IL-8, mentres que aumentou a secreción da citocina antiinflamatoria IL-4. Este último efecto pode atribuírse á alta afinidade das NLCs polos receptores de manosa (CD206) presentes na membrana das APCs producindo un efecto antiinflamatorio beneficioso.

Polo tanto, as NLCs desenvolvidas non só melloraron o seu recoñecemento e internalización polos macrófagos, senón que tamén foron capaces de modular a resposta

USC UNIVERSIDADE DE SANTIAGO DE COMPOSTELA

inflamatoria, detendo así o ciclo degradativo da patoloxía no punto de inflamación e facilitando o tratamento da mesma.

A segunda estratexia céntrase no deseño, desenvolvemento e caracterización de nanopartículas lipídico-poliméricas (LPNPs) cargadas con IL-4 para modular o fenotipo dos macrófagos. Elixiuse a IL-4 pola súa capacidade inmunomoduladora. As LPNPs xurdiron como novos sistemas de administración que combinan as propiedades das NPs poliméricas e lipídicas en termos de estabilidade e capacidade de funcionalización. Polo tanto, seleccionáronse como DDS para encapsular a proteína immunomoduladora seleccionada. Estes sistemas estaban compostos por un núcleo polimérico no que se encapsulaba a molécula terapéutica, e unha coroa lipídica pegilada que incluía grupos reactivos na cadea terminal de polietilenglicol proporcionando estabilidade estérica e unha funcionalización eficaz da superficie.

Empregáronse ferramentas de intelixencia artificial para determinar cal é a mellor composición de LPNPs para obter NPs estables. As LPNPs preparáronse, nun primeiro paso, empregando albúmina sérica bovina (BSA) soa como carga seguindo un método de nanoprecipitación modificado. A continuación, empregáronse os modelos obtidos para deseñar LPNPs cargadas coa proteína immunomoduladora coa composición que conduce aos mellores atributos das LPNPs. Ademais, caracterizouse a estrutura núcleo-coroa destes sistemas, así como o recubrimento superficial, empregando espectroscopia de fluorescencia de correlación cruzada (FCCS), unha técnica moi sensible que estuda a dinámica molecular. Ata onde sabemos, é a primeira vez que se utiliza a FCCS para caracterizar LPNPs. Para iso, os compoñentes das nanopartículas marcáronse con fluoróforos. A cuberta lipídica marcouse mediante a inserción hidrofóbica de DOPE-ATTO488, a manosa marcouse tras a formación dunha base de Schiff a través da reacción de Maillard con ATTO488-NH_2 e o núcleo polimérico marcouse mediante a incorporación de DiD' á dispersión polimérica durante a síntese das LPNPs. Esta técnica permite determinar a colocalización dos fluoróforos, corroborando así a estrutura das LPNPs.

Ademais, realizáronse estudos celulares *in vitro* para avaliar a viabilidade celular e a súa captación por macrófagos proinflamatorios. Empregouse microscopía confocal para obter imaxes do citoplasma celular e dos endosomas temperáns, previamente etiquetados. Para garantir a estabilidade da IL-4, preservando así a súa capacidade inmunomoduladora, estes LPNPs deberían evitar a degradación lisosomal. A actividade e capacidade inmunomoduladora avaliouse analizando a secreción de citoquinas proinflamatorias e antiinflamatorias tras o tratamento de macrófagos pro-inflamatorios cos sistemas desenvolvidos cargados de proteínas.

USC UNIVERSIDADE DE SANTIAGO DE COMPOSTELA

Os resultados mostraron que as LPNPs cargadas con IL-4 obtidas presentan distribucións de tamaño de partícula pequenas e uniformes (< 200 nm) así como un potencial zeta negativo (≈ - 20 mV) que lles confiren, xunto coa cuberta lipídica pegilada, estabilidade coloidal evitando a formación de agregados durante o almacenamento. Ademais, conseguiuse unha alta eficiencia de asociación (≈ 99,0%), non observándose perdas de proteína no período estudado, o que significa que a proteína encapsulada permanece dentro dos sistemas desenvolvidos polo menos 24 horas. Ademais, logrouse unha alta eficiencia de funcionalización, mellorando a observadas anteriormente para NLCs. Este efecto podería atribuírse a unha maior dispoñibilidade dos grupos funcionais para reaccionar coa manosa grazas ao enlazador de polietilenglicol. Polo tanto, os sistemas desenvolvidos presentan características adecuadas para ser captados por macrófagos.

Os estudos FCCS mostraron unha elevada función de correlación cruzada entre as especies marcadas con fluorescencia, o que confirma a estrutura núcleo-coroa, así como o recubrimento de manosa. A estrutura da manosa marcada fluorescentemente confirmouse de novo mediante unha análise ^{1}H-NMR. A confirmación da estrutura das LPNPs é esencial para comprender mellor a súa interacción coas células. Así pois, esta técnica serve como potente ferramenta para caracterizar estruturas complexas como as LPNPs funcionalizadas.

En canto á avaliación celular *in vitro* con LPNPs cargados con IL-4, os sistemas desenvolvidos conduciron a unha maior proliferación ou actividade metabólica tanto en macrófagos como en fibroblastos. O aumento da actividade metabólica observado atribuíuse principalmente á IL-4, unha molécula pro-rexenerativa e anti-inflamatoria. Ademais, as imaxes de confocal revelaron que tanto as formulacións funcionalizadas con manosa como as non funcionalizadas foron altamente internalizadas. Con todo, observáronse LPNPs dentro de endosomas temperáns. Curiosamente, nos endosomas temperáns co-localizaronse máis as formulacións funcionalizadas con manosa que as non funcionalizadas, o que indica que aquelas con recubrimento de manosa foron captadas por endocitosis mediada por receptores. Con todo, o núcleo polimérico aniónico permitiría o escape endosomal tardío das LPNPs ao cambiar a súa carga superficial en resposta ao cambio de pH a medida que a vesícula endosomal madura. Ademais, o escape de LPNPs dos endosomas tardíos confirmouse co efecto inmunomodulador mostrado polos sistemas desenvolvidos. O tratamento de macrófagos proinflamatorios cos LPNPs conduciu a un aumento significativo da secreción de IL-10, mentres que se produciu unha redución significativa da IL-8. Curiosamente, o aumento da secreción de IL-10 foi máis pronunciado no caso das formulacións de IL-4 que para o anteriormente publicado para proteína soa, o que indica un posible efecto beneficioso da combinación de manosa e IL-4.

USC DE COMPOSTELA

Estes resultados sinalan que as LPNPs cargadas con IL-4 evitan a degradación proteica, á vez que proporcionan unha modulación do fenotipo do macrófago cara a un fenotipo antiinflamatorio e, por tanto, a súa idoneidade como DMOADs.

A última estratexia tivo como obxectivo deseñar microesferas poliméricas cargadas cun fármaco senolítico para restaurar o dano da cartilaxe e a homeostasis tisular. Seleccionouse o fenofibrato como fármaco debido á súa actividade senolítica, que pode diminuír a degradación da cartilaxe modulando a senescencia e a autofaxia, polo que, considerase unha nova molécula terapéutica modificadora da enfermidade.

A pesar de que as microesferas poliméricas utilízanse amplamente como DDS, a falta dun procedemento xeral para producilas con características predicibles fai que o seu desenvolvemento quede relegado a enfoques de proba-erro.

Neste traballo preparáronse microesferas poliméricas mediante un proceso de emulsión simple con evaporación do disolvente empregando un polímero de baixo peso molecular. Estableceuse a relación entre as variables que interveñen no proceso de preparación e os parámetros de calidade das microesferas poliméricas mediante ferramentas de intelixencia artificial. Validouse o modelo e obtivéronse con éxito as microesferas con características desexadas que se caracterizaron minuciosamente. Ademais, pretendíase que estes sistemas permanecesen dentro da cavidade articular durante un período máis prolongado en comparación coas NPs desenvolvidas anteriormente para liberar o fármaco a nivel extracelular. Para conseguir un perfil de liberación do fármaco máis sostido, incorporouse á formulación un polímero de maior peso molecular e menor taxa de degradación.

Ademais, estudouse o efecto das microesferas desenvolvidas sobre a viabilidade celular, a senescencia celular (detención irreversible da división celular), e a indución da autofaxia, un proceso de reciclaxe celular, empregando condrocitos osteoartríticos primarios. Así mesmo, empregáronse fibroblastos murinos para demostrar o efecto senolítico específico do fármaco seleccionado.

Por outra banda, tamén se estudou *in vivo* a actividade terapéutica das microesferas cargadas con fenofibrato. Para iso, empregouse un modelo de rato con artrose inducida cirurxicamente, e inxectáronse por vía intraarticular microesferas a dúas doses de fenofibrato: 1 e 10 µg.

As ferramentas de intelixencia artificial empregadas foron capaces de xerar modelos de alta predictibilidade (> 85%) para as propiedades das microesferas. Ademais, o conxunto de regras lingüísticas obtidas, regras *IF-THEN*, permitiron ditar pautas xerais para seleccionar mellor os parámetros de formulación das microesferas poliméricas seguindo o proceso de emulsión simple con evaporación do disolvente.

USC UNIVERSIDADE DE SANTIAGO DE COMPOSTELA

Seguindo as regras obtidas, obtivéronse microesferas coas características desexadas validando o modelo. As microesferas cargadas con fármaco desenvoltas mostraron tamaños de partícula pequenos e uniformes (≈ 30 μm), adecuados para ser administrados por vía intraarticular. Ademais, alcanzáronse altas cargas de fármaco (1%) e eficiencias de encapsulación (≈ 100%). Por outra banda, estudouse o perfil de liberación de fenofibrato en formulacións que contiñan dúas composicións poliméricas: 1) un polímero de baixo peso molecular e degradación rápida ou 2) unha mixtura dun polímero de baixo peso molecular e degradación rápida cun polímero de alto peso molecular e perfil de degradación lenta. Os resultados mostraron unha redución significativa da constante de liberación para a formulación que inclúe a mixtura de polímeros (375,99 ± 52,46 e 210,56 ± 7,85 día$^{-1/2}$, respectivamente), que pode relacionarse coa velocidade de degradación do polímero. En ambos os casos, o perfil de liberación do fenofibrato prolongouse ata tres meses. Estes resultados demostran a idoneidade das microesferas desenvolvidas como sistemas de liberación de fenofibrato.

Realizáronse ensaios de viabilidade en condrocitos senescentes para avaliar o impacto das microesferas ou do fármaco libre. Observouse unha notable redución da viabilidade celular tras o tratamento tanto coas microesferas como co fármaco libre, asociada á actividade senolítica do fármaco. Ademais, para avaliar se o fármaco podía inducir unha diminución inespecífica da viabilidade celular, realizáronse estudos de viabilidade en fibroblastos. Os datos obtidos confirmaron o efecto senolítico específico do fenofibrato. Así pois, as microesferas cargadas con fenofibrato desenvolvidas podían exercer un efecto senolítico específico en células senescentes sen mostrar toxicidade para as células sans.

Tamén se avaliou a capacidade das microesferas cargadas co fármaco para diminuír o número de células senescentes en condrocitos osteoartríticos primarios. Observouse unha redución da senescencia celular tras o tratamento coas microesferas cargadas de fármaco en comparación co fármaco libre, independentemente da súa composición polimérica. Tamén se avaliou a capacidade das microesferas deseñadas para aumentar a autofaxia dos condrocitos osteoartríticos. Aínda que non se observaron diferenzas significativas na indución da autofaxia en comparación co fármaco libre, os resultados obtidos mostraron que as microesferas desenvolvidas son adecuadas para a administración do fenofibrato.

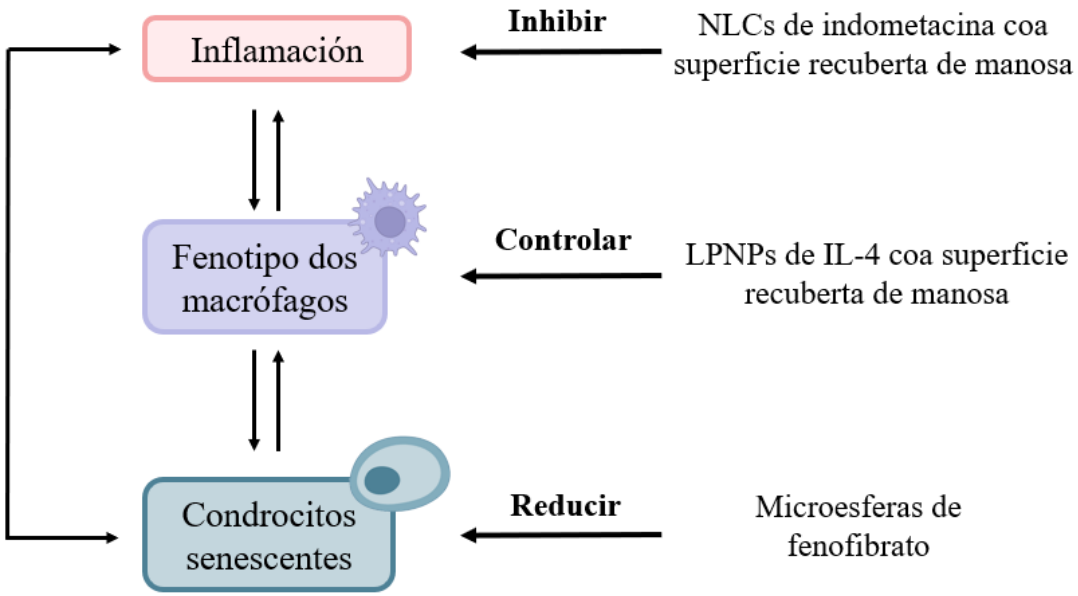
Seleccionouse a formulación que presentou unha liberación máis sostida do fármaco para probala nun modelo *in vivo* de artrose. Os resultados mostraron unha mellora significativa da morfoloxía da cartilaxe tras o tratamento coas microesferas cargadas de fármaco nas dúas doses ensaiadas.

USC UNIVERSIDADE DE SANTIAGO DE COMPOSTELA

Os resultados obtidos demostran a utilidade das ferramentas de intelixencia artificial para deseñar microesferas coas propiedades fisicoquímicas desexadas para a administración intraarticular. Ademais, a composición polimérica pode adaptarse para conseguir perfís de liberación de fármaco máis prolongados. A diminución dos cambios asociados á artrose na cartilaxe articular de ratos con artrose trala administración das microesferas demostrou o potencial destas formulacións como DMOADs.

Os resultados prometedores obtidos nesta tese, poñen de manifesto o importante papel das ferramentas de intelixencia artificial no deseño, desenvolvemento e optimización de DDS. Ademais, os DDS desenvolvidos non só foron capaces de encapsular con éxito as moléculas terapéuticas seleccionadas, senón que tamén melloraron a súa actividade terapéutica. Estes sistemas demostraron o seu potencial como DMOADs dirixidos ás dúas principais características da artrose: a inflamación e a degradación da cartilaxe mediante tres estratexias independentes, pero estreitamente relacionadas (**Resumo gráfico**): o control da inflamación, a modulación do fenotipo dos macrófagos e a redución da senescencia dos condrocitos, controlando a progresión da enfermidade. Polo tanto, xa sexa individualmente ou empregados en combinación, estes DDS presentan un gran potencial no tratamento da OA.

Resumo gráfico



USC UNIVERSIDADE DE SANTIAGO DE COMPOSTELA

USC
UNIVERSIDADE
DE SANTIAGO
DE COMPOSTELA

1 INTRODUCTION

USC
UNIVERSIDADE
DE SANTIAGO
DE COMPOSTELA

USC
UNIVERSIDADE
DE SANTIAGO
DE COMPOSTELA

1.1 OSTEOARTHRITIS

Osteoarthritis (OA) is a complex and chronic degenerative joint disease characterized by subchondral bone remodelling, cartilage degradation, and osteophyte formation. It primarily affects weight-bearing joints such as hips and knees, as well as cervical and lumbar spine, but it also can extend to non-weight-bearing joints such as hands, particularly interphalangeal and metacarpophalangeal joints (Heberden's nodes and Bouchard's nodes)[1–5].

Globally, OA impacts around 7% of the population, with a steady increasing incidence, causing mobility limitations, pain, joint stiffness, instability, and inflammation in 80% of patients. About 25% of them struggle with basic tasks, significantly affecting their quality of life. Risks factors include obesity or inflammatory diets. Age and gender are also risk factors, with a higher prevalence in woman and those over 60 years-old [4–7].

The joint involves the synovium or synovial membrane, cartilage, and subchondral bone [8]. Synovium is characterized by housing synovial fibroblasts or synoviocytes and macrophages, all of them involved in preserving joint homeostasis by the secretion of synovial fluid components. The secreted synovial fluid fills the joint cavity, preventing friction and providing shock absorption [9,10]. This fluid is composed by water, mucopolysaccharides, proteins as lubricin, mineral salts, and other small molecules [3].

Cartilage covers the bone surface allowing smooth movements to be produced. It is a challenging tissue to repair. Chondrocytes are the only cells present in the articular cartilage They produce lubricin and hyaluronic acid (HA), maintaining the extracellular matrix (ECM) biomechanical properties. Cartilage ECM is mainly composed of aggrecan, chondroitin sulphate, and collagen fibres, mostly type II, IX, and XI [11].

Subchondral bone, comprised by the subchondral plate and trabecula, is also crucial for joint homeostasis, providing nutritional and structural support, as well as load absorption [12].

OA pathogenesis, although not fully understood, is believed to be triggered by traumas and abnormal or excessive mechanical loads (**Figure 1.1**). In this situation, joint cells, including fibroblasts, macrophages, and chondrocytes induce the expression of pro-inflammatory cytokines and inflammatory mediators initiating the pathological degradative cascade [4,13,14].

In this situation, an increase of degradative enzymes (metalloproteinases, aggrecanases, and serine proteases, among others) is produced, causing subchondral bone sclerosis, synovitis, cartilage angiogenesis, and osteophyte formation along with bone-to-bone friction, pain, and poor mobility. These alterations further influence ECM composition and organization, resulting in cartilage deterioration (**Figure 1.1**)[14–19].

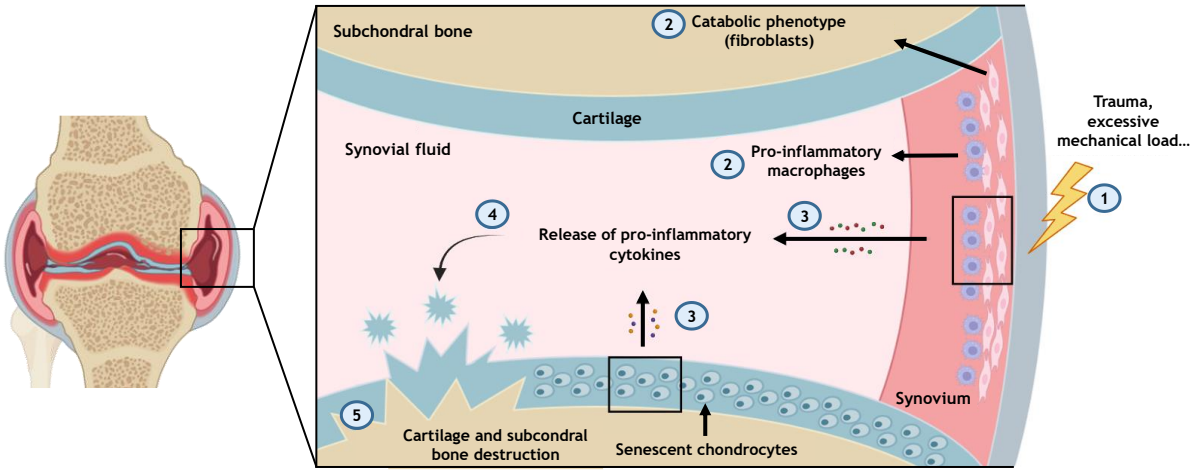


Figure 1.1. Schematic representation of the activation of the inflammatory pathway following trauma or excessive mechanical load. This leads to a change in the phenotype of the fibroblasts, macrophages, and chondrocytes, resulting in pain, synovitis, or osteophyte formation, among others. Image created with Biorender®.

A healthy human knee contains about 2 mL of synovial fluid with 2-4 mg/mL of high molecular weight HA (> 6,000 kDa) [20,21]. At the initial stage of OA the synovial fluid undergoes alterations, increasing in volume and decreasing in HA molecular weight and concentration, resulting in elevated intra-articular (IA) pressure and reduced viscosity, compromising joint lubrication and protection [22–24]. This shift contributes to joint pain and a decline in the synovial fluid damping function [22,25].

Currently approved OA treatments primarily target pain and symptoms improvement as there is no treatment capable of reversing or stopping disease progression [18,26,27]. Treatments approaches, selected based on disease severity, include non-pharmacological, pharmacological, and surgical options [7]. Early-phase interventions involve lifestyle modifications like exercise, weight loss, physiotherapy, and diet [28–30]. Pharmacological pain management includes oral analgesics (paracetamol), and non-steroidal anti-inflammatory drugs (NSAIDs) (ibuprofen, naproxen…), which frequently are associated with gastrointestinal and cardiovascular side effects. For severe phases, short-term opioid use (tramadol) is an option. However, all these treatments fail to prevent the progression of joint damage [30].

Surgical interventions (total knee arthroplasties, knee joint replacements, or osteotomies) are reserved for advanced stages of OA when other treatments are ineffective [1,30]. They are considered the last option due to the associated risks, including infections, thrombosis, postoperative discomfort, or potential mortality [9,15].

Given these challenges, there is a pressing need for treatments addressing disease progression in OA. An alternative to systemic administration is IA drug delivery, offering enhanced local bioavailability, reduced systemic side effects, and cost-

effectiveness [26,31]. Despite its advantages, IA administration still faces challenges in achieving long-term high local concentration of drug and minimizing its systemic toxicity [32,33].

1.2 INTRAARTICULAR TREATMENTS CURRENTLY USED IN CLINIC

1.2.1 Immediate release IA formulations: solutions and dispersions of therapeutic molecules

1.2.1.1 Anti-inflammatory drugs

NSAIDs are considered the first-line drugs for pain management, as they inhibit the synthesis of prostaglandins, the main actors in inflammation [6]. Despite NSAIDs are currently administered topically or orally, its IA injection should reduce the associated side effects. However, only Olfen, a diclofenac sodium injection for OA pain reduction, is approved in Croatia (**Table 1.1**).

On the other hand, intra-articular corticosteroids injections (IACI) are commonly used for managing inflammation when oral medications fail. Nevertheless, their effectiveness in pain relief or joint mobility varies widely among individuals, with positive effects observed in 70-80% of patients within the first four weeks of treatment [6,8,34,35].

The corticosteroids mechanism of action involves reducing inflammation and promoting immunosuppression, inhibiting the accumulation of inflammatory cells in the synovial membrane, suppressing the synthesis of inflammatory mediators (prostaglandins or IL-1) and reducing the activity of collagenases and matrix metalloproteinases (MMPs) [36,37]. Conversely, some *in vivo* studies suggest potential harm to articular cartilage [6,38].

Common formulations include crystalline suspensions of triamcinolone acetate, methylprednisolone acetate, and a mixture of betamethasone sodium phosphate and betamethasone acetate (**Table 1.1**) [6,24,39–42].

USC UNIVERSIDADE DE SANTIAGO DE COMPOSTELA

Table 1.1. Overview of the therapeutic molecules, European Union (EU) countries where they are commercialized, and examples of brand names.

Therapeutic Molecules	Commercialized Countries	Brand Names
Diclofenac Sodium	Croatia	Olfen®
Betamethasone (acetate) Betamethasone dipropionate Betamethasone sodium phosphate	Belgium, Slovenia	Celestan Biphase®, Diprofos Depot®, Diprophos®, Diprospan®, Flosteron®
Dexamethasone (phosphate) Dexamethasone palmitate Dexamethasone (di) sodium phosphate	Bulgaria, Croatia, Cyprus, Finland, France, Germany, Greece, Hungary, Ireland, Italy, Latvia, Lithuania, Netherlands, Poland, Portugal, Romania, Slovenia, Spain	Dexamed®, Dexamethasone Kabi®, Dexamethasone Phosphate Noridem®, Fortecortin®, Oradexon®
Hydrocortisone (acetate) Hydrocortisone sodium succinate Prednisolone (acetate) Prednisolone phosphate Prednisolone sodium succinate Methylprednisolone acetate	Cyprus, Finland, France, Germany, Hungary, Italy, Netherlands	Hydrocortison Richter®, Actocortina®, Depo-Medrol®, Depo-Medrone®, Medopred®
Triamcinolone acetonide Triamcinolone hexacetonide	Austria, Cyprus, France, Germany, Italy, Slovenia, Spain	Kenacort®, Kenalog®, Lederlon®, Lederspan®, Triacort®, Trica®

The choice of esters (acetate) or non-esters (sodium phosphate) of corticoids significantly influences the physicochemical properties and formulation effectiveness. Non-ester compounds are more water-soluble and provide a faster therapeutic effect, while the less water-soluble derivatives have a longer residence time in the synovial fluid, reducing systemic exposure and potential side effects [36,40,43].

1.2.1.2 Autologous blood products

Autologous blood products (platelet-rich plasma, autologous conditioned serum, and autologous protein solution) contain high concentrations of growth factors and other bioactive compounds. These therapies are emerging to offer a new safe alternative with reduced associated side effects that can be used to promote healing and tissue regeneration. However, their efficacy remains uncertain [15,42,44].

Platelet-rich plasma (PRP) is a plasma fraction rich in platelets containing growth factors and beneficial bioactive components, such as platelet-derived growth factor (PDGF), transforming growth factor beta (TGF-β), vascular endothelial growth factor

(VEGF), interleukin-1 receptor antagonist (IL-1RA), interleukin-4 (IL-4), interleukin-10 (IL-10), interleukin-13 (IL-13), and interferon-γ (IFN-γ) among others [27,45]. The cocktail of PRP components can control the expression of several inflammatory mediators and degradative enzymes, reduce pain, inhibit chondrocyte apoptosis, regulate metabolism, promote tissue regeneration, collagen synthesis, or cartilage and bone restoration [15,46,47].

PRP can be processed employing several disposable devices that are currently commercialized. Some examples include, SmartPReP® (Terumo blood and cell technologies), PurePRP®AB60, and AbsolutePRP® (AcCELLerated Biologics) [48].

Currently, there has been a growing trend in the use of PRP for managing OA. As an autologous product, immune reactions or adverse effects are reduced, thus appears promising as injectable treatment for improving OA symptoms [44]. However, the Osteoarthritis Research Society International (OARSI) does not recommend it, as no definitive statements can be made about the actual effects in OA. Despite controversy over its efficacy, PRP therapy offers a convenient, low-cost, and quick non-surgical option [49,50].

Similarly, autologous conditioned serum (ACS) is rich in growth factors and endogenous anti-inflammatory cytokines, such as IL-1RA, IL-4, IL-10, or IL-13 [15,51–53].

Interleukin-1 (IL-1), a pro-inflammatory cytokine with two isoforms (IL-1α and IL-1β), triggers a pro-inflammatory cascade in OA, causing cartilage degradation and inhibiting ECM synthesis [54–56]. ACS contains IL-1RA, an IL-1 receptor antagonist that can block both IL-1 isoforms, reducing inflammation [42,56,57].

ACS is also a patient-derived product, which reduces the risk of severe adverse effects. It is usually acquired and processed employing commercial kits such as Orthokine® [53]. Despite is a safe and well-tolerated therapy, ACS does not improve cartilage damage, which may be justified by the fast clearance of the synovial fluid [56,58,59].

Additionally, autologous protein solution (APS) also known as plasma rich in growth factors (PRGF) contains high levels of growth factors. Some of them are epidermal growth factor (EGF) which stimulates cell proliferation and differentiation, insulin-like growth factor-1 (IGF-1) which promotes cell growth, PDGF involved in cell proliferation, cell differentiation and angiogenesis, VEGF, and TGF-β1 along with high concentrations of anti-inflammatory mediators such as IL-1RA, soluble interleukin-1 receptor type II (sIL-1RII) and, soluble tumour necrosis factor receptor type I and II (sTNF-RI and sTNF-RII). These molecules can modulate inflammatory responses by interacting with pro-inflammatory cytokines, such as IL-1 and TNF-α, regulating the immune response and inflammation [42,60].

USC UNIVERSIDADE DE SANTIAGO

The nSTRIDE APS (Zimmer Biomet) is a commercialized kit that contains a cell separator and a cell concentrator employed to concentrate the anti-inflammatory cytokines and growth factors from the peripheral blood extracted from patients to obtain APS [60–62].

APS therapy appears to be safe and effective, potentially avoiding severe adverse effects by using the patient's own serum and cytokines, thus mitigating immune responses. However, additional studies are needed to determine the benefit of APS compared to other IA therapies [42,61].

1.2.2 Controlled drug delivery systems for IA injection

New controlled drug delivery systems (DDS) for IA administration have recently been developed for treating OA to address the rapid clearance of free therapeutic molecules from the joint cavity (**Figure 1.2**). These systems, including micrometric and nanometric particles, as well as hydrogels, aim to retain the drug within the joint, ensuring prolonged local concentrations and therapeutic effects [17,63–66]. Such DDS for IA administration minimize systemic side effects, facilitate controlled drug release, and potentially reduce the frequency of injections, enhancing patient compliance [67].

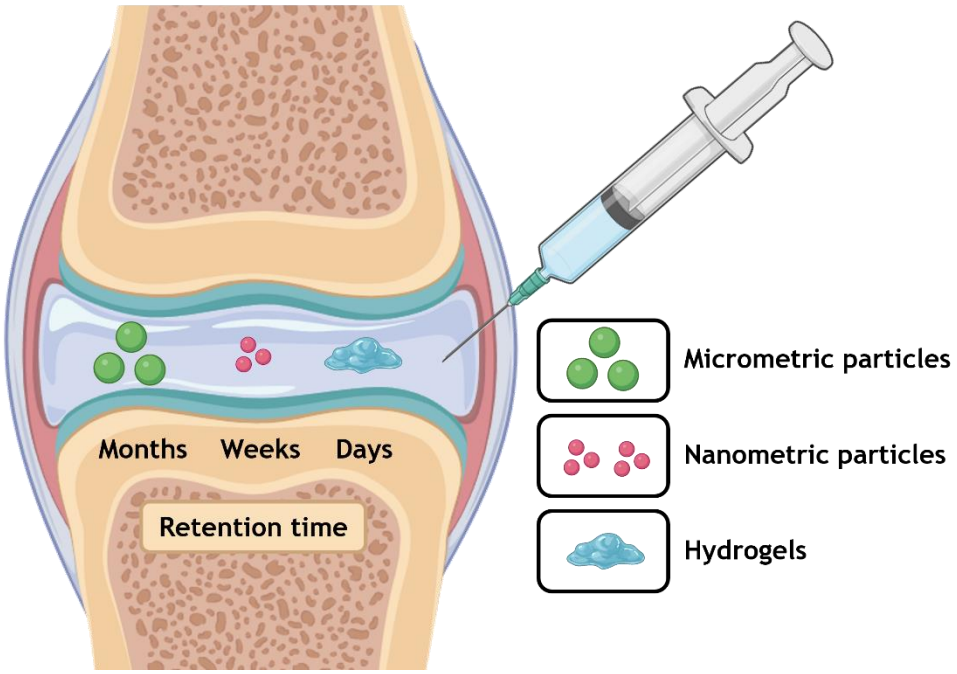


Figure 1.2. Drug delivery systems proposed for IA administration and their ideal retention times. Figure created with BioRender® and adapted from Maudens *et al.* [3].

USC UNIVERSIDADE DE SANTIAGO DE COMPOSTELA

1.2.2.1 Nanometric particles

Nanoparticles (NPs) are colloidal systems ranging from 10 to 1000 nm that have shown the ability to transport active molecules through biological barriers. They improve drug stability, local retention, and cellular uptake, allow controlled drug release, and reduced toxicity. They also enable the simultaneous administration of several drugs [67–69].

These systems can be developed using different procedures including nanoprecipitation, ultrasonication, high-shear homogenization, emulsion solvent evaporation, or hydrothermal methods, employing many different materials, such as inorganic and organic compounds [70–72].

In addition to the above-mentioned advantages, NPs allow for targeted delivery, as their surface can be coated or functionalized with certain ligands or materials (polysaccharides, antibodies, peptides, vitamins…) to interact with cell receptors or other tissue constituents [69,73,74].

Liposomes are a type of nanoparticles that can be used as DDS due to their close similarity to biological membranes and versatility [75]. Liposomes are spherical structures composed by phospholipid bilayers. This unique feature allows them to effectively encapsulate both hydrophilic drugs within their aqueous core and lipophilic drugs within the phospholipid bilayer. Moreover, their surface can be also functionalized [76,77].

Lipotalon® (available in Germany) based on dexamethasone palmitate loaded liposomes, has received authorization from the European Medicines Agency (EMA) for the treatment of OA via IA [33,78]. However, this DDS, presents certain limitations, including low chemical and physical stability, limited drug loading, and fast drug release requiring multiple injections. Furthermore, its IA has been associated with some adverse events such as infection, subchondral fracture, or osteonecrosis, associated to the administration of corticosteroids factors that continue to constrain its clinical application [76,77].

1.2.2.2 Micrometric particles

Microparticles (MPs), particles within the 1-100 μm size range, offer an innovative approach for controlled drug release in joint treatments, effectively extending therapeutic effects and decreasing drug clearance [79,80]. These DDS can be produced using a wide array of materials including natural (e.g., cellulose, sodium alginate, or chitosan), synthetic polymers (e.g., poly-caprolactone (PCL), poly-lactic acid (PLA), or poly-lactic-co-glycolic acid (PLGA)), and inorganic materials. Polymeric MPs are well-explored as DDS due to their biocompatibility and biodegradability [81,82].

USC
DE COMPOSTELA

The MPs particle size plays a crucial role in their residence time within the joint cavity [3]. Small MPs (< 10 μm) are thought to be taken up by chondrocytes and synoviocytes, while larger ones (> 10 μm) can be retained within the joint cavity for months depending on their size and composition [79,83].

Zilretta® is a Food and Drug Administration (FDA) approved formulation for knee OA pain management. It is a PLGA microsphere-based formulation that has demonstrated well-tolerability and efficacy in providing significant pain relief compared to the IA administration of placebo or triamcinolone acetonide crystalline suspension. The developed system consists of biodegradable microspheres with a mean diameter of 45 μm loaded with 25% of triamcinolone acetonide. Zilretta® is presented as a lyophilized powder, to be reconstituted in 5 mL of saline solution for IA administration after synovial fluid aspiration [84].

Nevertheless, despite its promising results in terms of residence time and symptom reduction, Zilretta® is not classified as a disease modifying osteoarthritis drug (DMOAD) since it cannot avoid further cartilage degradation neither induce cartilage regeneration [84,85].

1.2.2.3 Hydrogels

Hydrogels are promising materials in the field of regenerative medicine, offering a versatile platform for drug or biologicals molecules delivery. These 3D networks can be designed to mimic ECM and exhibit cartilaginous features. Moreover, hydrogels can display exceptional mechanical properties (elasticity), support, and lubricating characteristics coupled with significant biological properties that facilitate cell interaction, migration, differentiation, or proliferation [79,86].

Hydrogels are composed by polymers, either natural or synthetic, embedded within an aqueous solution, that can be chemically or physically crosslinked to achieve the desired characteristics [78,87–89]. Among natural polymers to produce hydrogels, HA is the most used in OA.

Cingal® and Condrotide® Plus are examples of loaded hydrogels classified as medical devices currently approved in Canada and EU for OA therapy [79]. Cingal® is an example of HA hydrogel loaded with triamcinolone hexacetonide for pain relief. It has the advantage of providing viscosupplementation and inflammation reduction. However, similar results were obtained in terms of pain relief compared to the free drug at 26 weeks [67,78,79]. On the other hand, Condrotide® Plus is also a HA hydrogel loaded with purines, pyrimidines, deoxyribonucleotides, and deoxyribonucleosides. Research suggests that it may offer pain relief and promote tissue regeneration, nevertheless, it still needs to be evaluated.

USC UNIVERSIDADE DE SANTIAGO DE COMPOSTELA

1.3 INTRAARTICULAR TREATMENTS UNDER CLINICAL TRIALS

1.3.1 Immediate release IA formulations: solutions and dispersions of therapeutic molecules

1.3.1.1 Corticosteroids

In recent years, several clinical trials have been initiated to compare the efficacy and safety of corticosteroids with other currently employed therapies, such as PRP (NCT06032039), HA (NCT04980105), PRGF (NCT05837494), bone marrow aspirate concentrate (NCT05288725), or even between different IACI (NCT05139875). Most of them are currently active, and their results have not been published yet.

1.3.1.2 Non-steroidal anti-inflammatory drugs

The IA administration of NSAIDs is being considered as an alternative to the oral administration to mitigate their side effects while maintaining their potent anti-inflammatory properties [90].

However, there is limited research regarding NSAIDs IA injections. Recently, an interventional phase IV clinical trial (NCT05336968) has been initiated to assess the efficacy of the IA ketorolac administration, a NSAID commonly used in orthopaedics and sports medicine, typically administered intramuscularly. This clinical trial aims to evaluate not only its efficacy when administered alone or in combination with corticosteroids but also to determine whether the combination of ketorolac and corticosteroids is superior in terms of pain relief and function improvement compared to either treatment alone. However, results have not been posted yet.

1.3.1.3 Analgesics

Therapeutic molecules including resiniferatoxin (RTX) or botulinum toxin-A (BoNT-A) that can have analgesic properties are attracting clinical interest.

Regarding RTX, only two recent clinical trials have been initiated (NCT04885972 and NCT04044742). They aim to assess the efficacy and safety of RTX single IA injections in patients with moderate to severe knee OA pain, comparing them with placebo or the commercially available triamcinolone acetonide MPs (Zilretta®).

Only two clinical trials involving BoNT-A have been found (NCT03891680 and NCT03726788). However, their results are pending.

1.3.1.4 Antagonists of pro-inflammatory cytokines

Pro-inflammatory cytokines play a crucial role in the OA pathogenesis, contributing to inflammation and pain. Antagonists of these cytokines have emerged as potential therapeutic options. **Table 1.2** details on IL-1 and tumor necrosis factor-alpha

USC UNIVERSIDADE DE SANTIAGO DE COMPOSTELA

(TNF-α) antagonists, along with relevant clinical trials conducted to assess the safety of different doses, efficacy, tolerability, and biodistribution.

Regarding IL-1 antagonists, results indicate a lack of reduction in pain or inflammation. No statistically significant differences were found between Anakinra and placebo (NCT00110916) and only a weak analgesic effect was observed for Canakinumab (NCT01160822). Furthermore, some of these clinical trials are ongoing, while others have been completed but their results remain unpublished, making it difficult to draw definitive conclusions.

Regarding TNF-α antagonists, only two clinical trials have recently been initiated. However, in a phase IV clinical trial conducted to assess the safety and anti-inflammatory properties of infliximab IA injections in early-stages of knee OA, a significant reduction in pain was observed compared to placebo (NCT01144143).

Table 1.2. Overview of clinical trials of pro-inflammatory cytokines antagonists as potential treatments for knee OA.

Group	Product/Brand name	Clinical Trial Identifier	Status	Results	Ref.
IL-1 Receptor Antagonist (IL-1RA)	Anakinra/Kineret®	NCT02790723	Completed	No results posted.	[91]
	Anakinra/Kineret®	NCT00110916	Completed	No significant differences between doses and placebo.	[92]
	FX201	NCT04119687	Active, not recruiting	No results posted.	[93]
IL-1 β neutralizing antibody	Canakinumab	NCT04814368	Recruiting	No results posted.	[94]
		NCT01160822	Completed	Weaker analgesic effect compared to placebo and naproxen.	[95]
Antibody fragment against TNFα	DLX105	NCT00819572	Completed	No results posted.	[18]
TNF inhibitor	Etanercept/Enbrel®	NCT02722772	Unknown status	No results posted.	[96]
	Infliximab	NCT01144143	Completed	Greater pain relief compared to placebo or other biologics.	[95]

1.3.1.5 Bioactive proteins and peptides

LNA043 and LMWF-5A are two proteins recently evaluated for OA treatments. LNA043, a novel protein derived from angiopoietin-like 3 (ANGPTL3) exhibits

USC UNIVERSIDADE DE SANTIAGO DE COMPOSTELA

chondrogenic properties by binding to the fibronectin receptor on mesenchymal stem cells (MSCs) and chondrocytes, stimulating anabolic pathways and suppressing the expression of OA progression mediators [97]. Three clinical trials (NCT04864392, NCT04814368, and NCT04564053) have recently been initiated to evaluate its safety, efficacy, and tolerability. However, results have not been posted yet, and, therefore, conclusions regarding their effectiveness cannot be drawn.

LMWF-5A or Ampion is a low molecular weight (< 5 kDa) ultrafiltrate fraction of 5% human serum albumin that presents anti-inflammatory and immune modulating properties [98–101]. A phase III clinical trial (NCT03988023) has been conducted to assess its safety, efficacy, and optimal dose selection. Despite its anti-inflammatory properties, results showed this protein did not lead to a significant improvement in pain reduction or joint function compared to placebo 12 weeks post-administration.

1.3.1.6 Senotherapeutic therapies

Senescence plays crucial roles in joint homeostasis and is implicated in the development of age-related diseases such as OA. Senotherapeutic molecules can either induce apoptosis of senescence cells (senolytics) or modified the phenotype of senescent cells (senomorphics). UBX0101 has been identified as a senolytic agent, with promising chondrogenic properties [102]. A phase I clinical trial has been conducted to evaluate the effectiveness, safety profile, and tolerability of UBX0101 IA injections in patients with moderate to severe knee OA. Different UBX0101 doses have been tested, but the results are still pending to be published (NCT04229225) [102,103].

A subsequent phase II clinical trial was also conducted with a single IA injection of UBX0101 at different doses or placebo in patients with moderate to severe knee OA. Results showed no significant differences between either group or placebo (NCT04129944).

1.3.1.7 Autologous blood products

Several clinical trials have been recently started centred on the use of platelet rich plasma in the management of OA. Some examples include trials aimed at assessing the synergistic effects when administered with other therapies, including viscosupplementation therapies (e.g. HA) (NCT04443166), or comparing their efficacy or superiority against other currently used therapies, including IACI as triamcinolone (NCT06032039 or NCT05742061), viscosupplementation therapies (e.g. HA) (NCT03167333 or NCT03801564), or topical options such as diclofenac (NCT05877027), among others.

USC UNIVERSIDADE DE SANTIAGO DE COMPOSTELA

Despite the large number of clinical trials already completed, the results have not been posted yet, and, therefore, conclusions regarding the efficacy of IA injections of PRP cannot be drawn.

1.3.1.8 Gene therapy

Gene therapy represents an innovative approach in OA treatments, aimed at correcting or modulating specific genes implicated in the disease. This process involves the introduction of anabolic and anti-inflammatory genes (IL-1RA, IL-10, IL-4, interferon-beta (IFN-β), TFG-β, IGF-1), or the silencing of catabolic and pro-inflammatory genes (TNF-α, matrix metalloproteimase-13 (MMP13), a disintegrin metalloproteinase with thrombospondin motifs 5 (ADAMTS5)) [104]. These therapeutic interventions are designed to decelerate tissue degradation, enhance repair, and promote cartilage regeneration using nucleic acids, including deoxyribonucleic acid (DNA), messenger ribonucleic acid (mRNA), micro ribonucleic acid (miRNA), short interfering RNA (siRNA), or short oligonucleotides.

These therapeutic agents can be encapsulated in viral vectors such as adenovirus (AV), adeno-associated virus (AAV), recombinant adeno-associated viral vector (rAAV), retrovirus (RV), lentivirus (LV), and baculovirus (BV), or in non-viral vectors such as liposomes, exosomes, and lipid or polymeric NPs, among others. The treatment strategies encompass both *in vivo* (direct injection) or *ex vivo* approaches. In the *ex vivo* strategy, autologous or allogenic cells are isolated, cultured, treated with the loaded therapeutic vector, and reintroduced into the patient [102,105,106].

The *ex vivo* treatment strategy was the first developed for OA management, with initial human clinical trials employing TGF-β1 and RV in OA knees using allogeneic chondrocytes. However, the short retention time of the administered cells was the limitation of this approach [105,107].

The selection of the therapeutic transgene is a complex task. Several clinical trials are evaluating the safety, tolerability, and efficacy of different anti-inflammatory transgenes (IL-1RA, TGF-β, IFN-β, IL-10, and NKX3.2) and viral vectors (RT, AAV, helper-dependent adenovirus (HC-adenovirus), or plasmids) [107]. Currently, the *in vivo* strategy is the most used in clinical trials as it allows for extended periods of gene expression. Clinical trials following this approach have employed different transgenes using variable vectors such as IL-1RA in AAV (NCT02790723) or IL-1RA in HC-adenovirus (NTC04119687), IL-10 in plasmids (NTC03477487 and NCT04124042), or NKX3.2 in AAV (NCT04875754 and NCT05454566) [18,107].

Non-viral vector approaches are currently under development; however, they have not reached clinical trials yet for OA [105].

USC UNIVERSIDADE DE SANTIAGO DE COMPOSTELA

1.3.2 Controlled drug delivery systems for IA injection

1.3.2.1 Nanometric particles

Dexamethasone sodium phosphate-loaded liposomes are currently in clinical trials (TLC599) [108]. A phase II clinical trial involving 102 patients was conducted to determine the pharmacokinetic profile of TLC599 in patients with mild to moderate knee OA treated with a single IA injection of TLC599 or with a single IA injection of the free drug. Healthy volunteers, on the other hand, received a single intra-venous injection of dexamethasone sodium phosphate. Although the study was recently completed (Nov.2023), results have not been posted yet (NCT03754049).

1.4 SYSTEMS CURRENTLY UNDER DEVELOPMENT

From the preceding paragraphs it is evident that IA injections have limitations but also promising prospects for treating OA. An important challenge lies in overcoming the restrictions associated with the rapid clearance formulations from the joint cavity [109]. This phenomenon hinders the sustained delivery of therapeutic agents, and consequently the therapeutic efficacy.

Furthermore, despite the big efforts to use the IA route for the administration of corticosteroids or proteins such as pro-inflammatory cytokines antagonists, the achievement of the desired therapeutic outcomes remains challenging. Treatments have reached partially success in relieving pain and inflammation, but full efficacy has not been attained.

Controlled DDS administered locally into the joint (NPs, MPs, or hydrogels), seem to have potential to become the best alternative [110]. They can present appropriate physicochemical properties for the IA route, providing drug stability or controlled drug release profiles that would provide an enhanced drug concentration within the joint. This approach will allow to reduce the number of injections, and, therefore, improve patient compliance and systemic drug exposure reduction [111]. Despite their remarkable characteristics, currently, commercially available drug delivery systems are not able to halt the progression of OA, which remains as a priority research target and is still the subject of continuous research [26].

FDA have recognized the importance of developing treatments that can prevent or reduce structural cartilage damage by highlighting the need for therapies that not only relieve symptoms such as pain, but also address these structural changes in joints associated with the pathology [112].

DMOADs defined as drug that not only inhibit of reverse disease progression, but also provide clinical and symptomatic improvements for patient, still represent an unmet medical need [26,32,113].

To this end, several therapeutic agents with the potential to act as DMOADs are under investigation, and some of them have already reached clinical trials to assess their safety and efficacy [111]. The current focus of the research is primarily on new therapeutic molecules targeting cellular senescence and inflammatory mechanisms.

Senescence, a cellular aging process, is characterized by the permanent arrest of cell division and the secretion of pro-inflammatory cytokines and extracellular degradative enzymes, all together referred as senescence-associated secretory phenotype (SASP). These factors contribute to tissue degradation and the development of age-related diseases such as OA [114]. Clearing senescent cells with drugs such as dasatinib, quercetin, or fenofibrate, a peroxisome proliferator-activated receptor alpha (PPARα) agonist that has recently demonstrated senolytic properties, can prevent cartilage degradation [111,114].

On the other hand, inflammation also plays an important role in OA progression. Macrophages are key players in modulating inflammation, as they can change their phenotype in response to their environment. When exposed to pro-inflammatory cytokines, they switch to a pro-inflammatory phenotype, known as M1 phenotype. Conversely, when exposed to anti-inflammatory cytokines they switch to an anti-inflammatory phenotype, known as M2 phenotype, promoting inflammation reduction [115]. Therefore, promoting the specific transition of macrophages to an anti-inflammatory phenotype with the use of anti-inflammatory drugs (indomethacin, naproxen, meloxicam, celecoxib…) or through the administration of paracrine mediators such as immunomodulatory cytokines (IL-4, IL-10, IL-13…), could represent a viable strategy for treating OA [116].

Recent clinical trials on DMOADs primarily use them in free form, but face solubility and bioavailability limitations. Efforts are focused on developing DDS to overcome these issues and improve therapeutic outcomes, nevertheless, DDS development is ongoing [111]. Several DDS as NPs, MPs, or hydrogels loaded with the therapeutic molecules have been developed.

1.4.1 Nanometric particles

Currently, different organic NPs, polymeric and lipid, are under research for IA administration. In addition, these nanometric systems can be also employed to develop composite systems by embedding them into hydrogels providing not only a reduced and controlled drug release, but also reduced friction and wear. These composite systems have been loaded with cationic liposomes containing celecoxib, or with liposomes containing rapamycin or kartogenin [81,111].

Polymeric NPs, made from natural (e.g., chitosan, alginate, or cellulose) or synthetic (e.g., PLA, PCL, or PLGA) polymers offer improved drug tolerance, reduced side

effects, and enhanced drug permeability compared to free drug. Moreover, they are biodegradable, biocompatible, and depict low toxicity [51,84].

These polymeric-based NPs have been loaded not only with NSAIDs (etoricoxib, piroxicam, or indomethacin), but also with therapeutic molecules that can modify disease progression such as kartogenin, exhibiting high biocompatibility and a controlled drug release profile [67].

On the other hand, lipid-based NPs including liposomes, solid lipid nanoparticles, nanostructured lipid carriers, and exosomes have gained popularity due to their biodegradable and biocompatible properties [111].

Liposomes were first developed and, as above mentioned, their amphiphilic nature allow them to encapsulate both, hydrophilic and lipophilic drugs [77]. Liposomes are highly versatile DDS characterized by providing good biocompatibility and by providing sustained drug release, and cartilage lubrication [111].

These DDS have been also loaded with several therapeutic molecules including NSAIDs (diclofenac, ibuprofen, indomethacin, lornoxicam, meloxicam, and celecoxib), corticosteroids (dexamethasone), or senotherapeutics (dasatinib, quercetin, or rapamycin), among others [111]. These systems can be also employed for drug co-administration, as those designed to carry two different senolytic drugs (dasatinib and quercetin) or those cationic liposomes designed to carry both, lornoxicam and microRNA-140 [117,118].

Additionally, liposomes as many other NPs, can be coated or functionalized for targeted delivery. Examples include the use of aptamers targeting senescent fibroblasts. This functionalization allows for reduced toxicity to healthy cells (fibroblasts and chondrocytes), while achieving controlled drug release and anti-inflammatory and analgesic effects [117]. Another example includes the use of liposomes loaded with triamcinolone acetonide camouflaged with an apoptotic neutrophil membrane [119].

Solid lipid nanoparticles (SLNs) are colloidal particles characterized by being composed of biocompatible solid lipids, generally steroids, diglycerides or triglycerides, surfactants, and water. However, they present some drawbacks being the most relevant the low drug loading capacity [74]. SLNs loaded with rhein have been tested for IA delivery achieving better outcomes compared to the drug suspension in terms of joint retention and reduced inflammatory markers when tested in an OA animal model [120].

To address the limitations of the SLNs, nanostructured lipid carriers (NLCs) have been developed. NLCs are composed of liquid and solid lipids, surfactants, and water. They present an imperfect matrix that confers them improved characteristics including

USC UNIVERSIDADE DE SANTIAGO DE COMPOSTELA

enhanced drug loading and stability during storage, as well as controlled drug release [111,121].

Exosomes are biological and spherical structures produced by cells such as MSCs or chondrocytes that are composed by lipid bilayers [109]. These natural NPs present several advantages over other synthetic lipid-based NPs including reduced toxicity and increased tissue and cell specificity. Exosomes have been loaded with therapeutic molecules such as RNA molecules as miRNA-140 for IA administration showing a decrease in cartilage degradative enzymes secretion after their administration [33,111].

Lipid-based NPs can also be developed by combining a polymeric core and a lipid shell to form lipid-polymer hybrid NPs. These systems have been shown to enhance stability of the encapsulated therapeutic molecules. Additionally, their lipid shell can be modified to provide increased joint retention and cartilage targeting. These systems have been loaded with small molecules such as MK-8722, a 5´adenosine monophosphate-activated protein kinase (AMPK) activator involved in chondrocyte metabolism [75,111,122–124].

1.4.2 Micrometric particles

Several MPs made of natural (chitosan, HA, gelatine, heparin, or silk fibroin) or synthetic polymers (PLGA, PLA, or PCL) are under research for IA administration. These polymeric MPs are extensively researched due to their high joint retention time, biocompatibility and biodegradability properties [82].

As mentioned above, hybrid systems can be developed not only using nanometric particles but also micrometric particles. For instance, polymeric microspheres loaded with diclofenac were embedded into thermosensitive hydrogels to enhance joint retention [81]. Another example involves the development of polymeric microspheres loaded with dexamethasone, embedded into an agarose hydrogel to provide sustained drug release and exert a chondroprotective effect [81].

Additionally, MPs made from natural polymers have been loaded with different therapeutic molecules, showing a prolonged retention time within the joint and an inflammation reduction [125,126]. As an example, chitosan microspheres loaded with lornoxicam have been developed. Their administration provides an anti-inflammatory effect, along with a decrease in the concentration of inflammatory markers [127].

On the other hand, MPs made from synthetic polymers loaded with therapeutic molecules including NSAIDS (lornoxicam, ketorolac, aceclofenac, celecoxib or diclofenac sodium), corticosteroids (triamcinolone acetonide, dexamethasone or mometasone furoate), small molecules able to modify disease progression (rapamycin or rhein), and autologous blood products (superactive platelet lysate) have been studied.

USC DE COMPOSTELA

These systems were able to maintain adequate therapeutic levels over a prolonged period while minimizing associated systemic side effects. Additionally, many of them exhibit anti-inflammatory activity, and some promote chondrocyte proliferation, thus improving cartilage integrity [125].

1.4.3 Hydrogels

Different hydrogels have been tested for IA administration after their loading with therapeutic molecules, liposomes, or even cells [110,111]. These systems have undergone extensive exploration due to their potential not only in controlling drug release, but also in providing viscoelasticity and lubrication [110].

Hydrogels can be produced using natural polymers such as HA, alginate, fibrin, chitosan, and glucosamine, synthetic polymers like polyvinyl alcohol (PVA), polyethylene glycol (PEG), carboxymethyl cellulose (CMC), poly(N-isopropylacrylamide) (PNIPAM) or a combination them. Furthermore, they can be functionalized to enhance their properties, creating sensitive hydrogels including thermo-sensitive, pH-sensitive, or photosensitive DDS [110,128].

Hydrogels have also been utilized for loading NSAIDs (celecoxib, diclofenac sodium, or meloxicam), corticosteroids (dexamethasone or triamcinolone acetonide), cell components (adipose-derived stem cells, rabbit mesenchymal stem cells, or chondrocytes), and blood components (platelet lysate) as previously described for MPs. These hydrogels offer various benefits, including slow and controlled release of therapeutic agents and promotion of cartilage regeneration. Additionally, they have demonstrated good biocompatibility and effectiveness *in vitro* and *in vivo* [110].

In recent years, the development of multicomponent hybrid hydrogels for various biomedical purposes has sparked significant interest [129].

1.5 Artificial intelligence tools in drug delivery systems development

The use of Artificial Intelligence (AI) tools to obtain tailor made DDS for OA, according to specific requirements, has great potential, paving the way for innovative developments in IA delivery systems. Currently, AI techniques are actively employed to deepen our understanding of the various factors impact in the formulation process. These techniques allow to establish relationships between input variables (such as ingredients and operational conditions) and output parameters (the final characteristics of the DDS), thereby enable manufacturing protocols refinement and complex DDS designs **[82,130,131]**.

USC UNIVERSIDADE DE SANTIAGO DE COMPOSTELA

1.5.1 Nanometric particles designed by artificial intelligence tools.

Different nanometric systems depicting variable structures as liposomes, SLN, NLCs, and lipid-polymer hybrid NPs have been successfully designed and optimized using AI tools (**Figure 1.3**).

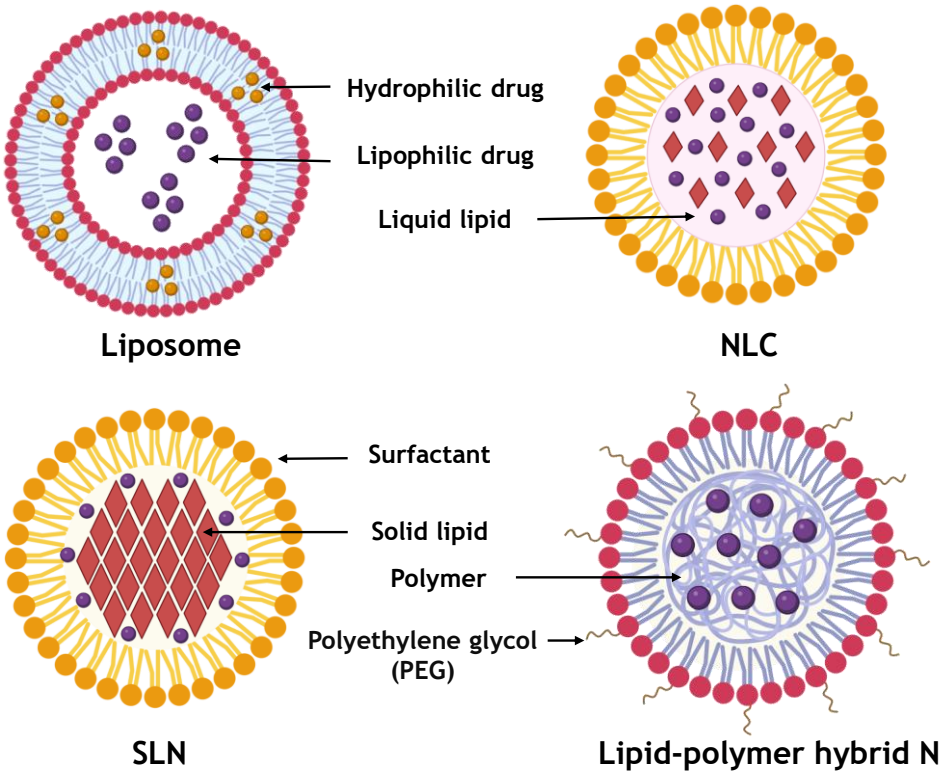


Figure 1.3. Schematic representation of lipid-based NPs. Figure created with BioRender®.

These tools have recently been applied to predict the characteristics like hydrodynamic diameter, dispersity, or the colloidal stability of liposomes, considering different formulation variables such as flow rate, lipid concentration, temperature, or drug concentration [132–134]. They have also been used to understand how ingredients and operation conditions like lipid, drug or surfactants concentration, and stirring speed influence the final characteristics of NLCs or lipid-polymer hybrid NPs [131,135].

Among the AI tools, molecular dynamics have also been employed to examine the interaction between drugs and lipid matrix of SLN, establishing a relationship between binding energy and drug loading capacity in these systems [136,137].

Furthermore, the surfaces of these lipid-based NPs can be coated or functionalized with certain components such as carbohydrates (glucose, mannose, galactose…), antibodies, vitamins, or aptamers, leading to targeted systems (**Figure 1.4**). Functionalized systems

USC UNIVERSIDADE DE SANTIAGO DE COMPOSTELA

exhibit interactions with specific cell receptors, improving cell selectivity and uptake [73,138,139].

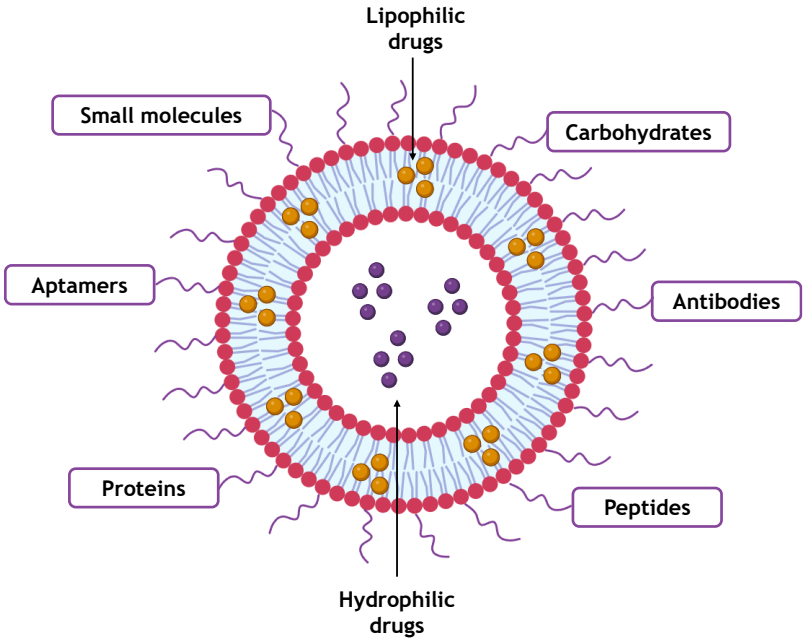


Figure 1.4. Illustrative example of functionalized lipid-based nanosystems (liposome) with the potential ligands for functionalization. Figure created with BioRender® and adapted from Wang S. *et al.* [77].

Human mannose receptor (CD206 or MRC1) is a glycoprotein expressed on the membrane of almost all macrophages, including tissue specific macrophages. This membrane receptor exhibit capacity to recognize pathogens comprising N-acetylglucosamine, mannose and fucose residues on their surface, such as bacteria or fungi. Moreover, CD206 plays a role in homeostasis, infections, and inflammatory response [140,141]. Given the essential role of macrophages in inflammation control, they emerge as crucial players in chronic inflammatory diseases [142]. The development of mannose-functionalized DDS may be a good strategy to ensure their recognition and internalization by macrophages. This new technique offers potential for creating DDS customized to successfully address inflammation associated disorders such as OA.

Nevertheless, the development of functionalized NPs sometimes requires the addition of further components (functionalization linkers). The incorporation of these extra ingredients entails the modification of their composition and properties, demanding additional studies to ensure the formation and stability of the modified systems. Generally, these variations towards functionalization are not considered in the optimization process, instead, optimized systems are obtained and subsequently, functionalized following a trial-and-error strategy [143]. This approach, focused primarily on the functionalization effect on NPs physicochemical properties (size and

USC
DE SANTIAGO
DE COMPOSTELA

surface charge), does not ensure the functionalized NPs show the best drug loading and functionalization efficiency. Therefore, the use of AI tools can be useful in the design, optimization, and functionalization of functionalized drug-loaded NPs.

1.5.2 Micrometric particles designed by artificial intelligence tools

MPs have been extensively explored in regenerative medicine either alone or embedded in 3D constructs. Among the different MPs types, polymeric ones are of particular interest due to their degradation profiles and biocompatibility [144]. Furthermore, polymeric MPs are suitable carriers for therapeutic molecules allowing their controlled release and the creation of intricate drug-delivery platforms, such as dual release profile systems [145]. These systems provide stability to encapsulated drugs and reduce the risk of side effects associated with fluctuations in the drug concentration [146–149]. Therefore, fulfilling the requirements for drug delivery during tissue development and repair.

Despite the profuse literature on the polymeric MPs development, there are no general protocols for producing MPs with predictable encapsulation efficiency, particle size, size distribution, and drug loading [150]. Nowadays, most researchers still follow the limited trial-and-error strategy using different methods as emulsion-solvent evaporation, supercritical CO_2 technology, electrospray, spray drying, microfluidics or hydrogel template [148,150,151]. The emulsion-solvent evaporation method, whether single or double emulsion, is one of the most widely used strategies for small-scale microparticle development, as it is simple, inexpensive, reproducible, and compatible with a wide variety of polymers and therapeutic molecules without requiring specialized equipment [146–148,152]. The single emulsion strategy is used when the drug is medium-highly soluble in the organic phase, usually the phase containing the polymer. On the other hand, when the drug is not soluble in this organic solution a double emulsion strategy is generally required. Despite the apparent simplicity of this method, the development of new microparticulate-based systems through emulsion-solvent evaporation is challenging as the production procedure involves several operations, most of them barely described in the literature.

Identifying and understanding the critical variables in MPs development is not an easy task. As mentioned, AI tools have been proposed as useful techniques for establishing general patterns by extracting knowledge from large databases. Machine learning techniques can be used to improve dosage systems formulation, establishing relationships between inputs (ingredients and operation conditions) and outputs (formulation properties), and even to optimize procedures without carrying out a single additional experiment [153–155].

USC UNIVERSIDADE DE SANTIAGO DE COMPOSTELA

These AI tools have been recently employed to study how different variables (polymer concentration, polymer viscosity, polymer molecular weight, surfactant concentration…) influences particle final characteristics as size, morphology…[156,157].

However, these approaches have never been tested for the development and design of DDS aimed at IA administration.

USC
UNIVERSIDADE DE SANTIAGO DE COMPOSTELA

USC
UNIVERSIDADE
DE SANTIAGO
DE COMPOSTELA

2 OBJECTIVES

USC
UNIVERSIDADE
DE SANTIAGO
DE COMPOSTELA

USC
UNIVERSIDADE
DE SANTIAGO
DE COMPOSTELA

The main objective of the current work is the design of innovative intra-articular (IA) drug delivery systems (DDS) that could serve as disease modifying OA drugs (DMOADs). This approach will be achieved by developing nanoparticulated and microparticulated DDS focused on the management of one of the two hallmarks of disease: articular inflammation and cartilage destruction. Therefore, the desired characteristics of the developed systems will be selected based on the requirements of the selected approach. The use of artificial intelligence (AI) tools will play a central role in the design of the systems, allowing for a deep understanding of the composition and procedure effects over the final DDS properties and an efficient optimization. These cutting-edge DDS will be based on following three therapeutic approaches; 1) Decrease inflammation by the intracellular delivery, in antigen presenting cells (APCs), of a nonsteroidal anti-inflammatory drug, indomethacin, currently used in the management of OA by oral administration; 2) Modulate macrophage phenotype by the intracellular delivery of the immunomodulatory cytokine IL-4 in pro-inflammatory macrophages, and 3) Control chondrocyte senescence by a long-term controlled release of a senotherapeutic drug, fenofibrate, in the joint cavity.

Therefore, this general objective is embodied in three specific objectives that explore the potential of AI tools to design and optimize DDS for IA administration.

SPECIFIC OBJECTIVE 1

The specific objective 1 is devoted to the design and optimization of nanostructured lipid carriers (NLCs) loaded with indomethacin for specific intracellular drug delivery in antigen presenting cells (APCs). This approach aims at reducing the secretion of pro-inflammatory mediators in APCs, more specifically pro-inflammatory macrophages, by the NLCs functionalization with membrane receptor ligands. Therefore, undesirable effects on other cells are avoided while high intracellular concentrations are achieved. The effectiveness of hybrid AI tools, specifically Artificial Neural Networks (ANNs) combined with fuzzy logic or genetic algorithms, will be evaluated in developing stable mannose-functionalized drug-loaded NLCs. A sequential approach will be adopted, constructing a comprehensive database integrating outcomes at each stage of the process. This database will aid in creating a model to delineate the final design space for functionalized and stable NLCs. Additionally, the work will assess whether the mannose incorporation will endow NLCs with the desired cell-selectivity and internalization. Furthermore, the impact of the optimized indomethacin loaded NLCs on the secretion of pro-inflammatory mediator on macrophage will be explored, aiming to identify the therapeutic potential of the developed NLCs.

USC UNIVERSIDADE DE SANTIAGO DE COMPOSTELA

SPECIFIC OBJECTIVE 2

The second specific objective is focused on the design and optimization of lipid-polymer hybrid nanoparticles (LPNPs) loaded with IL-4 and functionalized with mannose. These systems should be able to induce the specific release of IL-4 into the cytoplasm of macrophages. The LPNPs design will be assisted by AI tools to select the most adequate LPNPs composition. Furthermore, a deep LPNPs structure characterization will be performed using fluorescence cross-correlation spectroscopy (FCCS), a sensitive technique providing information on chemical dynamics and molecular interactions between fluorescently labelled species. The research will also determine whether the optimized lipid shell-polymeric core systems loaded with IL-4: 1) control the phenotype of osteoarthritic synovial macrophages and 2) ensure the stability of the protein and the suitability as DMOAD.

SPECIFIC OBJECTIVE 3

The third specific objective is centred in the design and optimization of biodegradable polymeric microspheres (MS) loaded with fenofibrate for long-term IA release. Machine learning techniques will be employed to generate general rules for the formulation of fenofibrate loaded MS via the single emulsion-solvent evaporation technique. The impact of several composition and production process operation parameters, on the critical quality attributes of the MS, will be studied. A manufacturing protocol will be established to consistently produce MS with the desired characteristics. The optimized MS will be deeply characterized, and their capacity to induce osteoarthritic chondrocytes apoptosis and autophagy will be studied in primary cells. Lastly, the obtained MS will be IA administered in a surgically mice model of OA to analyse their effect over cartilage damage.

USC
UNIVERSIDADE DE SANTIAGO DE COMPOSTELA

3 MATERIALS AND METHODS

USC
UNIVERSIDADE
DE SANTIAGO
DE COMPOSTELA

USC
UNIVERSIDADE
DE SANTIAGO
DE COMPOSTELA

3.1 FUNCTIONALIZED INDOMETHACIN-LOADED NANOSTRUCTURED LIPID CARRIERS

3.1.1 Materials

Indomethacin (IND) was purchased from Acros Organics (Belgium). Transcutol® P (highly purified diethylene glycol monoethyl ether), Capryol® 90 (propylene glycol monocaprylate), Labrafac® lipophile WL 1349 (triglycerides medium-chain), Labrafac® PG (propylene glycol dicaprylate), Labrafil® M 2125 CS (linoleoyl macrogol-6 glycerides), Labrafil® M 1944 CS (oleoyl macrogol-6 glycerides), and Labrasol® ALF (caprylocaproyl macrogol-8 glycerides) were used as liquid lipids (LL). Compritol® 888 ATO (glyceryl behenate), and Precirol® ATO 5 (glyceryl distearate) were selected as solid lipids (SL). Both LL and SL were kindly provided by Gattefossé (France). Epikuron® 145 V (deoiled phosphatidyl choline-enriched lecithin) was a kind gift from Cargill (USA). Polysorbate 80 (Tween® 80), Coumarin-6, octadecylamine (stearylamine) (SA), phorbol 12-myristate 13-acetate (PMA), and the D-(+)-Mannose were acquired from Sigma Aldrich (USA). Sodium cyanoborohydride (95%) and Anthranilic acid (98%) were acquired from Acros Organics (Belgium). Dialysis membrane (3.5 kDa MWCO) was provided by Spectrum Labs (USA). Acetate buffer at pH 4 was prepared using acetic acid 0.2 M from Sigma Aldrich (USA) and sodium acetate 0.2M from Scharlab (Spain).

THP-1 (TIB-202), BALB/3T3A31 (CCL-163) and RAW 264.7 (TIB-71) cell lines were obtained from ATCC (USA). AlexaFluor 647 phalloidin, ProLong® Gold Antifade reagent with DAPI, TrypLE Express Enzyme, fetal bovine serum (FBS), Roswell Park Memorial Institute 1640 Medium (RPMI 1640), phosphate buffered saline (PBS), and Dulbecco's phosphate-buffered saline (DPBS) were obtained from Thermo Fisher Scientific (USA). Dulbecco's Modified Eagle Medium (DMEM) was purchased from Corning (USA). Interferon-gamma (IFN-γ) was acquired from PeproTech (USA). Antibiotic solution (10,000 units/mL penicillin, 10,000 μg/mL streptomycin) was acquired from GE Healthcare Life Sciences (USA). Cell viability kit CCK-8 (2-(2-methoxy-4-nitrophenyl)-3-(4-nitrophenyl)-5-(2,4-disulfophenyl)-2H-tetrazolium monosodium salt) was purchased from Sigma Aldrich (USA). Glycerine was acquired from Fluka BioChemika (Switzerland). Ultrapure water (Milli-Q® plus, Millipore Ibérica, Spain) was used throughout all the experiments and the remaining solvents and reagents were analytical or HPLC grade.

3.1.2 Selection of NLCs components

To select the most appropriate liquid lipid (LL) for the development of NLCs able to encapsulate IND, a solubility study was conducted similar to previously described by Gaspar *et al*. with slight modifications [158]. To this end, 200 mg of IND were added to

USC UNIVERSIDADE DE COMPOSTELA

1 mL of each LL and stirred for 48 hours at 300 rpm. Then samples were centrifuged at 12,000 rpm and 20°C for 30 minutes to remove drug crystals. Subsequently, samples were suitably diluted in acetonitrile, and the IND concentration was quantified spectrophotometrically (UV-VIS 8453 spectrophotometer, Agilent Technologies, Spain) at 322 nm. Solubility studies were carried out in triplicate.

On the other hand, the most suitable solid lipid (SL) was selected by evaluating the solubility of IND in Compritol® 888 ATO (melting range between 65°C and 77°C) and Precirol® ATO 5 (melting range between 50°C and 60°C). To accomplish this, aliquots of each SL, weighing 200 mg were heated in a water bath at 80°C until fully melted. Gradually increased amounts of IND were added to each lipid until a precipitate of non-solubilized drug became visible. The solubility of IND in the SL is expressed as the maximum amount that can be solubilized without the presence of precipitate.

The miscibility of the selected LL and both SL was examined blending them in various proportions (75:25, 50:50, 25:75). The mixtures were then heated in a water bath at 80°C for 5 minutes. The presence of phase separation upon observation indicated lack of miscibility.

Finally, an *in silico* docking was performed to analyse the affinity of the selected lipids and stearylamine (SA), the linker used for NLCs surface functionalization, with the drug (IND). The 2D structure of IND, Transcutol® P, Compritol® 888 ATO, and SA were designed with ChemDraw professional v.17 (PerkinElmer, USA), while 3D structures were obtained by Chem3D v.17 (PerkinElmer, USA) and minimized using Merck molecular force field 94 (MMFF94) implemented in the program to find the most stable energetic conformation. Then, the minimized 3D structures were converted in .pdb file using PyMol v.2.4.0 (Schrödinger, USA). Autodock Tools v. 4.2.6 software (Molecular Graphics Lab., USA) was used to perform *in silico* computational molecular docking studies. In a first set of docking studies, the IND was used as flexible ligand, while Transcutol, Compritol, and SA were used as rigid receptor. On a second set of experiments, the IND was set as receptor, while Transcutol, Compritol, and SA were used as flexible ligand. In all the experiments, a grid box of 80 x 80 x 80 was set around receptor and ligand, using a default spacing of 0.375 Å. The docking parameters were set as default using a number of GA runs of 50, and Lamarckian genetic algorithm was used for the docking calculation [159]. The best in rank docking pose was chosen and free energy of binding (ΔG binding) and affinity constant (K_i) values were obtained [160,161]. The docking poses were successively visualized and analysed using BIOVIA Discovery Studio (France).

USC UNIVERSIDADE DE SANTIAGO DE COMPOSTELA

3.1.3 Experimental design

Nanostructured lipid carriers (NLCs) were prepared by hot shear homogenization following a general protocol, similar to previously reported [162]. In brief, a lipid phase (300 mg) comprising the selected lipids (Transcutol® P and Compritol® 888 ATO) at variable proportions, with or without IND, was prepared. Simultaneously, a separate aqueous phase (10 mL) containing lecithin (Epikuron® 145 V) and Tween® 80 at different concentrations was also prepared. Both phases were obtained as specified in **Table 3.1** and then, heated in a water bath at 80°C for 5 minutes. Subsequently, the aqueous phase was added to the lipid phase, and the mixture was homogenized for 10 minutes at 14,800 rpm using an Ultra-Turrax T25 (IKA Labortechnik, Germany). The obtained dispersion was rapidly cooled in an ice bath with gentle agitation for 2 min. Each formulation was characterized before and after dialysis (3.5 kDa MWCO) for the time specified in **Table 3.1** to eliminate the non-incorporated components [131,162].

The optimization of mannose-functionalized IND-loaded NLCs was performed following a two-step sequential design as presented in **Figure 3.1**. First, a reduced experimental design for four variables (LL/SL ratio, Tween 80 concentration, amount of lecithin, and dialysis time) with a minimum pattern of 3 was established using DataForm® v3.1 software (Intelligensys Ltd, UK). Both unloaded (blank) and IND-loaded NLCs formulations were prepared as indicated in **Table 3.1** (Formulations N01 to N30). The amount of drug used for each loaded formulation was the maximum one not leading to a drug precipitate. The obtained database (highlighted in grey) was modelled (see section *3.1.4*) and the obtained model, Model A, was then validated producing a new experimental formulation (Formulation N31).

In a second step, an additional variable, stearylamine (SA), required for mannose functionalization to endow NLCs with moieties able to covalently link this molecule, was incorporated [163,164]. These new formulations were prepared by adding SA to the lipid blend following the conditions shown in **Table 3.1** (Formulations N32 to N44). Subsequently, the entire database encompassing formulations from N01 to N44 was modelled (see section *3.1.4*). The resulting model, Model B, was validated by experimentally producing the selected optimal formulation (IND-NLC-SA), and the stability of the formulation was assessed after three months of storage. Finally, the stable formulation containing the functionalization linker was covalently functionalized with mannose though the Maillard reaction and characterized.

USC UNIVERSIDADE DE SANTIAGO DE COMPOSTELA

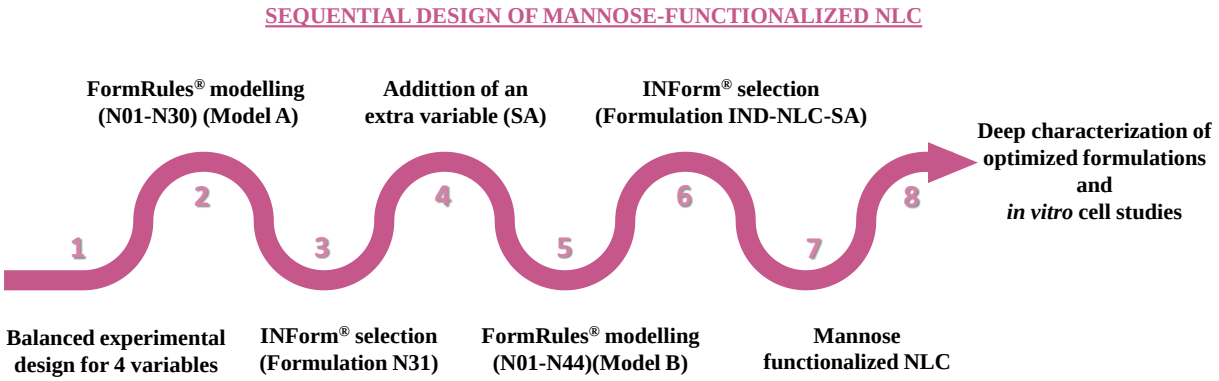


Figure 3.1. Stepwise optimization procedure to obtain optimized mannose-functionalized nanostructured lipid carriers (NLCs) using hybrid artificial intelligence (AI) tools.

3.1.4 NLCs modelling and optimization

The NLCs characterization data of the first-step formulations (Annex 1 Table S1; N01-N30) was modelled using FormRules®v4.03 (Intelligensys Ltd., UK) (Model A). FormRules® is a commercial software that combines two AI techniques, artificial neural networks (ANN) and fuzzy logic. This software uses the Adaptive Spline Modelling of Data (ASMOD) algorithm to generate models that relate inputs (ingredients and operation conditions) and outputs (formulation properties). Its ability to generate *IF-THEN* linguistic rules makes the effects of the different ingredients and operating conditions on the process or products produced easier to understand. This allows generating knowledge about the key variables to obtain IND-loaded NLCs. FormRules enables the use of different fitting statistical criteria. Among them, Structural Risk Minimization (SRM) was selected as it provided the highest predictability along with the simplest and most intelligible rules. Five variables were introduced as inputs: LL/SL ratio, Tween 80 concentration, amount of lecithin, dialysis time, and the amount of IND. On the other hand, four parameters were included as outputs: Size, polydispersity index (PDI), zeta potential (ZP), and drug loading (DL).

USC UNIVERSIDADE DE SANTIAGO DE COMPOSTELA

Table 3.1. Formulations prepared for Model A (grey) and Model B (grey and white) along with the distinctive composition and purification conditions.

Formulation	LL/SL Ratio (%)	Tween® 80 (%)	Lecithin (mg)	Dialysis time (h)	IND (mg)	SA (mg)
N01	50.0	0.5	2.0	12.3	0.0	0.0
N02	30.0	2.0	1.5	0.5	0.0	0.0
N03	10.0	1.3	1.0	24.0	0.0	0.0
N04	10.0	1.3	2.0	12.3	0.0	0.0
N05	50.0	0.5	1.0	0.5	0.0	0.0
N06	30.0	2.0	1.5	24.0	0.0	0.0
N07	30.0	0.5	2.0	12.3	0.0	0.0
N08	10.0	2.0	1.5	24.0	0.0	0.0
N09	50.0	1.3	1.0	0.5	0.0	0.0
N10	30.0	2.0	1.0	24.0	0.0	0.0
N11	50.0	1.3	2.0	12.3	0.0	0.0
N12	10.0	0.5	1.5	0.5	0.0	0.0
N13	50.0	2.0	1.0	24.0	0.0	0.0
N14	10.0	0.5	2.0	0.5	0.0	0.0
N15	30.0	1.3	1.5	12.3	0.0	0.0
N16	50.0	0.5	2.0	12.3	6.1	0.0
N17	30.0	2.0	1.5	0.5	14.5	0.0
N18	10.0	1.3	1.0	24.0	4.8	0.0
N19	10.0	1.3	2.0	12.3	4.8	0.0
N20	50.0	0.5	1.0	0.5	5.9	0.0
N21	30.0	2.0	1.5	24.0	14.4	0.0
N22	30.0	0.5	2.0	12.3	4.4	0.0
N23	10.0	2.0	1.5	24.0	4.8	0.0
N24	50.0	1.3	1.0	0.5	12.3	0.0
N25	30.0	2.0	1.0	24.0	14.3	0.0
N26	50.0	1.3	2.0	12.3	6.3	0.0
N27	10.0	0.5	1.5	0.5	4.8	0.0
N28	50.0	2.0	1.0	24.0	18.2	0.0
N29	10.0	0.5	2.0	0.5	4.6	0.0
N30	30.0	1.3	1.5	12.3	10.8	0.0
N31	50.0	1.7	2.0	2.0	16.5	0.0
N32	10.0	0.5	2.0	0.5	4.6	4.3
N33	10.0	0.5	2.0	0.5	4.6	7.7
N34	50.0	0.5	1.0	0.5	5.9	4.4
N35	50.0	0.5	1.0	0.5	6.0	7.7
N36	50.0	1.7	2.0	2.0	16.3	1.4
N37	50.0	1.7	2.0	2.0	17.2	4.2
N38	50.0	1.7	2.0	2.0	16.4	6.3
N39	48.1	1.8	1.5	3.0	12.2	0.0
N40	48.1	1.8	1.5	3.0	11.7	7.7
N41	48.1	1.8	1.5	3.0	11.7	0.6
N42	48.1	1.8	1.5	3.0	11.5	1.7
N43	48.1	1.8	1.5	3.0	11.2	4.5
N44	48.1	1.8	1.5	3.0	11.7	6.9

USC UNIVERSIDADE DE SANTIAGO DE COMPOSTELA

The training parameters used by FormRules software were the following: ridge regression factor of 1.0 e^{-6}, number of set densities: 2, set densities: 2 and 3, maximum inputs per submodel: 2, maximum nodes per input: 15, adapt nodes: true, C1 values over 0.75.

The determination coefficient of the training set (R^2) was used to establish the predictability of the models and calculated as stated in Eq. (**3.1**). The greater the value of the training set R^2, the higher the predictability of the model.

$$R^2 = \left[1 - \frac{\sum_{i=1}^{n} (y_i - y_i')^2}{\sum_{i=1}^{n} (y_i - y_i'')^2}\right] x\ 100\% \qquad (\mathbf{3.1})$$

where y_i is the actual value in the data set, y_i' is the value calculated by the model, and y_i'' is the mean of the dependent variable [165]. The comparison between predicted and experimental values has been conducted using an ANOVA. The absence of differences between both sets indicates the accuracy of the model. Computed *f* ratio values higher than critical *f* values for the specified degrees of freedom indicate no statistical significance between predicted and experimental results and hence, good model performance.

On the other hand, INForm®v5.01 software (Intelligensys Ltd, United Kingdom), integrates two AI technologies, ANN and genetic algorithms (GA), and was specifically designed for optimizing pharmaceutical formulations. INForm was used to obtain an optimized formulation using the initial dataset (Formulation N31). The training parameters used for the models were: 1 hidden layer, 2 nodes, transfer type (Asymmetric Sigmoid), output transfer type (Asymmetric Sigmoid), back propagation type (RPROP), target interactions (2000), target mean squared error (0.001), and random seed (10000), the optimization parameters were: number of populations = 1, number of interactions = 100, population size = 100, percentage of replacement = 50, mutation standard deviation = 0.1, and random seed = 1.

FormRules was employed to model the database under the same conditions as previously described, adding the amount of SA (mg) as an additional input. This second model, Model B, was developed using the data from formulations with and without the functionalization linker (Annex 1 Table S1; N01-N44).

Based on these models, a protocol (composition and appropriate purification conditions) for suitable and stable NLCs including the functionalization linker was established. Specifically, the protocol aimed at obtaining NLCs with small particle size (< 120 nm), maximum surface charge, and the highest drug loading (> 2%) not showing differences in their physicochemical properties after three months of storage. For this purpose, INForm was again employed. The training parameters used for the models were: 1

USC UNIVERSIDADE DE SANTIAGO DE COMPOSTELA

hidden layer, 3 nodes, transfer type (Asymmetric Sigmoid), output transfer type (linear), Back propagation type (RPROP), target interactions (1000), target mean squared error (0.0001), and random seed (10000).

3.1.5 Mannose-labelling

Mannose was labelled with anthranilic acid (2-aminobenzoic acid) (2AA) through a Maillard reaction to quantify its incorporation to the NPs surface [166]. Briefly, 6 mg of 2AA was dissolved in 100 µL of dimethyl sulfoxide: acetic acid (7:3, v:v) containing 1M of sodium cyanoborohydride ($NaBH_3CN$). Then, mannose (25.2 mg) was dissolved in the previously prepared solution. The resulting mixture was vigorously vortexed at maximum speed (Fisherbrand, USA), protected from light, and incubated for 12 hours at 37°C. After this time, the labelled mannose was diluted in acetate buffer, purified employing a Chromabond® cyano-modified silica gel-SPE column from Macherey-Nagel, (Germany), and lyophilized (Telstar, LyoQuest, Spain).

Proton nuclear magnetic resonance spectroscopy analysis (^{1}H-NMR) was conducted to confirm the labelling. For this purpose, fluorescently labelled mannose and unlabelled mannose were dissolved in deuterated water (D_2O) obtained from Sigma Aldrich (USA) at 200 mM, while anthranilic acid was dissolved in deuterated dimethyl sulfoxide (DMSO-D6; Cambridge Isotope Laboratories, Inc. (USA)) at the same concentration. The solutions were then placed in NMR tubes (600 µL) and characterized using a Bruker NEO-750 equipment (Germany).

3.1.6 NLCs functionalization with mannose

Dispersions of the optimized drug-loaded NLCs containing SA (IND-NLC-SA) were incubated with 50 mM fluorescently labelled D-(+)-mannose solution (MAN) in acetate buffer at pH 4. Various molar ratios of SA:MAN (1:2, 1:3, and 1:5) and incubation time points (24, 48, and 72h) were tested to select the best functionalization strategy. Mixtures were kept under magnetic stirring at 300 rpm (Fisherbrand, USA) protected from light. Subsequently, to eliminate unreacted components, formulations underwent a 12-hour dialysis using a cellulose membrane (3.5 kDa MWCO) under stirring in Milli-Q® water.

Additionally, to assess the functionalization effectiveness, the non-linked MAN was quantified. For this purpose, after incubation with mannose, formulations underwent ultrafiltration using Amicon® 100 kDa ultrafilters (Millipore, USA) at 10,000 g and 4°C for 15 minutes. Subnatants were collected, and fluorescence was measured (Excitation at 360 nm and Emission at 425 nm) using a plate reader (FLUOstar Omega, BMG Labtech, Germany). A calibration curve with MAN was also prepared for fluorescence determination.

USC UNIVERSIDADE DE SANTIAGO DE COMPOSTELA

Based on experimental results, IND-NLC-SA formulation functionalized with D-(+)-mannose at 1:2 SA:MAN ratio for 72 hours (IND-NLC-MAN) was selected for further experiments. Moreover, formulations of blank NLCs without (NLC) or with MAN (NLC-MAN) and non-functionalized IND-loaded formulations (IND-NLC) were selected as controls for further studies.

3.1.7 NLCs characterization

3.1.7.1 Particle size, polydispersity index, zeta potential, and drug loading

NLCs were characterized before and after dialysis in terms of particle size (size), polydispersity index (PDI), and surface charge (ZP) using a Zetasizer Pro (Malvern Instruments, UK). Samples were 1:10 diluted with Milli-Q® water, placed in a specific cuvette (DTS 1070), and measured in triplicate using the parameters automatically selected by the software. All the measurements were performed at 25°C ± 1°C.

Drug loading (DL) of the lipid network after purification (dialysis) of each formulation was calculated before and after three months storage using Eq. (**3.2**). To determine the actual drug content, samples were dissolved in acetonitrile and centrifuged at 12,000 rpm and 4°C for 30 minutes. The supernatants were filtered through 0.45 μm and properly diluted in acetonitrile. IND quantification was performed spectrophotometrically (UV-VIS 8453 spectrophotometer, Agilent Technologies, Spain) at 322 nm.

$$DL\ (\%) = \left[\frac{actual\ drug\ content\ (mg)}{weight\ of\ nanoparticles\ (mg)}\right] x\ 100 \qquad (\mathbf{3.2})$$

3.1.7.2 Drug leaking studies

Drug leaking studies were performed in quadruplicate using horizontal Franz diffusion cells at 37°C for both IND-NLC and IND-NLC-MAN formulations. A dialysis membrane of 3.5 kDa MWCO was placed between the donor and the receptor chambers. The formulations were diluted at a 1:6 ratio in phosphate-buffered saline (PBS) at pH 7.4 and introduced into the donor chamber (3mL), while the receptor chamber was filled with 3mL of PBS. At preset times, samples were collected from the receptor chamber, and the same volume of fresh PBS was replaced. IND was quantified spectrophotometrically at 322 nm.

3.1.7.3 Transmission electron microscopy

The morphology of the formulations was studied through transmission electron microscopy (TEM). The obtained colloidal dispersions were deposited onto cooper grids coated with a carbon membrane and treated for 2 minutes with a solution of

USC UNIVERSIDADE DE SANTIAGO DE COMPOSTELA

phosphotungstic acid (2%) [167]. Micrographs were taken employing a JEOL microscope (JEM 2010, Tokyo, Japan) with a Gatan Orius^{TM} camera (Gatan, Inc., USA).

3.1.7.4 Differential scanning calorimetry

Differential Scanning Calorimetry (DSC) studies were carried out using TA instruments Universal Analysis 2000 (USA) under a continuous flow of nitrogen at 50 mL/min. Samples of approximately 5 mg were placed into aluminium pans and analysed between -20°C and 350°C at a heating rate 10°C/min. Thermograms of IND, as well as, those for NLC, NLC-SA, IND-NLC, and IND-NLC-SA were recorded. An empty aluminium sample holder was employed to determine the baseline.

3.1.8 *In vitro* cell studies

In vitro studies were conducted using human monocytes (derived from acute lymphocytic leukemia, THP-1), murine macrophages (RAW 264.7), and fibroblasts (BALB/3T3A31). THP-1 were cultured in RPMI 1640 supplemented with 10% fetal bovine serum (FBS), 1% penicillin/streptomycin, and 2-mercaptoethanol 0.05 mM. Media was changed every other day. Before the studies, THP-1 at a density of $2x10^5$ cells/mL were activated with 400 nM of phorbol-12-myristate-13-acetate (PMA) in complete RPMI 1640 media for 72 hours to induce their differentiation into macrophages. Following differentiation, cell monolayers were washed with DPBS, and the PMA medium was replaced by fresh complete RPMI 1640, allowing them to set for 24 hours at 37°C and 5% of CO_2 before seeding.

RAW 264.7 and BALB/3T3A31 cell lines were cultured in DMEM medium containing 10% FBS and 1% penicillin/streptomycin at 37°C and 5% of CO_2. Media was changed every other day, and cells were maintained in culture until the time of the experiment. Cells were split when reaching 80% confluency.

3.1.8.1 Cell proliferation

Cell proliferation studies were performed in RAW 264.7 and BALB/3T3 cell lines. Cells were seeded at a density of $1.5x10^4$ cells/well in 96-well plates and allowed to attach for 24 hours. Subsequently, RAW 264.7 cells were either stimulated or not with IFN-γ (10 ng/mL) for 24 hours. Following stimulation, formulations (NLC, NLC-MAN, IND-NLC, and IND-NLC-MAN) were added at three different concentrations (300 μg/mL, 120 μg/mL, and 60 μg/mL solid mass per volume) for 24 hours. Cells without treatment and not stimulated with IFN-γ served as control. Additionally, free drug (IND), dissolved in ethanol, was added at an equivalent concentration.

To assess cell proliferation the Cell Counting Kit-8 (CCK-8) was used. The cell culture media was removed, and monolayers were washed with DPBS. Subsequently, 15 μL of

CCK-8 reagent, along with 150 µL of supplemented DMEM medium, was added to the wells. As a blank, CCK-8 reagent with medium and without cells was employed. The plate was incubated for 2 hours at 37°C and 5% of CO_2. The absorbance at 440 nm was measured using a plate reader (Bio-Rad 680, Spain). Cell viability was calculated using the following Eq. (**3.3**).

$$Cell\ proliferation = \left[\frac{sample\ absorbance - blank}{control\ absorbance}\right] \quad \textbf{(3.3)}$$

3.1.8.2 Cell uptake

Cell uptake studies were conducted in RAW 264.7 and BALB/3T3 cells. Cells were initially seeded at $1.5x10^4$ cells/well in 96-well plates for 24 hours. Subsequently, only RAW 264.7 were either stimulated with or without IFN-γ (10 ng/mL) for additional 24 hours. Following this period, fluorescently labelled formulations (NLC, NLC-MAN, IND-NLC, and IND-NLC-MAN) prepared by adding 4 µg/mL of coumarin-6 to the lipid phase during their synthesis, were added to the cells at the previously mentioned concentrations. As a control, untreated cells that were not stimulated with IFN-γ were included.

Immediately after NLCs addition, the initial fluorescence (Excitation at 485 nm and Emission at 520 nm) was measured using a plate reader (FLUOstar Omega, BMG Labtech, Germany) and cells were incubated for 2 hours at 37°C and 5% of CO_2. Then monolayers were washed 3 times with 200 µL/well of glycerine (20 mM) and PBS (pH 7.4) to remove and quench the non-internalized coumarin-6. After the wash step, 100 µL of 1% triton X-100 (Merck; Portugal) was added to each well to induce cell lysis so that the internalized fluorescently labelled NLCs were released. Post-lysis fluorescence was then measured using the plate reader. The percentage of NLCs internalization was determined by following Eq. **(3.4**).

$$Cell\ uptake\ (\%) = \left[\frac{post-lysis\ fluorescence}{initial\ fluorescence}\right] x\ 100 \quad \textbf{(3.4)}$$

Moreover, the specificity of the developed NLCs to be internalized by stimulated macrophages was determined by calculating the uptake index following Eq. **(3.5**).

$$Uptake\ index = \frac{Stimulated\ macrophage\ uptake}{Fibroblasts\ uptake} \quad \textbf{(3.5)}$$

3.1.8.3 Internalization of NLCs through confocal microscopy

NLCs internalization was also qualitatively evaluated using a confocal microscopy. For this purpose, RAW 264.7 cells were employed. The day before the experiment, cells were seeded at a density of $5x10^4$ cells/cm^2 in 8-well chambered cell culture slides (Nunc Lab-Tek Chamber Slide System, USA) and cultivated in complete DMEM with or without IFN-γ (10 ng/mL). Then, fluorescently labelled nanoparticles

(IND-NLC and IND-NLC-MAN) were added at a final concentration of 300 µg/mL (solid mass per volume) and monolayers were incubated for 2 hours at 37°C with 5% of CO_2. As a control untreated cells, not stimulated with IFN-γ, were used. Subsequently, the cell culture media was removed, and cells were washed twice with DPBS. Cell fixation was performed using formaldehyde solution (3.7% - 4.0%) (ITW Reagents, Spain) for 2 hours at room temperature (RT), followed by two washing steps with DPBS. Cells were then permeabilized with a Triton X-100 solution (0.1%) for 15 minutes, followed by two washing steps with DPBS. Subsequently, an incubation with Alexa Fluor 647 phalloidin (dilution 1:41) (Thermo Fisher Scientific, USA) was carried out for 40 minutes. Following this, cells were washed twice with DPBS and mounted with ProLong® Gold Antifade reagent with DAPI (4´,6-diamino-2-phenylindole) (Thermo Fisher Scientific, USA) (1 µg/mL). Finally, confocal microscopy images were obtained using a Leica SP5 confocal laser microscopy (Leica Microsystems, Germany).

3.1.8.4 Anti-inflammatory activity of IND-loaded NLCs

NLCs anti-inflammatory activity was tested using activated THP-1 cells. Cells were seeded at a density of $1.5x10^4$ cells/well in 96-well plates and allowed to attach for 18 hours. Cells were then stimulated with IFN-γ (10 ng/mL) for 24 hours. Following stimulation with IFN-γ, the developed formulations (IND-NLC, and IND-NLC-MAN) were added at a 60 µg/mL final concentration for an additional 24 hours. Cells stimulated with IFN-γ (10 ng/mL) and treated with NLC-MAN formulation were used as a control. Free drug (IND) dissolved in ethanol was added at an equivalent concentration. Cell culture supernatants were collected after the 24 hours treatment. Afterwards, the secreted concentration of different pro or anti-inflammatory cytokines was determined. Pro-inflammatory cytokines included TNF-α, IL-6, and IL-8, while anti-inflammatory cytokines included IL-4 and IL-10. Their quantification was performed using a magnetic bead-based multiplex assay Luminex® platform (R&D systems, USA) according to the manufacturer's instructions. To this end, 50 µL of each sample was incubated with 50 µL of the microparticle cocktail for 2 hours at RT on an orbital microplate shaker (Germany) at 800 rpm. Samples were then washed three times employing a magnetic device. Then 50 µL of biotin-antibody cocktail were added to each well and incubated for 1 hour at RT on the orbital microplate shaker at 800 rpm. Samples were washed again three times employing the magnetic device. Subsequently, 50 µL of streptavidin-PE were added to each well and incubated for 30 minutes at RT on the orbital microplate shaker at 800 rpm. Samples were washed again and the magnetic microparticles were resuspended by adding 100 µL of wash buffer to each well, followed by a 2 minutes incubation in the orbital microplate shaker at 800 rpm. Finally, the concentration of the secreted cytokines was measured employing a Bio-Plex MAGPIX Multiplex Reader (Milliplex® MAP multiplexing Assays, Millipore, USA).

USC DE COMPOSTELA

In parallel, the number of cells on each well was determined using the CCK-8 reagent as previously described for fibroblasts and murine macrophages. Additionally, known numbers of cells were included as standards to stablish the correlation between the obtained CCK-8 signal and the number of cells. The concentration of the secreted cytokines was normalized by the obtained number of cells.

3.1.9 Statistical analysis

GraphPad Prism 8 software was employed to analyse the obtained data. Group comparisons were performed through one-way analysis of variance (ANOVA) followed by post hoc Tukey's Multiple Comparison Test. The significant levels were categorized as follows: differences were considered significant at $p < 0.05$ or $p < 0.01$, highly significant at $p < 0.001$, and extremely significant at $p < 0.0001$. Results are presented as mean ± SD. The use of (*) represent statistically significant differences compared to the control, while (#) indicate statistically significant differences between the samples.

USC UNIVERSIDADE DE SANTIAGO DE COMPOSTELA

3.2 LIPID-POLYMER HYBRID NANOPARTICLES LOADED WITH IL-4 TO MODULATE MACROPHAGE PHENOTYPE.

3.2.1 Materials

Poly (D,L-lactide-co-glycolide) (PLGA; Resomer® RG 502H) was supplied by Evonik, Ltd. (Germany). Recombinant Human IL-4 was acquired from PeproTech (USA) and Bovine Serum Albumin (BSA) from Sigma Aldrich (USA). DSPE-PEG2000 (1,2-distearoyl-sn-glycero-3-phosphoethanolamine-N-[amino(polyethylene glycol)-2000] (ammonium salt)) and DSPE-PEG-NH_2 (1,2-distearoyl-sn-glycero-3-phosphoethanolamine-polyethylene glycol-amine) were supplied by Avanti® Polar Lipids (USA). DiD' solid (1,1'-dioctadecyl-3,3,3',3'-tetramethylindodicarbocyanine, 4-chlorobenzenesulfonate salt) and DOPE-ATTO 488 (1,2-dioleoyl-sn-glycero-3-phosphoethanolamine labelled with Atto 488) were supplied by Molecular Probes® Invitrogen™ (USA). Amino modified ATTO 488 was supplied from ATTO-TEC GmbH (Germany). Epikuron® 145V (deoiled phosphatidyl choline-enriched lecithin) was a kind gift from Cargill (USA). D-(+)-Mannose was acquired from Sigma Aldrich (USA). Sodium cyanoborohydride (95%) and Anthranilic acid (98%) (2-aminobenzoic acid) were acquired from Acros Organics (Belgium). Acetate buffer at pH 4 was prepared using acetic acid 0.2 M from Sigma Aldrich (USA) and sodium acetate 0.2M from Scharlab (Spain).

THP-1 (TIB-202), BALB/3T3A31 (CCL-163) and RAW 264.7 (TIB-71) cell lines were obtained from ATCC (USA). Phorbol 12-myristate 13-acetate (PMA) was acquired from Sigma Aldrich (USA). Rhodamine Phalloidin (R415), Rab5 Polyclonal Antibody (PA5-29022), Goat anti-Rabbit IgG (H+L) Alexa Fluor 594 Secondary Antibody (A11037), SlowFade Diamond Antifade Mountant, and normal goat serum were acquired from Invitrogen (USA). DAPI (4′,6-diamidino-2-phenylindole) was purchased from Sigma-Aldrich (USA). Formaldehyde (3.7-4.0% w/v) buffered to pH=7 and stabilized with methanol was acquired from PanReac AppliChem GmbH (Germany). Fetal Bovine Serum (FBS), Roswell Park Memorial Institute 1640 Medium (RPMI 1640), Phosphate Buffered Saline (PBS), and Dulbecco's Phosphate-Buffered Saline (DPBS) were obtained from Thermo Fisher Scientific (USA). Dulbecco's Modified Eagle Medium (DMEM) was purchased from Corning (USA). Cell culture slides (Nunc Lab-Tek Chamber Slide System) were adquired from Thermo Fischer Scientific (USA). Antibiotic solution (10,000 units/mL penicillin, 10,000 µg/mL streptomycin) was acquired from GE Healthcare Life Sciences (USA). TrypLE Express Enzyme was acquired from Gibco (USA). Cell viability assay kit (AlamarBlue) was purchased from ThermoFisher Scientific (USA). Ultrapure water (Milli-Q® plus, Millipore Ibérica, Spain) was used throughout the experiments and the remaining solvents and reagents were analytical or HPLC grade.

3.2.2 Experimental design

Lipid-polymer hybrid nanoparticles (LPNPs) were obtained following a modified nanoprecipitation method described in **Figure 3.2** [167]. Initially, only bovine serum albumin (BSA) was included as the cargo protein to afterwards incorporate IL-4 (BSA-LPNP). In brief, an organic phase was prepared by dissolving the required amount of PLGA in acetone (1 mL). Then, an aqueous solution of BSA was added to the organic phase at different concentrations regarding the PLGA amount (1%, 3%, or 5% w/w), as specified in **Table 3.2**. Subsequently, the prepared organic phase containing the protein was dropped onto 10 mL of an aqueous solution (4% ethanol, pH= 7.4) containing lecithin (Epikuron 145V; 200 μg) and DSPE-PEG2000 (637 μg). The mixture was stirred magnetically at 400 rpm for one hour to reach complete acetone evaporation. The formed LPNPs were ultrafiltered through 100 kDa MWCO filters (Millipore Amicon®, USA) at 10,000 rpm, 4°C for 10 minutes to remove the non-encapsulated protein. Lipid-polymer hybrid NPs were then washed, resuspended with the initial volume of Milli-Q® water, characterized, and stored at 4°C until use.

Table 3.2. Composition characteristics selected to develop the BSA-loaded LPNPs

Formulation	PLGA (mg)	BSA (% w/w)
BSA-LPNP 1	1.0	1.0
BSA-LPNP 2	3.0	1.0
BSA-LPNP 3	5.0	1.0
BSA-LPNP 4	1.0	3.0
BSA-LPNP 5	3.0	3.0
BSA-LPNP 6	1.0	5.0
BSA-LPNP 7	3.0	5.0
BSA-LPNP 8	5.0	5.0

The general protocol described above using the parameters stablished by the AI tools was followed to prepare unloaded or blank NPs (LPNP), as well as IL-4 loaded NPs (IL-4-LPNP). First, an organic phase was prepared by dissolving 3 mg of PLGA in 1mL of acetone. Then 30 μL of an aqueous solution containing 2 μg of IL-4 and 3% BSA was incorporated. The obtained mixture was directly dropped onto 10 mL of an aqueous solution (4% ethanol, pH= 7.4) containing lecithin (200 μg) and DSPE-PEG2000 (637 μg). Moreover, mannose functionalized blank (LPNP-MAN) and IL-4 loaded LPNPs were prepared (IL-4-LPNP-MAN). To obtain these formulations, the polymer-protein mixture was added to an aqueous solution (4% ethanol, pH= 7.4) containing lecithin (200 μg), DSPE-PEG2000 (477 μg), and DSPE-PEG-NH_2 (159 μg). Both nanoparticle dispersions were magnetically stirred at 400 rpm for one hour to reach complete acetone evaporation. For mannose coating, 2.9 μL of 20 mM mannose in acetate buffer (pH= 4) were added to 5 mL of the LPNPs dispersions and magnetically stirred at 400 rpm for one hour. Finally, functionalized, and non-functionalized LPNPs (LPNP, IL-4-LPNP,

LPNP-MAN, and IL-4-LPNP-MAN) were ultrafiltered through 100 kDa MWCO filters at 10,000 rpm, 4°C for 10 minutes to remove the non-encapsulated protein and the non-incorporated mannose (**Figure 3.2**). Filtrates were collected to quantify the non-incorporated IL-4 and mannose. Lipid-polymer hybrid NPs remained at the filter were then washed, resuspended with the initial volume of Milli-Q® water and stored at 4°C.

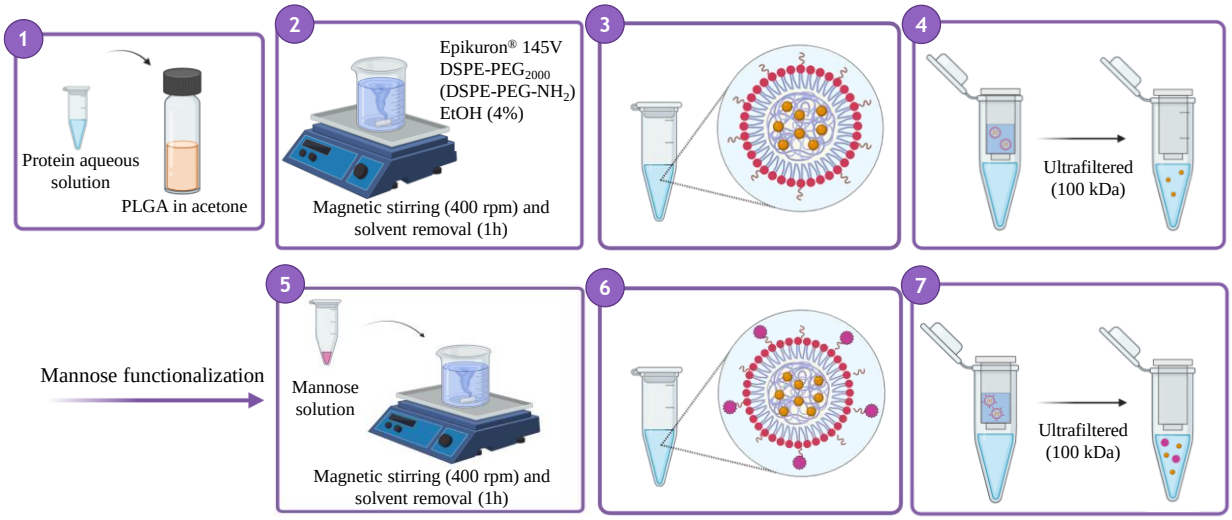


Figure 3.2. Synthesis protocol of polymer-lipid hybrid nanoparticles following the modified nanoprecipitation method. Figure created with Biorender®.

3.2.3 LPNPs modelling

The design of suitable protein-loaded LPNPs was performed taking advantage of AI tools. The characteristics of the LPNPs obtained as described in **Table 3.2** were selected as outputs while the composition variables were used as inputs. The database was modelled using FormRules® v4.03 (Intelligensys Ltd., UK), the commercial neurofuzzy logic software used previously (see section *3.1.4*). In this case, two composition variables were introduced as inputs: polymer amount and BSA concentration, while four variables were introduced as outputs: particle size, polydispersity index (PDI), zeta potential (ZP) and association efficiency (AE).

Among the FormRules statistical criteria for data fitting, Structural Risk Minimization (SRM) was selected as it provided the highest predictability along with the simplest and most comprehensible rules. The software was configured with specific training parameters, including a ridge regression factor of 1.0 e^{-6}, number of set densities: 2, set densities: 2 and 3, maximum inputs per submodel: 4, maximum nodes per input: 15, adapt nodes: true, C1 values over 0.75 and C2 values over 4.8.

As previously indicated in section *3.1.4*, the quality of the models was assessed. The predictability was established by the determination coefficient (R^2) as stated in Eq. (**3.1**).

USC UNIVERSIDADE DE SANTIAGO DE COMPOSTELA

To assess accuracy, an ANOVA was employed by comparing predicted and experimental values. Computed *f* ratio values higher than critical *f* values for the specified degrees of freedom indicate no statistical significance between predicted and experimental results and hence, good model performance.

3.2.4 Mannose labelling

Mannose was fluorescently labelled with 2AA, purified, and characterized as previously described (see section *3.1.5*). Additionally, mannose was also fluorescently labelled with an amino-modified ATTO 488 through a Maillard reaction to allow their determination by laser scanning microscopy. For this purpose, mannose (11.6 mg) was added to 400 µL NaOH (0.05 mM) containing the dye solution (50 µg/mL), pH was adjusted to 8.5 for optimal reaction. The mixture was protected from light and magnetically stirred at 500 rpm overnight at RT. After that time, the fluorescently labelled mannose was purified (Chromabond® cyano-modified silica gel-SPE column from Macherey-Nagel, Germany) and lyophilized (Telstar, LyoQuest, Spain).
Proton nuclear magnetic resonance spectroscopy analysis (^{1}H-NMR) was performed to confirm the correct labelling of mannose with ATTO 488. Fluorescently labelled mannose (200 mM) and D-(+)-mannose (200 mM) were dissolved in deuterated water (D_2O) (600 µL) (Sigma Aldrich, USA), placed in NMR tubes, and characterized using a Bruker DRX 500 (Germany).

3.2.5 LPNPs characterization

Lipid-polymer hybrid NPs were characterized in terms of particle size, polydispersity index (PDI), and surface charge (ZP) by dynamic light scattering (DLS) using a Zetasizer Pro (Malvern Instruments, Malvern, UK). For this purpose, samples were 1:10 diluted with Milli-Q® water and placed in a specific cuvette (DTS 1070). Measurements were carried out at 25°C ± 1°C in triplicate using the parameters automatically selected by the software.

The association efficiency (AE) of the BSA-loaded LPNPs (BSA-LPNP) was measured by directly quantifying the amount of BSA on the LPNPs using a micro-BCA protein assay. To this end, previously purified BSA-LPNP were concentrated using 100 kDa MWCO filters (Millipore Amicon®, USA) at 10,000 rpm, 4°C for 10 minutes, collected, and incorporated into an increasing amount of acetone until complete dissolution. Then, the obtained solution was diluted in Milli-Q® water (1:2) and centrifuged at 12,000 rpm and 20°C for 10 minutes to remove the precipitated polymer. The supernatants were collected and the released BSA was quantified following the manufacturer's instructions (Thermo Scientific, USA).

To determine the IL-4 AE in both, mannose-functionalized (IL-4-LPNP-MAN) and non-functionalized (IL-4-LPNP) formulations, the non-encapsulated IL-4 present in the

filtrate after LPNPs purification (*3.2.2*) was quantified. The concentration of IL-4 in the collected filtrates was determined by an enzyme-linked immunosorbent assay following the manufacturer's instructions (Human IL-4 ELISA Kit, ThermoFisher Scientific, USA).

Mannose functionalization efficiency was determined by the quantification of the non-attached 2AA-labelled mannose. The concentration of mannose on the collected filtrates during LPNPs purification (*3.2.2*) was determined by measuring fluorescence (Excitation at 360 nm and Emission at 425 nm) in a plate reader (FLUOstar Omega, BMG Labtech, Germany).

3.2.5.1 IL-4 leaking studies

Similarly to already described by NLCs, the capacity of the developed LPNPs to avoid the leaking of the protein before being uptake by cells was assessed. This step is crucial to allow local effect at the target tissue within the joint cavity. IL-4 loaded LPNPs dispersions (IL-4-LPNP and IL-4-LPNP-MAN) were kept at 37 ˚C for 24 hours. Afterwards, an aliquot was taken and ultrafiltered at 10,000 rpm, 4°C for 10 minutes. The released IL-4 was quantified in the filtrate by an enzyme-linked immunosorbent assay following the manufacturer's instructions (Human IL-4 ELISA Kit, ThermoFisher Scientific, USA).

3.2.6 Fluorescence cross-correlation spectroscopy

Fluorescence cross-correlation spectroscopy (FCCS) studies were performed to assess whether the selected protocol leads to LPNPs with the desired polymeric core-lipid shell structure. These studies were done employing non-functionalized LPNPs (LPNP). To this end, polymeric cores were stained by adding DiD´ (4 µL at 2.5 mg/mL) to the polymeric dispersion before nanoparticle preparation. On the other hand, the lipid shell was stained with ATTO 488 through the hydrophobic insertion technique. The staining was performed by incubating the obtained LPNPs with DOPE-ATTO 488 (4 µL at 2.5 mg/mL) for one hour. Afterwards, LPNPs were purified as previously described and used for FCCS.

To evaluate the correct mannose functionalization, mannose-functionalized LPNPs were used (LPNP-MAN). Polymeric cores stained with DiD´ as previously described were used. Subsequently, the obtained LPNPs containing DSPE-PEG-NH_2 were functionalized with mannose fluorescently labelled with ATTO 488 (2.87 µL at 20 mM). Afterwards, LPNPs were purified and used for FCCS.

A Laser Scanning Microscope Zeiss LSM 780 (Carl Zeiss AG, Germany) equipped with a Zeiss C-Apochromat 40X 1.2 NA water immersion objective with a correction collar was employed. An immersion water drop was placed in the objective and 0.17 mm

USC UNIVERSIDADE DE SANTIAGO DE COMPOSTELA

thickness coverslips were directly positioned on the immersion drop. LPNPs dispersions were then placed on the coverslip.

For fluorescence determination, DiD´ was excited using a 633 nm diode-pumped solid-state laser (DPSS laser) with an emission detection range from 634 nm to 692 nm, while ATTO 488 was excited with a 488 nm argon laser covering an emission detection range from 499 nm to 621 nm. A dichroic mirror MBS 488/561/633 was employed to separate excitation and emission fluorescence.

Prior to each measurement, pinhole alignment was performed to select the optimal size, aiming to maximize the brightness signal (counts per molecule or CPM) and achieve the most accurate and precise curve. Laser power was adjusted to its highest feasible level to maximize brightness while preventing saturation effects and photobleaching [168,169].

Long acquisition times (10 repetitions x 100 s) were selected and fluorescence time-traces of the labelled species moving in and out of the detection volume were obtained. These characteristic fluorescent time-traces represent fluctuations in fluorescence intensity over time. These measurements are essential for calculating the normalized autocorrelation function (G) which provides insights into the nature and periodicity of fluctuations, enhancing the understanding of the dynamics and interactions of fluorescently labelled species, that is, polymeric cores, lipids and mannose (Eq. **3.6**) [168,169].

$$G(\tau) = \frac{\langle \delta F(t) \delta F(t+\tau) \rangle}{\langle F(t) \rangle^2} \quad \textbf{(3.6)}$$

Where G (τ) represents average over time, F (*t*) denotes the time-averaged fluorescence intensity, δF (*t*) = F(*t*) – ‹F(*t*)› represent the time-dependent fluctuations, and τ represents the diffusion time [169,170].

3.2.7 *In vitro* cell studies

Cellular studies were performed in murine fibroblasts (BALB/3T3A31), murine macrophages (RAW 264.7), and human monocytes (THP-1). BALB/3T3 and RAW 264.7 cells were cultured in DMEM medium supplemented with FBS (10%), penicillin/streptomycin (1%) at 37°C and 5% of CO_2. The supplemented medium was changed every other day. These cell lines were split when reaching 80% confluency and maintained in culture until the time of the experiment.

THP-1 cells were cultured in RPMI 1640 medium supplemented with FBS (10%), penicillin/streptomycin (1%), and 2-mercaptoethanol (0.05 mM). The cell culture media was changed every other day. Before the studies, THP-1 cells were activated by culturing them at a density of $2x10^5$ cells/mL in a complete RPMI 1640 medium

USC UNIVERSIDADE DE SANTIAGO DE COMPOSTELA

supplemented with 400 nM of PMA for 72 hours to promote their differentiation into macrophages. Following differentiation, RPMI 1640 medium supplemented with PMA was removed, and the cell monolayers were washed with DPBS before being cultured in fresh complete RPMI 1640 medium at 37°C and 5% of CO_2 for 24 hours before seeding.

3.2.7.1 Cell viability studies

Cell viability studies were performed in fibroblasts (BALB/3T3A31) and in murine macrophages (RAW 264.7). To this end, cells were seeded at $1.5x10^4$ cells/well in 96-well culture plates and allowed to attach for 24 hours. After this incubation time, complete DMEM was removed, and the cells were washed with DPBS. Subsequently, formulations (LPNP, LPNP-MAN, IL-4-LPNP, and IL-4-LPNP-MAN) were added at different final concentrations, 30 μg/mL, 12 μg/mL, and 6 μg/mL of LPNPs solid mass per volume and cells were incubated for 24 hours. Cells without treatment were used as a control.

Cell viability was assessed using AlamarBlue assay kit. The plate was incubated with the 1:10 diluted AlamarBlue reagent for 2 hours at 37°C and 5% of CO_2, and the fluorescence (Excitation at 540 nm and Emission at 580 nm) was measured employing a plate reader (FLUOstar Omega, BMG Labtech, Germany). The diluted reagent in medium and without cells served as blank. Cell viability was calculated as stated in Eq. **(3.7**).

$$Cell\ viability = \left[\frac{sample\ absorbance - blank}{control\ absorbance}\right] \quad (\mathbf{3.7})$$

3.2.7.2 Intracellular distribution of LPNPs through confocal microscopy

Macrophage uptake of non-functionalized and mannose-functionalized LPNPs was qualitatively evaluated using confocal microscopy. Murine macrophages (RAW 264.7) were seeded ($5x10^4$ cells/cm^2) in 8-well chambered cell culture slides and allowed to attach. After incubation, DMEM medium was removed, and the wells were washed with DPBS. LPNPs with DiD´ labelled polymeric cores (LPNP and LPNP-MAN), as previously described for FCCS studies, were added at a final concentration of 30 μg/mL. The monolayers were then incubated with LPNPs for 2 hours at 37°C and 5% of CO_2. Cells without treatment served as control. Afterwards, DMEM medium was removed, and cells were washed twice with DPBS before fixation with a 3.7% - 4.0% formaldehyde solution overnight.

To study the intracellular distribution of LPNPs cell cytoplasm and endosomes were stained. The latter ones were visualized through immunostaining by detecting Rab 5, a key regulator of clathrin-mediated endocytosis present in early endosomes [171,172]. Hence, fixed cells were washed twice with DPBS and permeabilized with 0.1% Triton

X-100 for 15 minutes at RT. After removing Triton X-100, cells were washed twice with DPBS and then blocked for 30 minutes at RT with DPBS containing 5% goat serum and 1% BSA. The blocking solution was then removed, and cells were incubated with the primary antibody (anti-Rab5, 1:100 dilution in blocking solution) for 2 hours at RT. The primary antibody was then removed, and cells were washed twice with DPBS and incubated with the secondary antibody (goat anti-Rabbit Alexa Fluor 594, 1:1000 dilution in blocking solution) for 45 minutes at RT. Afterwards, the secondary antibody was removed, cells were washed thrice with DPBS and incubated with DAPI (1 μg/mL) for 5 minutes at RT. DAPI solution was then removed, cells washed twice with DPBS, and samples were mounted with SlowFade Diamond Antifade.

For cytoplasm staining, cells were washed twice with DPBS and permeabilized with Triton X-100 as previously described. Triton X-100 was then removed, cells were washed again twice with DPBS and incubated with rhodamine phalloidin (50 μg/mL) for 45 minutes at RT. Afterwards, rhodamine phalloidin was removed, cells were washed twice with DPBS, and incubated with DAPI (1 μg/mL) for 5 minutes at RT. DAPI solution was then removed, cells were washed twice with DPBS, and samples were mounted with SlowFade Diamond Antifade.

Finally, cells were visualized at 63X using a Laser Scanning Microscope Zeiss LSM 780 (Carl Zeiss AG, Germany).

3.2.7.3 Immunomodulatory activity

The immunomodulatory activity of the developed systems was assessed in PMA differentiated THP-1 cells. Cells were seeded at a density of $1.0x10^4$ cells/well in 96-well plates for at least 2 hours. Cells were then stimulated with lipopolysaccharide (LPS) (100 ng/mL) and treated with the IL-4 loaded and unloaded functionalized LPNPs (IL-4-LPNP-MAN and LPNP-MAN) at a final concentration of 30 μg/mL (LPNPs solid mass per volume) for 24 hours. This concentration represents an equivalent IL-4 concentration of 20 ng/mL. As controls, cells stimulated with LPS (100 ng/mL) but not treated with the developed systems were used. After 24 hours, cell culture supernatants were collected, and the secreted concentrations of various cytokines (TNF-α, IL-8, IL-6, and IL-10) were determined by using a magnetic bead-based multiplex assay (R&D systems, USA), according to the manufacturer's instructions as mentioned above (see section *3.1.8.4*).

In parallel, the number of cells on each well was determined using the AlamarBlue reagent as previously described for fibroblasts and murine macrophages (see section *3.2.7.1*). Additionally, known numbers of cells were included as standards to stablish the correlation between the obtained AlamarBlue signal and the number of cells.

USC UNIVERSIDADE DE SANTIAGO DE COMPOSTELA

3.2.8 Statistical analysis

The data, presented as mean ± SD, was analysed using GraphPad Prism 8 software as above mentioned (see section *3.1.9*).

USC
UNIVERSIDADE DE SANTIAGO DE COMPOSTELA

3.3 DESIGN AND EVALUATION OF SENOLYTIC LOADED MICROSPHERES

3.3.1 Materials

Fenofibrate (FN) was purchased from Acros Organics (Belgium). Poly (D,L-lactide-co-glycolide) (PLGA) (Resomer® RG 502H (502H) (viscosity 0.21 dL/g) and Resomer® RG 755S (755S) (viscosity 0.60 dL/g)) were supplied by Evonik, Ltd. (Germany). Polyvinyl alcohol (PVA) (87-90% hydrolyzation, Av. Mol. Wt. 30,000-70,000 Da) was supplied by Sigma Aldrich (USA). Dichloromethane (DCM) of high-performance liquid chromatography grade was obtained from Merck (Germany). BALB/3T3A31 (CCL-163) cell line was obtained from ATCC (USA). Dulbecco's Modified Eagle Medium (DMEM) was purchased from Corning (USA). Antibiotic solution (10,000 units/mL penicillin, 10,000 μg/mL streptomycin) was acquired from GE Healthcare Life Sciences (USA). Phosphate buffered saline (PBS), TrypLE Express Enzyme, fetal bovine serum (FBS), and Dulbecco's phosphate-buffered saline (DPBS) were obtained from Thermo Fisher Scientific (USA). IL-6 was acquired from (Gibco, USA). Pronase and collagenase-P were obtained from Roche Molecular Biochemicals (Germany). Cell viability assay kit (AlamarBlue) and Pierce™ RIPA Buffer were purchased from ThermoFisher Scientific (USA). All experiments were carried out using Milli-Q® water (Milli-Q® plus, Millipore Ibérica, Spain).

3.3.2 Experimental design

Polymeric microspheres were developed using the single emulsion-solvent evaporation method outlined in **Figure 3.3**. Initially, an organic phase (O) containing fenofibrate (FN) (0% - 2%), Resomer RG 502H (10% - 20%), and 1 mL of dichloromethane (DCM) was prepared and added to an aqueous phase (W) (0.5% - 2% of PVA) using aqueous phase volumes between 2.5 mL and 10 mL to obtain the different O/W ratios (0.1 - 0.4) as indicated in **Table 3.3**. Both phases were mixed using a vortex (Fisherbrand, USA) at the preset speed (1,000 rpm - 3,000 rpm) for a preestablished time (60 s - 120 s) to form the emulsion. Subsequently, the emulsion was added to an aqueous solution (0.2% of PVA; volume between 3.5 mL to 99.0 mL), to obtain different dilution ratios (2 - 10) and maintained at 400 rpm using a magnetic stirrer (Fisherbrand, USA) for 2 h to reach complete DCM evaporation. Finally, microspheres were filtered using a membrane disk filter (GHP, 0.45 μm, 47 mm diameter, Waters), washed repeatedly with Milli-Q® water, freeze-dried (Telstar, LyoQuest, Spain), and stored at 4°C until use.

A reduced experimental design, shown in **Table 3.3**, was stablished by DataForm®v.3.1 software (Intelligensys Ltd., UK) using a balanced density method for seven variables relative to the composition and operation conditions during the microspheres production

process at three levels with a minimum pattern of eight: drug concentration, polymer concentration, surfactant (PVA) concentration during the emulsification process, organic/aqueous phase ratio (O/W ratio), stirring speed during the emulsification process, stirring time, and the dilution ratio (total volume/emulsion volume ratio) during solvent evaporation. Fenofibrate (LogP = 5.2, MW ≈ 360.8 Da) was used for the whole experimental design as well as for the further model validation step. The variables and their limits listed in **Table 3.3** were selected based on data found in the literature [147].

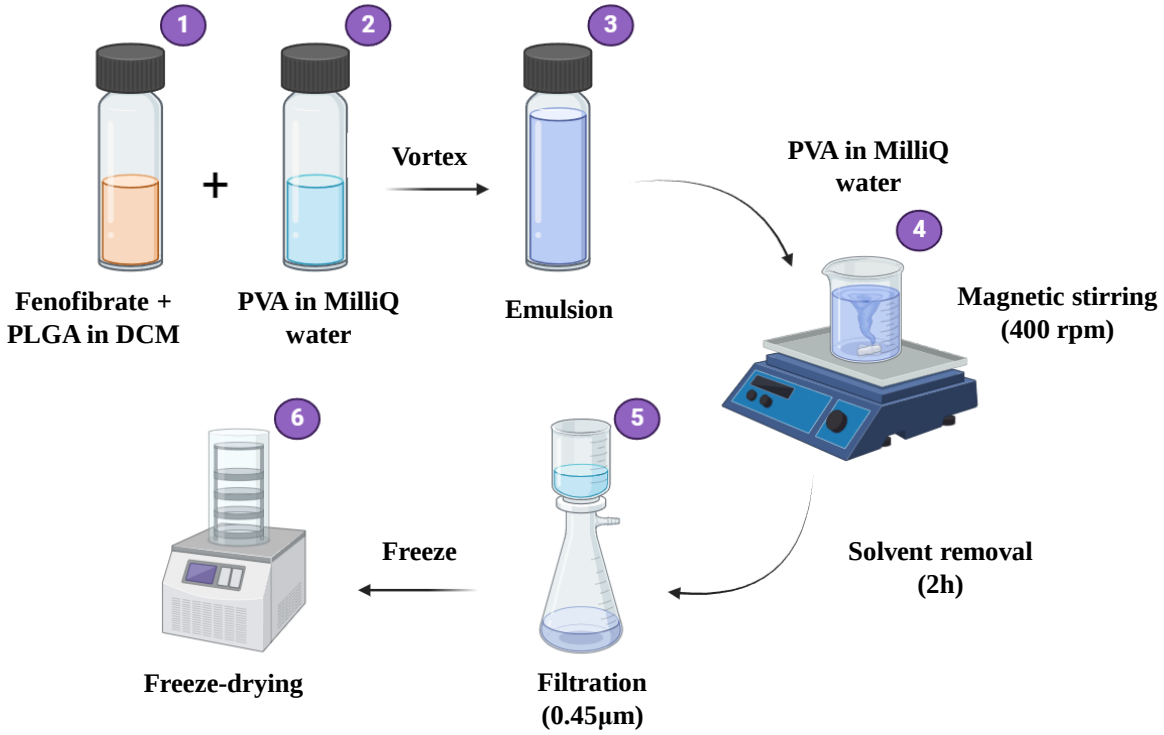


Figure 3.3. Microspheres preparation protocol by a single emulsion-solvent evaporation method. Figure created with Biorender®.

3.3.3 Microspheres modelling

The complete dataset including the seven variables as inputs (drug concentration, polymer concentration, PVA concentration, O/W ratio, stirring speed, stirring time, and the dilution ratio) and the values of the four formulation parameters studied as outputs (mean particle size, uniformity, drug loading (DL) and encapsulation efficiency (EE)) (**Table 3.3**) was modelled using the commercial neurofuzzy logic software, FormRules® v4.03 (Intelligensys Ltd., UK). As previously described, the models were 'pruned' to make them as simple as possible and to generate sets of linguistic *IF-THEN* rules relatively easy to understand.

The training parameters used by FormRules were the following: ridge regression factor of 1.0 e^{-6}, number of set densities: 2, set densities: 2 and 3, maximum inputs per

submodel: 4, maximum nodes per input: 15, adapt nodes: true. Among the five fitting statistical criteria offered by FormRules, Structural Risk Minimization (SRM) was used since it gave the highest predictability together with the simplest and more intelligible rules [165].

As indicated in section *3.1.4*, for assessing the quality of the models, the determination coefficient (R^2) (Eq. **3.1)** and an ANOVA were employed to establish predictability and accuracy, respectively.

FormRules models are expressed as a set of simple and easy-to-understand rules (Annex 3, Tables S1 to S4) which were used to establish the protocol to obtain microspheres of desirable specific characteristics.

Table 3.3. Characteristics of formulations established by DataForm experimental design using balanced density method for 7 variables and minimum patterns of 8.

Formulation	[Drug] (%)	[PLGA] (%)	[PVA] (%)	O/W ratio	Speed (rpm)	Time (s)	Dilution ratio
M01	1	10	2.00	0.10	1,000	60	6
M02	2	20	0.50	0.40	3,000	120	2
M03	0	15	1.25	0.25	2,000	90	10
M04	1	10	0.50	0.25	1,000	120	6
M05	0	15	1.25	0.40	3,000	90	2
M06	2	20	2.00	0.10	2,000	60	10
M07	1	15	1.25	0.40	2,000	60	6
M08	0	10	2.00	0.25	1,000	90	10
M09	2	20	0.50	0.10	3,000	120	2
M10	1	15	0.50	0.40	3,000	120	6
M11	0	10	1.25	0.10	1,000	90	10
M12	2	20	2.00	0.25	2,000	60	2
M13	2	10	1.25	0.40	2,000	120	2
M14	1	20	0.50	0.25	1,000	90	6
M15	0	15	2.00	0.10	3,000	60	10
M16	1	20	0.50	0.25	3,000	60	2
M17	0	15	2.00	0.10	1,000	120	10
M18	2	10	1.25	0.40	2,000	90	6
M19	1	10	0.50	0.40	3,000	60	10
M20	0	20	1.25	0.25	2,000	120	6
M21	2	15	2.00	0.10	1,000	90	2
M22	1	10	2.00	0.40	1,000	60	10
M23	0	15	0.50	0.10	3,000	90	6
M24	2	20	1.25	0.25	2,000	120	2

USC UNIVERSIDADE DE SANTIAGO DE COMPOSTELA

3.3.4 Preparation of microspheres for intra-articular delivery

The formulation obtained based on the generated models (F502) was selected and produced (**Table 3.4**). Firstly, it was used to validate the model, and, secondly for further characterization as a potential system for controlled drug delivery in OA management.

Additionally, to study how the incorporation of a polymer with a higher lactic:glicolic ratio (L:G) and molecular weight may affect the release profile of the drug, a second formulation employing a polymeric blend of 90% Resomer RG 502H (502H; 50:50 L:G) and Resomer RG 755S (755S; 75:25 L:G) was also prepared (F502:755) as indicated in **Table 3.4**. Unloaded or blank formulations were prepared following the same protocols, to be used as controls.

Table 3.4. Composition and operation variables followed for the production of unloaded and fenofibrate loaded microspheres for IA delivery.

Formulation	[Drug] (%)	[502H] (%)	[755S] (%)	[PVA] (%)	O/W ratio	Speed (rpm)	Time (s)
F502	1.0	20.0	0.0	1.0	0.25	2,400	60
F502:755	1.0	18.0	2.0	1.0	0.25	3,000	60
B502	0.0	20.0	0.0	1.0	0.25	2,400	60
B502:755	0.0	18.0	2.0	1.0	0.25	3,000	60

3.3.5 Microspheres characterization

3.3.5.1 Particle size, uniformity, drug loading, and encapsulation efficiency

Microspheres were evaluated in terms of particle size by light diffraction using a Mastersizer 2000 (Malvern Instruments, UK). Particle size distributions were characterized by two parameters, the mean particle size and the uniformity (Mastersizer 2000 user manual-Malvern Instruments). Mean particle size was calculated using one of the derived diameters D[m,n] stablished by the British standard BS2955:1993. Particularly, D (v, 0.5) or median of the distribution volume, this corresponds to the size in microns at which 50% of the microsphere's population is smaller and 50% is larger, while uniformity is a measure of the absolute deviation from the median.

Drug loading (DL) and encapsulation efficiency (EE) were determined using Eq. **(3.8)** and Eq. **(3.9)**, respectively. To this end, 3.0 mg of the obtained microspheres were dissolved in 3.0 mL DCM. The obtained drug concentration was quantified spectrophotometrically at 287 nm using a spectrophotometer (UV-VIS 8453 spectrophotometer, Agilent Technologies, Spain).

$$DL\ (\%) = \left[\frac{actual\ drug\ content\ (mg)}{weight\ of\ microspheres\ (mg)}\right] x\ 100 \qquad \textbf{(3.8)}$$

USC UNIVERSIDADE DE SANTIAGO DE COMPOSTELA

$$EE\ (\%) = \left[\frac{actual\ drug\ content\ (mg)}{theoretical\ drug\ content\ (mg)}\right]\ x\ 100 \quad (\mathbf{3.9})$$

3.3.5.2 Scanning electron microscopy

The morphology of the microspheres was examined by scanning electron microscopy (SEM) after silver coating. Imaging was performed on a Zeiss EVO LS 15 microscope (Germany) at a 500X magnification.

3.3.5.3 Differential scanning calorimetry

Thermal analysis was performed on fenofibrate (FN), PLGA (502H), physical mixtures of both PLGAs (90:10), and on the obtained microspheres (F502, F502:755, B502, and B502:755) using differential scanning calorimetry (DSC) on a Waters TA instruments Universal Analysis 2000 (USA) under a continuous flow of nitrogen at 50 mL/min. Samples (≈ 4.0 mg) were placed in aluminium pans and analysed from -20°C to 250°C at a 10°C/min heating rate. An empty aluminium sample holder was used to determine the baseline.

3.3.5.4 *In vitro* drug release studies

In vitro release studies of drug-loaded microspheres (F502 and F502:755) were conducted using a 1% aqueous solution of sodium dodecyl sulphate (SDS) as release media to maintain sink conditions. Samples (25.0 mg) were incubated in 1.5 mL of release media at 37°C in a shaking bath for three months. At preset points, samples were centrifuged (1,200 rpm, 4 min, RT) and 83% of the supernatant was collected and replaced with fresh media. Samples were then vortexed for 30 seconds at maximum speed and returned to the shaking bath. The amount of released fenofibrate was quantified after appropriate dilution of the collected supernatant at 287 nm using a validated spectrophotometric method. Unloaded microspheres (B502 and B502:755) underwent the same procedure to serve as blanks at the corresponding time points.

3.3.6 *In vitro* cell studies

Murine fibroblasts (BALB/3T3A31) and primary human osteoarthritic chondrocytes (OACs) were used for cell studies. BALB/3T3 were cultured in DMEM supplemented with 10% FBS and 1% penicillin/streptomycin at 37°C and 5% of CO_2. Media was changed every other day and cells were split when reached 80% confluence.

OACs were isolated from OA human cartilage slides provided by the Cellular Communication in Cancer and Age-related diseases Group at the Instituto de Investigación Biomédica de A Coruña (INIBIC), following previously established protocols [128,173]. Samples were washed twice with DPBS and cultured for 12 hours in DMEM supplemented with 2% FBS and 1% penicillin/streptomycin at 37°C and 5% of CO_2. After incubation, the medium was removed, and samples were treated with

pronase (1 mg/mL) for 30 minutes at 37°C in a shaking bath. Following two washes with DPBS, the samples were treated with collagenase P (1 mg/mL) for 8 hours at 37°C under shaking. The resulting cell suspension was then filtered through a 40 μm cell strainer and centrifuged twice at 1,200 rpm for 4 minutes washing with DPBS between centrifugations. The resulting cell pellet was resuspended in supplemented culture media and seeded in 6-well culture plates. Cell culture media was changed every other day and monolayers were split when reaching 80% confluency. All the experiments were performed with passage 3 cells.

3.3.6.1 Senescent cells viability

OACs were seeded at a density of $18x10^3$ cells/well in 24-well culture plates and allowed to adhere for 24 hours. Then cells were stimulated with IL-6 (20 ng/mL) to induce senescence. Transwell® permeable supports (5.0 μm polycarbonate membrane) (Sigma Aldrich, USA) were placed on each well. Subsequently, stimulated OACs were treated with either free fenofibrate at a final concentration of 3.12 μg/mL or with the obtained microspheres at an equivalent drug concentration, placing the treatments on top of the Transwell. The amount of microspheres used to achieve the equal drug concentration was calculated using the obtained *in vitro* release constants. Cells stimulated with IL-6 and left untreated were used as a control.

Cell viability studies were also performed using fibroblasts (BALB/3T3). Cells were seeded at a density of $10x10^3$ cells/well in 96-well culture plates and allowed to attach for 24 hours. Then, cells were treated with free fenofibrate at a final concentration of 3.12 μg/mL. Untreated cells were used as control.

Cell viability in both OACs and BALB/3T3 after 72 hours of treatment was quantified using the commercial AlamarBlue assay kit according to the manufacturer protocol. To assess viability, cell culture media and Transwell holders were removed, and the monolayers were washed with DBPS. Then, the 1:10 diluted AlamarBlue in complete media was added to each well, followed by a 2-hour incubation at 37°C and 5% of CO_2. Supernatants were afterwards transferred to 96-well plates and fluorescence (Excitation at 540 nm and Emission at 580 nm) was measured using a plate reader (Fluorostar Optima, BMG LABTECH, Germany). Wells without cells were used as blank. Cell proliferation was calculated as stated in Eq. (**3.7**) (section *3.2.7.1*).

USC UNIVERSIDADE DE SANTIAGO DE COMPOSTELA

3.3.6.2 Senolytic activity and autophagy induction

Cell senescence was evaluated by analysing the β-galactosidase activity of OACs using the senescence cells histochemical staining kit (Sigma Aldrich, USA) following the manufacturer's instructions. Cells were seeded and treated as described in the previous section (*3.3.6.1*). After, 72 hours of treatment, cell culture media and Transwell holders were removed. The cell monolayers were washed three times with DPBS and fixed with 400 μL per well of fixation buffer provided by the manufacturer. Afterwards, staining solution was added to the cell monolayers and kept at 37°C at least 24 hours monitoring staining intensity in an inverted microscope Olympus CKX53 (Olympus Life Science, Japan). Cells were then washed three times with DPBS and 500 μL per well of glycerol solution (70%) were added. Images of the stained cells were acquired with the mentioned microscope equipped with an Olympus EP50 microscope digital camera (Olympus Life Science, Japan). Images were analysed by employing the EP view (Olympus Life Science) software. Images were divided into quadrants, and both the total number of cells and positive cells for β-galactosidase staining (stained in blue) were counted. The percentage of positive cells was obtained dividing the stained cells by the total amount of cells and multiplying by 100.

For autophagy evaluation, senescent OACs treated for 72 hours with free drug or microspheres, were washed three times with DPBS. Autophagy was studied quantifying the expression of the autophagosomal marker LC3-II using the Autophagy ELISA Kit (Cell Biolabs, Inc., USA). To this end, the cytosolic pro-LC3 and the LC3-I were removed by adding 446 μL per well of cytosolic LC3 removal reagent provided by the manufacturer followed by a 5 minutes incubation at RT. Cells were then washed again three times with DPBS and lysed by adding 200 μL per well of ice-cold RIPA buffer and incubated on ice for 10 minutes. The obtained cell lysate was harvested and centrifugated at 12,000 rpm for 10 minutes at 4°C. LC3-II protein levels in the cell lysate were then quantified by an ELISA following the manufacturer's instructions. Total protein content was quantified using a micro-BCA protein assay kit following the manufacturer's instructions (Thermo Scientific, USA). LC3-II protein expression was normalized by the total amount of protein present in the cell lysates, and this was further normalized versus control (senescent not treated OACs).

3.3.7 *In vivo* studies

The efficacy of F502:755 microspheres to avoid OA disease progression was evaluated by employing a surgically induced OA model in mice. This is a predictive preclinical model of disease that resembles pathological joint changes occurring in the human cartilage and synovium.

USC UNIVERSIDADE DE SANTIAGO DE COMPOSTELA

3.3.7.1 Surgically induced OA

All animal experiments were performed according to protocols approved by the Institutional Animal Care and Use Committee at Instituto de Investigación Biomédica de A Coruña (INIBIC) by the Cartilage Biology Group. Experimental OA was induced in 3-month-old male C57BI/6J mice by transection of the medial meniscotibial ligament and the medial collateral ligament (MMTL + MCL) in the right knee as previously described [174]. The left knee was not subjected to surgery, only the joint capsule was opened, and was used as a sham control. Body weight was evaluated every two weeks.

3.3.7.2 Intra-articular administration of microspheres

Microspheres were administered to OA mice by a single IA injection at two fenofibrate doses, 1 and 10 μg. To evaluate the efficacy, three study groups were used (8 mice/each group). Mice were randomly assigned to each of the three groups. Group 1 or Control Group: mice treated with empty microspheres (B502:755); Group 2: mice treated with F502:755 at an equivalent drug dose of 1 μg; and Group 3: mice treated with F502:755 at an equivalent drug dose of 10 μg. Treatment was started one week after surgery recovery in all groups, meaning that the joint capsule had healed and closed before the IA injection.

3.3.7.3 Histological analysis of mouse knee joints

After three months of the injection, mice were euthanized, knee joints were fixed in 10% zinc-buffered formalin for 24 hours, decalcified in TBD for 6 hours, followed by paraffin embedding. Serial sections (4 μm) were cut, stained with Safranin O-fast green, and examined for histopathological changes using a semiquantitative scoring system for preclinical evaluation of whole joint changes according to OARSI guidelines [175]. In this system the scores are defined as follows: 0= normal cartilage; 0.5= loss of proteoglycan with intact surface;1= superficial fibrillation without loss of cartilage; 2= vertical clefts and loss of surface lamina (any % or joint surface area); 3= vertical clefts/erosion to the calcified layer lesion for 1-25% of the quadrant width; 4=lesion reaches the calcified cartilage for 25-50% of the quadrant width; 5= lesion reaches the calcified cartilage for 50-75% of the quadrant width; 6= lesion reaches the calcified cartilage for more than 75% of the quadrant width.

3.3.8 Statistical analysis

Results were analysed using GraphPad Prism 8 software as above mentioned (see section *3.1.9*).

USC UNIVERSIDADE DE SANTIAGO DE COMPOSTELA

USC
UNIVERSIDADE
DE SANTIAGO
DE COMPOSTELA

4 RESULTS AND DISCUSSION

USC
UNIVERSIDADE
DE SANTIAGO
DE COMPOSTELA

USC
UNIVERSIDADE
DE SANTIAGO
DE COMPOSTELA

4.1 FUNCTIONALIZED INDOMETHACIN-LOADED NANOSTRUCTURED LIPID CARRIERS

Nanoparticles depict several advantages for IA administration allowing for prolonged retention time of the therapeutic molecules within the joint and a higher tissue penetration when compared to free drugs [69]. Moreover, the capacity of nanoparticles to be targeted to specific cells by using surface moieties ensures the therapeutic molecule reach the target tissue while avoiding undesirable effects. In this regard, when nanoparticles are designed to control inflammation, a hallmark of OA, ideally, they should present enhanced affinity for the synovium, the homing tissue of immune cells [116].

In this section, NLCs loaded with the anti-inflammatory drug indomethacin (IND) were proposed to control inflammation in OA. These systems were functionalized with mannose to enable their specific distribution towards inflammation control cells, mainly macrophages. Human mannose receptor (CD206 or MRC1) is a glycoprotein expressed on the membrane of antigen presenting cells (APCs) including synovial macrophages. This membrane receptor exhibit capacity to recognize pathogens comprising N-acetylglucosamine, mannose and fucose residues on their surface, such as bacteria or fungi [140,141]. Moreover, CD206 plays a role in homeostasis, infections and inflammatory responses [140].

However, the development of NLCs able to depict the suitable physicochemical and stability properties is already a complex task where many variables are involved (ingredients and operation conditions). This process is even more challenging when additional steps are required for functionalization. A sequential design process was selected to obtain the desired NLCs following different steps: 1) Design of indomethacin (IND)-loaded NLCs with adequate physicochemical properties and drug loading by selecting the suitable composition and production procedure; 2) Design of IND-loaded NLCs containing the functionalization linker ensuring suitable drug loading, size and polydispersity index; 3) Design of mannose functionalized IND-loaded NLCs showing the desired properties of the previous step together with high functionalization efficiency. Once the optimized NLCs were obtained their capacity to be internalized by macrophages and anti-inflammatory response were evaluated.

4.1.1 Liquid lipid and solid lipid selection

The IND solubility in different liquid lipids (LL) is presented in **Figure 4.1**. Based on the obtained results, Transcutol P (HLB not applicable; logP = 0.5) was selected as the LL for the development of the NLCs. The IND solubilization capacity for Transcutol P (197.22 ± 3.12 mg/mL) was significantly higher ($p < 0.0001$) compared to all the other LL. On the other hand, Labrafac lipophile WL 1349 and Labrafac PG (HLB=1) were the LL showing the lowest solubilization capacity. No significant differences in IND

USC DE COMPOSTELA

solubility were observed between Capryol 90 (HLB=5), Labrafil M 2125 CS (HLB=9), and Labrafil M 1944 CS (HLB=9). IND presents also high solubility (85.97 ± 9.46 mg/mL) in Labrasol ALF (HLB=12). These differences in solubility can be mainly associated with interactions between the drug and the lipid. Despite drugs with high logP are usually better dissolved in substances with low HLB value, the molecular structure of IND, presenting ionizable functional groups (-COOH), can form hydrogen bonds with oily components that exhibit different degrees of polarity (Capryol 90, Labrafil M2125 CS, Labrafil M 1944 CS…)[176].

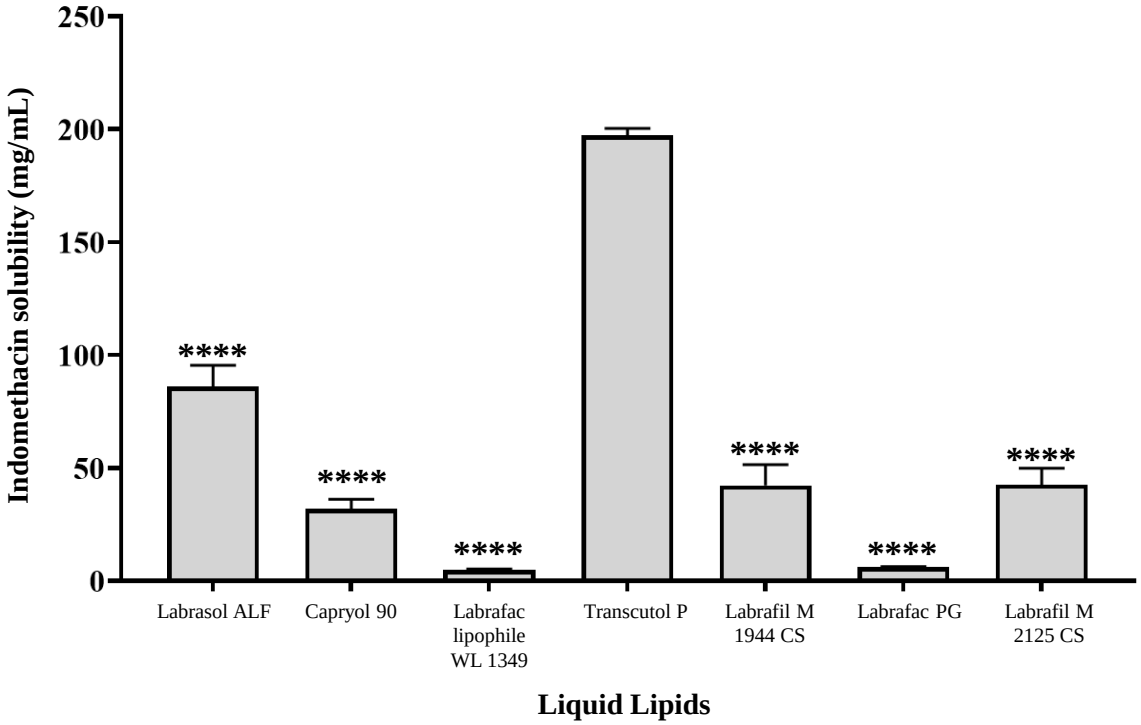


Figure 4.1. Solubility of indomethacin (IND) in the different liquid lipids (LL). Values are mean ± SD of three independent studies (*$p<0.0001$ *vs. Transcutol P*).

Furthermore, IND exhibited comparable solubility in both SL. No phase separation occurred when mixing Transcutol P with either SL, therefore, preliminary formulations were prepared to identify the best LL/SL ratio to achieve NLCs with superior characteristics. Following a thorough evaluation of the data, both SL provided similar NLCs characteristics. The two SL are categorized within generally recognized as safe (GRAS) status and their use for pharmaceutical products is approved. Therefore, they can be used as lipid carriers for both, solid lipid nanoparticles (SLNs) and nanostructured lipid carriers (NLCs). Considering this, Compritol 888 ATO was selected as the SL for the NLCs as it was previously used to develop IND-loaded NLCs [177,178]. Furthermore, other authors indicated that Precirol ATO 5 is not a suitable SL for IND encapsulation, as the drug can be easily released [179].

USC UNIVERSIDADE DE SANTIAGO DE COMPOSTELA

4.1.2 NLCs design and optimization

The characteristics of the initial experimental design formulations (Annex1 N01 - N30) are detailed in Annex1 Table S1 (highlighted in grey). This first step aims at selecting the best composition and protocol to obtain IND-loaded NLCs within the limits of the experimental design. NLCs with sizes ranging from 96.6 nm to 265.1 nm and PDI values between 0.1 and 0.3 were achieved, indicating narrow and homogeneous size distributions [162,180]. In all cases, the ZP values were negative, ranging between -3.7 mV and -16.7 mV. On the other hand, the achieved drug loading felt within the limits of 0.7% to 3.8%.

Table 4.1. Model A results and quality parameters. Inputs and submodels generated by FormRules for the different outputs. The most relevant submodels affecting each output are bolded.

Output	Submodel	Inputs from FormRules	R^2	Computed *f* value	ANOVA freedom degrees	α
Size (nm)	1	Ratio (LL/LS) x [Tween 80]	85.22	12.81	9 and 20	<0.01
	2	**IND x [Tween 80]**				
PDI	**1**	**IND x [Tween 80]**	75.30	1.60	19 and 10	-
	2	Lecithin x IND				
	3	Ratio (LL/LS)				
	4	Dialysis				
ZP (mV)	**1**	**Ratio (LL/LS) x [Tween 80]**	70.72	7.59	7 and 22	<0.01
	2	IND				
	3	Lecithin				
	4	Dialysis				
DL (%)	**1**	**IND**	87.63	25.97	3 and 11	<0.01

As indicated in **Table 4.1**, FormRules successfully modelled three out of the four formulation properties with high predictability (R^2 > 70%) and accuracy (α < 0.01). However, when it comes to PDI, the model struggled to accurately explain variations in this parameter. This discrepancy can be attributed to the narrow PDI values distribution, suggesting consistently adequate PDI throughout the design space.

According to the obtained models, NLCs size is conditioned by three variables: Ratio (LL/SL), Tween 80 concentration, and amount of IND. Variations in particle size are explained, by the interaction between (LL/SL) ratio and Tween 80 concentration (Submodel 1 - **Figure 4.2A**) and, on the other hand, by the interaction between the amount of IND and the Tween 80 concentration (Submodel 2 - **Figure 4.2B**), being the last submodel the one presenting the strongest effect on NLCs size.

USC UNIVERSIDADE DE SANTIAGO DE COMPOSTELA

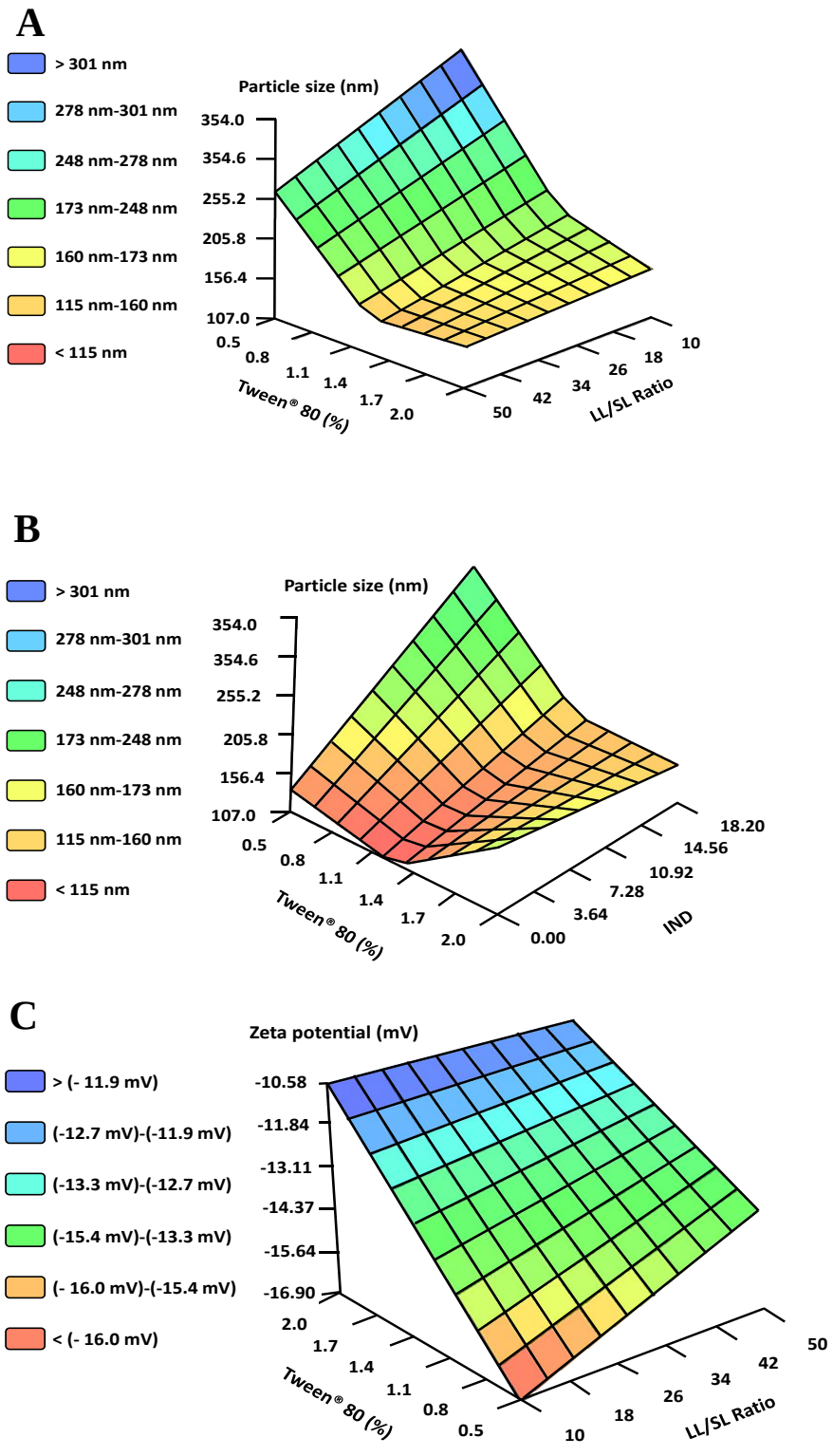


Figure 4.2. Values predicted by neurofuzzy logic Model A for (A) the NLCs particle size explained by submodel 1 for a constant 16.4 mg IND amount; (B) the NLCs particle explained by submodel 2 for a constant 50% LL/LS ratio and (C) zeta potential explained by its submodel 1 and for constant values of lecithin (2%), dialysis time (2h), and amount of IND (16.4 mg).

USC UNIVERSIDADE DE SANTIAGO DE COMPOSTELA

FormRules allows to express the developed models as a set of linguistic rules for each parameter (*IF-THEN* rules) (Annex1 Table S2) clarifying the factors conditioning the formulation development [82].

Figure 4.2 shows graphical examples of the predictions that can be derived from the models and rule sets. When more than 2 variables are involved, those that are not represented on the Cartesian axes have been kept constant. As depicted in **Figure 4.2** and outlined in the rule set for particle size (Annex1 Table S2), achieving small particulate systems requires high LL/SL ratios and elevated concentrations of Tween 80 (> 1.4%) (**Figure 4.2A**). By increasing the concentration of Tween 80 a more favourable environment for the formation of small and stable particles is created [181]. Additionally, the smallest IND-loaded NLCs are obtained with the inclusion of high concentrations of Tween 80 (≈ 1.4%) along with reduced amounts of IND (**Figure 4.2B** and Annex 1, Table S2, Rule 7). Notably, the use of low concentrations of Tween 80 (<1%) results in NLCs above 200 nm, irrespective of the employed LL/SL ratios (**Figure 4.2A**). Furthermore, the IND incorporation consistently leads to an increase in the NLCs particle size when low Tween 80 concentrations are used (**Figure 4.2B**).

Variations in ZP are mainly explained by the interaction between LL/SL ratio and Tween 80 concentration (Submodel 1 - **Figure 4.2C**). NLCs were prepared using negatively charged lipids and a non-ionic surfactant, Tween 80, which can diminish their surface net charge. As expected, high Tween 80 concentrations led to less negative ZP values being this difference in surface charge less pronounced at higher LL/SL ratios (Annex1 Table S2- **Figure 4.2C**)[181].

Drug loading is directly influenced by the quantity of drug added during the formulation process, higher amounts of IND are required to achieve elevated DL (Annex1 Table S2).

Components such as lecithin do not seem to play a decisive role in the characteristics of the NLCs. Although lecithin serves as an amphipathic lipid contributing to the stabilization of the NLCs dispersion and reducing its aggregation, variations in this parameter, within the studied design space, only result in slight variations in the ZP (Annex1 Table S2) [181].

INForm software was then used to select the optimal composition and preparation protocol to achieve an IND-loaded NLCs formulation with small particle size (< 120 nm), a PDI ranging from 0.2 - 0.3, the lowest surface charge, and the highest DL (> 2%). The software successfully modelled the N01 - N30 database (data not shown) and identify the parameters to obtain the desirable formulation. **Table 4.2** shows the variables selected by INForm's genetic algorithms along with the predicted values for the studied parameters to find a compromise solution with maximum desirability. These

USC UNIVERSIDADE DE SANTIAGO DE COMPOSTELA

conditions were used to produce the optimal formulation. The obtained systems show characteristics that closely matches the model's predictions.

Table 4.2. Composition selected by INForm optimization, values predicted by the model and those obtained experimentally.

Variables		Characteristics	Predicted values	Experimental values
Ratio (LL/SL)	50	**Size (nm)**	119.6	123.4
Tween 80 (%)	1.7	**ZP (mV)**	-15.2	-14.8
Lecithin (mg)	2.0	**PdI**	0.2	0.2
Dialysis (h)	2.0	**DL (%)**	3.1	2.5
IND (mg)	16.4			

The developed optimized NLCs present uniform size distributions (PDI < 0.3) and small particle sizes (< 120 nm), adequate to diffuse trough biological barriers [69]. Moreover, the developed systems presented moderate negative zeta potential (ZP < -10 mV) that can confer stability to the colloidal dispersion [162]. Regarding DL, a high drug content was obtained (> 2%), likely attributed to the high solubility of IND in the selected LL together with the NLCs unstructured lipid matrix, which enhances drug incorporation [182].

The experimental values of the optimized formulation were added to the initial database as formulation N31. Moreover, mannose functionalization requires the inclusion of an extra component to the NLCs structure, stearylamine (SA). This ingredient enable the reaction of the amino group of SA, within the NLCs structure, with the aldehyde group of mannose, forming a Schiff's base (-N=CH-) [183].

Therefore, a new process variable was introduced during the formulation procedure, expanding the design space. Consequently, the database was increased with new formulations (N32 to N44 in **Table 3.1**), featuring SA amounts within the range of 1.4 - 7.7 mg.

The database integrating these new formulations characteristics (Annex1, N01 - N44 in Table S1) was successfully modelled using FormRules (Model B). The resulting model parameters are presented in **Table 4.3**. Like previous assessments, the quality of the models was evaluated for predictability (R^2 > 70% for all formulation properties) and accuracy (α < 0.01 for all formulation parameters).

USC UNIVERSIDADE DE SANTIAGO DE COMPOSTELA

Table 4.3. Model B results and quality parameters. Inputs and submodels generated by FormRules for the different outputs. The most relevant submodels for each output are bolded.

Output	Submodel	Inputs from FormRules	R^2	Computed *f* value	ANOVA freedom degrees	α
Size (nm)	**1**	**[Tween 80] x SA**	91.97	60.77	13 and 69	<0.01
	2	Ratio (LL/LS)				
PDI	**1**	**[Tween 80] x SA**	77.55	15.89	15 and 69	<0.01
	2	[Tween 80] x IND				
ZP (mV)	**1**	**[Tween 80] x SA**	98.00	482.92	8 and 79	<0.01
	2	IND				
	3	Dialysis				
DL (%)	**1**	**[Tween 80] x IND**	96.78	405.72	6 and 81	<0.01

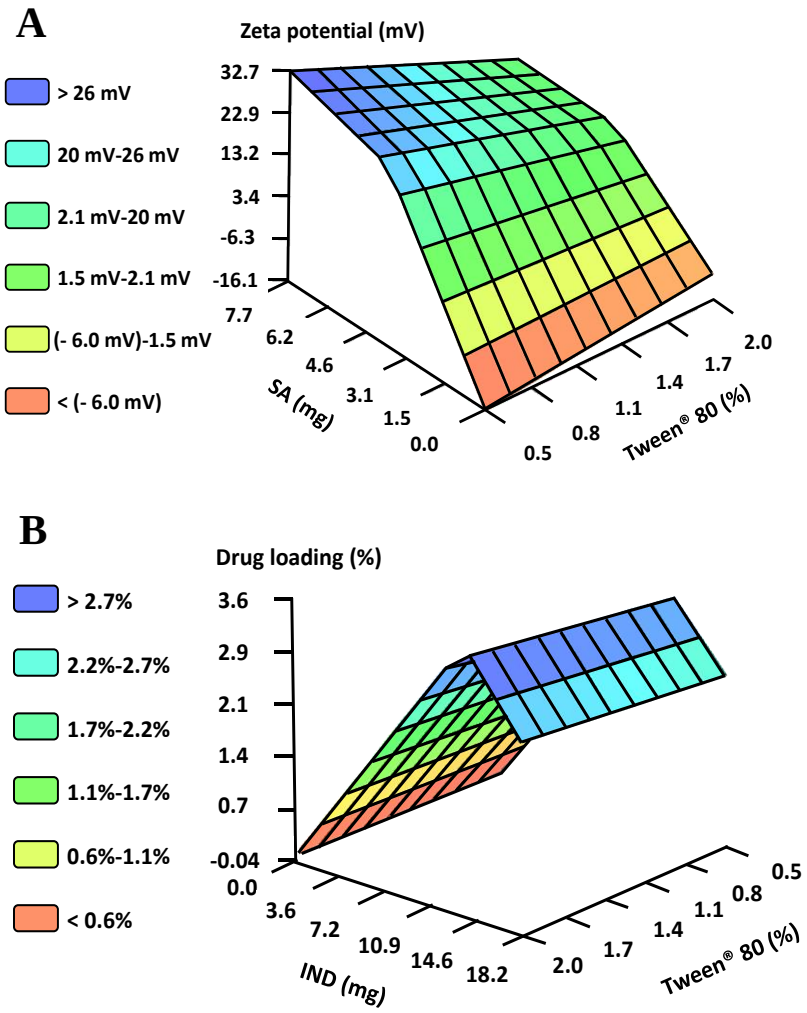


Figure 4.3. Predicted values by FormRules for (A) NLCs ZP explained by submodel 1 for a constant ratio 50% LL/SL, and (B) NLCs DL explained by the interaction between the amount of drug added and the Tween 80 concentration.

USC UNIVERSIDADE DE COMPOSTELA

As gathered from the inputs selected by FormRules for Model B, the amount of SA has an impact on almost all the studied parameters, highlighting the need to consider this variable for a correct formulation design. The amount of incorporated SA interacts with the Tween 80 in such a way that the smallest particle sizes are achieved for high values Tween 80 (> 1.6%) and medium-high values of SA (> 3 mg) (Annex1 Rule 11 Table S3). SA also influences the PDI but without great relevance since all the obtained values for PDI were lower than 0.3. Furthermore, the amount of incorporated SA extraordinarily conditions the ZP value, shifting from negative to positive after just the addition of a small amount of SA (**Figure 4.3A**). This effect has been previously reported by other authors when developing rifampicin-loaded NLCs [163].

On the other hand, Model B does not show an effect of SA on DL which variations are explained by the interaction between Tween 80 and the amount of IND added (**Figure 4.3B**). The model recommends using medium-high amounts of IND (over 7 mg) to achieve a high DL, regardless of the employed SA amounts (Annex1 Rules 27-30, Table S3).

Moreover, a throughout analysis of the database (Annex1 Table S1) shows that the addition of SA above 6.5 mg to formulations including IND (> 10 mg) leads to the production of NLCs with markedly lower size (N39 vs N40 and N39 vs N44). To elucidate the reason behind this effect, *in silico* docking was performed. The docking was conducted under two different conditions: 1) the IND was set as free-ligand, and the single excipient was used as rigid receptor (Annex 1 Figure S1); 2) the IND was set as rigid receptor and the single excipient as free-ligand. The calculated free binding energy relies on intra- and inter-molecular free-energy and the formation of favourable bonds and interactions. By alternately setting the drug and excipient as the free ligand, we gained insight into each component's contribution to total free energy and the newly established interactions. Additionally, setting excipients as rigid receptors better simulated the self-assembled NLCs system, where they adopt a stacked, straight alkyl chain conformation, typically energetically favourable in the solid state. On the other hand, when IND was set as rigid receptor, the excipients were free to move and adapt their conformation to the drug, thus better simulate the lipid liquid state [184].

The resulting binding energy (ΔG) and affinity constant (K_i) are reported in **Figure 4.4**. The results revealed that IND exhibits a stronger affinity for SA compared to other excipients, as evidenced by the lower ΔG and K_i values. These results are attributed to the establishment of more hydrogen bond formations and hydrophobic interactions, resulting in decreased free-energy and increased affinity between both components. The higher affinity is largely dependent on the formation of two hydrogen bonds between the amino group of SA and the carboxylic group of IND (**Figure 4.4C**). Indeed, when SA was set as free ligand, it was able to partially compensate the free energy loss passing

from linear alkyl chain to flexible chain, thanks to the established hydrogen bonds. Moreover, the numerous formations of hydrophobic p-alkyl interaction between ring of IND and the alkyl chain of SA, along with an additional pi-lone pair interaction, further contributed to a lower free-energy and stabilized the assumed pose (**Figure 4.4C**).

Interestingly, the poses of Compritol demonstrated that the formation of hydrophobic interactions alone does not result in a strong affinity for IND. Indeed, the affinity of Compritol for IND significantly decreased when it was unable to establish the hydrogen bond (**Figure 4.4B** and Figure S1 Annex l). This concept was further supported by the results obtained for Transcutol. While Transcutol was able of forming a hydrogen bond with IND in both docking poses, the fewer hydrophobic interactions were insufficient to fully compensate for the energy loss associated to the transition from a linear to a non-linear chain (**Figure 4.4A** and Figure S1 Annex l). Nevertheless, the presence of both hydrophobic and hydrogen bond interactions resulted in a higher affinity than Compritol in its flexible form (**Figure 4.4B**).

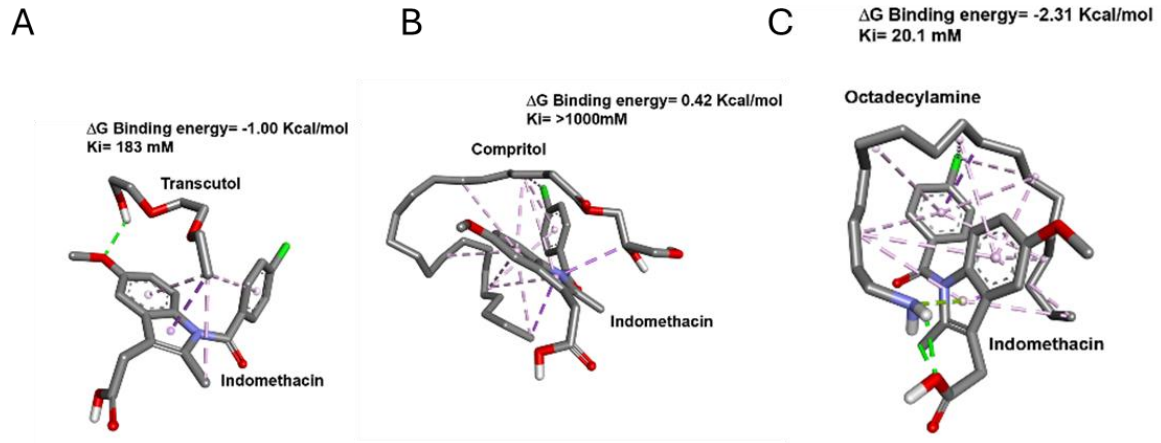


Figure 4.4. Binding pose of indomethacin with (A) Transcutol, (B) Compritol, and (C) Stearylamine and the respective estimated ΔG binding energy and affinity constant (K_i). In the structures, carbon atoms are shown in grey, oxygen atoms in red, nitrogen atoms are shown in blue, while chlorine atoms are shown in green. Indomethacin was set as rigid receptor, while the excipients were set as flexible ligands.

The observed high affinity of IND for SA could modify the dynamic behind the formation of NLCs and lead to the formation of smaller nanoparticles. Afterwards, INForm was used again to model the expanded database (Formulations N01 to N44) (data not shown). This tool was also used to identify the conditions leading to NLCs formulations including IND and SA with a small particle size (< 120 nm), a PDI ranging between 0.2 and 0.3, the highest positive surface charge, and a high drug loading (> 2%). **Table 4.4** shows the variables selected by the INForm model to obtain such formulation, along with the predicted values for the studied properties.

USC UNIVERSIDADE DE SANTIAGO DE COMPOSTELA

Table 4.4. Composition selected by INForm (Formulation IND-NLC-SA) together with the predicted properties values and those obtained experimentally before and after storage at 5°C for 3 months (n= 3 ± SD).

Variables		Characteristics	Predicted values	Experimental values	Experimental values (after storage)
Ratio (LL/SL)	48.1	**Size (nm)**	57.6	59.7 ± 0.8	61.7 ± 5.3
Tween® 80 (%)	1.8	**ZP (mV)**	23.4	22.6 ± 3.6	17.1 ± 2.5
Lecithin (mg)	1.5	**PDI**	0.3	0.3 ± 0.1	0.3 ± 0.0
Dialysis (h)	3.0	**DL (%)**	3.4	1.2 ± 0.2	1.2 ± 0.1
IND (mg)	11.0				
SA (mg)	7.7				

The optimized IND-loaded formulations, ready to be functionalized (IND-NLC-SA), were experimentally produced under the conditions outlined in **Table 4.4,** yielding values similar to those predicted by the model. Therefore, the model was successful at integrating the complex effect of SA-IND interaction over particle size. However, the DL was slightly lower than anticipated, indicating a discrepancy in this parameter that can be attributed to the limited number of loaded formulations with SA in the database.

Furthermore, the properties of IND-NLC-SA after a 3-month storage period were re-analysed to evaluate the stability of the NLCs. The formulated IND-NLC-SA were stable over the specified duration, with no statistically significant differences observed in the NLCs characteristics, including size, PDI, ZP, and DL over time.

4.1.3 NLCs functionalization of the optimized formulation

Mannose was fluorescently labelled to allow for the analysis of the NLCs functionalization process. Nuclear magnetic resonance (NMR) spectroscopy was performed to confirm the successful mannose modification. This analysis enables the detailed structural chemical characterization of different materials including carbohydrates [185]. **Figure 4.5** shows the ^{1}H NMR spectrum of the D-(+)-mannose (violet) overlapped with the fluorescently labelled mannose derived from the Maillard reaction (green) and with free anthranilic acid (red). These findings suggest that mannose was bounded to the fluorophore observing a shift in the anthranilic acid peaks after conjugation. Moreover, two additional peaks could be observed for the labelled mannose coming from the acetate buffer used for dilution and purification before lyophilization.

USC UNIVERSIDADE DE SANTIAGO DE COMPOSTELA

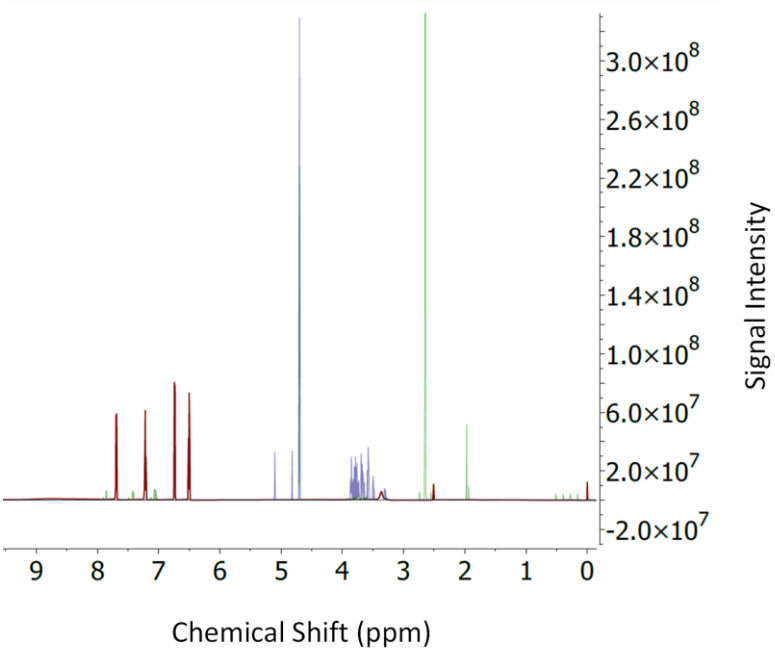


Figure 4.5. ^{1}H NMR spectrum of D-(+)-Mannose (violet spectrum) overlapped with the derived product from the Maillard reaction to fluorescently label mannose (green spectrum), and with anthranilic acid (red spectrum).

The use of fluorescently labelled mannose allowed the NLCs functionalization efficiency quantification, expressed as the percentage of the added component incorporated to the NLCs surface. Moreover, this approach is useful to optimize the functionalization procedure. As far as we know, this method has not been previously used. Based on literature, different SA:MAN proportions and incubation times have been selected to include most of the previously reported settings. **Table 4.5** exhibits the IND-NLC-SA mannose functionalization efficiency in the different studied conditions, along with the naïve NLCs characteristics (particle size, PDI, and ZP).

As depicted in **Table 4.5**, the functionalization process following all the studied protocols results in NLCs with significantly higher particle size ($p < 0.0001$) compared to naïve IND-NLC-SA, aligning with previously reported findings [164]. Despite no statistically significant changes were observed in the ZP between naïve and functionalized NLCs, as a general trend, higher ZP values were obtained in functionalized NLCs.

No statistically significant differences were found in the NLCs properties between variable incubation times at any of the used ratios. Moreover, elevated SA:MAN molar ratios (> 1:3) contributed to amplified variability in NLCs functionalization efficiency. On the other hand, the functionalization efficiency exceeds 85% for 1:2 ratios, suggesting that the optimized formulation developed through the sequential procedure (IND-NLC-SA; **Table 4.4**), is well suited for mannose functionalization at this ratio.

Despite no differences were observed between incubation time, the 72 hours incubation condition was selected to obtain the optimized IND-NLC-MAN.

Table 4.5. Results of mannose-functionalization efficiency of IND-NLC-SA optimal formulation and NLC characteristics after their incubation with D-(+)-mannose (50 mM) at various SA:MAN molar ratio and incubation times. (n= 3 ± SD).

SA:MAN	Incubation time (h)	Functionalization efficiency (%)	Size (nm)	PDI	ZP (mV)
1:2	24	86.59 ± 4.21	73.94 ± 2.24	0.27 ± 0.03	21.69 ± 3.59
1:2	48	85.15 ± 7.26	70.88 ± 0.58	0.26 ± 0.03	23.34 ± 3.06
1:2	72	86.24 ± 6.23	71.98 ± 1.24	0.26 ± 0.03	24.84 ± 4.62
1:3	24	71.98 ± 16.45	74.22 ± 2.26	0.27 ± 0.01	23.12 ± 2.45
1:3	48	70.71 ± 20.01	73.32 ± 0.87	0.27 ± 0.01	23.41 ± 0.08
1:3	72	67.85 ± 21.15	71.54 ± 2.87	0.27 ± 0.01	25.24 ± 4.15
1:5	24	65.83 ± 13.40	71.80 ± 3.08	0.25 ± 0.02	23.50 ± 1.75
1:5	48	61.62 ± 17.85	72.91 ± 1.10	0.26 ± 0.02	24.91 ± 0.26
1:5	72	62.48 ± 16.38	72.91 ± 2.88	0.26 ± 0.01	24.06 ± 0.53
Non-functionalized NLCs **(IND-NLC-SA)**			59.72 ± 0.84	0.30 ± 0.05	22.62 ± 3.56

This optimized functionalized formulation (IND-NLC-MAN), highlighted in grey in **Table 4.5**, shows a uniform particle size distribution (PDI 0.3), small particle sizes (≈ 70 nm), and a high positive zeta potential (> 20 mV), which fall below the ideal threshold. Nevertheless, the stability is not compromised, ensuring colloidal stability [162]. Several studies have indicated that particle characteristics such as size, charge, shape, and surface coating influence their uptake by antigen-presenting cells (APCs) and residence time within the joint cavity [69,73,186]. Nanometric systems can be internalized via various mechanisms including phagocytosis, pinocytosis, caveolin-mediated endocytosis, or clathrin-mediated endocytosis [187]. However, when surface coated nanoparticles depict a specific ligand for membrane receptors, as is the case for mannose with CD 206 in APCs, it is anticipated that NPs will predominantly undergo receptor-mediated endocytosis [73]. In this scenario, cell uptake will be beneficiated in NLCs showing a diameter of approximately 50 nm and round morphology [73,188,189]. Additionally, positively charged nanoparticles show enhanced interaction with the cell membrane and, therefore, facilitate cell uptake [190].

On the other hand, the residence time of nanoparticles within the joint after IA administration is also highly influenced by size. High nanoparticles (900 nm) are proven to stay longer than smaller particles (500 nm) [191]. Therefore, a compromise should be achieved to ensure enough time at the joint and, at the same time, efficient uptake. Additionally, positively charged NPs have shown enhanced retention times associated

USC UNIVERSIDADE DE SANTIAGO DE COMPOSTELA

with an interaction with the negatively charged hyaluronic acid component of the synovial fluid [192].

Based on the above-mentioned properties, the developed IND-NLC-MAN shows suitable properties to be highly internalized by APCs while could depict enhanced retention in the joint cavity thanks to the highly positive charge. This optimized formulation was selected for furthers studies to deeply analyse the nanoparticle morphology and structure and confirm the adequate cell uptake and anti-inflammatory capacity. In parallel, unfunctionalized loaded nanoparticles (IND-NLC) and blank nanoparticles without (NLC) and with mannose functionalization (NLC-MAN) with identical operational conditions were also prepared to be used as controls.

Table 4.6 shows the physicochemical properties of the developed formulations. As expected, the three new batches of the optimized formulation (IND-NLC-MAN) show the same properties as previously described in **Table 4.5** indicating the reproducibility of the developed protocol. Moreover, in the case of unfunctionalized NLCs, the inclusion of IND leads to a slight decrease in particle size as previously pointed out by Model A (**Figure 4.2B**), with negligible effects on PDI or ZP. However, the addition of SA, as part of the functionalization process, causes a notable shift in ZP towards high positive values for both unloaded and IND-loaded systems, also previously noted in Model B (**Figure 4.3A**). Functionalization with mannose also contributes to the formation of broader particle size distributions.

Table 4.6. NLCs characterization in terms of particle size (Size), polydispersity index (PDI), zeta potential (ZP), and drug loading (DL) (n= 3 ± SD).

Formulations	Size (nm)	PDI	ZP (mV)	DL (%)
NLC	290.13 ± 14.66	0.20 ± 0.01	-12.23 ± 0.12	-
NLC-MAN	292.93 ± 39.22	0.40 ± 0.01	32.42 ± 1.76	-
IND-NLC	249.91 ± 3.04	0.25 ± 0.01	-17.80 ± 0.78	2.44 ± 0.48
IND-NLC-MAN	67.98 ± 11.96	0.36 ± 0.03	20.10 ± 6.05	2.96 ± 0.14

The significant reduction in particle size observed for IND-NLC-MAN is particularly noteworthy, especially considering that it contradicts findings from other studies involving mannose-coated NLCs, where no reductions in particle size were reported [193,194]. This unexpected observation based on literature, is explained by the strong interaction between IND and SA previously found (**Figure 4.4**), suggesting a distinct behaviour during NLCs preparation when SA is incorporated, rather than an effect of the surface coating phenomenon itself. Indeed, the addition of mannose, although not significantly, increase the size of the systems, from a mean diameter of 58.83 ± 4.81 nm for unfunctionalized NLCs (IND-NLC-SA) to a mean diameter of 67.98 ± 11.96 nm for functionalized NLCs (IND-NLC-MAN) similarly to already shown in **Table 4.5**.

USC UNIVERSIDADE DE SANTIAGO DE COMPOSTELA

Similar findings were found by Burgarelli Lages *et al*., who conducted a study on solid lipid nanoparticles with and without the functionalization linker. They also observed a significant decrease in particle size for both unloaded and drug-loaded formulations after the addition of SA. This reduction was attributed to the introduction of the new ingredient in the NLCs composition, resulting in a less structured matrix [195]. To clarify this possible effect on the developed NLCs, a thermal analysis (DSC) of the raw materials and nanoparticles was developed (**Figure 4.6** and **Table 4.7**). Non-functionalized systems, with (IND-NLC) and without the drug (NLC), as well as systems prepared with SA with (IND-NLC-SA) and without the drug (NLC-SA) were prepared. Additionally, the thermogram of the free drug (IND) was performed.

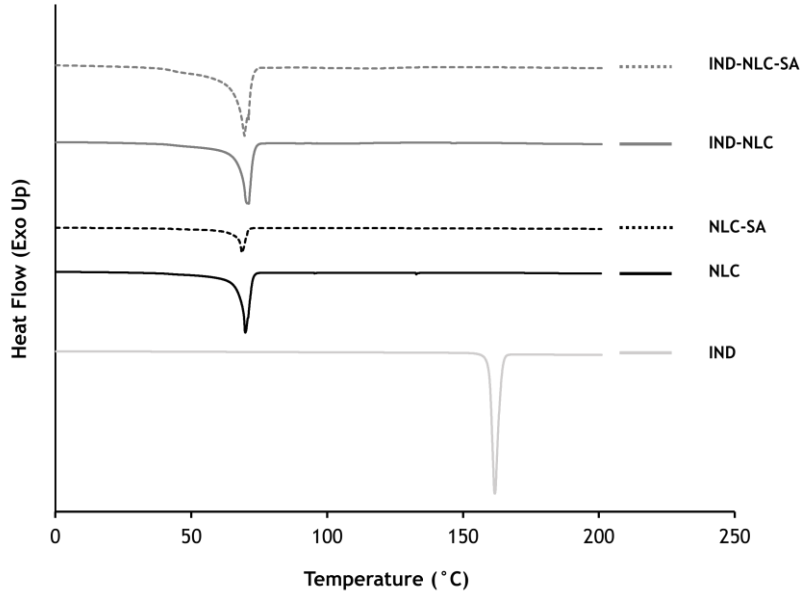


Figure 4.6. DSC thermograms of the developed NLCs with or without the drug and with or without the functionalization linker (NLC, NLC-SA, IND-NLC, and IND-NLC-SA), as well as the thermogram of the free drug (IND).

IND shows the characteristic melting peak at approximately 160°C, previously reported [196]. This event was absent in the thermograms of the drug-loaded formulations (IND-NLC and IND-NLC-SA) suggesting either complete dissolution of the IND within the melted lipids or its presence in an amorphous state [197].

Table 4.7. Melting enthalpies and temperatures determined by DSC for the developed NLCs and free drug.

Formulation	Melting Enthalpy (ΔH) (J/g)	Melting Temperature (°C)
NLC	99.07	68.64
NLC-SA	82.79	67.51
IND-NLC	82.84	67.90
IND-NLC-SA	79.35	66.12

USC UNIVERSIDADE DE SANTIAGO DE COMPOSTELA

Moreover, NLCs thermogram shows an endothermic peak at 68.64ºC corresponding to the melting of the nanoparticles. The drug incorporation to the lipid matrix either without (IND-NLC) or with SA (IND-NLC-SA) results in a reduction in melting enthalpy and temperature. This reduction can be attributed to the less ordered structure of the lipid matrix caused by the incorporation of drug molecules [193,197]. Additionally, the inclusion of the functionalization linker further contributes to a reduction in melting enthalpy and temperature (**Table 4.7**). Therefore, our findings agree with those already mentioned, where the incorporation of additional ingredients other than SL and LL leads to a less structured lipid matrix [195].

4.1.4 Deep characterization of optimized formulations

As already mentioned, the internalization efficiency of NLCs can be influenced by their morphology [186]. Spherical shapes are known to exhibit the highest internalization efficiency compared to other shapes such as rods or stars, among others [69]. **Figure 4.7** displays representative TEM images of the optimized formulation (IND-NLC-MAN) and the corresponding controls (NLC, NLC-MAN, and IND-NLC). All the developed nanoparticles displayed a uniform spherical shape with smooth surfaces. Images agree with the previous results obtained by DLS (**Table 4.6)**, confirming the significant smaller size of mannose functionalized drug-loaded NLCs (**Figure 4.7D**). Importantly, the incorporation of mannose did not alter the spherical shape of the nanoparticlesaligning with the findings of Chae *et al.* [198]. Furthermore, no significant morphological differences were observed between blank (**Figure 4.7A and 4.7B**) and drug-loaded (**Figure 4.7C and 4.7D**) nanoparticles.

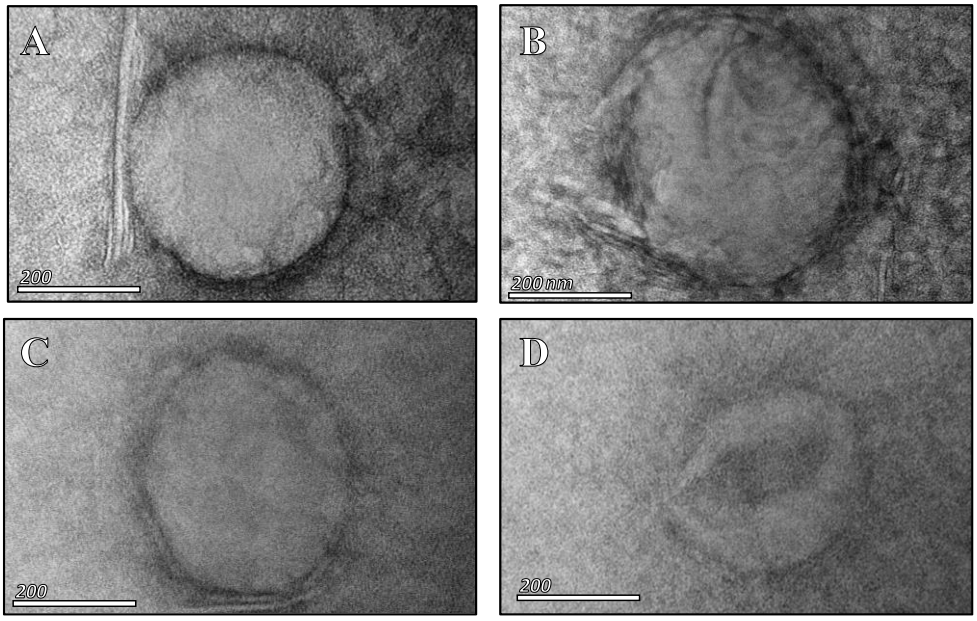


Figure 4.7. TEM images of (A) NLC, (B) NLC-MAN, (C) IND-NLC, and (D) IND-NLC-MAN formulations. Scale bar 200 μm.

USC DE COMPOSTELA

The spherical morphology depicted by the developed optimized nanoparticles together with the already described size (≈ 70 nm) provides suitable characteristics to achieve an efficient cell uptake. However, to ensure an adequate therapeutic response, the drug should not be leaked from the NLCs to the synovial fluid before being taken up by cells. The release of the drug to the general joint cavity would not guarantee the desired local effect to the inflamed synovial tissue. To test whether the developed nanoparticles would release the drug in this situation they were diluted in PBS at pH 7.4 and placed at 37°C under stirring over a 24-hour period. This time-point was selected based on the retention time reported for small size nanoparticles (7 nm) that showed a half-period of 29 hours [192].

Figure 4.8 illustrates the *in vitro* IND release profiles from IND-NLC and IND-NLC-MAN. The drug release data were analysed using various kinetic models, including zero-order, first-order, Higuchi, Hixon-Crowell, and Korsmeyer-Peppas models. The correlation coefficient (R^2) was used to assess the fit between each model and the experimental data [199]. The highest R^2 values were obtained for zero-order kinetics, entailing a constant release rate independent of the remaining concentration within the lipid matrix [199,200].

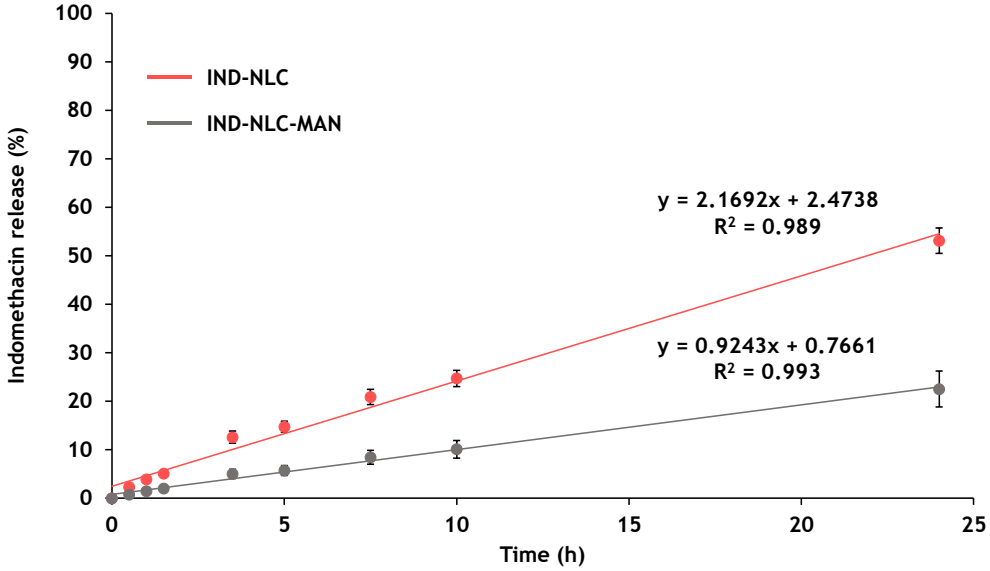


Figure 4.8. Drug release profiles for IND-NLC (red) and IND-NLC-MAN (grey) formulations in PBS (pH 7.4) at 37°C (n= 3 ± SD).

Moreover, the non-functionalized formulation (IND-NLC) exhibited a faster release profile than the functionalized one (IND-NLC-MAN). Approximately 53.1 ± 2.6% of the encapsulated IND was release within 24 hours from IND-NLC while only 22.5 ± 3.7% of the IND was released from IND-NLC-MAN in the same period. This difference in release rates can be primarily attributed to the presence of the mannose

coating. This coating likely acts as a diffusion barrier, hindering the release of the encapsulated IND. Additionally, the high affinity of IND for SA, which facilitates the previously confirmed smaller particle size, could play a contributory role in the slower release observed for this formulation [183,200]. The strong interaction between IND and SA within the NLCs matrix may further impede the release of the drug leading to the specific intracellular delivery.

4.1.5 Cell proliferation and internalization studies

The proliferation of fibroblasts (BALB/3T3A31) treated with the developed nanoparticles (NLC, NLC-MAN, IND-NLC, or IND-NLC-MAN) for 24 hours at different concentrations (300 μg/mL and 60 μg/mL) was assessed. Not treated cell monolayers were used as control and denoted as 0 μg/mL. Notably, all the tested formulations and free drug demonstrated high cytocompatibility at both tested concentrations, not showing statistically significant differences compared to the control (**Figure 4.9A**).

Similarly, the proliferation of macrophages (RAW 264.7) subjected to a 24-hour treatment with 300 μg/mL, 120 μg/mL or 60 μg/mL of the developed formulations was evaluated. Cell uptake was also analysed on macrophages using the same treatment conditions. As illustrated in **Figure 4.9B**, macrophages proliferation exhibited a decrease with increasing concentrations of NLCs and free drug. No significant differences were observed between the free drug (IND) and neither of the drug-loaded NLCs, IND-NLC or IND-NLC-MAN. However, a significant reduction in macrophage proliferation was evident after treatment with medium and high concentrations (120 μg/mL or 300 μg/mL) of the mannose-functionalized NLCs (NLC-MAN and IND-NLC-MAN). This phenomenon can be attributed to the enhanced internalization of these functionalized NLCs compared to non-functionalized counterparts, as demonstrated in **Figure 4.9C**. This observation aligns with the findings of Vieira *et al.*, who reported a similar reduction in cell proliferation following the treatment with functionalized NLCs (both unloaded and drug-loaded). The potential mechanism for this phenomenon associated with mannose-coated formulations is likely linked to their high interaction with the cell surface. Moreover, studies suggest that cationic nanoparticles, like these mannose-coated NLCs, can be more cytotoxic than those with negative or neutral charges due to their potential to damage cell membranes [73,193].

Additionally, macrophages were also treated with Interferon-gamma (IFN-γ; 10 ng/mL) to induce their differentiation towards the main phenotype implicated in OA inflammation, the pro-inflammatory phenotype. Stimulated macrophages were treated with the formulations as previously described for unstimulated cells to assess cell uptake. Nanoparticles showed high uptake efficiency with almost 100% of internalized

USC DE SANTIAGO DE COMPOSTELA

nanoparticles for all the formulations besides the NLC formulation. As for un-stimulated cells, mannose functionalization also led to an enhancement in NLCs uptake, especially for unloaded formulation (NLC-MAN) (**Figure 4.9D**).

Lastly, the NLCs uptake in fibroblasts was studied following the same protocol as for macrophages. The specificity of the NLCs to be internalized by IFN-γ macrophages was determined by calculating the uptake index (**Figure 4.9E**). This index is defined as the ratio between the percentage of internalized NLCs in IFN-γ macrophages and the percentage of internalized NLCs in fibroblasts. Uptake indexes over 1 indicates preferential uptake by macrophages compared to fibroblasts, suggesting their potential for targeted delivery to APCs. Conversely, an index of 1 suggests non-selective uptake, while a value below 1 indicates a higher internalization rate in fibroblasts compared to macrophages and limited targeting specificity towards macrophages. All formulations (functionalized and non-functionalized NLCs) exhibited high uptake index (>1) confirming macrophage targeting and internalization with no significant differences observed between formulations. This effect could be associated to the inherent higher uptake activity of pro-inflammatory macrophages when compared to fibroblasts.

USC
UNIVERSIDADE DE SANTIAGO DE COMPOSTELA

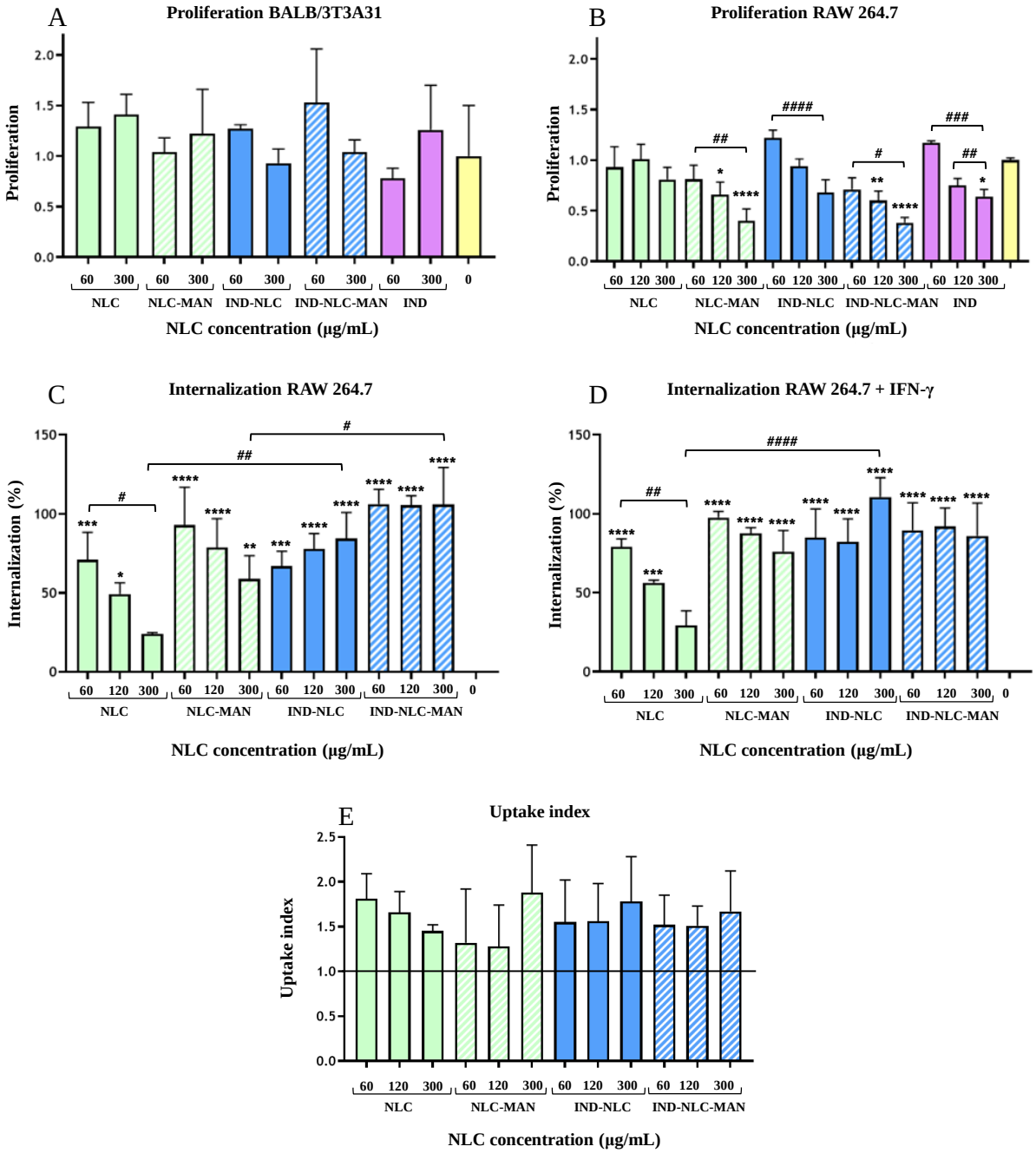


Figure 4.9. Cell proliferation and internalization results after the treatment with the developed systems or the free drug at equivalent concentration (IND) at different concentrations (300 µg/mL, 120 µg/mL, and 60 µg/mL). Untreated cells were used as a control (0 µg/mL). (A) Cell proliferation in BALB/3T3A31 cells, (B) Cell proliferation in RAW 264.7 cells, (C) Internalization in RAW 264.7 cells, (D) Internalization in RAW 264.7 cells stimulated with IFN-γ (10 ng/mL), and (E) Uptake index. Proliferation results were normalized vs. control. Values are mean ± SD of three independent studies. (*) Indicates differences compared to control (*$p < 0.05$, **$p < 0.01$, ***$p < 0.001$, ****$p < 0.0001$). (#) Indicates differences between samples ($^{\#}p < 0.05$, $^{\#\#}p < 0.01$, $^{\#\#\#}p < 0.001$, $^{\#\#\#\#}p < 0.0001$).

Confocal microscopy images were also taken to analyse the nanoparticles uptake. This analysis revealed qualitative aspects of NLCs internalization by macrophages. Macrophages were stimulated or not with IFN-γ and treated with the highest drug-loaded formulation concentration (300 μg/mL). Mannose-functionalized NLCs were specifically designed to depict enhanced uptake by APCs.

As mentioned, nanoparticles can enter cells through various pathways, including phagocytosis, receptor-mediated endocytosis, macropinocytosis, clathrin-dependent endocytosis, or caveolae-mediated endocytosis [188,201]. NLCs with a size below 100 nm (IND-NLC-MAN) are likely to be internalized via receptor-mediated endocytosis, while NLCs exceeding 200 nm are more likely to undergo phagocytosis [188]. Following internalization, the NLCs will traffic through cellular compartments. Initially, they will reside in the early endosome, where the pH progressively decreases. Upon reaching the late endosome (pH < 5.5), fusion with a lysosome occurs. Lysosomes contain a repertoire of acidic enzymes capable of degrading the NLCs, thereby releasing the encapsulated drug [202]. The inherent stability of IND at acidic pH ensures the preservation of its properties after release in the cytoplasm [203].

Confocal microscopy images confirmed the efficient uptake of both NLCs formulations by macrophages (**Figure 4.10**). Interestingly, the distribution of nanoparticles within the cell cytoplasm is different between unfunctionalized and mannose functionalized nanoparticles. While unfunctionalized systems show a homogenous distribution in the cell cytoplasm, mannose functionalized systems lead to particle aggregates with morphologies that could be associated to their incorporation in endocytic vesicles.

The distinct particle sizes between the functionalized (IND-NLC-MAN~70 nm) and non-functionalized (IND-NLC~250 nm) systems together with the mannose coating likely contribute to their different distribution associated to different internalization pathways. IND-NLC-MAN, due to its smaller size and mannose coating, is expected to be internalized via receptor-mediated endocytosis, potentially leading to clustering within endosomes. Conversely, the larger, non-functionalized IND-NLC might be internalized through phagocytosis, with some particles potentially undergoing degradation in lysosomes while others are released into the cytoplasm [204].

USC
UNIVERSIDADE DE SANTIAGO DE COMPOSTELA

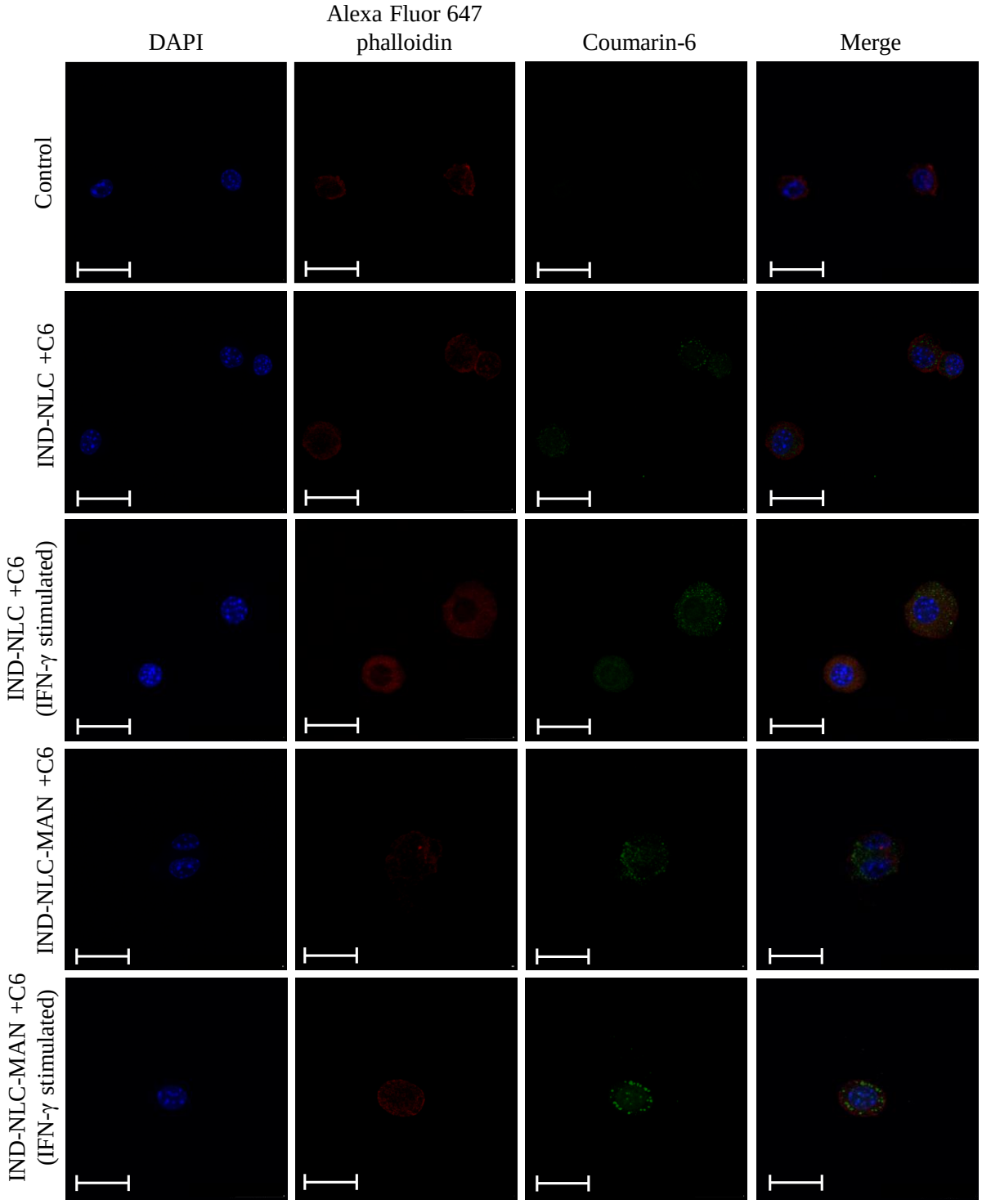


Figure 4.10. Confocal microscopy images of NLCs internalization by macrophages stimulated or not with IFN-γ and treated with the drug-loaded formulations (IND-NLC and IND-NLC-MAN). As control untreated cells were used. Cell cytoplasm is represented in red colour (Alexa Fluor 647 phalloidin), cell nuclei is represented in blue colour (DAPI), and NLCs (IND-NLC and IND-NLC-MAN) are represented in green colour (coumarin-6). Scale bar 20 μm.

USC
UNIVERSIDADE DE SANTIAGO DE COMPOSTELA

4.1.6 Anti-inflammatory activity

Activated THP-1 cells, stimulated with IFN-γ (10 ng/mL) were treated with, unloaded nanoparticles (NLC-MAN) (Control), drug loaded nanoparticles (IND-NLC and IND-NLC-MAN) and the equivalent free drug (IND) to evaluate their impact on cytokine secretion. Treatment duration (24 hours) and concentration (60 μg/mL) were stablished based on the previously described expected retention time within the joint cavity and the cell viability data. The secretion of pro-inflammatory cytokines (TNF-α, IL-6, and IL-8) and anti-inflammatory cytokines (IL-4 and IL-10) was assessed though a multiplex assay and normalized by the number of cells.

No significant differences were observed between the drug-loaded formulations (IND-NLC and IND-NLC-MAN) and free drug (IND) in the pro-inflammatory cytokines TNF-α and IL-6 secretion. However, a significant reduction in the secretion of the pro-inflammatory cytokines TNF-α and IL-8 was observed after the treatment with the functionalized and drug-loaded formulations (IND-NLC-MAN) or the free drug (IND) compared to control (**Figure 4.11A-B**). The same trend was observed in the secretion of IL-6 however, it did not reach statistical significance (**Figure 4.11C**). These findings suggest a potentially beneficial effect of the drug-loaded formulations indicating their suitability to encapsulate the drug (**Figure 4.11A-C**).

Additionally, we noted a significant increase in the secretion of IL-4, an anti-inflammatory cytokine, after the administration of the functionalized drug-loaded NLCs (IND-NLC-MAN) compared to the free drug (IND) (**Figure 4.11E**). Despite, no differences were observed in IL-10 secretion after the treatment with the drug-loaded formulations (**Figure 4.11D**) these findings indicate that the developed drug-loaded NLCs are effective in encapsulating the drug and, additionally, may modulate the inflammatory response (**Figure 4.11D-E**).

Despite several immune cells are implicated in tissue inflammation in OA, macrophages stand out by their implications in inflammation initiation and resolution [205]. The depletion of macrophages has been demonstrated to decrease cartilage degradation in OA [206]. Macrophages are known to depict two main phenotypes also known as pro-inflammatory phenotypes or M1 and anti-inflammatory phenotype or M2. The first ones are characterized by the secretion of pro-inflammatory cytokines exacerbating the already stablished inflammation and inducing the degradation of the extracellular matrix. On the other hand, M2 cells secrete anti-inflammatory cytokines with pro-regenerative effects [207].

USC UNIVERSIDADE DE SANTIAGO DE COMPOSTELA

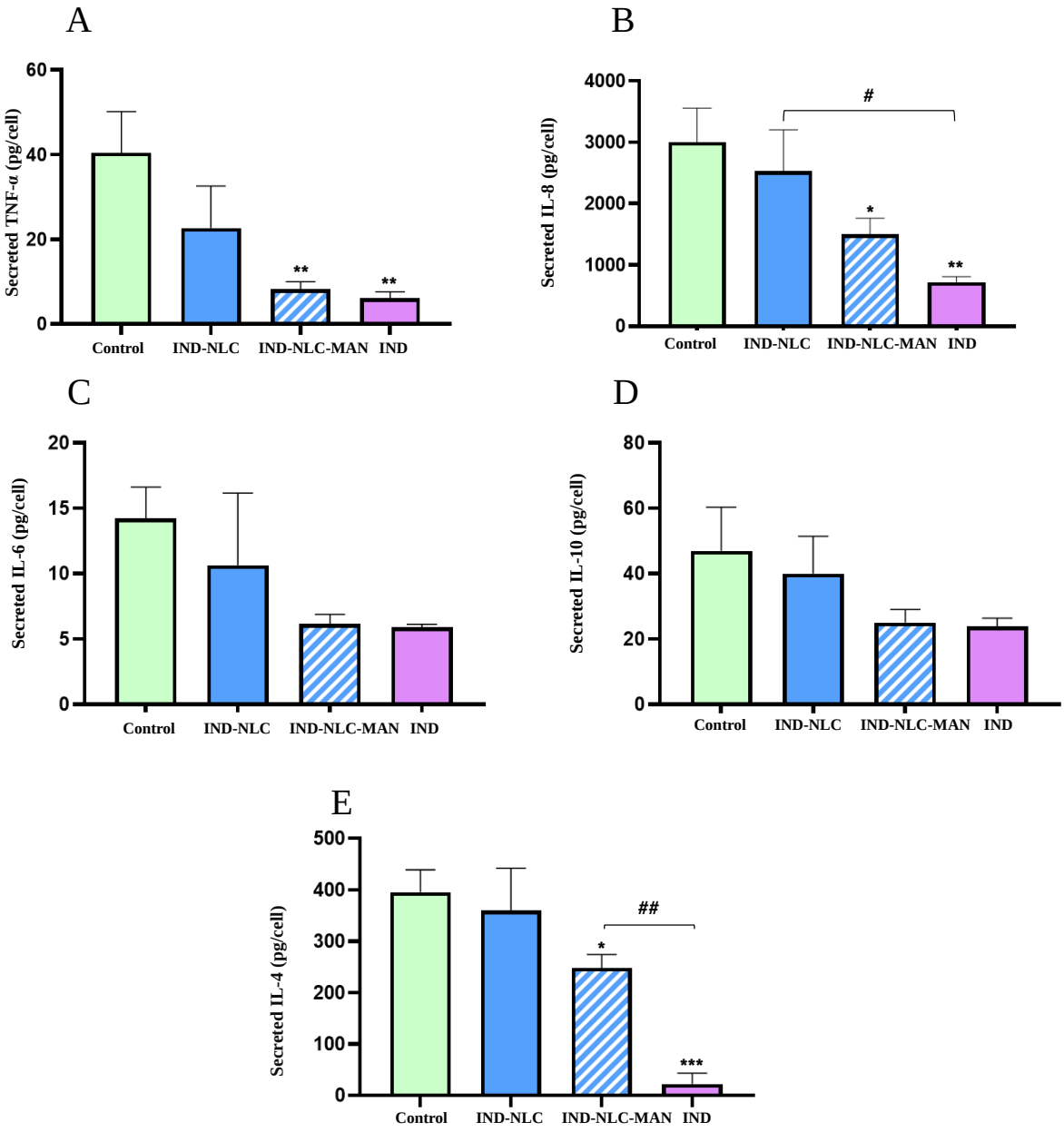


Figure 4.11. Release of pro-inflammatory (TNF-α, IL-6, and IL-8) and anti-inflammatory (IL-4 and IL-10) cytokines after the treatment with the developed systems (IND-NLC and IND-NLC-MAN) or the free drug (IND). NLC-MAN was used as control. (A) Secreted TNF-α, (B) secreted IL-8, (C) secreted IL-6, (D) secreted IL-10, and (E) secreted IL-4. Values are mean ± SD of three independent studies. (*) Indicates differences compared to control (*$p < 0.05$, **$p < 0.01$, ***$p < 0.001$). (#) Indicates differences between the indicated samples ($^{\#}p < 0.05$, $^{\#\#}p < 0.01$).

Low doses of IND have been described to be beneficial in decreasing cartilage damage in OA, associated to an anti-inflammatory effect [208]. However, the effect of this drug in tissue healing is controversial as for any other non-steroidal anti-inflammatory drug

USC
UNIVERSIDADE DE SANTIAGO DE COMPOSTELA

(NSAIDs) [209]. Therefore, to avoid any undesirable effects, IND-loaded NLCs were successfully functionalized with mannose to allow their targeting to APCs. The developed nanoparticles showed an efficient and specific uptake by pro-inflammatory macrophages. Moreover, this strategy shows a similar anti-inflammatory effect than the free drug while avoiding undesirable effects. Remarkably, the developed IND-NLC-MAN shows an enhancement in IL-4 secretion compared to the free-drug that could be beneficial for a pro-regenerative effect. This effect could be associated to the presence of the mannose coating as CD206 ligands has been reported to induce the differentiation of macrophages towards M2 phenotype [210].

USC
UNIVERSIDADE DE SANTIAGO DE COMPOSTELA

4.2 LIPID-POLYMER HYBRID NANOPARTICLES LOADED WITH IL-4 TO MODULATE MACROPHAGE PHENOTYPE

As already mentioned, recent studies pointed out the important role of inflammation in OA progression [128,211]. The degenerative process of OA is enhanced by the release of pro-inflammatory cytokines such as interleukin-1 (IL-1), interleukin-6 (IL-6), and tumour necrosis factor-α (TNF-α) to the synovial membrane that simultaneously led to a further enhanced synovial inflammation. Under this self-perpetuating cycle, a catabolic-anabolic imbalance is established making tissue repair more challenging [211].

Macrophages, the most prevalent cells in the synovial membrane, present a high potential for immunomodulation and inflammation control[5,212]. They can modify their phenotype in response to changes in the microenvironment. These cells adopt a pro-inflammatory secretory phenotype when exposed to pro-inflammatory cytokines leading to increased local inflammation [115]. By contrast, they can depict an anti-inflammatory secretory phenotype when exposed to anti-inflammatory cytokines [115]. OA is characterized by an increase in the proportion of pro-inflammatory macrophages over anti-inflammatory cells directly correlated with synovitis and disease severity [213,214]. Therefore, the phenotype modulation of pro-inflammatory macrophages towards an anti-inflammatory phenotype could be an strategy to control inflammation and pathology progression [116,215].

IL-4 is an immunomodulatory cytokine showing capacity to induce an anti-inflammatory response in pro-inflammatory macrophages [216,217]. Therefore, its administration could generate an anti-inflammatory response while blocking the inflammatory phenotype [216–218]. However, this protein shows short half-life and no vectorization capacity to specific cells [219].

In this context, the use of lipid-polymer hybrid NPs (LPNPs) as delivery systems for biomolecules have proved to enhance the stability of the encapsulated therapeutic molecules while ensuring adequate activity [135]. Furthermore, their surface can be functionalized with targeting moieties to interact exclusively with the desired cells and tissues [167].

Based on the previously described information, lipid-polymer hybrid NPs loaded with IL-4 have been proposed as a potential delivery system to modulate macrophage phenotype, thereby reducing OA progression.

USC UNIVERSIDADE DE SANTIAGO DE COMPOSTELA

4.2.1 Effect of the studied variables on hybrid nanoparticles properties

Table 4.8 shows the properties of the developed BSA-LPNP for the four studied parameters (Size, PDI, ZP, and AE). All LPNPs presented small particle sizes (size < 300 nm), variable size distributions (0.2 – 0.4), and negative surface charges (ZP < -20 mV). In addition, a wide range of AE have been obtained, with percentages ranging from 55% to 100%.

Table 4.8. Experimental values for the BSA-loaded NPs (BSA-LPNP) (n= 3 ± SD).

Formulation	Size (nm)	PDI	ZP (mV)	AE (%)
BSA-LPNP1	214.8 ± 22.6	0.4 ± 0.01	-20.9 ± 3.4	> 99.0
BSA-LPNP2	179.7 ± 13.6	0.3 ± 0.03	-23.6 ± 1.0	> 99.0
BSA-LPNP3	172.9 ± 10.0	0.2 ± 0.02	-24.5 ± 1.1	> 99.0
BSA-LPNP4	241.2 ± 50.8	0.4 ± 0.03	-21.2 ± 1.7	> 99.0
BSA-LPNP5	187.2 ± 21.0	0.3 ± 0.03	-22.2 ± 3.4	74.8 ± 9.5
BSA-LPNP6	179.4 ± 8.1	0.4 ± 0.05	-19.5 ± 7.0	80.3 ± 39.3
BSA-LPNP7	222.6 ± 101.0	0.4 ± 0.02	-21.8 ± 0.6	59.6 ± 16.0
BSA-LPNP8	273.8 ± 14.4	0.3 ± 0.08	-23.7 ± 0.9	54.5 ± 14.8

Despite of the small number of formulations, the software successfully modelled the database (**Table 4.8**) with high predictability (R^2 > 80%) and accuracy for all the characteristics (Size, PDI, ZP, and AE). The inputs selected by the model to explain the variability of the different outputs, together with the model quality parameters are shown in **Table 4.9**. The complete set of rules (*IF-THEN* Rules) can be found at Annex 2 (Table S1).

Table 4.9. Inputs and submodels selected by FormRules for the different outputs and models quality parameters. The most relevant submodels affecting each output are bolded.

Output	Submodel	Inputs from FormRules	R^2	Computed *f* value	ANOVA freedom degrees	*α*
Particle size (nm)	**1**	**BSA x PLGA**	98.39	10.20	6 and 1	0.01
PDI	**1**	**PLGA**	86.77	8.74	3 and 4	0.05
	2	BSA				
ZP (mV)	**1**	**PLGA**	80.44	10.28	2 and 5	0.05
AE (%)	**1**	**BSA**	85.85	8.09	3 and 4	0.05
	2	PLGA				

The LPNPs particle size is influenced by the interaction between the employed amount of PLGA and the concentration of BSA. Largest particles were obtained when high polymer amounts (5 mg) together with high BSA concentrations were used, resulting in particles reaching 273.8 ± 14.4 nm, in accordance with the established rules (Annex 2, Rule 6 Table 1S).

USC UNIVERSIDADE DE SANTIAGO DE COMPOSTELA

Moreover, not all the obtained LPNPs demonstrated uniform size distributions. High BSA loads and particularly, the combination of these high loads with low PLGA percentages (Annex 2, Rules 7 and 10, Table 1S) result in PDI values higher than 0.3, the threshold for homogeneous particle size distributions [162].

Surface charge serves as an indicator of colloidal stability and is typically assessed by measuring ZP. All the developed formulations exhibited negative ZP values (ZP ≈ -20 mV). Although these values fall below the ideal threshold, the stability is not compromised as the hydrophilic PEG shell present on the LPNPs will provide high colloidal stability through steric repulsion [220]. As expected, formulations containing higher amounts of PLGA, regardless of the BSA concentration, displayed even more negative surface charges (Rule 12 Table 1S) (**Figure 4.12**). This fact can be attributed to the inherent negative charge of the polymer.

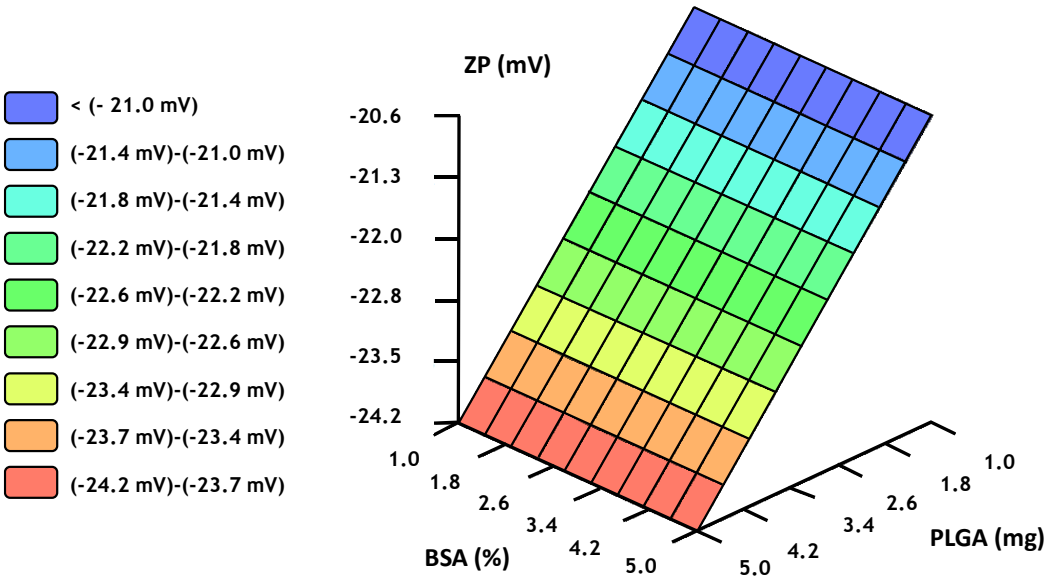


Figure 4.12. Predicted values by FormRules for surface charge (ZP) as a function of BSA and PLGA.

Nearly all the developed systems exhibited a remarkable high protein load, with AEs exceeding 99% as detailed in **Table 4.8**. However, formulations containing 5% BSA demonstrated a slightly lower AE, as indicated by Rule 14 in Annex 2 Table S1.

Based on the characteristics of BSA-loaded NPs, BSA-LPNP2 formulation (highlighted in grey in **Table 4.8**), consisting of 1% BSA and 3 mg of PLGA, was selected among the potential candidates for the preparation of IL-4-loaded NPs. This composition exhibited favourable physicochemical properties, including a small and uniform size (179.7 ± 13.6 nm and PDI of 0.3 ± 0.03, respectively), high AE (> 99%), and a high negative zeta potential (-23.6 ± 1.0 mV).

USC UNIVERSIDADE DE SANTIAGO DE COMPOSTELA

4.2.2 Characterization of the obtained IL-4-LPNPs

Lipid-polymer hybrid NPs where then loaded with the anti-inflammatory cytokine IL-4 and developed under the specific conditions outlined in the preceding paragraph. The results for particle size and ZP of both, unloaded and IL4-loaded LPNPs as well as non-functionalized and mannose-functionalized particles (LPNP, LPNP-MAN, IL-4-LPNP, and IL-4-LPNP-MAN), are presented in **Figure 4.13**. The physicochemical properties of the obtained LPNP, LPNP-MAN, IL-4-LPNP, and IL-4-LPNP-MAN (particle size and ZP) are presented in **Figure 4.13**. In agreement with our previous data and similar works, all the formulations exhibited a mean particle size around 150 nm being all within the 129.5 nm - 153.3 nm range. Moreover, the obtained systems show narrow particle size distributions (PDI < 0.3) and ZP lower than -18.5 mV, with no statistically significant differences between them[70,167].

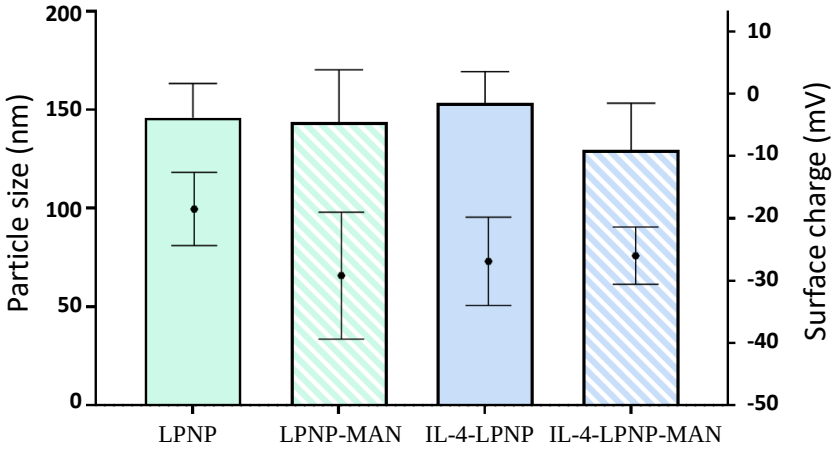


Figure 4.13. Mean particle size (bars & left Y axis) and ZP values (black points & right Y axis) for the obtained LPNPs (n= 3 ± SD).

No IL-4 was detected on the filtrate of the NPs dispersions during purification, indicating the complete incorporation of the protein. The same behaviour was found for both non-functionalized and mannose-functionalized formulations (IL-4-LPNP and IL-4-LPNP-MAN). Therefore, the selected conditions were suitable for IL-4 encapsulation.

Furthermore, IL-4 release studies were conducted over a 24-hour period. This time-point was settle based on the time macrophages require for LPNPs uptake and the retention time in the joint cavity (half-life 29 hours for 7 nm NPs) [192]. The obtained results indicate no leaking of the protein from the developed LPNPs ensuring its stability and specific effect on the cells after NPs uptake. However, it was observed that non-functionalized formulations (IL-4-LPNP) exhibit a faster protein release (0.65 ± 0.23%) than functionalized formulations (IL-4-LPNP-MAN) (0.18 ± 0.07%) in the same period.

USC DE COMPOSTELA

As already anticipated based on the data in NLCs (section *4.2*), and as previously reported by Vieira *et al*. this difference in release rates can be attributed to the presence of mannose coating [193].

The functionalization capacity of the LPNPs was determined by quantifying the non-incorporated 2-AA labelled mannose. The developed systems were effectively functionalized with mannose, achieving a functionalization efficiency of 99.5 ± 8.4% for LPNP-MAN. This parameter is usually not studied for the mannose functionalization of NPs, limiting the discussion with current literature. However, the efficiency of mannose functionalization of LPNPs was significantly higher than the values achieved for NLCs (section *4.2*) despite a much lower amino: mannose ratio was used in this case. These differences can be attributed to a different distribution of the reactive moieties. The incorporation of the amino group to the lipid shell using a PEG linker will allow for a higher NH_2 groups availability while in the case of NLCs the amino groups provided by stearylamine are evenly distributed in the lipid matrix. Additionally, the obtained functionalization efficiency was also higher than those previously reported for aptamers and antibodies using similar LPNPs [167].

4.2.3 Fluorescence cross-correlation spectroscopy

The FCCS technique can offer insight into the structure of core-shell NPs by detecting molecular movements and interactions through fluctuations in fluorescently labelled molecules [221,222]. This can be achieved by labelling the core with one fluorophore, in our case DiD´ and the shell with another fluorophore, in our case using a commercially lipid-ATTO 488. The diffusion of these molecules (fluorophores) generates single signals, known as auto-correlation curves, in two distinct channels. Green auto-correlation curves (G_G) describe the single dynamics of the fluorescently labelled polymeric cores, while red auto-correlation curves (G_R) describe the single dynamics of the fluorescently labelled lipid shells (**Figure 4.14A** and **Figure 4.14B**, respectively). When both dyes diffuse together through the confocal volume, both signals are co-localized obtaining a cross-correlation curve (G_X) (**Figure 4.14C**) indicating their co-localization or binding [169,221].

USC UNIVERSIDADE DE SANTIAGO DE COMPOSTELA

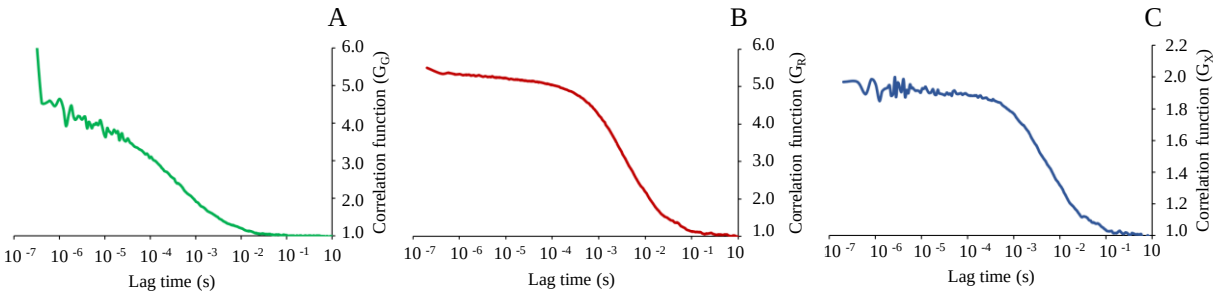


Figure 4.14. Fluorescent auto-correlation and cross-correlation curves for LPNPs formulations. (A) Auto-correlation curve for the polymeric core labelled with DiD´, (B) auto-correlation curve for the lipid shell labelled with DOPE-ATTO 488, (C) cross-correlation curve obtained for the core-shell structure of the LPNPs.

A high cross-correlation ($G_X \approx 1.8$) was observed confirming the desired core-shell structure of the developed NPs. This technique has been recently employed to characterize the core-shell structure of lipid-polycation-nuclei acid NPs, as well as the structure of lipoplexes and EVs-membrane coated polymeric cores [169,221,222]. However, to the best of our knowledge, this is the first time this technique has been employed to characterize the core-shell structure of lipid-polymer hybrid NPs. The confirmation of the NPs structure is crucial to understand their interaction with cells and tissue. Therefore, this technique is a powerful tool in the characterization of complex NPs for biomedical applications.

Moreover, we have proven that FCCS can be employed to determine the structure of mannose-coated formulations. To this end, mannose was labelled with ATTO 488. To confirm the correct labelling of the targeting ligand, proton nuclear magnetic resonance spectroscopy analysis (^{1}H-NMR) was performed. **Figure 4.15** illustrates the reaction product obtained after the reaction of mannose with amino-modified ATTO 488 through the Maillard reaction. The spectrum displays the characteristic peaks corresponding to mannose (light blue) and the resulting product (red), obtained through the formation of the Schiff´s base (-N=CH-). This covalent bonding was formed by the reaction between the aldehyde group of mannose and the amino group located in the aliphatic chain of the fluorophore, thus confirming the correct labelling.

USC
UNIVERSIDADE DE SANTIAGO DE COMPOSTELA

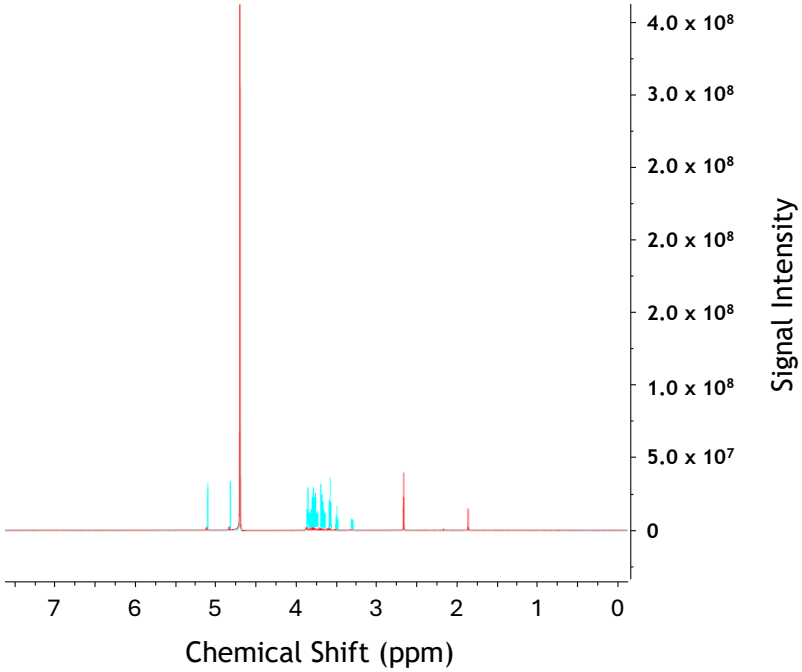


Figure 4.15. ^{1}H NMR spectrum of D-(+)-Mannose (light blue spectrum) overlapped with the product derived from the Maillard reaction to fluorescently label mannose with an amino-modified ATTO 488 (red spectrum).

FCCS was afterwards performed by labelling the polymeric cores with DiD´ and functionalizing the LPNPs with the developed ATTO 488-labelled mannose. Therefore, green auto-correlation curves (G_G) describe the single dynamics of the fluorescently labelled polymeric cores, while red auto-correlation curves (G_R) describe the single dynamics of the ATTO 488 labelled mannose (**Figure 4.16A** and **Figure 4.16B**, respectively). A positive cross-correlation curve ($G_X \approx 1.2$) was obtained for those mannose-functionalized LPNPs (**Figure 4.16C**) confirming the correct mannose-functionalization. This is the first time that this technique is employed to characterize the surface coating of LPNPs.

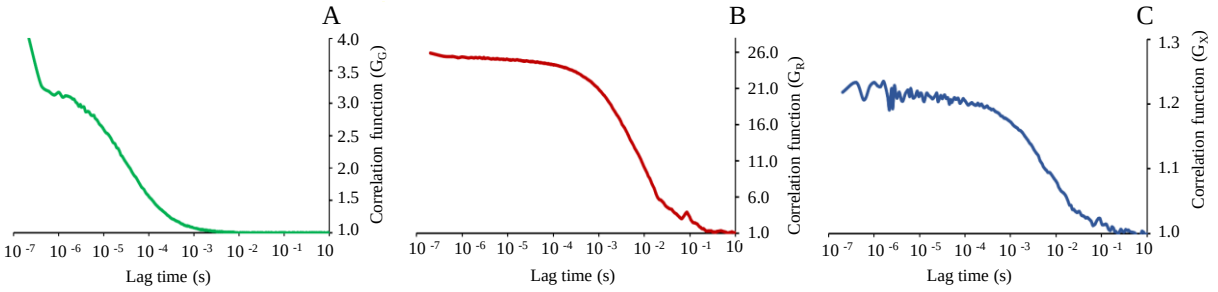


Figure 4.16. Fluorescent auto-correlation and cross-correlation curves for LPNP-MAN formulations. (A) auto-correlation curve for the polymeric core labelled with DiD´, (B) auto-correlation curve for the fluorescently labelled mannose with ATTO 488, and (C) cross-correlation curve obtained for the LPNP-MAN.

USC UNIVERSIDADE DE SANTIAGO DE COMPOSTELA

4.2.4 Cell viability

Figure 4.17 displays the cell viability data for both cell lines treated with the developed formulations at a concentration of 30 μg/mL. Despite two more concentrations were tested (12 μg/mL and 6 μg/mL), this figure exclusively showcases the proliferation response at the highest concentration as no toxic effects were observed at any concentration as previously observed for other mannose-coated NPs [223,224]. However, the higher concentration, 30 μg/mL, shows a significant induction of cell viability over the control which ultimately means an enhancement on cell proliferation and/or metabolic activity. This latter effect is derived from the technique selected to study cell viability that is based on the capacity of the cells to reduce the AlamarBlue reagent. Indeed, this reagent has also been used to determine cell metabolism [225].

Despite similar effects were observed in fibroblasts and macrophages, a more pronounced outcome could be observed on the last ones (**Figure 4.17A** and **Figure 4.17B**). Additionally, significant differences in macrophage proliferation/metabolic activity were observed between mannose functionalized formulations containing or not IL-4 (IL-4-LPNP-MAN vs LPNP-MAN). Greater proliferation/metabolic activity values were obtained for protein-loaded formulations (1.63 ± 0.11) compared to blank formulations (1.41 ± 0.03) (**Figure 4.17A**). These LPNPs are intended to directly deliver the encapsulated protein in cell cytoplasm. Once in the cell cytoplasm, the encapsulated protein will be released. The intracellular delivery of IL-4, a pro-regenerative and anti-inflammatory molecule, could either induce the cell proliferation and/or modulate metabolic activity [216,217]. These pro-proliferative effects of IL-4 have been previously proven in fibroblasts and macrophages and could explain the obtained results [226,227].

On the other hand, the increase in proliferation/metabolic activity in cells treated with unloaded NPs can be attributed to the presence of biodegradable particles. When macrophages come into contact with biodegradable particles, they secrete acids that modify the degradation of these particles, potentially accelerating it [228]. In this situation, cell homeostasis may be altered, which may affect cell metabolic activity as reflected in **Figure 4.17A**. In our work, this effect has been observed not only in macrophages, but also in fibroblasts (**Figure 4.17B**).

USC UNIVERSIDADE DE SANTIAGO DE COMPOSTELA

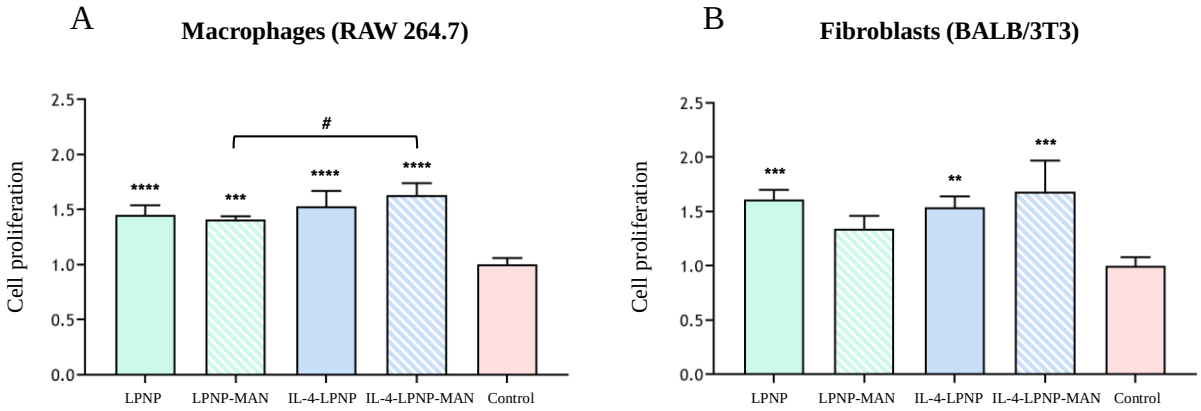


Figure 4.17. Cell proliferation results after the treatment with 30 μg/mL of LPNPs. Proliferation results were normalized vs. control (untreated cells). Results are expressed as mean ± SD of four well per condition. (*) Indicates statistically significant differences compared to control (**p < 0.01, ***p < 0.001, ****p < 0.0001). (#) Indicates statistically significant differences between formulations ($^{\#}p < 0.05$).

4.2.5 Cell uptake

NPs exhibit different routes for cellular internalization, involving phagocytosis, macropinocytosis, receptor-mediated endocytosis, clathrin-dependent endocytosis, or caveolae-mediated endocytosis [188,201]. After uptake, NPs undergo several intracellular processes. Initially, the phagosome fuses with the early endosome, which can be identified by the presence of proteins such as Rab5 [229]. Within the early endosomes, the pH gradually decreases due to the activity of proton pumps, particularly vacuolar ATPases. This acidification continues until the late endosome (pH < 5.5). Finally, fusion occurs between the late endosome and a lysosome [202]. Proteins loaded in NPs would be degraded in the lysosomes acidic medium, losing their therapeutic activity.

To avoid protein degradation and ensure effective delivery of their payload, protein-loaded NPs should show either fusogenic behaviour, that is, instead of suffering the above-mentioned process they fuse with the cell membrane or depict endosomal escape features. Particle size is recognized to play a critical role in the mechanisms of internalization within macrophages. However, not only particle size plays an important role, but also surface charge, lipid composition or surface modifications [197]. Therefore, the fusogenic behaviour of the developed NPs can be achieved tailoring the lipid composition and the use of PEGylated lipids. Previous studies indicate that PEGylated lipids play a significant role in conferring this fusogenic behaviour [204]. Additionally, several strategies can be followed to allow for endosomal escape as the proton sponge effect, the osmotic lysis, the sweeling of the endosome, the endosome membrane disruption or fusion and the interaction with the endosome membrane [230].

USC UNIVERSIDADE DE SANTIAGO DE COMPOSTELA

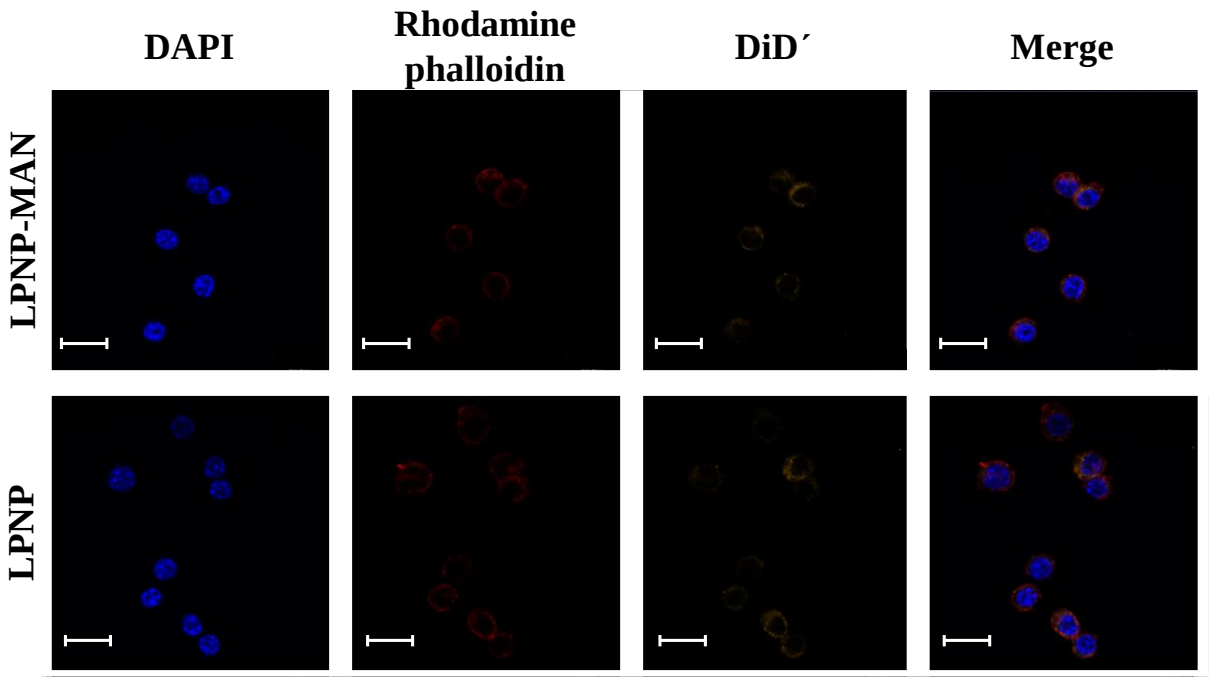


Figure 4.18. Confocal microscopy images showing distribution of developed NPs within macrophages. Nuclei stained with DAPI (blue), cytoplasm with rhodamine phalloidin (red), and polymeric cores with DiD´(yellow). Scale bar 20 μm.

Figure 4.18 shows the intracellular distribution of both LPNP and LPNP-MAN. LPNPs were fluorescently labelled with DiD´ and cytoplasm was stained with rhodamine phalloidin. Numerous LPNPs (yellow) were distributed within the cytoplasm of macrophages, as evidenced by the co-localization of the rhodamine phalloidin and DiD´ fluorophores indicating adequate uptake. However, as depicted in **Figure 4.19**, functionalized and non-functionalized LPNPs (yellow) can be found within early endosomes, as indicated by the co-localization of the Alexa fluor 594 and DiD´. Interestingly, higher co-localization was observed for LPNP-MAN. These findings indicate that, despite incorporating fusogenic components, the developed LPNPs are internalized by endocytosis. This outcome could be associated with the presence of the mannose on the surface of the LPNPs that could induce a receptor-mediated endocytosis.

Nevertheless, the incorporation of PLGA in the LPNPs will lead to the endosomal escape of the systems before fusion with the lysosome through the selective inversion of the LPNPs surface charge. This effect is achieved by the change in charge of PLGA from anionic to cationic as the pH of the endosome decreases, leading to a high interaction with the endosomal membrane and their escape through translocation into the cytosol, where the encapsulated protein will be subsequently released [231].

USC UNIVERSIDADE DE SANTIAGO DE COMPOSTELA

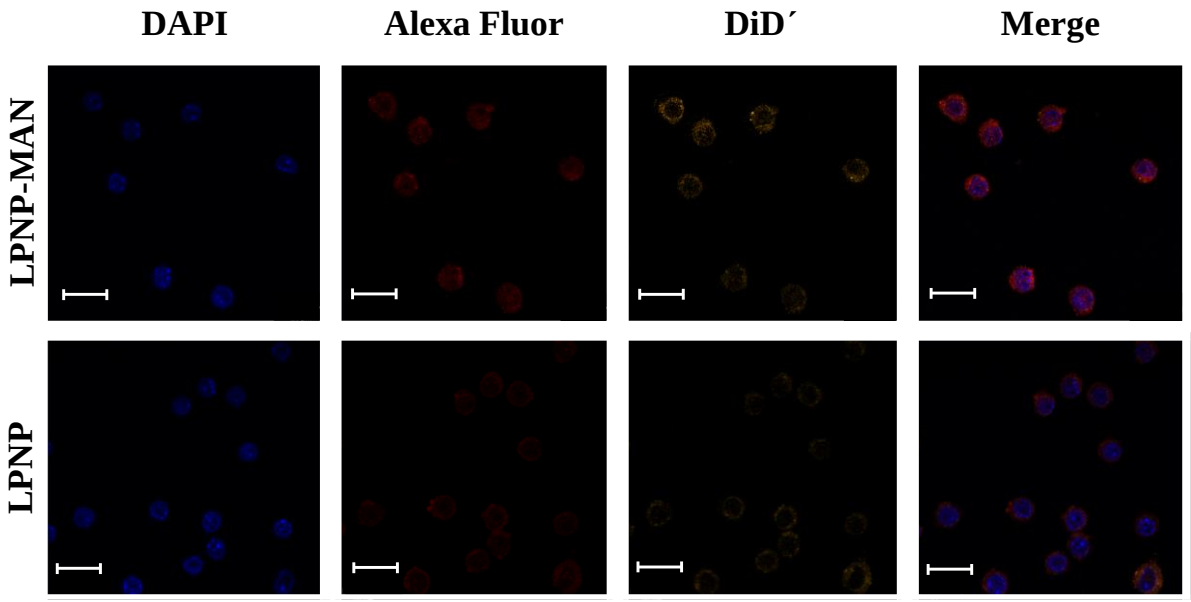


Figure 4.19 Confocal microscopy images showing distribution of developed LPNPs within the macrophages. Nuclei stained with DAPI (blue), cell endosomes with Alexa Fluor 594 (red), and polymeric cores with DiD´ (yellow). Scale bar, 20 μm.

4.2.6 Anti-inflammatory activity

To analyse the effect of the developed LPNP-MAN and IL-4-LPNP-MAN formulations on modulating LPS stimulated macrophages phenotype, the secretion of pro-inflammatory (IL-6, IL-8, and TNF-α) and anti-inflammatory cytokines (IL-10) was analysed. During OA, there is an increase in the levels of pro-inflammatory cytokines in the synovial fluid associated to a higher population of pro-inflammatory macrophages [232]. TNF-α is a pro-inflammatory cytokine secreted by stimulated macrophages that induces the extracellular matrix (ECM) degradation. In addition, cytokines such as IL-6 or IL-8 also contribute to cartilage damage [232,233]. On the other hand, IL-10 is an anti-inflammatory cytokine secreted by macrophages presenting an anti-inflammatory phenotype (M2), thus promoting cartilage repair [234].

As expected, no statistically significant differences in cytokine secretion, were observed between the control group (untreated and stimulated macrophages) and macrophages treated with unloaded nanoparticles (LPNP-MAN), as depicted in **Figure 4.20**. In contrast, after the treatment with the IL-4 loaded NPs (IL-4-LPNP-MAN) a statistically significant reduction was observed in the secretion of IL-8 (**Figure 4.20B**). The same trend was followed for the other pro-inflammatory cytokines, TNF-α and IL-6, although not statistically significant differences were observed in these cases (**Figures 4.20A** and **Figure 4.20C**). Simultaneously, a statistically significant increase in IL-10 secretion compared to the control group was observed (**Figure 4.20D**). This finding suggests that the treatment with IL-4-LPNP-MAN can induce an anti-inflammatory response. Interestingly, as previously observed in section *4.1*, the presence of mannose on the NPs

surface could also suggest a beneficial effect on promoting anti-inflammatory macrophages observing higher effects on IL-10 secretion induction than pure IL-4 treatment at the same concentration and time-point on LPS-stimulated THP-1 [235].

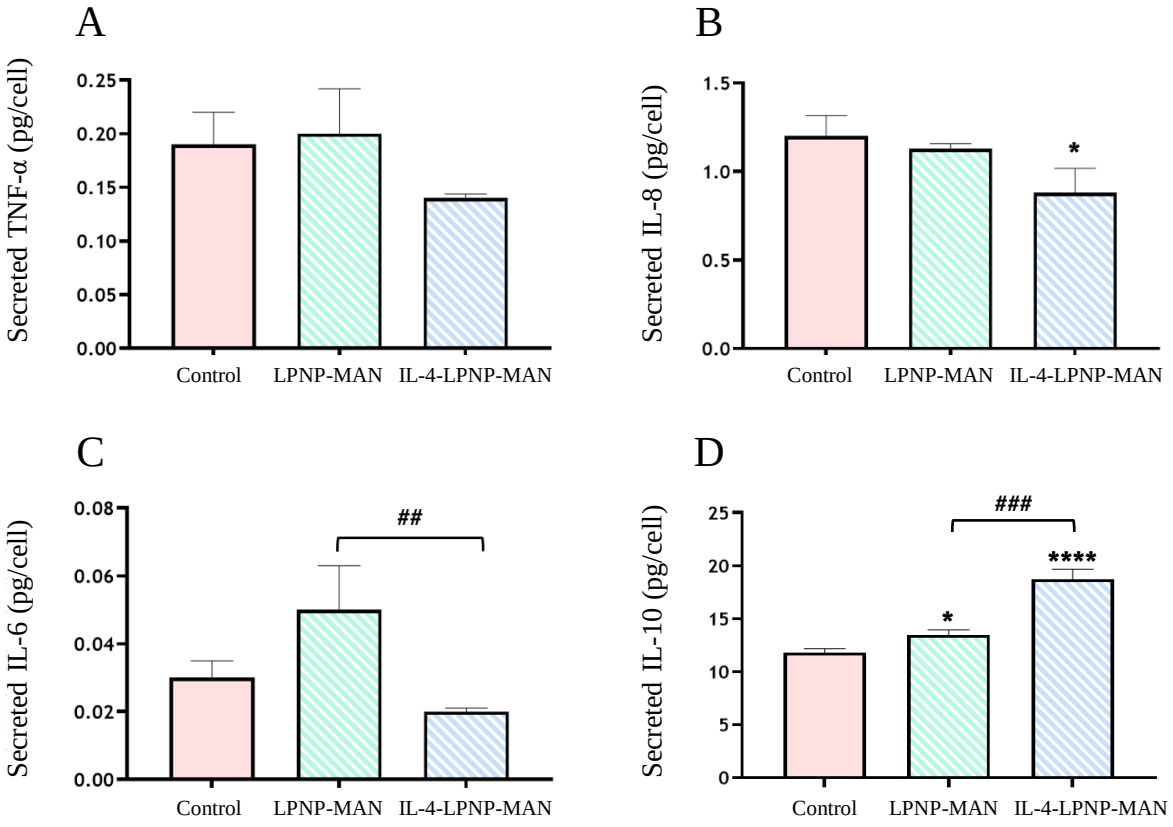


Figure 4.20. Secreted pro-inflammatory (A) TNF-α (B) IL-8, and (C) IL-6 and anti-inflammatory (D) IL-10 cytokines by macrophages (THP-1) displaying a pro-inflammatory phenotype (stimulated with LPS at 100 ng/mL) after being treated with the developed nanoparticles (LPNP-MAN and IL-4-LPNP-MAN) (30 μg/mL). Control cells were stimulated with LPS but not treated with LPNPs. Results are expressed as mean ± SD of three wells per condition (*) Indicates statistically significant differences in secreted cytokines compared to control (*$p < 0.05$, ****$p < 0.0001$). (#) Indicates statistically significant differences in secreted cytokines between formulations ($^{\#\#}p < 0.01$, $^{\#\#\#}p < 0.001$).

The developed LPNPs, depicting the desired core-shell structure, were successfully internalized by macrophages showed capacity to modulate the phenotype of pro-inflammatory macrophages. IL-8 is one of the major pro-inflammatory cytokines in OA, directly associated with clinical severity, and responsible for mediating the secretion of matrix degradative enzymes and hypertrophy in osteoarthritic chondrocytes [236]. On the other hand, IL-10 have proven protective effects on osteoarthritic cartilage inducing an increase in the synthesis of cartilage ECM components as glycosaminoglycans [237]. Therefore, these systems able to decrease IL-8 and increase IL-10 secretion, show a high

potential to slower the disease progression by controlling synovitis and macrophages paracrine signalling towards the recovery of the healthy tissue homeostasis. Therefore, they could represent a new type of disease modifying therapeutic strategies centred on modulating synovial macrophages.

.

USC
UNIVERSIDADE DE SANTIAGO DE COMPOSTELA

4.3 DESIGN AND EVALUATION OF SENOLYTIC LOADED MICROSPHERES

To date, there are not available disease modifying drugs able to restore cartilage damage in osteoarthritis. Cartilage degradation can be modified and reduced by eliminating senescent cells and promoting autophagy to restore tissue homeostasis [114]. Autophagy is an essential process for cellular homeostasis. It is characterized by the autophagosomes formation where cells can degrade and recycle damaged or dysfunctional macromolecules [238,239]. Autophagy appears to be crucial for cellular integrity, function, and survival maintenance [238]. However, it is well known that age-related diseases such as OA are characterized by a deficient autophagy capacity [114].

Furthermore, age-related diseases are also characterized by accumulation of senescent cells [114]. Senescence is a cellular aging process characterized by the permanent arrest of cell division and the secretion of pro-inflammatory cytokines and ECM degradative enzymes, which contribute to tissue degradation and thus to OA development [114].

In this context, the use of senotherapeutics, that decrease or control senescent cells, may be a good strategy for controlling OA progression. However, the fast drug clearance due to quick turnover rate of the synovial fluid limits its therapeutic potential for IA injections. In this situation, the development of drug delivery systems such as polymeric microspheres, well known for their biocompatible and biodegradable properties, could keep the senotherapeutic agent within the joint while offering localized therapeutic benefits.

Nevertheless, the lack of general protocols for producing polymeric microspheres, makes their design and development a complex task. In this perspective, artificial intelligence tools will be used to identify and understand the role of the involved variables to design senotherapeutic-loaded microspheres with the desired characteristics.

4.3.1 Effect of the studied variables on microspheres properties

Table 4.10 shows the results of the experimental design for the four parameters studied (mean particle size, uniformity, encapsulation efficiency, and drug loading). Microspheres were always obtained within the established limits of the design space, but they presented variable mean particle sizes, in the range 17.22 µm - 827.60 µm, and disparate distributions (uniformity range 0.21 - 1.19). Variations in the manufacturing procedure also had an impact on the drug incorporation into the microspheres, as reflected in the EE values (e.g. M10 EE = 47.82%).

USC UNIVERSIDADE DE SANTIAGO DE COMPOSTELA

Table 4.10. Experimental values for the studied parameters.

Sample	Mean particle size (µm)	Uniformity	EE (%)	DL (%)
M01	369.72	0.58	59.00	0.56
M02	26.52	0.33	91.05	1.98
M03	21.25	0.26	-	-
M04	193.38	0.63	89.06	1.29
M05	22.33	0.39	-	-
M06	45.53	0.27	104.83	2.08
M07	20.69	0.25	100.41	1.10
M08	431.93	0.57	-	-
M09	33.00	0.25	95.94	2.25
M10	26.22	0.97	46.95	0.47
M11	173.77	0.45	-	-
M12	24.72	0.26	101.22	1.90
M13	33.31	0.50	78.47	1.35
M14	827.60	0.28	95.28	0.85
M15	22.60	0.73	-	-
M16	19.38	0.27	102.35	0.97
M17	212.03	0.38	-	-
M18	17.22	0.21	87.91	1.77
M19	26.47	0.40	101.61	1.05
M20	23.68	0.21	-	-
M21	210.69	1.05	105.70	2.06
M22	185.09	1.19	96.85	1.01
M23	23.61	0.22	-	-
M24	23.89	0.26	98.26	2.02

Despite the small number of experiments, FormRules managed to model all the parameters with high predictability (R^2 > 85%) and accuracy as shown in **Table 4.11**. Additionally, it was able to select the main inputs that explain the variability of each output. Only one variable, dilution ratio, does not seem to exert significant effects on any of the studied parameters. The ASMOD performed by FormRules splits each model into submodels to point out single or combined effects of variables. The highlighted submodels in **Table 4.11** correspond to the inputs with the greatest effect on each output. FormRules also generates a set of simple linguistic IF-THEN rules for each model together with membership degrees ranging between 0 and 1 (Annex 3 Tables S1-S4). For each of these rules the "membership degree" specifies how a "low or high value" belongs to that fuzzy subset using the technique called fuzzy qualifier [240]. When precise information is needed, the domains of an output can be observed and quantified, depending on the degree of membership, the specific value predicted by the model [241]. In this way, the rules generated by FormRules can be transformed into decision trees (Annex 3 Figures S1-S5).

USC UNIVERSIDADE DE SANTIAGO DE COMPOSTELA

Table 4.11. Model results and quality parameters Inputs and submodels generated by FormRules for the different outputs. The most relevant submodels affecting each output are bolded.

Model	Submodel	Inputs selected by FormRules	R^2	calcultated *f*	d.f (v1, v2)	α
Mean particle size (μm)	**1**	**[Polymer] x Speed**	92.90	20.35	9, 14	<0.01
Uniformity	**1**	**[Drug] x Speed**	85.26	4.45	13, 10	<0.05
	2	[PVA]				
	3	Time x O/W ratio				
	4	Dilution ratio				
EE (%)	**1**	**[Polymer] x O/W ratio**	90.08	3.30	11, 4	0.13
	2	[Drug] x Time				
DL (%)	**1**	**[Drug] x [Polymer]**	94.86	87.62	4, 19	<0.01

Particle size is a critical quality attribute directly affecting drug release and, therefore, the therapeutic utility of the developed microparticle-based systems [147]. The variations in particle size within the database are explained in a 92.9% by a single submodel involving the interaction between the polymer concentration and stirring speed.

The combined effect of stirring speed and polymer concentration in microparticle size is presented in **Figure 4.21**. Additionally, the set of IF-THEN rules is shown in Annex 3 Table S1 (Rules 1-9). When the polymer concentration is high (> 17.5%), the use of low stirring speed (< 1,500 rpm) leads to big microspheres (Annex 3 Figure S1). On the other hand, stirring speeds over 2,000 rpm during the emulsification process allow to obtain always small size microspheres regardless of the polymer used concentration (Annex 3 Rules 1-9 Table S1 and Figure S1).

These findings are in agreement with several authors who suggested microparticle size and morphology are conditioned by the energy input during emulsification [241,242]. However, no effect of the surfactant concentration (PVA) on microspheres characteristics was observed in our work. In this case, the percentage of polymer in the formulation is critical, which determines the viscosity of the organic phase, and therefore, the energy balance necessary for the formation of the emulsion [243]. More than 12.5% of PLGA, and a high input of energy (> 1,500 rpm) is necessary to achieve small-sized microspheres (Annex 3 Figure S1).

Narrow microparticle size distributions (low uniformity values) are desirable to ensure adequate dosing [244,245]. Moreover, variations in uniformity can have important consequences on cellular uptake or drug release and compromise the therapeutic effect of the microspheres formulation [246]. The model obtained for uniformity also shows

high predictability (R^2 > 85%) and accuracy (α < 0.05), but is complex, involving six out of the seven studied variables. FormRules split the model in four submodels including the interaction between percentage of drug and stirring speed which has the strongest effect, and the interaction of O/W ratio and the stirring time, together with the single effects of surfactant concentration (PVA) and the dilution ratio.

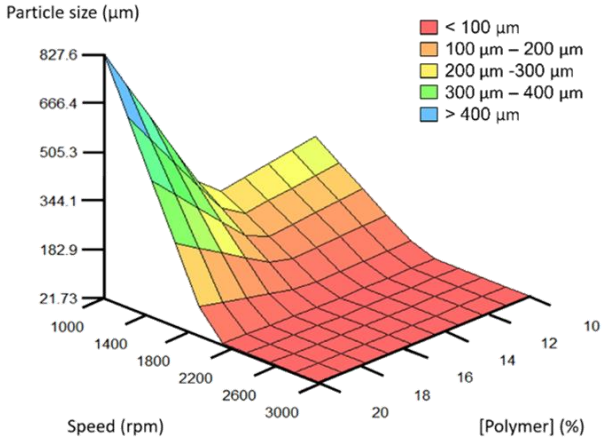


Figure 4.21. 3D plot developed by FormRules displaying the effect of stirring speed and polymer concentration on the predicted particle size.

Analysing the surfactant concentration and the dilution ratio individual effects, as shown in **Figure 4.22A** and **Figure 4.22B**, respectively, it is desirable to use low surfactant concentrations (< 1.25%) and low dilution ratios (< 6) to obtain low size distribution values and consequently, homogeneous size distributions (Annex 3 Rules 7-8 and 15-16 Table S2). On the contrary, Li *et al*. indicate that as PVA concentration increases, the particle size decreases, the specific surface area increases and the particles become more uniform, that is, low size distributions are obtained [247].

Two submodels contribute to explain the variations in the encapsulation efficiencies with high predictability (90%). However, probably due to the reduced degrees of freedom, the accuracy could not be adequately demonstrated (**Table 4.11**). The variations in EE are mainly explained by the interaction between the polymer concentration and the O/W ratio. In addition, the effect of the interaction between the drug concentration and the stirring time is observed. In agreement with our findings, Yasin *et al.* have previously reported higher encapsulation efficiencies when greater polymer concentrations were used [248]. Our models suggest that high polymer concentrations are required to achieve high encapsulation efficiencies, irrespective of the O/W ratios used. This effect has been previously reported by Santoyo *et al*., who found that high polymer concentrations increase the emulsion viscosity, thereby preventing drug loss and consequently enhancing encapsulation efficiency (Annex 3 Rules 4-6 Table S3) [249]. Nevertheless, as derived from Rules 1-3 (Annex 3 Table S3), when low polymer concentrations are used, higher encapsulation efficiencies are

achieved with medium O/W ratios (≈ 0.2 - 0.3), corresponding to the use of approximately five times the volume of aqueous phase over the organic phase volume (**Figure 4.22C**). The use of higher O/W ratios has been reported to enhance the encapsulation efficiency of PLGA nanoparticles [250]. Our model confirms this effect when O/W ratios between 0.1 and 0.25 are used. However, at higher ratios, a decrease in the EE was observed. This non-linear relationship between O/W ratio and EE could be attributed to the detrimental effect of high O/W ratios (> 0.25) on microparticle uniformity, resulting in erratic EE (Annex 3 Table 2S).

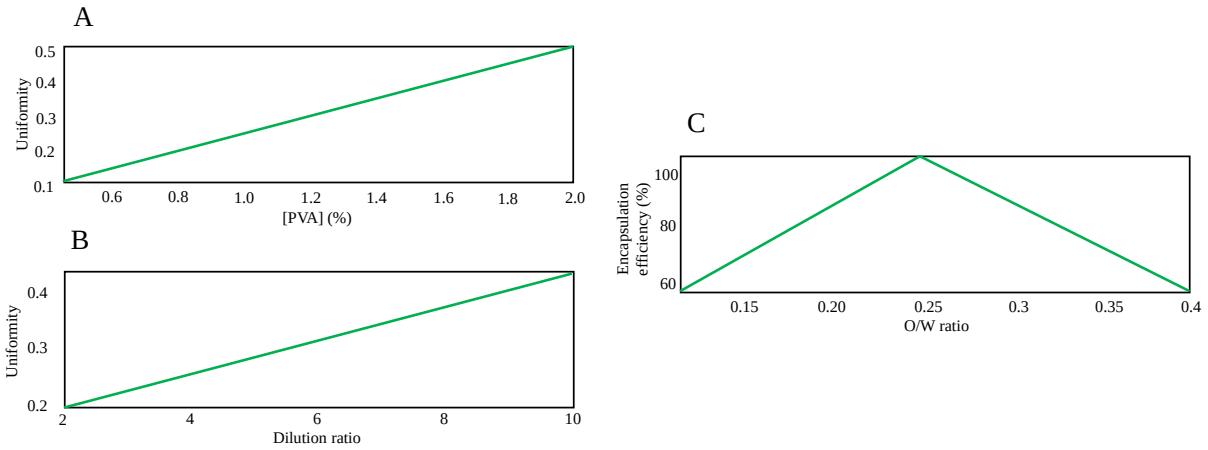


Figure 4.22. Individual partial effects of the variables on microparticle parameters estimated by the FormRules. (A) effect of surfactant concentration (%) on uniformity, (B) effect of dilution ratio on uniformity, and (C) effect of O/W ratio on encapsulation efficiency.

High drug loading is usually desirable to achieve the adequate therapeutic activity. Variations in drug loading within the database are explained in a 94.86% by the interaction between the drug and polymer concentration in the formulation.

As expected, high drug loading is achieved when high percentage of drug is used. In this situation, the increase in the percentage of polymer improves the drug microencapsulation (Annex 3 Rules 1-4 Table S4) (**Figure 4.23**).

USC
UNIVERSIDADE DE SANTIAGO DE COMPOSTELA

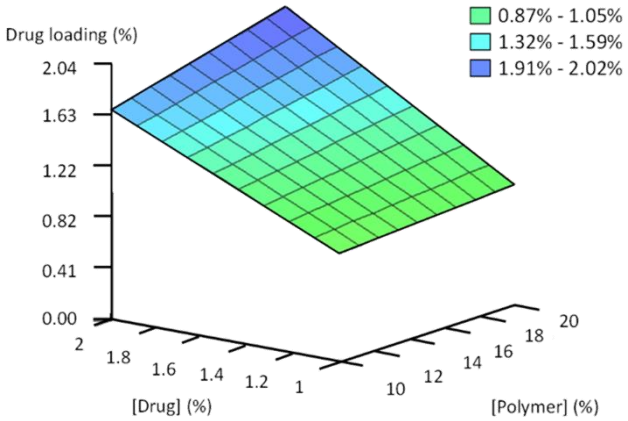


Figure 4.23. 3D plot developed by FormRules displaying the effect of polymer and drug concentrations on predicted drug loading.

4.3.2 Evaluation of microsphere formulations for intra-articular delivery

Controlled IA drug delivery depicts several advantages, including long-term therapeutic effects requiring few administrations. However, this approach requests the use of systems, usually micrometric particles and hydrogels, that should be easily administered and retained within the joint cavity for long periods, without compromising functionality. Therefore, successful microparticulated IA delivery systems must fulfil specific requirements, including high encapsulation efficiency, homogenous size distribution, and appropriate drug loading based on its therapeutic effect. Particle size is also a specific condition as polymeric microspheres larger than 10 μm are preferred for optimal joint retention, while those smaller than 300 μm ensure homogeneous polymer degradation [83,251].

The required conditions to obtain microspheres able to meet these characteristics for IA administration have been selected based on the FormRules model. The IF-THEN rules generated by the software allow a better understanding of how the different variables influence the critical attributes of microspheres (Annex 3 Figures S1-S5). To validate the obtained rules, the composition and operating conditions were selected to prepare a formulation (F502) of uniform polymeric microspheres (**Table 3.4**). High polymer concentrations (> 17.5%), together with medium or high (> 1,500 rpm) stirring speeds were used to obtain small particles (Annex 3 Rules 6 and 9 Table S1). Moreover, medium O/W ratios (≈ 0.2 - 0.3) together with low stirring times (< 75 s), and high drug concentrations (≈ 1 %) were chosen to obtain high encapsulation efficiencies (> 70%) (**Table 3.4**) (Annex 3 Rule 5 Table S3). Another variable that must also be considered is the surfactant concentration. Low surfactant concentrations (< 1.25%) are desirable to obtain a narrow microparticle size distribution. Therefore, 1% of PVA was selected.

The new formulation, F502, was produced following these described conditions (**Table 3.4**). Their characteristics are shown in **Table 4.12**. The critical microspheres attributes

were aligned with the established desirability criteria, since small (≈ 24 μm) and monodisperse microspheres (uniformity ≈ 0.3) were obtained. The formulation showed the anticipated high encapsulation efficiency. These results confirm the validity of the obtained neurofuzzy logic models. Therefore, the followed strategy is suitable to design the procedures to obtain microspheres with the required attributes. In this way, we proved the obtained IF-THEN rules are suitable for the selection of the manufacture conditions to obtain microspheres with the required properties.

Moreover, a slow-release rate is required to obtain long-term therapeutic effects once the microspheres are administered. Despite PLGA-based microspheres depict an already well-described diffusion/erosion controlled drug release, the molecular weight and lactide:glycolide ratio (L:G ratio) of the polymer modulated drug release. Polymers with a greater L:G ratio and higher molecular weight, tend to degrade at a slower rate than those with a lesser L:G ratio [252]. Therefore, to obtain microspheres with a slower release rate an additional formulation was prepared incorporating 10% of a PLGA with 75:25 L:G ratio and viscosity 0.60 dL/g (Resomer RG 755S) to a 90% of the initial PLGA 50:50 L:G and viscosity of 0.21 dL/g obtaining the formulation F502:755. This formulation was prepared also using the previously selected parameters: high polymer concentration (20%), medium O/W ratios (0.25), low stirring times (60 s), high drug concentration (1%) and 1% PVA. In parallel, blank formulations without incorporating the drug were prepared (**Table 3.4**).

Table 4.12 Characteristics of the developed microspheres.

Formulation	Mean particle size (μm)	Uniformity	DL (%)	EE (%)
F502	23.75 ± 3.96	0.32 ± 0.09	1.10 ± 0.10	110.28 ± 10.25
F502:755	35.69 ± 0.70	0.35 ± 0.01	0.99 ± 0.05	99.25 ± 5.40
B502	23.89 ± 1.16	0.34 ± 0.06	-	-
B502:755	41.11 ± 1.56	0.57 ± 0.01	-	-

This new formulation presented similar properties than the one prepared with a single PLGA (F502) showing small size (< 50 μm), monodisperse particle size distribution (uniformity ≈ 0.3) and high encapsulation efficiency (≈ 100) (**Table 4.12**). Therefore, both formulations present adequate characteristics for IA administration and retention in the joint cavity [79,83]. Indeed, the mean particle size is similar to those of already commercialized triamcinolone acetonide loaded polymeric microspheres (45 μm) for OA IA administration. These microspheres demonstrated prolonged retention time and reduced systemic exposure compared to the free drug administration [83,84,251]. Furthermore, the obtained drug loading and encapsulation efficiency values indicate the drug has been effectively encapsulated within the microspheres.

USC UNIVERSIDADE DE SANTIAGO DE COMPOSTELA

4.3.3 Characterization of the obtained microspheres

Differential scanning calorimetry (DSC) was performed on the raw materials (fenofibrate and polymers) and fenofibrate-loaded microspheres (F502 and F502:755) (**Figure 4.24**). The fenofibrate (FN) thermogram displays a sharp peak at 81.4°C (ΔH= 96.6 J/g) as previously reported, corresponding to the melting point [253]. Endothermic peaks at 49.8°C and 55.1°C were observed for the PLGA (502H) and the 90:10 physical mixture (502H and 755S), respectively. Distinctive features can be noted between raw materials and the developed microspheres, characterized by less intense and broader peaks of the PLGAs glass transition phenomena in F502 and F502:755. This observation could be attributed to the presence of additional components within the microspheres that can interact with the molecular organization of the polymeric chains [254]. Moreover, the absence of the FN melting peak in the drug-loaded microspheres (F502 and F502:755) suggests the presence of the drug in an amorphous state within the microspheres network. Pointing to a good compatibility between the drug and the polymers.

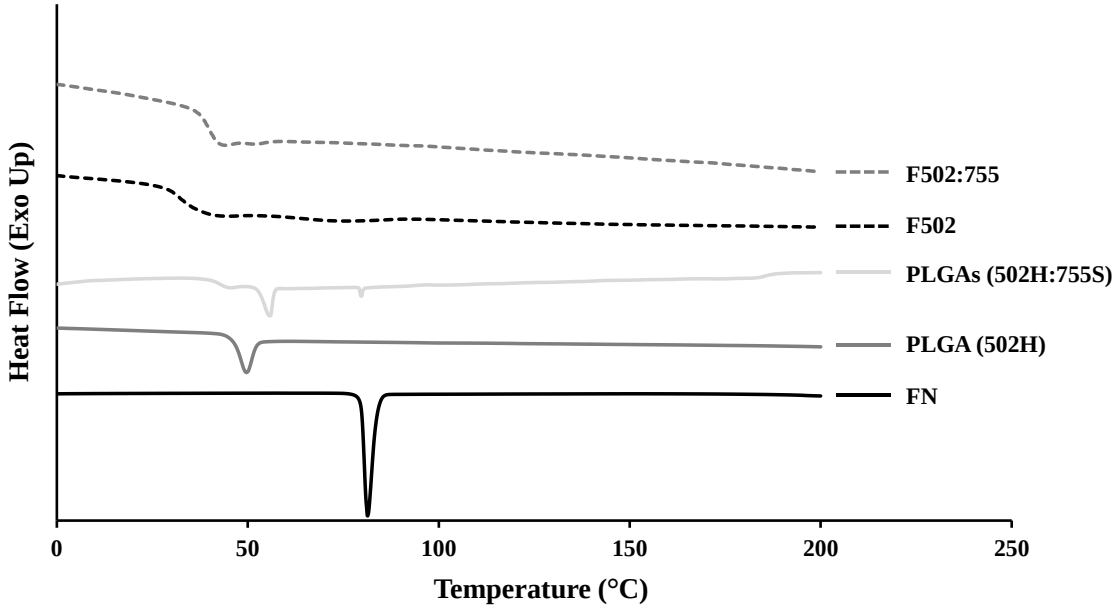


Figure 4.24. DSC thermograms of FN, PLGA (502H), the physical mixture of both PLGAs (502H:755S; 90:10), and microspheres (F502 and F502:755).

Figure 4.25 shows SEM images for two formulations of the initial experimental design representing the smallest (M10; **Figure 4.25A**) and largest (M14; **Figure 4.25B**) according to light diffraction measures. These were chosen to assess manufacturing protocol variations on particle morphology (**Table 4.10**). The SEM images confirm the observed size differences and show smooth, spherical microspheres with uniform distribution. Moreover, no discernible morphological differences were observed between microspheres prepared with a single PLGA polymer and the polymeric mixture

(**Figure 4.25C** vs **Figure 4.25D**) or between loaded and unloaded microspheres (**Figure 4.25C** vs **Figure 4.25E**; **Figure 4.25D** vs **Figure 4.25F**).

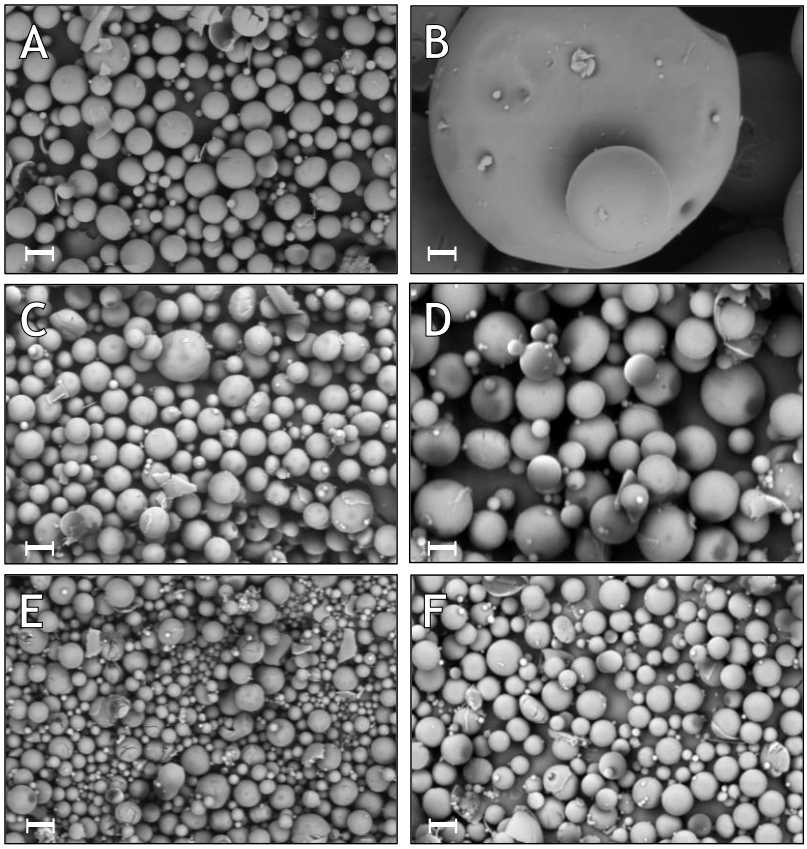


Figure 4.25. Scanning electron micrographs of (A) M10, (B) M14, (C) F502, (D) F502:755, (E) B502, and (F) B502:755. Magnification of 500X. Scale bar 20 μm.

The release profile over 3 months of the formulations designed for IA administration is shown in **Figure 4.26**. As previously reported by other authors for PLGA-based systems, the drug was released from the polymeric microspheres in two phases (biphasic release) [252]. Moreover, the release mechanisms were further investigated by applying various kinetic models, including zero-order, first-order, Higuchi, Hixson-Crowell, and Korsmeyer-Peppas models to the acquired data. The correlation coefficient (R^2) was used as a metric to assess the fit between the model and the experimental data [255].

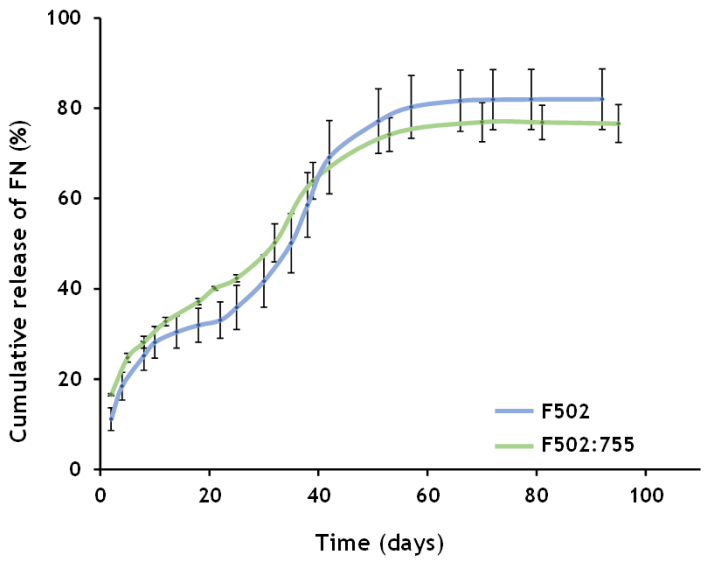
The first release phase fitted zero-order kinetics for both F502 and F502:755. This phase is characterized by a slow and constant drug release. Although the obtained release constant was slightly higher for F502, no significant differences were observed between both formulations (**Figure 4.26B**). In contrast to other studies, where significant differences in the duration of the initial phase were found between high (lasting 21 days) and low (lasting 2 days) molecular weight polymers, we only observed a slightly different between both formulations, lasting 10 days for F502 and 12 days for F502:755.

USC UNIVERSIDADE DE SANTIAGO DE COMPOSTELA

This fact may be attributed to the low amount (10%) of high molecular weight and L:G ratio PLGA added [252].

On the other hand, the second release phase fitted to a Higuchi kinetic model also for both formulations (F502 and F502:755). This phase is characterized by the polymer degradation where the release of FN is controlled by the hydrolysis of the polymer in their oligomers (lactic and glycolic acid). This situation results in the creation of pores facilitating the entry of the release media, the dissolution and diffusion of the encapsulated drug [256]. A significant increase in the FN release constant was observed between F502 and F502:755 microspheres (375.99 vs. 210.56 $day^{-1/2}$) (**Figure 4.26B**). This difference was already anticipated and attributed to the addition to the microspheres network of a PLGA with a higher L:G ratio and molecular weight that undergo slower degradation [150].

A



B

Formulation	K_0 (µg/day)	R^2	Formulation	k_H ($day^{-1/2}$)	R^2
F502-Phase 1	22.74 ± 3.16	0.98	F502-Phase 2	375.99 ± 52.46	0.98
F502:755-Phase 1	21.64 ± 1.09	0.99	F502:755-Phase 2	210.56 ± 7.85	0.99

Figure 4.26 Drug release profiles (A) and obtained kinetics (B) for F502 and F502:755 formulations in SDS (1%) at 37°C. Values are mean ± SD of three independent studies.

4.3.4 Senescent cells viability

Cell senescence is generally defined by an irreversible arrest in proliferation, resistance to apoptosis, and the release of ECM-degrading and pro-inflammatory molecules known as senescence-associated secretory phenotypes (SASP). These SASP can trigger alterations in the structure and function of nearby cells and tissues playing a

USC UNIVERSIDADE DE SANTIAGO DE COMPOSTELA

crucial role in age-related diseases such as atherosclerosis, macular degeneration, sarcopenia, and osteoarthritis [257]. Several studies point out to an accumulation of senescent cells in OA joints, indicating an important function of senescence on pathology progression. These cells contribute to the established inflammation by secreting SASP and also propagate senescence through paracrine and autocrine signalling [258]. Based on these effects, the modulation of senescence using senotherapeutics has been pointed out as a novel strategy to control OA progression. In this regard, two different therapeutic approaches can be followed: 1) apoptosis induction of senescent cells by the so called senolytic drugs where the initiation of programmed cell death leads to a decrease in the number of senescent cells, or 2) modulation of the SASP profile using senomorphic drugs that control the effect of senescent cells on the surrounding tissues [259].

Fenofibrate, a member of the fibrates family, widely used for dyslipidemia treatment, has been identified as a senotherapeutic agent, exhibiting therapeutic effects in OA as a senolytic [260]. **Figure 4.27A** depicts the cell viability of senescent OACs treated with either of the developed formulations or an equivalent drug concentration. A significant decrease in cell viability was observed in all the treatment conditions compared to senescent cells that were not treated, with no statistically significant differences between them. Therefore, the developed microspheres were able to maintain the senolytic activity previously reported for the drug, demonstrating their suitability as FN carriers (**Figure 4.27A**).

Moreover, to elucidate whether the drug could extend an unspecific decrease in cell viability, fibroblasts were also treated with FN at the same dose to ensure no toxic effects are induced in healthy cells. The obtained experimental data (**Figure 4.27B**) indicate there is no toxic effect on fibroblast viability when cells were treated with FN. Therefore, our results are in agreement with previous studies in which FN was able to selective reduce the number of senescent cells, demonstrating senolytic properties [114].

USC
UNIVERSIDADE DE SANTIAGO DE COMPOSTELA

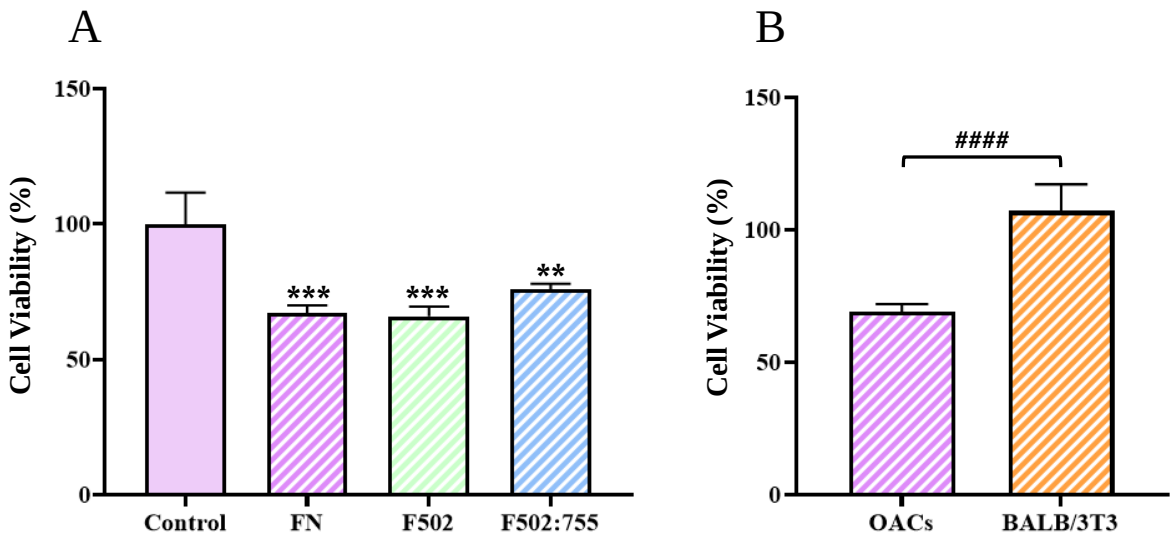


Figure 4.27. (A) Viability results of senescent OACs (control) treated with FN (3.12 µg/mL) or with the developed microspheres (F502 and F502:755) for 72h. Viability results were normalized vs. control. (B) Viability results for BALB/3T3 and senescent OACs treated with FN (3.12 µg/mL) for 72 hours, Values are mean ± SD of three well/condition. (*) Indicates significant differences compared to control (**p < 0.01, ***p < 0.001). (#) Indicates significant differences between samples ($^{\#\#\#\#}p < 0.0001$).

4.3.5 Senolytic activity and autophagy induction

The determination of the β-galactosidase activity is the gold-standard to identify senescent cells [259]. The number of OACs stained positive for β-galactosidase was quantified after 72 hours treatment with either free FN or the loaded microspheres (F502 and F502:755). As reflected in **Figure 4.28A**, a significant reduction on the percentage of senescent cells was observed when cell monolayers were treated with the developed microspheres (F502 and F502:755) compared to the free drug (FN). Therefore, the treatment with the developed microspheres showed improved therapeutic activity over the free senotherapeutic (**Figure 4.28A**).

Additionally, autophagy, a process used by cells to recycle endogenous or exogenous cytoplasmatic substances, is known to be decreased in OA. That is, the pathology is characterized by presenting a higher population of senescent cells and a lower population of cells with high autophagy activity. Several works have pointed out that the induction of autophagy have beneficial effects in osteoarthritic chondrocytes decreasing cartilage degradation [261]. Autophagy can be studied using different check points during the process: autophagy induction, autophagosome production, vesicle fusion, and autophagosome breakdown. Microtubule-associated protein 1A/1B-light chain 3 (LC3), is a soluble protein that is conjugated in the cytoplasm to phosphatidylethanolamine leading to LC3-II, and afterwards, recruited to autophagosomal membranes [262]. The expression levels of this protein are commonly

used to study the autophagosome production and, therefore, as a measure of the autophagy activity.

Some authors have already pointed out that fenofibrate, besides decreasing senescence, also enhances autophagy [114,263]. Therefore, the expression levels of LC3-II were also studied for OACs treated with either free drug or the drug-loaded microspheres. The experimental results (**Figure 4.28B**) shows no significant differences between the administration of free drug or the drug-loaded microspheres.

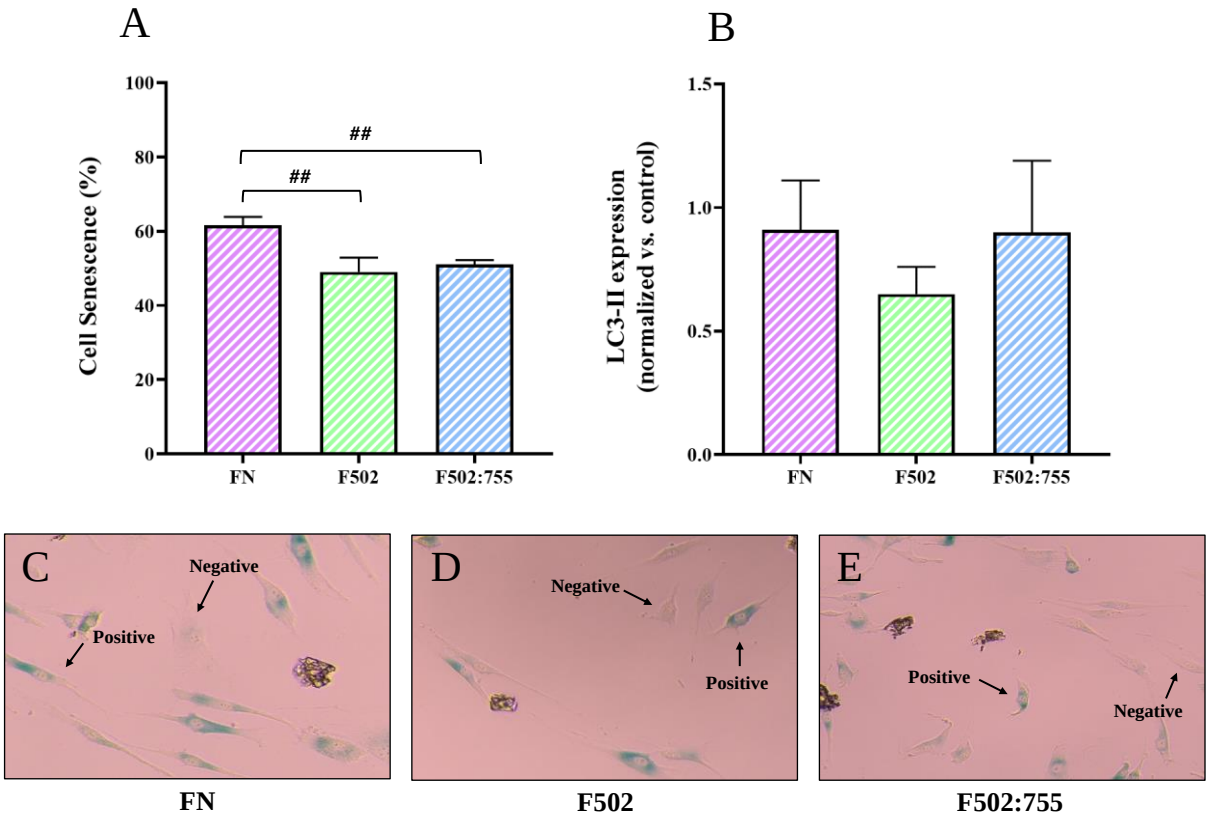


Figure 4.28. (A) Senescence results of senescent OACs treated with FN or with the developed microspheres (F502 and F502:755) for 72h. (B) LC3-II expression results of senescent OACs treated with FN or with the developed microspheres (F502 and F502:755) for 72h. LC3-II expression was related to the total protein amount, and this was further normalized vs. control (senescent OACs). (C) Image of senescent OACs treated with FN, (D) F502 microspheres, and (E) F502:755 microspheres. Values are mean ± SD of three well/condition. (#) Indicates significant differences between samples ($^{\#\#}$ $p < 0.01$).

Therefore, based on the obtained results, the developed microspheres were able to successfully encapsulate FN while maintaining the same activity in decreasing senescent cell viability and LC3-II than free drug. Interestingly, the treatment with F502 (**Figure 4.28D**) and F502:755 (**Figure 4.28E**) showed a higher ability to decrease the number of cells stained positive for β-galactosidase than FN alone (**Figure 4.28C**), performing better than the free drug.

4.3.6 *In vivo* therapeutic effects of microspheres

The therapeutic activity of FN-loaded microspheres was evaluated in a mouse model of OA. F502:755 was selected for testing based on the aforementioned data. Although no differences in biological performance were observed between F502 and F502:755 formulations, F502:755 exhibited a slower release rate, potentially leading to a more prolonged therapeutic effect. Mice were treated with two FN doses (1 µg and 10 µg) through IA injection, animals were monitored, and the knee structures were evaluated eight weeks after treatment.

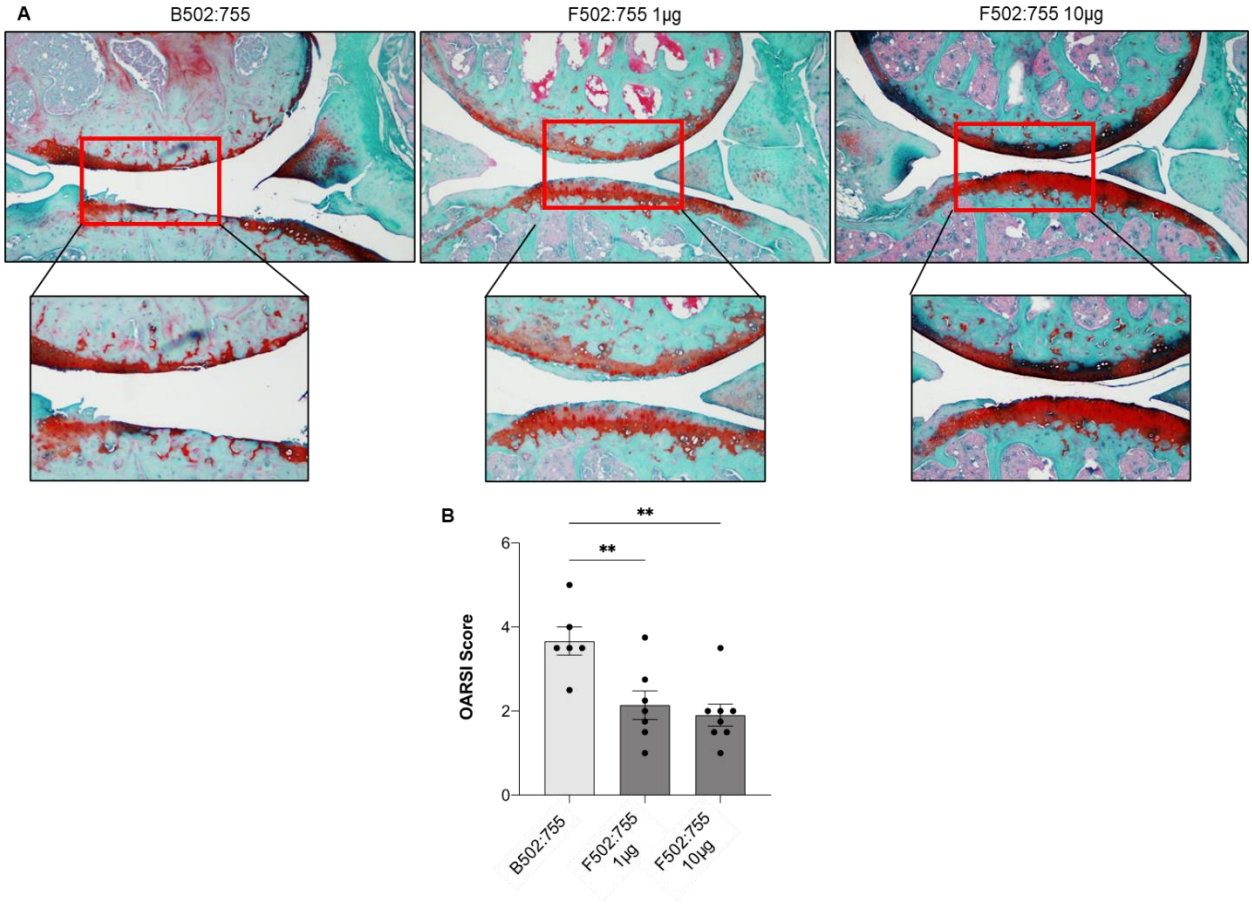


Figure 4.29. (A) Knee joints of animals treated either with the blank microspheres (B502:755) or FN-loaded microspheres (F502:755) analysed by staining with Safranin O-fast green. (B) Histological scores. Values are mean ± SEM. (**p<0.01) versus B502:755 condition. Magnification: 10X.

Mice knee joints treated with the blank formulation (B502:755) exhibited significant cartilage damage, including proteoglycan depletion, loss of surface lamina and cartilage fibrillations (**Figure 4.29A**). However, the treatment with F502:755 (1µg) and F502:755 (10µg) significantly decreased the severity of these OA-like changes. The analysis of OA pathology by a semiquantitative scoring system indicated a significant decrease in

USC UNIVERSIDADE DE SANTIAGO DE COMPOSTELA

the severity of the OA-like changes after the treatment with the developed formulations at both FN doses compared to blank microspheres ($p < 0.01$) (**Figure 4.29B**).

Fibrates are agonists of the peroxisome proliferator-activated receptor α (PPARα). The activation of this receptor inhibits the nuclear translocation of nuclear factor κB (NFκB) a pro-inflammatory pathway. Moreover, they also control other inflammatory pathways as mitogen activated protein kinase phosphorylation, exerting an anti-inflammatory effect on various cell types [264–266]. The mechanism by which fibrates induces apoptosis in senescent cells is still not fully understood, but some potential mechanisms are associated to its activity as PPARα activator, implicated in the control of genes involved in cell survival and apoptosis pathways. Moreover, fenofibrate has been reported to modulate metabolic reprogramming, and interact with other signalling pathways specific to senescent cells [267].

The anti-inflammatory profile of fibrates together with their senolytic effect could be beneficial in controlling disease progression and tissue function in age-relate pathologies as OA. Indeed, osteoarthritic patients treated with fibrates have shown improved joint functions and better mobility [114]. However, their systemic administration requires the use of high daily doses and the consequent effects on systemic lipid homeostasis. Therefore, the IA administration of such therapeutic molecules would avoid systemic effects, decreasing the required dose to be administered and increasing the therapeutic activity.

The obtained data proved, for the first time, that the IA administration of FN successfully reduces joint damage in a preclinical mice model of OA. Remarkably, only a 1 µg dose is required to obtain significant effects on cartilage OA-like changes. Similarly, the IA administration of (4 (2′-aminoethyl) amino-1, 8-dimethylimidazo (1,2-a) quinoxaline) (BMS-345541), also an inhibitor of the NF-κB signalling, has shown beneficial effects on the cartilage level of surgical induced OA. However, the administration of BMS-345541 was performed three times a week over the 8 weeks of treatment and led to a lesser decrease in OARSI score than the one observed in our study **[268]**. This difference could be associated to the use of controlled release systems able to sustain the drug within the joint. In agreement with this, the IA administration of PLGA microspheres loaded with the immunomodulator rapamycin showed improved therapeutic outcomes than the administration of the free drug **[269]**. Nevertheless, the observed improvement in tissue structure associated with OA was less marked than the effect obtained with the designed FN-loaded microspheres, despite being administered more frequently (3 doses at days 7, 24, and 42).

The combination of a controlled-release system with FN, which possesses several pharmacological effects in the pathology, has resulted in the development of a novel

USC DE SANTIAGO DE COMPOSTELA

therapeutic strategy that outperforms previously developed IA strategies in OA mice model. This approach holds promise as a disease modifying osteoarthritis drug.

USC
UNIVERSIDADE
DE SANTIAGO
DE COMPOSTELA

USC
UNIVERSIDADE
DE SANTIAGO
DE COMPOSTELA

5 CONCLUSIONS

USC
UNIVERSIDADE
DE SANTIAGO
DE COMPOSTELA

USC
UNIVERSIDADE
DE SANTIAGO
DE COMPOSTELA

The obtained results highlight the potential of artificial intelligence (AI) tools to design, develop, and optimize drug delivery systems leading to novel formulations with potential as disease modifying osteoarthritis drugs (DMOADs). In this regard, artificial intelligence tools enabled the establishment of robust protocols to prepare nanoparticles and microspheres of desired characteristics. Based on this approach, three different drug-loaded systems were obtained.

1. Anti-inflammatory nanostructured lipid carriers (NLCs) loaded with indomethacin and efficiently functionalized with mannose. The use of intelligence artificial tools allowed for the use of a sequential methodology to obtain stable and functionalized NLCs. These NPs exhibit small and uniform nanometric particle sizes, as well as a substantial positive surface charge adequate to interact with cell membranes. Moreover, high drug loading and low drug leakage were achieved.

   The optimized NLCs exhibited a specific and effective uptake by APCs and an intracellular distribution compatible with a receptor-mediated endocytosis internalization pathway. This feature was due to their high affinity for mannose receptors present on the cell membrane.

   The NLCs reduced the secretion of pro-inflammatory cytokines, while increasing the secretion of anti-inflammatory cytokines, most likely due to the mannose functionalization. These properties demonstrated the suitability of the developed systems to modulate the inflammatory response, thereby stopping the pathology degradative cycle at the inflammation point.

2. Lipid-polymer hybrid nanoparticles (LPNPs) depicting a core-shell structure, high IL-4 association efficiency and immunomodulatory properties. The use of artificial intelligence tools allowed for the selection of the best composition able to obtain stable LPNPs. The optimized LPNPs exhibited small and uniform nanometric particle sizes, as well as a substantial negative zeta potential which, together with the pegylated lipid layer, confer them colloidal stability.

   The core-shell structure, and mannose coating were confirmed by fluorescence cross-correlation spectroscopy, a technique that, to the best of our knowledge, has never been used before to characterize LPNPs.

   The optimized NPs were highly internalized by pro-inflammatory macrophages through endocytosis. Nevertheless, the immunomodulatory effect shown by the systems confirmed their ability to escape from the late endosome due to their surface charge change driven by the endosome pH shift. The treatment of pro-inflammatory macrophages with the developed systems significantly increased

USC UNIVERSIDADE DE SANTIAGO DE COMPOSTELA

the secretion of anti-inflammatory cytokines while significantly reducing pro-inflammatory cytokines.

Therefore, the developed protein-loaded LPNPs prevent IL-4 degradation while modulating macrophage phenotype towards an anti-inflammatory state, highlighting their suitability as DMOAD.

3. Polymeric microspheres with tailored physicochemical properties and drug release profiles depicting disease modifying capacity *in vivo*. The use of artificial intelligence tools provided general guidelines for a better selection of the polymeric microspheres formulation parameters following the single emulsion-solvent evaporation process. Drug loaded microspheres showed small and uniform micrometric particle sizes, high drug loading, and encapsulation efficiencies, making them suitable for intra-articular administration.

   The drug release profile of the optimized microspheres extended up to three months, demonstrating its suitability as fenofibrate delivery systems. The microspheres exerted a specific senolytic effect on senescent cells without exhibiting toxicity to healthy cells. A significant reduction in cell senescence was achieved after treating osteoarthritic chondrocytes with the developed microspheres compared to the free drug.

   Finally, *in vivo* studies demonstrated the significant potential of fenofibrate-loaded microspheres as DMOAD, showing an improvement in cartilage morphology compared to unloaded formulations following a single intra-articular administration.

The drug delivery systems developed in this thesis demonstrated its potential as DMOADs by targeting the two main hallmarks of OA: inflammation and cartilage degradation. These new systems not only successfully encapsulated the selected therapeutic molecules but also improved their therapeutic activity through enhanced drug stability and targeted delivery strategies. The use of AI tools was pivotal in achieving these advancements, offering innovative methodologies that surpassed traditional approaches in drug delivery systems design. Moreover, the combined administration of these systems would allow to address the disease through three independent but closely related strategies; inflammation control, macrophage phenotype modulation and reversing disease progression by modulating chondrocyte senescence. Therefore, either individually or in combination these drug delivery systems depict high potential in the management of OA.

USC
UNIVERSIDADE DE SANTIAGO DE COMPOSTELA

6 REFERENCES

USC
UNIVERSIDADE
DE SANTIAGO
DE COMPOSTELA

USC
UNIVERSIDADE
DE SANTIAGO
DE COMPOSTELA

1. Dantas, L.O.; Salvini, T.D.F.; McAlindon, T.E. Knee Osteoarthritis: Key Treatments and Implications for Physical Therapy. *Brazilian Journal of Physical Therapy* **2021**, *25*, 135–146, doi:10.1016/j.bjpt.2020.08.004.
2. Favero, M.; Belluzzi, E.; Ortolan, A.; Lorenzin, M.; Oliviero, F.; Doria, A.; Scanzello, C.R.; Ramonda, R. Erosive Hand Osteoarthritis: Latest Findings and Outlook. *Nat Rev Rheumatol* **2022**, *18*, 171–183, doi:10.1038/s41584-021-00747-3.
3. Maudens, P.; Jordan, O.; Allémann, E. Recent Advances in Intra-Articular Drug Delivery Systems for Osteoarthritis Therapy. *Drug Discovery Today* **2018**, *23*, 1761–1775, doi:10.1016/j.drudis.2018.05.023.
4. Motta, F.; Barone, E.; Sica, A.; Selmi, C. Inflammaging and Osteoarthritis. *Clinic Rev Allerg Immunol* **2022**, *64*, 222–238, doi:10.1007/s12016-022-08941-1.
5. Sanchez-Lopez, E.; Coras, R.; Torres, A.; Lane, N.E.; Guma, M. Synovial Inflammation in Osteoarthritis Progression. *Nat Rev Rheumatol* **2022**, *18*, 258–275, doi:10.1038/s41584-022-00749-9.
6. Richard, M.J.; Driban, J.B.; McAlindon, T.E. Pharmaceutical Treatment of Osteoarthritis. *Osteoarthritis and Cartilage* **2023**, *31*, 458–466, doi:10.1016/j.joca.2022.11.005.
7. Veronese, N.; Ecarnot, F.; Cheleschi, S.; Fioravanti, A.; Maggi, S. Possible Synergic Action of Non-Steroidal Anti-Inflammatory Drugs and Glucosamine Sulfate for the Treatment of Knee Osteoarthritis: A Scoping Review. *BMC Musculoskelet Disord* **2022**, *23*, 1084, doi:10.1186/s12891-022-06046-6.
8. Latourte, A.; Kloppenburg, M.; Richette, P. Emerging Pharmaceutical Therapies for Osteoarthritis. *Nat Rev Rheumatol* **2020**, *16*, 673–688, doi:10.1038/s41584-020-00518-6.
9. Sacitharan, P.K. Ageing and Osteoarthritis. In *Biochemistry and Cell Biology of Ageing: Part II Clinical Science*; Harris, J.R., Korolchuk, V.I., Eds.; Subcellular Biochemistry; Springer Singapore: Singapore, 2019; Vol. 91, pp. 123–159 ISBN 9789811336805.
10. Toropitsyn, E.; Pravda, M.; Rebenda, D.; Ščigalková, I.; Vrbka, M.; Velebný, V. A Composite Device for Viscosupplementation Treatment Resistant to Degradation by Reactive Oxygen Species and Hyaluronidase. *J Biomed Mater Res* **2022**, *110*, 2595–2611, doi:10.1002/jbm.b.35114.
11. Goldring, M.B. Chondrogenesis, Chondrocyte Differentiation, and Articular Cartilage Metabolism in Health and Osteoarthritis. *Therapeutic Advances in Musculoskeletal* **2012**, *4*, 269–285, doi:10.1177/1759720X12448454.
12. Hu, W.; Chen, Y.; Dou, C.; Dong, S. Microenvironment in Subchondral Bone: Predominant Regulator for the Treatment of Osteoarthritis. *Ann Rheum Dis* **2021**, *80*, 413–422, doi:10.1136/annrheumdis-2020-218089.
13. Kiełbowski, K.; Herian, M.; Bakinowska, E.; Banach, B.; Sroczyński, T.; Pawlik, A. The Role of Genetics and Epigenetic Regulation in the Pathogenesis of Osteoarthritis. *IJMS* **2023**, *24*, 11655, doi:10.3390/ijms241411655.
14. Liu, S.-C.; Tsai, C.-H.; Wang, Y.-H.; Su, C.-M.; Wu, H.-C.; Fong, Y.-C.; Yang, S.-F.; Tang, C.-H. Melatonin Abolished Proinflammatory Factor Expression and Antagonized

USC UNIVERSIDADE DE SANTIAGO DE COMPOSTELA

Osteoarthritis Progression in Vivo. *Cell Death Dis* **2022**, *13*, 215, doi:10.1038/s41419-022-04656-5.

15. Fotouhi, A.; Maleki, A.; Dolati, S.; Aghebati-Maleki, A.; Aghebati-Maleki, L. Platelet Rich Plasma, Stromal Vascular Fraction and Autologous Conditioned Serum in Treatment of Knee Osteoarthritis. *Biomedicine & Pharmacotherapy* **2018**, *104*, 652–660, doi:10.1016/j.biopha.2018.05.019.
16. Freitag, J.; Bates, D.; Boyd, R.; Shah, K.; Barnard, A.; Huguenin, L.; Tenen, A. Mesenchymal Stem Cell Therapy in the Treatment of Osteoarthritis: Reparative Pathways, Safety and Efficacy – a Review. *BMC Musculoskelet Disord* **2016**, *17*, 230, doi:10.1186/s12891-016-1085-9.
17. Maudens, P.; Jordan, O.; Allémann, E. Recent Advances in Intra-Articular Drug Delivery Systems for Osteoarthritis Therapy. *Drug Discovery Today* **2018**, *23*, 1761–1775, doi:10.1016/j.drudis.2018.05.023.
18. Toyoda, E.; Maehara, M.; Watanabe, M.; Sato, M. Candidates for Intra-Articular Administration Therapeutics and Therapies of Osteoarthritis. *IJMS* **2021**, *22*, 3594, doi:10.3390/ijms22073594.
19. Xia, B.; Di Chen; Zhang, J.; Hu, S.; Jin, H.; Tong, P. Osteoarthritis Pathogenesis: A Review of Molecular Mechanisms. *Calcif Tissue Int* **2014**, *95*, 495–505, doi:10.1007/s00223-014-9917-9.
20. Hunter, D.J. Viscosupplementation for Osteoarthritis of the Knee. *N Engl J Med* **2015**, *372*, 1040–1047, doi:10.1056/NEJMct1215534.
21. Webner, D.; Huang, Y.; Hummer, C.D. Intraarticular Hyaluronic Acid Preparations for Knee Osteoarthritis: Are Some Better Than Others? *CARTILAGE* **2021**, *13*, 1619S-1636S, doi:10.1177/19476035211017320.
22. Kang, M.L.; Im, G.-I. Drug Delivery Systems for Intra-Articular Treatment of Osteoarthritis. *Expert Opinion on Drug Delivery* **2014**, *11*, 269–282, doi:10.1517/17425247.2014.867325.
23. Oo, W.M.; Liu, X.; Hunter, D.J. Pharmacodynamics, Efficacy, Safety and Administration of Intra-Articular Therapies for Knee Osteoarthritis. *Expert Opinion on Drug Metabolism & Toxicology* **2019**, *15*, 1021–1032, doi:10.1080/17425255.2019.1691997.
24. Snibbe, J.C.; Gambardella, R.A. Use of Injections for Osteoarthritis in Joints and Sports Activity. *Clinics in Sports Medicine* **2005**, *24*, 83–91, doi:10.1016/j.csm.2004.08.001.
25. O'Connell, B.; Wragg, N.M.; Wilson, S.L. The Use of PRP Injections in the Management of Knee Osteoarthritis. *Cell Tissue Res* **2019**, *376*, 143–152, doi:10.1007/s00441-019-02996-x.
26. Oo, W.M.; Little, C.; Duong, V.; Hunter, D.J. The Development of Disease-Modifying Therapies for Osteoarthritis (DMOADs): The Evidence to Date. *DDDT* **2021**, *Volume 15*, 2921–2945, doi:10.2147/DDDT.S295224.
27. Tang, J.Z.; Nie, M.J.; Zhao, J.Z.; Zhang, G.C.; Zhang, Q.; Wang, B. Platelet-Rich Plasma versus Hyaluronic Acid in the Treatment of Knee Osteoarthritis: A Meta-Analysis. *J Orthop Surg Res* **2020**, *15*, 403, doi:10.1186/s13018-020-01919-9.

USC DE SANTIAGO DE COMPOSTELA

28. Domżalski, M.; Migliore, A. A Review of the Clinical Effectiveness and Safety of Hybrid Cooperative Complexes in Intra-Articular Viscosupplementation. *Rheumatol Ther* **2022**, *9*, 957–974, doi:10.1007/s40744-022-00450-z.

29. Skou, S.T.; Roos, E.M. Physical Therapy for Patients with Knee and Hip Osteoarthritis: Supervised, Active Treatment Is Current Best Practice. *Clinical and Experimental Rheumatology* **2019**.

30. Wang, H.; Ma, B. Healthcare and Scientific Treatment of Knee Osteoarthritis. *Journal of Healthcare Engineering* **2022**, *2022*, 1–7, doi:10.1155/2022/5919686.

31. Craciunescu, O.; Icriverzi, M.; Florian, P.E.; Roseanu, A.; Trif, M. Mechanisms and Pharmaceutical Action of Lipid Nanoformulation of Natural Bioactive Compounds as Efficient Delivery Systems in the Therapy of Osteoarthritis. *Pharmaceutics* **2021**, *13*, 1108, doi:10.3390/pharmaceutics13081108.

32. Assi, R.; Quintiens, J.; Monteagudo, S.; Lories, R.J. Innovation in Targeted Intra-Articular Therapies for Osteoarthritis. *Drugs* **2023**, *83*, 649–663, doi:10.1007/s40265-023-01863-y.

33. Zhou, D.; Zhou, F.; Sheng, S.; Wei, Y.; Chen, X.; Su, J. Intra-Articular Nanodrug Delivery Strategies for Treating Osteoarthritis. *Drug Discovery Today* **2023**, *28*, 103482, doi:10.1016/j.drudis.2022.103482.

34. Donovan, R.L.; Edwards, T.A.; Judge, A.; Blom, A.W.; Kunutsor, S.K.; Whitehouse, M.R. Effects of Recurrent Intra-Articular Corticosteroid Injections for Osteoarthritis at 3 Months and beyond: A Systematic Review and Meta-Analysis in Comparison to Other Injectables. *Osteoarthritis and Cartilage* **2022**, *30*, 1658–1669, doi:10.1016/j.joca.2022.07.011.

35. Guermazi, A.; Neogi, T.; Katz, J.N.; Kwoh, C.K.; Conaghan, P.G.; Felson, D.T.; Roemer, F.W. Intra-Articular Corticosteroid Injections for the Treatment of Hip and Knee Osteoarthritis-Related Pain: Considerations and Controversies with a Focus on Imaging— *Radiology* Scientific Expert Panel. *Radiology* **2020**, *297*, 503–512, doi:10.1148/radiol.2020200771.

36. Hameed, F.; Ihm, J. Injectable Medications for Osteoarthritis. *PM&R* **2012**, *4*, doi:10.1016/j.pmrj.2012.02.010.

37. Im, G.-I. Perspective on Intra-Articular Injection Cell Therapy for Osteoarthritis Treatment. *Tissue Eng Regen Med* **2019**, *16*, 357–363, doi:10.1007/s13770-018-00176-6.

38. Liu, N.; Wang, W.; Zhao, Z.; Zhang, T.; Song, Y. Autophagy in Human Articular Chondrocytes Is Cytoprotective Following Glucocorticoid Stimulation. *Molecular Medicine Reports* **2014**, *9*, 2166–2172, doi:10.3892/mmr.2014.2102.

39. Derendorf, H.; Möllmann, H.; Grüner, A.; Haack, D.; Gyselby, G. Pharmacokinetics and Pharmacodynamics of Glucocorticoid Suspensions after Intra-Articular Administration. *Clin Pharmacol Ther* **1986**, *39*, 313–317, doi:10.1038/clpt.1986.45.

40. Douglas, R.J. Corticosteroid Injection into the Osteoarthritic Knee: Drug Selection, Dose, and Injection Frequency: Corticosteroid Injection into the Osteoarthritic Knee. *International Journal of Clinical Practice* **2012**, *66*, 699–704, doi:10.1111/j.1742-1241.2012.02963.x.

USC UNIVERSIDADE DE SANTIAGO DE COMPOSTELA

41. Li, S.; Zhang, W.; Lin, Y. Application of Intra-Articular Corticosteroid Injection in Juvenile Idiopathic Arthritis. *Front. Pediatr.* **2022**, *10*, 822009, doi:10.3389/fped.2022.822009.

42. Richards, M.M.; Maxwell, J.S.; Weng, L.; Angelos, M.G.; Golzarian, J. Intra-Articular Treatment of Knee Osteoarthritis: From Anti-Inflammatories to Products of Regenerative Medicine. *The Physician and Sportsmedicine* **2016**, *44*, 101–108, doi:10.1080/00913847.2016.1168272.

43. Stitik, T.P.; Kumar, A.; Foye, P.M. Corticosteroid Injections for Osteoarthritis: *American Journal of Physical Medicine & Rehabilitation* **2006**, *85*, S51–S65, doi:10.1097/01.phm.0000245508.35730.f3.

44. O'Connell, B.; Wragg, N.M.; Wilson, S.L. The Use of PRP Injections in the Management of Knee Osteoarthritis. *Cell Tissue Res* **2019**, *376*, 143–152, doi:10.1007/s00441-019-02996-x.

45. Prodromidis, A.D.; Charalambous, C.P.; Moran, E.; Venkatesh, R.; Pandit, H. The Role of Platelet-Rich Plasma (PRP) Intraarticular Injections in Restoring Articular Cartilage of Osteoarthritic Knees. A Systematic Review and Meta-Analysis. *Osteoarthritis and Cartilage Open* **2022**, *4*, 100318, doi:10.1016/j.ocarto.2022.100318.

46. Cui, Y.; Lin, L.; Wang, Z.; Wang, K.; Xiao, L.; Lin, W.; Zhang, Y. Research Trends of Platelet-Rich Plasma Therapy on Knee Osteoarthritis from 2011 to 2021: A Review. *Medicine* **2023**, *102*, e32434, doi:10.1097/MD.0000000000032434.

47. Wang, L.; He, C. Nrf2-Mediated Anti-Inflammatory Polarization of Macrophages as Therapeutic Targets for Osteoarthritis. *Front. Immunol.* **2022**, *13*, 967193, doi:10.3389/fimmu.2022.967193.

48. Jildeh, T.R.; Su, C.A.; Vopat, M.L.; Brown, J.R.; Huard, J. A Review of Commercially Available Point-of-Care Devices to Concentrate Platelet-Rich Plasma. *Cureus* **2022**, doi:10.7759/cureus.28498.

49. Berkani, S.; Courties, A.; Eymard, F.; Latourte, A.; Richette, P.; Berenbaum, F.; Sellam, J.; Louati, K. Time to Total Knee Arthroplasty after Intra-Articular Hyaluronic Acid or Platelet-Rich Plasma Injections: A Systematic Literature Review and Meta-Analysis. *JCM* **2022**, *11*, 3985, doi:10.3390/jcm11143985.

50. Tramś, E.; Malesa, K.; Pomianowski, S.; Kamiński, R. Role of Platelets in Osteoarthritis—Updated Systematic Review and Meta-Analysis on the Role of Platelet-Rich Plasma in Osteoarthritis. *Cells* **2022**, *11*, 1080, doi:10.3390/cells11071080.

51. Kavanaugh, T.E.; Werfel, T.A.; Cho, H.; Hasty, K.A.; Duvall, C.L. Particle-Based Technologies for Osteoarthritis Detection and Therapy. *Drug Deliv. and Transl. Res.* **2016**, *6*, 132–147, doi:10.1007/s13346-015-0234-2.

52. Shakouri, S.K.; Dolati, S.; Santhakumar, J.; Thakor, A.S.; Yarani, R. Autologous Conditioned Serum for Degenerative Diseases and Prospects. *Growth Factors* **2021**, *39*, 59–70, doi:10.1080/08977194.2021.2012467.

53. Tokawa, P.K.A.; Brossi, P.M.; Baccarin, R.Y.A. Autologous Conditioned Serum in Equine and Human Orthopedic Therapy: A Systematic Review. *Research in Veterinary Science* **2022**, *146*, 34–52, doi:10.1016/j.rvsc.2022.03.009.

USC UNIVERSIDADE DE SANTIAGO DE COMPOSTELA

54. Murakami, T.; Nakaminami, Y.; Takahata, Y.; Hata, K.; Nishimura, R. Activation and Function of NLRP3 Inflammasome in Bone and Joint-Related Diseases. *IJMS* **2022**, *23*, 5365, doi:10.3390/ijms23105365.

55. Raeissadat, S.A.; Rayegani, S.M.; Sohrabi, M.R.; Jafarian, N.; Bahrami, M.N. Effectiveness of Intra-Articular Autologous-Conditioned Serum Injection in Knee Osteoarthritis: A Meta-Analysis Study. *Future Science OA* **2021**, *7*, FSO759, doi:10.2144/fsoa-2021-0069.

56. Rutgers, M.; Saris, D.B.; Dhert, W.J.; Creemers, L.B. Cytokine Profile of Autologous Conditioned Serum for Treatment of Osteoarthritis, in Vitro Effects on Cartilage Metabolism and Intra-Articular Levels after Injection. *Arthritis Res Ther* **2010**, *12*, R114, doi:10.1186/ar3050.

57. Frizziero, A.; Giannotti, E.; Oliva, F.; Masiero, S.; Maffulli, N. Autologous Conditioned Serum for the Treatment of Osteoarthritis and Other Possible Applications in Musculoskeletal Disorders. *British Medical Bulletin* **2013**, *105*, 169–184, doi:10.1093/bmb/lds016.

58. Baltzer, A.W.A.; Moser, C.; Jansen, S.A.; Krauspe, R. Autologous Conditioned Serum (Orthokine) Is an Effective Treatment for Knee Osteoarthritis. *Osteoarthritis and Cartilage* **2009**, *17*, 152–160, doi:10.1016/j.joca.2008.06.014.

59. Vitali, M.; Ometti, M.; Drossinos, A.; Pironti, P.; Santoleri, L.; Salini, V. Autologous Conditioned Serum: Clinical and Functional Results Using a Novel Disease Modifying Agent for the Management of Knee Osteoarthritis. *Journal of Drug Assessment* **2020**, *9*, 43–51, doi:10.1080/21556660.2020.1734009.

60. Vitale, N.D.; Vandenbulcke, F.; Chisari, E.; Iacono, F.; Lovato, L.; Di Matteo, B.; Kon, E. Innovative Regenerative Medicine in the Management of Knee OA: The Role of Autologous Protein Solution. *Journal of Clinical Orthopaedics and Trauma* **2019**, *10*, 49–52, doi:10.1016/j.jcot.2018.08.019.

61. Kon, E.; Engebretsen, L.; Verdonk, P.; Nehrer, S.; Filardo, G. Autologous Protein Solution Injections for the Treatment of Knee Osteoarthritis: 3-Year Results. *Am J Sports Med* **2020**, *48*, 2703–2710, doi:10.1177/0363546520944891.

62. Kuwasawa, A.; Okazaki, K.; Noda, K.; Nihei, K. Clinical Results of Autologous Protein Solution Injection for Knee Osteoarthritis with Severe Disease Grade Is Inferior to Mild or Moderate Grade. *Sci Rep* **2023**, *13*, 6404, doi:10.1038/s41598-023-33659-1.

63. He, Z.; Wang, B.; Hu, C.; Zhao, J. An Overview of Hydrogel-Based Intra-Articular Drug Delivery for the Treatment of Osteoarthritis. *Colloids and Surfaces B: Biointerfaces* **2017**, *154*, 33–39, doi:10.1016/j.colsurfb.2017.03.003.

64. Li, H.; Gou, R.; Liao, J.; Wang, Y.; Qu, R.; Tang, Q.; Gan, J.; Zou, L.; Shi, S. Recent Advances in Nano-Targeting Drug Delivery Systems for Rheumatoid Arthritis Treatment. *Acta Materia Medica* **2023**, *2*, doi:10.15212/AMM-2022-0039.

65. Rai, M.F.; Pham, C.T. Intra-Articular Drug Delivery Systems for Joint Diseases. *Current Opinion in Pharmacology* **2018**, *40*, 67–73, doi:10.1016/j.coph.2018.03.013.

66. Wongrakpanich, A.; Khunkitchai, N.; Achayawat, Y.; Suksiriworapong, J. Ketorolac-Loaded PLGA-/PLA-Based Microparticles Stabilized by Hyaluronic Acid: Effects of

USC UNIVERSIDADE DE SANTIAGO DE COMPOSTELA

Formulation Composition and Emulsification Technique on Particle Characteristics and Drug Release Behaviors. *Polymers* **2023**, *15*, 266, doi:10.3390/polym15020266.

67. Song, P.; Cui, Z.; Hu, L. Applications and Prospects of Intra-Articular Drug Delivery System in Arthritis Therapeutics. *Journal of Controlled Release* **2022**, *352*, 946–960, doi:10.1016/j.jconrel.2022.11.018.

68. Dwivedi, P.; Nayak, V.; Kowshik, M. Role of Gold Nanoparticles as Drug Delivery Vehicles for Chondroitin Sulfate in the Treatment of Osteoarthritis: Biotechnol. Prog. *Biotechnol Progress* **2015**, *31*, 1416–1422, doi:10.1002/btpr.2147.

69. Wen, J.; Li, H.; Dai, H.; Hua, S.; Long, X.; Li, H.; Ivanovski, S.; Xu, C. Intra-Articular Nanoparticles Based Therapies for Osteoarthritis and Rheumatoid Arthritis Management. *Materials Today Bio* **2023**, *19*, 100597, doi:10.1016/j.mtbio.2023.100597.

70. García-García, P.; Reyes, R.; García-Sánchez, D.; Pérez-Campo, F.M.; Rodríguez-Rey, J.C.; Évora, C.; Díaz-Rodríguez, P.; Delgado, A. Nanoparticle-Mediated Selective Sfrp-1 Silencing Enhances Bone Density in Osteoporotic Mice. *J Nanobiotechnol* **2022**, *20*, 462, doi:10.1186/s12951-022-01674-5.

71. Gaur, M.; Maurya, S.; Akhtar, Mohd.S.; Yadav, A.B. Synthesis and Evaluation of BSA-Loaded PLGA–Chitosan Composite Nanoparticles for the Protein-Based Drug Delivery System. *ACS Omega* **2023**, *8*, 18751–18759, doi:10.1021/acsomega.3c00738.

72. Ghosal, K.; Chatterjee, S.; Thomas, S.; Roy, P. A Detailed Review on Synthesis, Functionalization, Application, Challenges, and Current Status of Magnetic Nanoparticles in the Field of Drug Delivery and Gene Delivery System. *AAPS PharmSciTech* **2022**, *24*, 25, doi:10.1208/s12249-022-02485-5.

73. Mitchell, M.J.; Billingsley, M.M.; Haley, R.M.; Wechsler, M.E.; Peppas, N.A.; Langer, R. Engineering Precision Nanoparticles for Drug Delivery. *Nat Rev Drug Discov* **2021**, *20*, 101–124, doi:10.1038/s41573-020-0090-8.

74. Viegas, C.; Patrício, A.B.; Prata, J.M.; Nadhman, A.; Chintamaneni, P.K.; Fonte, P. Solid Lipid Nanoparticles vs. Nanostructured Lipid Carriers: A Comparative Review. *Pharmaceutics* **2023**, *15*, 1593, doi:10.3390/pharmaceutics15061593.

75. Hadinoto, K.; Sundaresan, A.; Cheow, W.S. Lipid–Polymer Hybrid Nanoparticles as a New Generation Therapeutic Delivery Platform: A Review. *European Journal of Pharmaceutics and Biopharmaceutics* **2013**, *85*, 427–443, doi:10.1016/j.ejpb.2013.07.002.

76. Farooq, M.A.; Trevaskis, N.L. TPGS Decorated Liposomes as Multifunctional Nano-Delivery Systems. *Pharm Res* **2023**, *40*, 245–263, doi:10.1007/s11095-022-03424-6.

77. Wang, S.; Chen, Y.; Guo, J.; Huang, Q. Liposomes for Tumor Targeted Therapy: A Review. *IJMS* **2023**, *24*, 2643, doi:10.3390/ijms24032643.

78. Gao, J.; Xia, Z.; Mary, H.B.; Joseph, J.; Luo, J.N.; Joshi, N. Overcoming Barriers for Intra-Articular Delivery of Disease-Modifying Osteoarthritis Drugs. *Trends in Pharmacological Sciences* **2022**, *43*, 171–187, doi:10.1016/j.tips.2021.12.004.

79. DeJulius, C.R.; Gulati, S.; Hasty, K.A.; Crofford, L.J.; Duvall, C.L. Recent Advances in Clinical Translation of Intra-Articular Osteoarthritis Drug Delivery Systems. *Advanced Therapeutics* **2021**, *4*, 2000088, doi:10.1002/adtp.202000088.

USC UNIVERSIDADE DE SANTIAGO DE COMPOSTELA

80. Sangsuwan, R.; Yik, J.H.N.; Owen, M.; Liu, G.-Y.; Haudenschild, D.R.; Lewis, J.S. Intra-Articular Injection of Flavopiridol-Loaded Microparticles for Treatment of Post-Traumatic Osteoarthritis. *Acta Biomaterialia* **2022**, *149*, 347–358, doi:10.1016/j.actbio.2022.06.042.

81. Cao, Y.; Ma, Y.; Tao, Y.; Lin, W.; Wang, P. Intra-Articular Drug Delivery for Osteoarthritis Treatment. *Pharmaceutics* **2021**, *13*, 2166, doi:10.3390/pharmaceutics13122166.

82. Martinez-Borrajo, R.; Diaz-Rodriguez, P.; Landin, M. Rationalized Design to Explore the Full Potential of PLGA Microspheres as Drug Delivery Systems. *Drug Delivery* **2023**, *30*, 2219864, doi:10.1080/10717544.2023.2219864.

83. Pradal, J.; Maudens, P.; Gabay, C.; Seemayer, C.A.; Jordan, O.; Allémann, E. Effect of Particle Size on the Biodistribution of Nano- and Microparticles Following Intra-Articular Injection in Mice. *International Journal of Pharmaceutics* **2016**, *498*, 119–129, doi:10.1016/j.ijpharm.2015.12.015.

84. Paik, J.; Duggan, S.T.; Keam, S.J. Triamcinolone Acetonide Extended-Release: A Review in Osteoarthritis Pain of the Knee. *Drugs* **2019**, *79*, 455–462, doi:10.1007/s40265-019-01083-3.

85. Rasmussen, S.; Kjær Petersen, K.; Kristiansen, M.K.; Skallerup, J.; Aboo, C.; Thomsen, M.E.; Skjoldemose, E.; Jørgensen, N.K.; Stensballe, A.; Arendt-Nielsen, L. Gold Micro-particles for Knee Osteoarthritis. *European Journal of Pain* **2022**, *26*, 811–824, doi:10.1002/ejp.1909.

86. Gonzalez-Fernandez, P.; Rodríguez-Nogales, C.; Jordan, O.; Allémann, E. Combination of Mesenchymal Stem Cells and Bioactive Molecules in Hydrogels for Osteoarthritis Treatment. *European Journal of Pharmaceutics and Biopharmaceutics* **2022**, *172*, 41–52, doi:10.1016/j.ejpb.2022.01.003.

87. Wang, T.; Li, Y.; Liu, J.; Fang, Y.; Guo, W.; Liu, Y.; Li, X.; Li, G.; Wang, X.; Zheng, Z.; et al. Intraarticularly Injectable Silk Hydrogel Microspheres with Enhanced Mechanical and Structural Stability to Attenuate Osteoarthritis. *Biomaterials* **2022**, *286*, 121611, doi:10.1016/j.biomaterials.2022.121611.

88. Zhao, Y.; Zhu, Z.S.; Guan, J.; Wu, S.J. Processing, Mechanical Properties and Bio-Applications of Silk Fibroin-Based High-Strength Hydrogels. *Acta Biomaterialia* **2021**, *125*, 57–71, doi:10.1016/j.actbio.2021.02.018.

89. Zheng, H.; Zuo, B. Functional Silk Fibroin Hydrogels: Preparation, Properties and Applications. *J. Mater. Chem. B* **2021**, *9*, 1238–1258, doi:10.1039/D0TB02099K.

90. Xu, J.; Qu, Y.; Li, H.; Zhu, A.; Jiang, T.; Chong, Z.; Wang, B.; Shen, P.; Xie, Z. Effect of Intra-Articular Ketorolac Versus Corticosteroid Injection for Knee Osteoarthritis: A Retrospective Comparative Study. *Orthopaedic Journal of Sports Medicine* **2020**, *8*, 232596712091112, doi:10.1177/2325967120911126.

91. Study Details | Safety of Intra-Articular Sc-rAAV2.5IL-1Ra in Subjects With Moderate Knee OA | ClinicalTrials.Gov.

92. Chevalier, X.; Goupille, P.; Beaulieu, A.D.; Burch, F.X.; Bensen, W.G.; Conrozier, T.; Loeuille, D.; Kivitz, A.J.; Silver, D.; Appleton, B.E. Intraarticular Injection of Anakinra

USC UNIVERSIDADE DE SANTIAGO DE COMPOSTELA

in Osteoarthritis of the Knee: A Multicenter, Randomized, Double-blind, Placebo-controlled Study. *Arthritis & Rheumatism* **2009**, *61*, 344–352, doi:10.1002/art.24096.

93. Mehta, S.; He, T.; Bajpayee, A.G. Recent Advances in Targeted Drug Delivery for Treatment of Osteoarthritis. *Current Opinion in Rheumatology* **2021**, *33*, 94–109, doi:10.1097/BOR.0000000000000761.

94. Study Details | A Safety and Efficacy Study of Anti-Inflammatory (Canakinumab) and Cartilage Stimulating (LNA043) Drugs Injected Into the Knee Joint of Participants With Knee Osteoarthritis (OA) | ClinicalTrials.Gov.

95. Li, Y.; Mai, Y.; Cao, P.; Wen, X.; Fan, T.; Wang, X.; Ruan, G.; Tang, S.; Ding, C.; Zhu, Z. Relative Efficacy and Safety of Anti-Inflammatory Biologic Agents for Osteoarthritis: A Conventional and Network Meta-Analysis. *JCM* **2022**, *11*, 3958, doi:10.3390/jcm11143958.

96. Study Details | Efficacy of Intra-Articular Injection of Etanercept for Moderate and Severe Knee Osteoarthritis | ClinicalTrials.Gov.

97. Gerwin, N.; Scotti, C.; Halleux, C.; Fornaro, M.; Elliott, J.; Zhang, Y.; Johnson, K.; Shi, J.; Walter, S.; Li, Y.; et al. Angiopoietin-like 3-Derivative LNA043 for Cartilage Regeneration in Osteoarthritis: A Randomized Phase 1 Trial. *Nat Med* **2022**, *28*, 2633–2645, doi:10.1038/s41591-022-02059-9.

98. Jones, I.A.; Togashi, R.; Wilson, M.L.; Heckmann, N.; Vangsness, C.T. Intra-Articular Treatment Options for Knee Osteoarthritis. *Nat Rev Rheumatol* **2019**, *15*, 77–90, doi:10.1038/s41584-018-0123-4.

99. Nooh, M.H.; Alshehri, M.S.; Alzahrani, Z.S.; Alsolami, H.M.; Almutairi, A.O.; AlOtaibi, A.S.; Ajohani, A.N. The Efficacy and Safety of Intra-Articular Low Molecular Weight Fraction of Human Serum Albumin for the Management of Moderate to Moderately Severe Knee Osteoarthritis: A Systematic Review and Meta-Analysis. *Cureus* **2023**, doi:10.7759/cureus.41240.

100. Salottolo, K.; Cole, B.; Bar-Or, D. Intra-Articular Injection of the Anti-Inflammatory Compound LMWF-5A in Adults with Severe Osteoarthritis: A Double-Blind Prospective Randomized Controlled Multi-Center Safety and Efficacy Trial. *Patient Saf Surg* **2018**, *12*, 11, doi:10.1186/s13037-018-0158-0.

101. Yu, S.P.; Hunter, D.J. Intra-Articular Therapies for Osteoarthritis. *Expert Opinion on Pharmacotherapy* **2016**, *17*, 2057–2071, doi:10.1080/14656566.2016.1232396.

102. RODRIGUEZ-MERCHAN, E.C. The Current Role of Disease-Modifying Osteoarthritis Drugs. *ABJS* **2022**, doi:10.22038/abjs.2021.56530.2807.

103. Li, S.; Cao, P.; Chen, T.; Ding, C. Latest Insights in Disease-Modifying Osteoarthritis Drugs Development. *Therapeutic Advances in Musculoskeletal* **2023**, *15*, 1759720X2311698, doi:10.1177/1759720X231169839.

104. Mehta, S.; He, T.; Bajpayee, A.G. Recent Advances in Targeted Drug Delivery for Treatment of Osteoarthritis. *Current Opinion in Rheumatology* **2021**, *33*, 94–109, doi:10.1097/BOR.0000000000000761.

105. Grol, M.W. The Evolving Landscape of Gene Therapy Strategies for the Treatment of Osteoarthritis. *Osteoarthritis and Cartilage* **2024**, S1063458424000013, doi:10.1016/j.joca.2023.12.009.

106. Rodriguez-Merchan, E.C.; Valentino, L.A. The Role of Gene Therapy in Cartilage Repair. . *NUMBER* **2019**, *7*.

107. Evans, C.H.; Ghivizzani, S.C.; Robbins, P.D. Osteoarthritis Gene Therapy in 2022. *Current Opinion in Rheumatology* **2023**, *35*, 37–43, doi:10.1097/BOR.0000000000000918.

108. Hunter, D.J.; Chang, C.-C.; Wei, J.C.-C.; Lin, H.-Y.; Brown, C.; Tai, T.-T.; Wu, C.-F.; Chuang, W.C.-M.; Shih, S.-F. TLC599 in Patients with Osteoarthritis of the Knee: A Phase IIa, Randomized, Placebo-Controlled, Dose-Finding Study. *Arthritis Res Ther* **2022**, *24*, 52, doi:10.1186/s13075-022-02739-4.

109. Amirsaadat, S.; Amirazad, H.; Hashemihesar, R.; Zarghami, N. An Update on the Effect of Intra-Articular Intervention Strategies Using Nanomaterials in Osteoarthritis: Possible Clinical Application. *Front. Bioeng. Biotechnol.* **2023**, *11*, 1128856, doi:10.3389/fbioe.2023.1128856.

110. Ma, L.; Zheng, X.; Lin, R.; Sun, A.R.; Song, J.; Ye, Z.; Liang, D.; Zhang, M.; Tian, J.; Zhou, X.; et al. Knee Osteoarthritis Therapy: Recent Advances in Intra-Articular Drug Delivery Systems. *DDDT* **2022**, *Volume 16*, 1311–1347, doi:10.2147/DDDT.S357386.

111. Bordon, G.; Berenbaum, F.; Distler, O.; Luciani, P. Harnessing the Multifunctionality of Lipid-Based Drug Delivery Systems for the Local Treatment of Osteoarthritis. *Biomedicine & Pharmacotherapy* **2023**, *168*, 115819, doi:10.1016/j.biopha.2023.115819.

112. Osteoarthritis: Structural Endpoints for the Development of Drugs, Devices, and Biological Products for Treatment Guidance for Industry. **2018**.

113. Kim, H.; Seo, J.; Lee, Y.; Park, K.; Perry, T.A.; Arden, N.K.; Mobasheri, A.; Choi, H. The Current State of the Osteoarthritis Drug Development Pipeline: A Comprehensive Narrative Review of the Present Challenges and Future Opportunities. *Therapeutic Advances in Musculoskeletal* **2022**, *14*, 1759720X2210859, doi:10.1177/1759720X221085952.

114. Nogueira-Recalde, U.; Lorenzo-Gómez, I.; Blanco, F.J.; Loza, M.I.; Grassi, D.; Shirinsky, V.; Shirinsky, I.; Lotz, M.; Robbins, P.D.; Domínguez, E.; et al. Fibrates as Drugs with Senolytic and Autophagic Activity for Osteoarthritis Therapy. *EBioMedicine* **2019**, *45*, 588–605, doi:10.1016/j.ebiom.2019.06.049.

115. Oishi, Y.; Manabe, I. Macrophages in Inflammation, Repair and Regeneration. *International Immunology* **2018**, *30*, 511–528, doi:10.1093/intimm/dxy054.

116. Zhou, K.; Yang, C.; Shi, K.; Liu, Y.; Hu, D.; He, X.; Yang, Y.; Chu, B.; Peng, J.; Zhou, Z.; et al. Activated Macrophage Membrane-Coated Nanoparticles Relieve Osteoarthritis-Induced Synovitis and Joint Damage. *Biomaterials* **2023**, *295*, 122036, doi:10.1016/j.biomaterials.2023.122036.

117. Chen, X.; Zhang, L.; Shao, X.; Gong, W.; Shi, T.; Dong, J.; Shi, Y.; Shen, S.; He, Y.; Qin, J.; et al. Specific Clearance of Senescent Synoviocytes Suppresses the Development of Osteoarthritis Based on Aptamer-Functionalized Targeted Drug Delivery System. *Adv Funct Materials* **2022**, *32*, 2109460, doi:10.1002/adfm.202109460.

118. He, K.; Huang, X.; Shan, R.; Yang, X.; Song, R.; Xie, F.; Huang, G. Intra-Articular Injection of Lornoxicam and MicroRNA-140 Co-Loaded Cationic Liposomes Enhanced

USC UNIVERSIDADE DE SANTIAGO DE COMPOSTELA

the Therapeutic Treatment of Experimental Osteoarthritis. *AAPS PharmSciTech* **2021**, *23*, 9, doi:10.1208/s12249-021-02149-w.

119. Deng, C.; Chen, Y.; Zhao, X.; Yu, L.; Xiao, Y.; Li, H.; Zhang, Y.; Ai, K.; Zhou, D.; Bai, X.; et al. Apoptotic Neutrophil Membrane-Camouflaged Liposomes for Dually Targeting Synovial Macrophages and Fibroblasts to Attenuate Osteoarthritis. *ACS Appl. Mater. Interfaces* **2023**, *15*, 39064–39080, doi:10.1021/acsami.3c05861.

120. Ebada, H.M.; Nasra, M.M.; Nassra, R.A.; Solaiman, A.A.; Abdallah, O.Y. Cationic Nanocarrier of Rhein Based on Hydrophobic Ion Pairing Approach as Intra-Articular Targeted Regenerative Therapy for Osteoarthritis. *Colloids and Surfaces B: Biointerfaces* **2022**, *211*, 112285, doi:10.1016/j.colsurfb.2021.112285.

121. Rouco, H.; Diaz-Rodriguez, P.; Remuñán-López, C.; Landin, M. Recent Advances in Solid Lipid Nanoparticles Formulation and Clinical Applications. In *Nanomaterials for Clinical Applications*; Elsevier, 2020; pp. 213–247 ISBN 978-0-12-816705-2.

122. Khalili, L.; Dehghan, G.; Sheibani, N.; Khataee, A. Smart Active-Targeting of Lipid-Polymer Hybrid Nanoparticles for Therapeutic Applications: Recent Advances and Challenges. *International Journal of Biological Macromolecules* **2022**, *213*, 166–194, doi:10.1016/j.ijbiomac.2022.05.156.

123. Mukherjee, A.; Waters, A.K.; Kalyan, P.; Achrol, A.S.; Kesari, S.; Yenugonda, V.M. Lipid–Polymer Hybrid Nanoparticles as a next-Generation Drug Delivery Platform: State of the Art, Emerging Technologies, and Perspectives. *IJN* **2019**, *Volume 14*, 1937–1952, doi:10.2147/IJN.S198353.

124. Ai, X.; Duan, Y.; Zhang, Q.; Sun, D.; Fang, R.H.; Liu-Bryan, R.; Gao, W.; Zhang, L. CARTILAGE-TARGETING ULTRASMALL LIPID-POLYMER Hybrid Nanoparticles for the Prevention of Cartilage Degradation. *Bioengineering & Transla Med* **2021**, *6*, e10187, doi:10.1002/btm2.10187.

125. Wang, G.; Zhang, X.; Kapilevich, L.; Hu, M. Recent Advances in Polymeric Microparticle-Based Drug Delivery Systems for Knee Osteoarthritis Treatment. *Front. Bioeng. Biotechnol.* **2023**, *11*, 1290870, doi:10.3389/fbioe.2023.1290870.

126. Gambaro, F.M.; Ummarino, A.; Torres Andón, F.; Ronzoni, F.; Di Matteo, B.; Kon, E. Drug Delivery Systems for the Treatment of Knee Osteoarthritis: A Systematic Review of In Vivo Studies. *IJMS* **2021**, *22*, 9137, doi:10.3390/ijms22179137.

127. Abd-Allah, H.; Kamel, A.O.; Sammour, O.A. Injectable Long Acting Chitosan/Tripolyphosphate Microspheres for the Intra-Articular Delivery of Lornoxicam: Optimization and in Vivo Evaluation. *Carbohydrate Polymers* **2016**, *149*, 263–273, doi:10.1016/j.carbpol.2016.04.096.

128. Diaz-Rodriguez, P.; Mariño, C.; Vázquez, J.A.; Caeiro-Rey, J.R.; Landin, M. Targeting Joint Inflammation for Osteoarthritis Management through Stimulus-Sensitive Hyaluronic Acid Based Intra-Articular Hydrogels. *Materials Science and Engineering: C* **2021**, *128*, 112254, doi:10.1016/j.msec.2021.112254.

129. Garcia-del Rio, L.; Diaz-Rodriguez, P.; Landin, M. Multicomponent Hybrid Hydrogels for Biomedical Applications: Opportunities and Challenges. In *Multicomponent Hydrogels*; Dodda, J.M., Deshmukh, K., Bezuidenhout, D., Eds.; The Royal Society of Chemistry, 2023; pp. 313–345 ISBN 978-1-83916-727-0.

USC UNIVERSIDADE DE SANTIAGO DE COMPOSTELA

130. Garcia-del Rio, L.; Diaz-Rodriguez, P.; Landin, M. Design of Novel Orotransmucosal Vaccine-Delivery Platforms Using Artificial Intelligence. *European Journal of Pharmaceutics and Biopharmaceutics* **2021**, *159*, 36–43, doi:10.1016/j.ejpb.2020.12.018.

131. Rouco, H.; Diaz-Rodriguez, P.; Rama-Molinos, S.; Remuñán-López, C.; Landin, M. Delimiting the Knowledge Space and the Design Space of Nanostructured Lipid Carriers through Artificial Intelligence Tools. *International Journal of Pharmaceutics* **2018**, *553*, 522–530, doi:10.1016/j.ijpharm.2018.10.058.

132. Di Francesco, V.; Boso, D.P.; Moore, T.L.; Schrefler, B.A.; Decuzzi, P. Machine Learning Instructed Microfluidic Synthesis of Curcumin-Loaded Liposomes. *Biomed Microdevices* **2023**, *25*, 29, doi:10.1007/s10544-023-00671-1.

133. Rebollo, R.; Oyoun, F.; Corvis, Y.; El-Hammadi, M.M.; Saubamea, B.; Andrieux, K.; Mignet, N.; Alhareth, K. Microfluidic Manufacturing of Liposomes: Development and Optimization by Design of Experiment and Machine Learning. *ACS Appl. Mater. Interfaces* **2022**, *14*, 39736–39745, doi:10.1021/acsami.2c06627.

134. Sansare, S.; Duran, T.; Mohammadiarani, H.; Goyal, M.; Yenduri, G.; Costa, A.; Xu, X.; O'Connor, T.; Burgess, D.; Chaudhuri, B. Artificial Neural Networks in Tandem with Molecular Descriptors as Predictive Tools for Continuous Liposome Manufacturing. *International Journal of Pharmaceutics* **2021**, *603*, 120713, doi:10.1016/j.ijpharm.2021.120713.

135. García-García, P.; Briffault, E.; Landin, M.; Evora, C.; Diaz-Rodriguez, P.; Delgado, A. Tailor-Made Oligonucleotide-Loaded Lipid-Polymer Nanosystems Designed for Bone Gene Therapy. *Drug Deliv. and Transl. Res.* **2021**, *11*, 598–607, doi:10.1007/s13346-021-00926-5.

136. Hathout, R.M.; Metwally, A.A. Towards Better Modelling of Drug-Loading in Solid Lipid Nanoparticles: Molecular Dynamics, Docking Experiments and Gaussian Processes Machine Learning. *European Journal of Pharmaceutics and Biopharmaceutics* **2016**, *108*, 262–268, doi:10.1016/j.ejpb.2016.07.019.

137. Metwally, A.A.; Hathout, R.M. Computer-Assisted Drug Formulation Design: Novel Approach in Drug Delivery. *Mol. Pharmaceutics* **2015**, *12*, 2800–2810, doi:10.1021/mp500740d.

138. Burdușel, A.-C.; Andronescu, E. Lipid Nanoparticles and Liposomes for Bone Diseases Treatment. *Biomedicines* **2022**, *10*, 3158, doi:10.3390/biomedicines10123158.

139. Leong, E.W.X.; Ge, R. Lipid Nanoparticles as Delivery Vehicles for Inhaled Therapeutics. *Biomedicines* **2022**, *10*, 2179, doi:10.3390/biomedicines10092179.

140. Cummings, R.D. The Mannose Receptor Ligands and the Macrophage Glycome. *Current Opinion in Structural Biology* **2022**, *75*, 102394, doi:10.1016/j.sbi.2022.102394.

141. Costa, A.; Sarmento, B.; Seabra, V. Mannose-Functionalized Solid Lipid Nanoparticles Are Effective in Targeting Alveolar Macrophages. *European Journal of Pharmaceutical Sciences* **2018**, *114*, 103–113, doi:10.1016/j.ejps.2017.12.006.

142. Shapouri-Moghaddam, A.; Mohammadian, S.; Vazini, H.; Taghadosi, M.; Esmaeili, S.; Mardani, F.; Seifi, B.; Mohammadi, A.; Afshari, J.T.; Sahebkar, A. Macrophage

USC UNIVERSIDADE DE SANTIAGO DE COMPOSTELA

Plasticity, Polarization, and Function in Health and Disease. *J Cell Physiol* **2018**, *233*, 6425–6440, doi:10.1002/jcp.26429.

143. Pinheiro, M.; Couto, A.; Chaves, L.; Ferreira, D.; Sarmento, B.; Reis, S. Design and Statistical Modeling of Mannose-Decorated Dapsone-Containing Nanoparticles as a Strategy of Targeting Intestinal M-Cells. *IJN* **2016**, 2601, doi:10.2147/IJN.S104908.

144. Ogay, V.; Mun, E.A.; Kudaibergen, G.; Baidarbekov, M.; Kassymbek, K.; Zharkinbekov, Z.; Saparov, A. Progress and Prospects of Polymer-Based Drug Delivery Systems for Bone Tissue Regeneration. *Polymers* **2020**, *12*, 2881, doi:10.3390/polym12122881.

145. Oliveira, M.B.; Mano, J.F. Polymer-Based Microparticles in Tissue Engineering and Regenerative Medicine. *Biotechnol Progress* **2011**, *27*, 897–912, doi:10.1002/btpr.618.

146. Varde, N.K.; Pack, D.W. Microspheres for Controlled Release Drug Delivery. *Expert Opin. Biol. Ther.* **2004**, 17.

147. Mensah, R.A.; Kirton, S.B.; Cook, M.T.; Styliari, I.D.; Hutter, V.; Chau, D.Y.S. Optimising Poly(Lactic-Co-Glycolic Acid) Microparticle Fabrication Using a Taguchi Orthogonal Array Design-of-Experiment Approach. *PLoS ONE* **2019**, *14*, e0222858, doi:10.1371/journal.pone.0222858.

148. Han, F.Y.; Thurecht, K.J.; Whittaker, A.K.; Smith, M.T. Bioerodable PLGA-Based Microparticles for Producing Sustained-Release Drug Formulations and Strategies for Improving Drug Loading. *Front. Pharmacol.* **2016**, *7*, doi:10.3389/fphar.2016.00185.

149. Tran, V.-T.; Benoît, J.-P.; Venier-Julienne, M.-C. Why and How to Prepare Biodegradable, Monodispersed, Polymeric Microparticles in the Field of Pharmacy? *International Journal of Pharmaceutics* **2011**, *407*, 1–11, doi:10.1016/j.ijpharm.2011.01.027.

150. Park, K.; Skidmore, S.; Hadar, J.; Garner, J.; Park, H.; Otte, A.; Soh, B.K.; Yoon, G.; Yu, D.; Yun, Y.; et al. Injectable, Long-Acting PLGA Formulations: Analyzing PLGA and Understanding Microparticle Formation. *Journal of Controlled Release* **2019**, *304*, 125–134, doi:10.1016/j.jconrel.2019.05.003.

151. Henshaw, C.A.; Dundas, A.A.; Cuzzucoli Crucitti, V.; Alexander, M.R.; Wildman, R.; Rose, F.R.A.J.; Irvine, D.J.; Williams, P.M. Droplet Microfluidic Optimisation Using Micropipette Characterisation of Bio-Instructive Polymeric Surfactants. *Molecules* **2021**, *26*, 3302, doi:10.3390/molecules26113302.

152. Varela-Fernández, R.; Bendicho-Lavilla, C.; Martin-Pastor, M.; Herrero Vanrell, R.; Lema-Gesto, M.I.; González-Barcia, M.; Otero-Espinar, F.J. Design, Optimization, and in Vitro Characterization of Idebenone-Loaded PLGA Microspheres for LHON Treatment. *International Journal of Pharmaceutics* **2022**, *616*, 121504, doi:10.1016/j.ijpharm.2022.121504.

153. Colbourn, E.A.; Roskilly, S.J.; Rowe, R.C.; York, P. Modelling Formulations Using Gene Expression Programming – A Comparative Analysis with Artificial Neural Networks. *European Journal of Pharmaceutical Sciences* **2011**, *44*, 366–374, doi:10.1016/j.ejps.2011.08.021.

154. Rowe, R.C.; Colbourn, E.A. Neural Computing in Product Formulation. *The Chemical Educator* **2003**, 9.

155. Echezarreta-López, M.M.; Landin, M. Using Machine Learning for Improving Knowledge on Antibacterial Effect of Bioactive Glass. *International Journal of Pharmaceutics* **2013**, *453*, 641–647, doi:10.1016/j.ijpharm.2013.06.036.

156. Szlęk, J.; Pacławski, A.; Lau, R.; Jachowicz, R.; Kazemi, P.; Mendyk, A. Empirical Search for Factors Affecting Mean Particle Size of PLGA Microspheres Containing Macromolecular Drugs. *Computer Methods and Programs in Biomedicine* **2016**, *134*, 137–147, doi:10.1016/j.cmpb.2016.07.006.

157. Rodríguez-Dorado, R.; Landín, M.; Altai, A.; Russo, P.; Aquino, R.P.; Del Gaudio, P. A Novel Method for the Production of Core-Shell Microparticles by Inverse Gelation Optimized with Artificial Intelligent Tools. *International Journal of Pharmaceutics* **2018**, *538*, 97–104, doi:10.1016/j.ijpharm.2018.01.023.

158. Gaspar, D.P.; Faria, V.; Gonçalves, L.M.D.; Taboada, P.; Remuñán-López, C.; Almeida, A.J. Rifabutin-Loaded Solid Lipid Nanoparticles for Inhaled Antitubercular Therapy: Physicochemical and in Vitro Studies. *International Journal of Pharmaceutics* **2016**, *497*, 199–209, doi:10.1016/j.ijpharm.2015.11.050.

159. Morris, G.M.; Huey, R.; Lindstrom, W.; Sanner, M.F.; Belew, R.K.; Goodsell, D.S.; Olson, A.J. AutoDock4 and AutoDockTools4: Automated Docking with Selective Receptor Flexibility. *J Comput Chem* **2009**, *30*, 2785–2791, doi:10.1002/jcc.21256.

160. Pereira-da-Mota, A.F.; Vivero-Lopez, M.; Topete, A.; Serro, A.P.; Concheiro, A.; Alvarez-Lorenzo, C. Atorvastatin-Eluting Contact Lenses: Effects of Molecular Imprinting and Sterilization on Drug Loading and Release. *Pharmaceutics* **2021**, *13*, 606, doi:10.3390/pharmaceutics13050606.

161. Morris, G.M.; Goodsell, D.S.; Pique, M.E.; Huey, R.; Hart, W.E.; Halliday, S.; Belew, R.; Olson, A.J. Updated for Version 4.2.6.

162. Rouco, H.; Diaz-Rodriguez, P.; Gaspar, D.P.; Gonçalves, L.M.D.; Cuerva, M.; Remuñán-López, C.; Almeida, A.J.; Landin, M. Rifabutin-Loaded Nanostructured Lipid Carriers as a Tool in Oral Anti-Mycobacterial Treatment of Crohn's Disease. *Nanomaterials* **2020**, *10*, 2138, doi:10.3390/nano10112138.

163. Vieira, A.C.; Magalhães, J.; Rocha, S.; Cardoso, M.S.; Santos, S.G.; Borges, M.; Pinheiro, M.; Reis, S. Targeted Macrophages Delivery of Rifampicin-Loaded Lipid Nanoparticles to Improve Tuberculosis Treatment. *Nanomedicine* **2017**, *12*, 2721–2736, doi:10.2217/nnm-2017-0248.

164. Magalhães, J.; Pinheiro, M.; Drasler, B.; Septiadi, D.; Petri-Fink, A.; Santos, S.G.; Rothen-Rutishauser, B.; Reis, S. Lipid Nanoparticles Biocompatibility and Cellular Uptake in a 3D Human Lung Model. *Nanomedicine* **2020**, *15*, 259–271, doi:10.2217/nnm-2019-0256.

165. Shao, Q.; Rowe, R.C.; York, P. Comparison of Neurofuzzy Logic and Neural Networks in Modelling Experimental Data of an Immediate Release Tablet Formulation. *European Journal of Pharmaceutical Sciences* **2006**, *28*, 394–404, doi:10.1016/j.ejps.2006.04.007.

166. Kang, J.-Y.; Kwon, O.; Gil, J.Y.; Oh, D.-B. Data for Analysis of Mannose-6-Phosphate Glycans Labeled with Fluorescent Tags. *Data in Brief* **2016**, *7*, 1531–1537, doi:10.1016/j.dib.2016.04.042.

USC UNIVERSIDADE DE SANTIAGO DE COMPOSTELA

167. Rouco, H.; García-García, P.; Évora, C.; Díaz-Rodríguez, P.; Delgado, A. Screening Strategies for Surface Modification of Lipid-Polymer Hybrid Nanoparticles. *International Journal of Pharmaceutics* **2022**, *624*, 121973, doi:10.1016/j.ijpharm.2022.121973.

168. Bacia, K.; Schwille, P. Practical Guidelines for Dual-Color Fluorescence Cross-Correlation Spectroscopy. *Nat Protoc* **2007**, *2*, 2842–2856, doi:10.1038/nprot.2007.410.

169. Gómez-Varela, A.I.; Gaspar, R.; Miranda, A.; Assis, J.L.; Valverde, R.H.F.; Einicker-Lamas, M.; Silva, B.F.B.; De Beule, P.A.A. Fluorescence CROSS-CORRELATION Spectroscopy as a Valuable Tool to Characterize Cationic LIPOSOME-DNA Nanoparticle Assembly. *Journal of Biophotonics* **2021**, *14*, e202000200, doi:10.1002/jbio.202000200.

170. Krieger, J.W.; Singh, A.P.; Bag, N.; Garbe, C.S.; Saunders, T.E.; Langowski, J.; Wohland, T. Imaging Fluorescence (Cross-) Correlation Spectroscopy in Live Cells and Organisms. *Nat Protoc* **2015**, *10*, 1948–1974, doi:10.1038/nprot.2015.100.

171. Schnatwinkel, C.; Christoforidis, S.; Lindsay, M.R.; Uttenweiler-Joseph, S.; Wilm, M.; Parton, R.G.; Zerial, M. The Rab5 Effector Rabankyrin-5 Regulates and Coordinates Different Endocytic Mechanisms. *PLoS Biol* **2004**, *2*, e261, doi:10.1371/journal.pbio.0020261.

172. Falk, J.; Konopacki, F.A.; Zivraj, K.H.; Holt, C.E. Rab5 and Rab4 Regulate Axon Elongation in the *Xenopus* Visual System. *J. Neurosci.* **2014**, *34*, 373–391, doi:10.1523/JNEUROSCI.0876-13.2014.

173. Scotece, M.; Conde, J.; Abella, V.; López, V.; Francisco, V.; Ruiz, C.; Campos, V.; Lago, F.; Gomez, R.; Pino, J.; et al. Oleocanthal Inhibits Catabolic and Inflammatory Mediators in LPS-Activated Human Primary Osteoarthritis (OA) Chondrocytes Through MAPKs/NF-κB Pathways. *Cell Physiol Biochem* **2018**, *49*, 2414–2426, doi:10.1159/000493840.

174. Caramés, B.; Hasegawa, A.; Taniguchi, N.; Miyaki, S.; Blanco, F.J.; Lotz, M. Autophagy Activation by Rapamycin Reduces Severity of Experimental Osteoarthritis. *Ann Rheum Dis* **2012**, *71*, 575–581, doi:10.1136/annrheumdis-2011-200557.

175. Glasson, S.S.; Chambers, M.G.; Van Den Berg, W.B.; Little, C.B. The OARSI Histopathology Initiative – Recommendations for Histological Assessments of Osteoarthritis in the Mouse. *Osteoarthritis and Cartilage* **2010**, *18*, S17–S23, doi:10.1016/j.joca.2010.05.025.

176. El-Leithy, E.S.; Ibrahim, H.K.; Sorour, R.M. *In Vitro* and *in Vivo* Evaluation of Indomethacin Nanoemulsion as a Transdermal Delivery System. *Drug Delivery* **2015**, *22*, 1010–1017, doi:10.3109/10717544.2013.844742.

177. Balguri, S.P.; Adelli, G.R.; Majumdar, S. Topical Ophthalmic Lipid Nanoparticle Formulations (SLN, NLC) of Indomethacin for Delivery to the Posterior Segment Ocular Tissues. *European Journal of Pharmaceutics and Biopharmaceutics* **2016**, *109*, 224–235, doi:10.1016/j.ejpb.2016.10.015.

178. Ricci, M.; Puglia, C.; Bonina, F.; Giovanni, C.D.; Giovagnoli, S.; Rossi, C. Evaluation of Indomethacin Percutaneous Absorption from Nanostructured Lipid Carriers (NLC): In Vitro and In Vivo Studies. *Journal of Pharmaceutical Sciences* **2005**, *94*, 1149–1159, doi:10.1002/jps.20335.

USC DE COMPOSTELA

179. Pietkiewicz, J.; Sznitowska, M.; Placzek, M. The Expulsion of Lipophilic Drugs from the Cores of Solid Lipid Microspheres in Diluted Suspensions and in Concentrates. *International Journal of Pharmaceutics* **2006**, *310*, 64–71, doi:10.1016/j.ijpharm.2005.11.038.

180. Varela-Fernández, R.; García-Otero, X.; Díaz-Tomé, V.; Regueiro, U.; López-López, M.; González-Barcia, M.; Isabel Lema, M.; Javier Otero-Espinar, F. Lactoferrin-Loaded Nanostructured Lipid Carriers (NLCs) as a New Formulation for Optimized Ocular Drug Delivery. *European Journal of Pharmaceutics and Biopharmaceutics* **2022**, *172*, 144–156, doi:10.1016/j.ejpb.2022.02.010.

181. Zaky, M.F.; Megahed, M.A.; Hammady, T.M.; Gad, S.; Ghorab, M.M.; El-Say, K.M. Tailoring Apixaban in Nanostructured Lipid Carrier Enhancing Its Oral Bioavailability and Anticoagulant Activity. *Pharmaceutics* **2022**, *15*, 80, doi:10.3390/pharmaceutics15010080.

182. Castelli, F.; Puglia, C.; Sarpietro, M.G.; Rizza, L.; Bonina, F. Characterization of Indomethacin-Loaded Lipid Nanoparticles by Differential Scanning Calorimetry. *International Journal of Pharmaceutics* **2005**, *304*, 231–238, doi:10.1016/j.ijpharm.2005.08.011.

183. Ahalwat, S.; Bhatt, D.C.; Rohilla, S.; Jogpal, V.; Sharma, K.; Virmani, T.; Kumar, G.; Alhalmi, A.; Alqahtani, A.S.; Noman, O.M.; et al. Mannose-Functionalized Isoniazid-Loaded Nanostructured Lipid Carriers for Pulmonary Delivery: In Vitro Prospects and In Vivo Therapeutic Efficacy Assessment. *Pharmaceuticals* **2023**, *16*, 1108, doi:10.3390/ph16081108.

184. Small, D.M. Lateral Chain Packing in Lipids and Membranes. *Journal of Lipid Research* **1984**, *25*, 1490–1500, doi:10.1016/S0022-2275(20)34422-9.

185. Kolsi, R.B.A.; Salah, H.B.; Jardak, N.; Chaaben, R.; Jribi, I.; Feki, A.E.; Rebai, T.; Jamoussi, K.; Allouche, N.; Blecker, C.; et al. Sulphated Polysaccharide Isolated from Sargassum Vulgare : Characterization and Hypolipidemic Effects. *Carbohydrate Polymers* **2017**, *170*, 148–159, doi:10.1016/j.carbpol.2017.04.083.

186. Sakamoto, Y.; Fujii, S.; Takano, S.; Fukushima, J.; Ando, M.; Kodera, N.; Nishimura, T. Manipulation of Macrophage Uptake by Controlling the Aspect Ratio of Graft Copolymer Micelles. *Nano Lett.* **2024**, acs.nanolett.4c01054, doi:10.1021/acs.nanolett.4c01054.

187. Soni, S.S.; Kim, K.M.; Sarkar, B.; Rodell, C.B. Uptake of Cyclodextrin Nanoparticles by Macrophages Is Dependent on Particle Size and Receptor-Mediated Interactions. *ACS Appl. Bio Mater.* **2024**, acsabm.3c00985, doi:10.1021/acsabm.3c00985.

188. Li, F.; Zhu, A.; Song, X.; Ji, L.; Wang, J. The Internalization of Fluorescence-Labeled PLA Nanoparticles by Macrophages. *International Journal of Pharmaceutics* **2013**, *453*, 506–513, doi:10.1016/j.ijpharm.2013.06.033.

189. Hoshyar, N.; Gray, S.; Han, H.; Bao, G. The Effect of Nanoparticle Size on *in Vivo* Pharmacokinetics and Cellular Interaction. *Nanomedicine* **2016**, *11*, 673–692, doi:10.2217/nnm.16.5.

USC UNIVERSIDADE DE SANTIAGO DE COMPOSTELA

190. Zhang, R.; Qin, X.; Kong, F.; Chen, P.; Pan, G. Improving Cellular Uptake of Therapeutic Entities through Interaction with Components of Cell Membrane. *Drug Delivery* **2019**, *26*, 328–342, doi:10.1080/10717544.2019.1582730.

191. Singh, A.; Agarwal, R.; Diaz-Ruiz, C.A.; Willett, N.J.; Wang, P.; Lee, L.A.; Wang, Q.; Guldberg, R.E.; García, A.J. Nanoengineered Particles for Enhanced Intra-Articular Retention and Delivery of Proteins. *Adv Healthcare Materials* **2014**, *3*, 1562–1567, doi:10.1002/adhm.201400051.

192. Bajpayee, A.G.; Scheu, M.; Grodzinsky, A.J.; Porter, R.M. Electrostatic Interactions Enable Rapid Penetration, Enhanced Uptake and Retention of Intra-articular Injected Avidin in Rat Knee Joints. *Journal Orthopaedic Research* **2014**, *32*, 1044–1051, doi:10.1002/jor.22630.

193. Vieira, A.C.; Magalhães, J.; Rocha, S.; Cardoso, M.S.; Santos, S.G.; Borges, M.; Pinheiro, M.; Reis, S. Targeted Macrophages Delivery of Rifampicin-Loaded Lipid Nanoparticles to Improve Tuberculosis Treatment. *Nanomedicine* **2017**, *12*, 2721–2736, doi:10.2217/nnm-2017-0248.

194. Bera, H.; Zhao, C.; Tian, X.; Cun, D.; Yang, M. Mannose-Decorated Solid-Lipid Nanoparticles for Alveolar Macrophage Targeted Delivery of Rifampicin. *Pharmaceutics* **2024**, *16*, 429, doi:10.3390/pharmaceutics16030429.

195. Lages, E.B.; De Freitas, M.B.; Gonçalves, I.M.B.; Alves, R.J.; Vianna-Soares, C.D.; Ferreira, L.A.M.; De Oliveira, M.C.; De Oliveira, R.B. Evaluation of Antitumor Activity and Development of Solid Lipid Nanoparticles of Metronidazole Analogue. *Journal of Biomedical Nanotechnology* **2013**, *9*, 1939–1944, doi:10.1166/jbn.2013.1674.

196. Fael, H.; Demirel, A.L. Indomethacin Co-Amorphous Drug-Drug Systems with Improved Solubility, Supersaturation, Dissolution Rate and Physical Stability. *International Journal of Pharmaceutics* **2021**, *600*, 120448, doi:10.1016/j.ijpharm.2021.120448.

197. Akhoond Zardini, A.; Mohebbi, M.; Farhoosh, R.; Bolurian, S. Production and Characterization of Nanostructured Lipid Carriers and Solid Lipid Nanoparticles Containing Lycopene for Food Fortification. *J Food Sci Technol* **2018**, *55*, 287–298, doi:10.1007/s13197-017-2937-5.

198. Chae, J.; Choi, Y.; Hong, J.; Kim, N.; Kim, J.; Lee, H.-Y.; Choi, J. Anticancer and Antibacterial Properties of Curcumin-Loaded Mannosylated Solid Lipid Nanoparticles for the Treatment of Lung Diseases. *ACS Appl. Bio Mater.* **2024**, *7*, 2175–2185, doi:10.1021/acsabm.3c01145.

199. Yu, S.; Shao, X.; Wu, T.; Liu, Z.; Yu, P.; Xing, J. Preparation of PMMA-Based Temperature/pH Responsive Nanoparticles Encapsulating 5-Fluorouracil and Methotrexate In Situ by One-Pot Dispersion Photopolymerization. *Macromolecular Bioscience* **2024**, 2300469, doi:10.1002/mabi.202300469.

200. Chae, J.; Kang, S.H.; Kim, J.; Choi, Y.; Kang, S.H.; Choi, J. Targeted and Efficient Delivery of Rifampicin to Macrophages Involved in Non-Tuberculous Mycobacterial Infection *via* Mannosylated Solid Lipid Nanoparticles. *Nanoscale Adv.* **2023**, *5*, 4536–4545, doi:10.1039/D3NA00320E.

USC UNIVERSIDADE DE SANTIAGO DE COMPOSTELA

201. Phukan, K.; Devi, R.; Chowdhury, D. Insights into Anti-Inflammatory Activity and Internalization Pathway of Onion Peel-Derived Gold Nano Bioconjugates in RAW 264.7 Macrophages. *ACS Omega* **2022**, *7*, 7606–7615, doi:10.1021/acsomega.1c06131.

202. Wong, C.; Pratiwi, F.W.; Chen, P.; Mou, C.; Hsu, S. Revealing the Phagosomal pH Regulation and Inflammation of Macrophages after Endocytosing Polyurethane Nanoparticles by A Ratiometric pH Nanosensor. *Advanced Biology* **2021**, *5*, 2000200, doi:10.1002/adbi.202000200.

203. Hippalgaonkar, K.; Adelli, G.R.; Hippalgaonkar, K.; Repka, M.A.; Majumdar, S. Indomethacin-Loaded Solid Lipid Nanoparticles for Ocular Delivery: Development, Characterization, and *In Vitro* Evaluation. *Journal of Ocular Pharmacology and Therapeutics* **2013**, *29*, 216–228, doi:10.1089/jop.2012.0069.

204. Kim, B.; Pang, H.-B.; Kang, J.; Park, J.-H.; Ruoslahti, E.; Sailor, M.J. Immunogene Therapy with Fusogenic Nanoparticles Modulates Macrophage Response to Staphylococcus Aureus. *Nat Commun* **2018**, *9*, 1969, doi:10.1038/s41467-018-04390-7.

205. Orlowsky, E.W.; Kraus, V.B. The Role of Innate Immunity in Osteoarthritis: When Our First Line of Defense Goes On the Offensive. *J Rheumatol* **2015**, *42*, 363–371, doi:10.3899/jrheum.140382.

206. Blom, A.B.; Van Lent, P.L.; Libregts, S.; Holthuysen, A.E.; Van Der Kraan, P.M.; Van Rooijen, N.; Van Den Berg, W.B. Crucial Role of Macrophages in Matrix Metalloproteinase–Mediated Cartilage Destruction during Experimental Osteoarthritis : Involvement of Matrix Metalloproteinase 3. *Arthritis & Rheumatism* **2007**, *56*, 147–157, doi:10.1002/art.22337.

207. Chen, B.; Hong, H.; Sun, Y.; Chen, C.; Wu, C.; Xu, G.; Bao, G.; Cui, Z. Role of Macrophage Polarization in Osteoarthritis (Review). *Exp Ther Med* **2022**, *24*, 757, doi:10.3892/etm.2022.11693.

208. Liu, Q.; Wu, Z.; Hu, D.; Zhang, L.; Wang, L.; Liu, G. Low Dose of Indomethacin and Hedgehog Signaling Inhibitor Administration Synergistically Attenuates Cartilage Damage in Osteoarthritis by Controlling Chondrocytes Pyroptosis. *Gene* **2019**, *712*, 143959, doi:10.1016/j.gene.2019.143959.

209. Sandberg, O.; Aspenberg, P. Different Effects of Indomethacin on Healing of Shaft and Metaphyseal Fractures. *Acta Orthopaedica* **2015**, *86*, 243–247, doi:10.3109/17453674.2014.973328.

210. Gan, J.; Dou, Y.; Li, Y.; Wang, Z.; Wang, L.; Liu, S.; Li, Q.; Yu, H.; Liu, C.; Han, C.; et al. Producing Anti-Inflammatory Macrophages by Nanoparticle-Triggered Clustering of Mannose Receptors. *Biomaterials* **2018**, *178*, 95–108, doi:10.1016/j.biomaterials.2018.06.015.

211. Tang, L.; Sim, I.; Moqbel, S.; Wu, L. Dapansutrile Ameliorated Chondrocyte Inflammation and Osteoarthritis through Suppression of MAPK Signaling Pathway. *Hum Exp Toxicol* **2022**, *41*, 096032712211454, doi:10.1177/09603271221145401.

212. Emami, A.; Namdari, H.; Parvizpour, F.; Arabpour, Z. Challenges in Osteoarthritis Treatment. *Tissue and Cell* **2023**, *80*, 101992, doi:10.1016/j.tice.2022.101992.

USC UNIVERSIDADE DE SANTIAGO DE COMPOSTELA

213. Zhu, X.; Lee, C.-W.; Xu, H.; Wang, Y.-F.; Yung, P.S.H.; Jiang, Y.; Lee, O.K. Phenotypic Alteration of Macrophages during Osteoarthritis: A Systematic Review. *Arthritis Res Ther* **2021**, *23*, 110, doi:10.1186/s13075-021-02457-3.

214. Zhang, Y.; Ji, Q. Macrophage Polarization in Osteoarthritis Progression: A Promising Therapeutic Target. *Front. Cell Dev. Biol.* **2023**, *11*, 1269724, doi:10.3389/fcell.2023.1269724.

215. Fernandes, T.L.; Gomoll, A.H.; Lattermann, C.; Hernandez, A.J.; Bueno, D.F.; Amano, M.T. Macrophage: A Potential Target on Cartilage Regeneration. *Front. Immunol.* **2020**, *11*, 111, doi:10.3389/fimmu.2020.00111.

216. He, Y.; Gao, Y.; Zhang, Q.; Zhou, G.; Cao, F.; Yao, S. IL-4 Switches Microglia/Macrophage M1/M2 Polarization and Alleviates Neurological Damage by Modulating the JAK1/STAT6 Pathway Following ICH. *Neuroscience* **2020**, *437*, 161–171, doi:10.1016/j.neuroscience.2020.03.008.

217. Liu, S.; Deng, Z.; Chen, K.; Jian, S.; Zhou, F.; Yang, Y.; Fu, Z.; Xie, H.; Xiong, J.; Zhu, W. Cartilage Tissue Engineering: From Proinflammatory and Anti-inflammatory Cytokines to Osteoarthritis Treatments (Review). *Mol Med Rep* **2022**, *25*, 99, doi:10.3892/mmr.2022.12615.

218. Risser, G.E.; Machour, M.; Hernaez-Estrada, B.; Li, D.; Levenberg, S.; Spiller, K.L. Effects of Interleukin-4 (IL-4)-Releasing Microparticles and Adoptive Transfer of Macrophages on Immunomodulation and Angiogenesis. *Biomaterials* **2023**, *296*, 122095, doi:10.1016/j.biomaterials.2023.122095.

219. Yang, H.; Ulge, U.Y.; Quijano-Rubio, A.; Bernstein, Z.J.; Maestas, D.R.; Chun, J.-H.; Wang, W.; Lin, J.-X.; Jude, K.M.; Singh, S.; et al. Design of Cell-Type-Specific Hyperstable IL-4 Mimetics via Modular de Novo Scaffolds. *Nat Chem Biol* **2023**, *19*, 1127–1137, doi:10.1038/s41589-023-01313-6.

220. Shi, L.; Zhang, J.; Zhao, M.; Tang, S.; Cheng, X.; Zhang, W.; Li, W.; Liu, X.; Peng, H.; Wang, Q. Effects of Polyethylene Glycol on the Surface of Nanoparticles for Targeted Drug Delivery. *Nanoscale* **2021**, *13*, 10748–10764, doi:10.1039/D1NR02065J.

221. Paris, J.L.; Gaspar, R.; Coelho, F.; De Beule, P.A.A.; Silva, B.F.B. Stability Criterion for the Assembly of Core–Shell Lipid–Polymer–Nucleic Acid Nanoparticles. *ACS Nano* **2023**, *17*, 17587–17594, doi:10.1021/acsnano.3c07204.

222. Briffault, E.; Garcia-Garcia, P.; Martinez-Borrajo, R.; Evora, C.; Delgado, A.; Diaz-Rodriguez, P. Harnessing Extracellular Vesicle Membrane for Gene Therapy: EVs-Biomimetic Nanoparticles. *Colloids and Surfaces B: Biointerfaces* **2024**, 113951, doi:10.1016/j.colsurfb.2024.113951.

223. Craparo, E.F.; Cabibbo, M.; Scialabba, C.; Giammona, G.; Cavallaro, G. Inhalable Formulation Based on Lipid–Polymer Hybrid Nanoparticles for the Macrophage Targeted Delivery of Roflumilast. *Biomacromolecules* **2022**, *23*, 3439–3451, doi:10.1021/acs.biomac.2c00576.

224. Zhang, L.; Wu, S.; Qin, Y.; Fan, F.; Zhang, Z.; Huang, C.; Ji, W.; Lu, L.; Wang, C.; Sun, H.; et al. Targeted Codelivery of an Antigen and Dual Agonists by Hybrid Nanoparticles for Enhanced Cancer Immunotherapy. *Nano Lett.* **2019**, *19*, 4237–4249, doi:10.1021/acs.nanolett.9b00030.

USC UNIVERSIDADE DE COMPOSTELA

225. Rampersad, S.N. Multiple Applications of Alamar Blue as an Indicator of Metabolic Function and Cellular Health in Cell Viability Bioassays. *Sensors* **2012**, *12*, 12347–12360, doi:10.3390/s120912347.

226. Fujitsu, Y.; Fukuda, K.; Kumagai, N.; Nishida, T. IL-4-Induced Cell Proliferation and Production of Extracellular Matrix Proteins in Human Conjunctival Fibroblasts. *Experimental Eye Research* **2003**, *76*, 107–114, doi:10.1016/S0014-4835(02)00248-8.

227. Jenkins, S.J.; Ruckerl, D.; Thomas, G.D.; Hewitson, J.P.; Duncan, S.; Brombacher, F.; Maizels, R.M.; Hume, D.A.; Allen, J.E. IL-4 Directly Signals Tissue-Resident Macrophages to Proliferate beyond Homeostatic Levels Controlled by CSF-1. *Journal of Experimental Medicine* **2013**, *210*, 2477–2491, doi:10.1084/jem.20121999.

228. Anderson, J.M.; Shive, M.S. Biodegradation and Biocompatibility of PLA and PLGA Microspheres. *Advanced Drug Delivery Reviews* **1997**.

229. Da Costa Marques, R.; Hüppe, N.; Speth, K.R.; Oberländer, J.; Lieberwirth, I.; Landfester, K.; Mailänder, V. Proteomics Reveals Time-Dependent Protein Corona Changes in the Intracellular Pathway. *Acta Biomaterialia* **2023**, *172*, 355–368, doi:10.1016/j.actbio.2023.10.010.

230. Qiu, C.; Xia, F.; Zhang, J.; Shi, Q.; Meng, Y.; Wang, C.; Pang, H.; Gu, L.; Xu, C.; Guo, Q.; et al. Advanced Strategies for Overcoming Endosomal/Lysosomal Barrier in Nanodrug Delivery. *Research (Wash D C)* **2023**, *6*, 0148, doi:10.34133/research.0148.

231. Panyam, J.; Zhou, W.; Prabha, S.; Sahoo, S.K.; Labhasetwar, V. Rapid Endo-lysosomal Escape of Poly(DL-lactide- *Co* Glycolide) Nanoparticles: Implications for Drug and Gene Delivery. *FASEB j.* **2002**, *16*, 1217–1226, doi:10.1096/fj.02-0088com.

232. Luo, P.; Yuan, Q.; Wan, X.; Yang, M.; Xu, P. Effects of Immune Cells and Cytokines on Different Cells in OA. *JIR* **2023**, *Volume 16*, 2329–2343, doi:10.2147/JIR.S413578.

233. Yang, J.; Wang, X.; Zhang, Y.; He, R.; Fu, Z.; Wang, R.; Ma, Y.; Fu, D.; Meng, S.; Cai, W.; et al. Intra-Articular Injection of Interleukin-8 Neutralizing Monoclonal Antibody Effectively Attenuates Osteoarthritis Progression in Rabbits. *CARTILAGE* **2024**, 19476035241240361, doi:10.1177/19476035241240361.

234. Li, B.; Shen, E.; Wu, Z.; Qi, H.; Wu, C.; Liu, D.; Jiang, X. BMSC-Derived Exosomes Attenuate Rat Osteoarthritis by Regulating Macrophage Polarization through PINK1/Parkin Signaling Pathway. *CARTILAGE* **2024**, 19476035241245805, doi:10.1177/19476035241245805.

235. Arnosa-Prieto, Á.; Diaz-Rodriguez, P.; González-Gómez, M.A.; García-Acevedo, P.; De Castro-Alves, L.; Piñeiro, Y.; Rivas, J. Magnetic-Driven Interleukin-4 Internalization Promotes Magnetic Nanoparticle Morphology and Size-Dependent Macrophage Polarization. *Journal of Colloid and Interface Science* **2024**, *655*, 286–295, doi:10.1016/j.jcis.2023.11.004.

236. García-Manrique, M.; Calvet, J.; Orellana, C.; Berenguer-Llergo, A.; Garcia-Cirera, S.; Llop, M.; Albiñana-Giménez, N.; Galisteo-Lencastre, C.; Gratacós, J. Synovial Fluid but Not Plasma Interleukin-8 Is Associated with Clinical Severity and Inflammatory Markers in Knee Osteoarthritis Women with Joint Effusion. *Sci Rep* **2021**, *11*, 5258, doi:10.1038/s41598-021-84582-2.

USC UNIVERSIDADE DE SANTIAGO DE COMPOSTELA

237. Van Helvoort, E.M.; Van Der Heijden, E.; Van Roon, J.A.G.; Eijkelkamp, N.; Mastbergen, S.C. The Role of Interleukin-4 and Interleukin-10 in Osteoarthritic Joint Disease: A Systematic Narrative Review. *CARTILAGE* **2022**, *13*, 194760352210981, doi:10.1177/19476035221098167.

238. Caramés, B.; Taniguchi, N.; Otsuki, S.; Blanco, F.J.; Lotz, M. Autophagy Is a Protective Mechanism in Normal Cartilage, and Its Aging-related Loss Is Linked with Cell Death and Osteoarthritis. *Arthritis & Rheumatism* **2010**, *62*, 791–801, doi:10.1002/art.27305.

239. Gong, Y.; Li, S.; Wu, J.; Zhang, T.; Fang, S.; Feng, D.; Luo, X.; Yuan, J.; Wu, Y.; Yan, X.; et al. Autophagy in the Pathogenesis and Therapeutic Potential of Post-Traumatic Osteoarthritis. *Burns & Trauma* **2023**, *11*, tkac060, doi:10.1093/burnst/tkac060.

240. Gago, J.; Pérez-Tornero, O.; Landín, M.; Burgos, L.; Gallego, P.P. Improving Knowledge of Plant Tissue Culture and Media Formulation by Neurofuzzy Logic: A Practical Case of Data Mining Using Apricot Databases. *Journal of Plant Physiology* **2011**, *168*, 1858–1865, doi:10.1016/j.jplph.2011.04.008.

241. Vysloužil, J.; Doležel, P.; Kejdušová, M.; Mašková, E.; Mašek, J.; Lukáč, R.; Košťál, V.; Vetchý, D.; Dvořáčková, K. Influence of Different Formulations and Process Parameters during the Preparation of Drug-Loaded PLGA Microspheres Evaluated by Multivariate Data Analysis. *Acta Pharmaceutica* **2014**, *64*, 403–417, doi:10.2478/acph-2014-0032.

242. Yeo, Y.; Park, K. Control of Encapsulation Efficiency and Initial Burst in Polymeric Microparticle Systems. *Arch Pharm Res* **2004**, *27*, 1–12, doi:10.1007/BF02980037.

243. Vasileiou, K.; Vysloužil, J.; Pavelková, M.; Vysloužil, J.; Kubová, K. The Size-Reduced Eudragit® RS Microparticles Prepared by Solvent Evaporation Method – Monitoring the Effect of Selected Variables on Tested Parameters. 7.

244. Wang, H.; Zhang, G.; Ma, X.; Liu, Y.; Feng, J.; Park, K.; Wang, W. Enhanced Encapsulation and Bioavailability of Breviscapine in PLGA Microparticles by Nanocrystal and Water-Soluble Polymer Template Techniques. *European Journal of Pharmaceutics and Biopharmaceutics* **2017**, *115*, 177–185, doi:10.1016/j.ejpb.2017.02.021.

245. Damiati, S.A.; Rossi, D.; Joensson, H.N.; Damiati, S. Artificial Intelligence Application for Rapid Fabrication of Size-Tunable PLGA Microparticles in Microfluidics. *Sci Rep* **2020**, *10*, 19517, doi:10.1038/s41598-020-76477-5.

246. Operti, M.C.; Dölen, Y.; Keulen, J.; van Dinther, E.A.W.; Figdor, C.G.; Tagit, O. Microfluidics-Assisted Size Tuning and Biological Evaluation of PLGA Particles. *Pharmaceutics* **2019**, *11*, 590, doi:10.3390/pharmaceutics11110590.

247. Li, L.; Li, Z.; Guo, Y.; Zhang, K.; Mi, W.; Liu, J. Preparation of Uniform-Sized GeXIVA[1,2]-Loaded PLGA Microspheres as Long-Effective Release System with High Encapsulation Efficiency. *Drug Delivery* **2022**, *29*, 2283–2295, doi:10.1080/10717544.2022.2089297.

248. Yasin, H.; Al-Taani, B.; Salem, M. Preparation and Characterization of Ethylcellulose Microspheres for Sustained-Release of Pregabalin. *Res Pharma Sci* **2021**, *16*, 1, doi:10.4103/1735-5362.305184.

USC UNIVERSIDADE DE SANTIAGO DE COMPOSTELA

249. Santoyo, S.; de Jalón, E.G.; Ygartua, P.; Renedo, M.J.; Blanco-Príeto, M.J. Optimization of Topical Cidofovir Penetration Using Microparticles. *International Journal of Pharmaceutics* **2002**, *242*, 107–113, doi:10.1016/S0378-5173(02)00178-3.

250. Hu, H.; Liao, Z.; Xu, M.; Wan, S.; Wu, Y.; Zou, W.; Wu, J.; Fan, Q. Fabrication, Optimization, and Evaluation of Paclitaxel and Curcumin Coloaded PLGA Nanoparticles for Improved Antitumor Activity. *ACS Omega* **2023**, *8*, 976–986, doi:10.1021/acsomega.2c06359.

251. Lamela-Gómez, I.; Gonçalves, L.M.; Almeida, A.J.; Luzardo-Álvarez, A. Infliximab Microencapsulation: An Innovative Approach for Intra-Articular Administration of Biologics in the Management of Rheumatoid Arthritis—in Vitro Evaluation. *Drug Deliv. and Transl. Res.* **2023**, *13*, 3030–3058, doi:10.1007/s13346-023-01372-1.

252. Dhanabalan, K.M.; Gupta, V.K.; Agarwal, R. Rapamycin–PLGA Microparticles Prevent Senescence, Sustain Cartilage Matrix Production under Stress and Exhibit Prolonged Retention in Mouse Joints. *Biomater. Sci.* **2020**, *8*, 4308–4321, doi:10.1039/D0BM00596G.

253. Figari, G.; Gonçalves, J.L.M.; Diogo, H.P.; Dionísio, M.; Farinha, J.P.; Viciosa, M.T. Understanding Fenofibrate Release from Bare and Modified Mesoporous Silica Nanoparticles. *Pharmaceutics* **2023**, *15*, 1624, doi:10.3390/pharmaceutics15061624.

254. Lynnerup, J.T.; Eriksen, J.B.; Bauer-Brandl, A.; Holsæter, A.M.; Brandl, M. Insight into the Mechanism behind Oral Bioavailability-Enhancement by Nanosuspensions through Combined Dissolution/Permeation Studies. *European Journal of Pharmaceutical Sciences* **2023**, *184*, 106417, doi:10.1016/j.ejps.2023.106417.

255. Padmaa Paarakh, M.; Preethy Ani, J.; Setty, C.; Peter Christoper RELEASE KINETICS – CONCEPTS AND APPLICATIONS. *IJPRT* **2019**, *8*, doi:10.31838/ijprt/08.01.02.

256. Sun, Z.; Gu, X.; Hao, T.; Liu, J.; Gao, R.; Li, Y.; Yu, B.; Xu, H. Intra-Articular Injection PLGA Blends Sustained-Release Microspheres Loaded with Meloxicam: Preparation, Optimization, Evaluation *in Vitro* and *in Vivo*. *Drug Delivery* **2022**, *29*, 3317–3327, doi:10.1080/10717544.2022.2144545.

257. Gil, T.-H.; Zheng, H.; Lee, H.G.; Shin, J.-W.; Hwang, S.W.; Jang, K.-M.; Jeon, O.H. Senolytic Drugs Relieve Pain by Reducing Peripheral Nociceptive Signaling without Modifying Joint Tissue Damage in Spontaneous Osteoarthritis. *Aging* **2022**, *14*, 6006–6027, doi:10.18632/aging.204204.

258. Astrike-Davis, E.M.; Coryell, P.; Loeser, R.F. Targeting Cellular Senescence as a Novel Treatment for Osteoarthritis. *Current Opinion in Pharmacology* **2022**, *64*, 102213, doi:10.1016/j.coph.2022.102213.

259. Coryell, P.R.; Diekman, B.O.; Loeser, R.F. Mechanisms and Therapeutic Implications of Cellular Senescence in Osteoarthritis. *Nat Rev Rheumatol* **2021**, *17*, 47–57, doi:10.1038/s41584-020-00533-7.

260. Szychlinska, M.A.; Ravalli, S.; Musumeci, G. Pleiotropic Effect of Fibrates on Senescence and Autophagy in Osteoarthritis. *EBioMedicine* **2019**, *45*, 11–12, doi:10.1016/j.ebiom.2019.07.018.

USC UNIVERSIDADE DE SANTIAGO DE COMPOSTELA

261. Xiao, S.-Q.; Cheng, M.; Wang, L.; Cao, J.; Fang, L.; Zhou, X.-P.; He, X.-J.; Hu, Y.-F. The Role of Apoptosis in the Pathogenesis of Osteoarthritis. *International Orthopaedics (SICOT)* **2023**, *47*, 1895–1919, doi:10.1007/s00264-023-05847-1.

262. Tanida, I.; Ueno, T.; Kominami, E. LC3 and Autophagy. In *Autophagosome and Phagosome*; Deretic, V., Ed.; Methods in Molecular Biology™; Humana Press: Totowa, NJ, 2008; Vol. 445, pp. 77–88 ISBN 978-1-58829-853-9.

263. Zhang, Y.-Y.; Wang, J.-X.; Qiao, F.; Zhang, M.-L.; Luo, Y.; Du, Z.-Y. Pparα Activation Stimulates Autophagic Flux through Lipid Catabolism-Independent Route. *Fish Physiol Biochem* **2024**, doi:10.1007/s10695-024-01327-4.

264. Van Eekeren, I.C.M.; Clockaerts, S.; Bastiaansen-Jenniskens, Y.M.; Lubberts, E.; Verhaar, J.A.N.; Van Osch, G.J.V.M.; Bierma-Zeinstra, S.M. Fibrates as Therapy for Osteoarthritis and Rheumatoid Arthritis? A Systematic Review. *Therapeutic Advances in Musculoskeletal* **2013**, *5*, 33–44, doi:10.1177/1759720X12468659.

265. Abulaban, A.A.; Al-kuraishy, H.M.; Al-Gareeb, A.I.; Elekhnawy, E.; Alanazi, A.; Alexiou, A.; Papadakis, M.; Batiha, G.E.-S. Role of Fenofibrate in Multiple Sclerosis. *Eur J Med Res* **2024**, *29*, 113, doi:10.1186/s40001-024-01700-2.

266. Park, A.; Heo, T.-H. IL-17A-Targeting Fenofibrate Attenuates Inflammation in Psoriasis by Inducing Autophagy. *Life Sciences* **2023**, *326*, 121755, doi:10.1016/j.lfs.2023.121755.

267. Del Rey, M.J.; Valín, Á.; Usategui, A.; Ergueta, S.; Martín, E.; Municio, C.; Cañete, J.D.; Blanco, F.J.; Criado, G.; Pablos, J.L. Senescent Synovial Fibroblasts Accumulate Prematurely in Rheumatoid Arthritis Tissues and Display an Enhanced Inflammatory Phenotype. *Immun Ageing* **2019**, *16*, 29, doi:10.1186/s12979-019-0169-4.

268. Murahashi, Y.; Yano, F.; Kobayashi, H.; Makii, Y.; Iba, K.; Yamashita, T.; Tanaka, S.; Saito, T. Intra-Articular Administration of IκBα Kinase Inhibitor Suppresses Mouse Knee Osteoarthritis via Downregulation of the NF-κB/HIF-2α Axis. *Sci Rep* **2018**, *8*, 16475, doi:10.1038/s41598-018-34830-9.

269. Dhanabalan, K.M.; Dravid, A.A.; Agarwal, S.; Sharath, R.K.; Padmanabhan, A.K.; Agarwal, R. Intra-articular Injection of Rapamycin Microparticles Prevent Senescence and Effectively Treat Osteoarthritis. *Bioengineering & Transla Med* **2023**, *8*, e10298, doi:10.1002/btm2.10298.

USC UNIVERSIDADE DE SANTIAGO DE COMPOSTELA

ANNEXES

USC
UNIVERSIDADE
DE SANTIAGO
DE COMPOSTELA

USC
UNIVERSIDADE
DE SANTIAGO
DE COMPOSTELA

ANNEX 1

Table S1. Characteristics of the NLC studied (before and after dialysis). Grey area corresponds to the formulations used for the Model A. The complete database was used for Model B.

Formulation	Particle size (nm)	ZP (mV)	PDI	DL (%)
N01	124.2	-15.2	0.3	-
N02	160.3	-9.1	0.1	-
N03	148.3	-10.5	0.2	-
N04	139.8	-10.5	0.2	-
N05	127.8	-14.5	0.2	-
N06	174.1	-7.6	0.1	-
N07	185.8	-15.4	0.3	-
N08	171.5	-7.2	0.2	-
N09	98.3	-11.6	0.2	-
N10	168.4	-7.2	0.1	-
N11	111.9	-3.7	0.2	-
N12	232.1	-14.6	0.2	-
N13	182.2	-6.4	0.2	-
N14	233.8	-15.6	0.3	-
N15	128.8	-11.4	0.2	-
N16	179.7	-16.1	0.2	-
N17	161.3	-11.0	0.2	-
N18	149.2	-12.8	0.2	-
N19	172.5	-12.4	0.2	-
N20	184.0	-15.3	0.2	-
N21	162.6	-9.9	0.2	-
N22	230.6	-15.2	0.2	-
N23	165.8	-8.5	0.2	-
N24	104.9	-12.3	0.2	-
N25	170.6	-10.2	0.2	-
N26	122.4	-9.4	0.2	-
N27	240.1	-16.7	0.2	-
N28	181.1	-11.3	0.2	-
N29	265.1	-16.4	0.2	-
N30	151.1	-12.9	0.2	-
N01	122.5	-7.9	0.3	-
N02	160.5	-8.0	0.1	-
N03	161.0	-13.0	0.2	-
N04	149.9	-10.3	0.2	-
N05	124.1	-13.4	0.2	-
N06	211.3	-10.8	0.1	
N07	203.1	-12.9	0.3	-
N08	194.1	-10.8	0.2	-
N09	96.6	-10.9	0.2	-
N10	190.2	-11.1	0.1	-
N11	117.7	-11.6	0.2	-
N12	224.3	-13.8	0.2	-

USC UNIVERSIDADE DE SANTIAGO DE COMPOSTELA

N13	219.5	-10.7	0.2	-
N14	220.9	-14.7	0.3	-
N15	142.2	-12.2	0.2	-
N16	179.7	-14.2	0.2	1.0
N17	169.7	-10.9	0.2	3.8
N18	153.0	-13.4	0.2	0.9
N19	187.3	-12.9	0.2	1.6
N20	184.0	-13.9	0.2	1.4
N21	185.0	-11.6	0.2	3.4
N22	230.6	-15.2	0.2	0.7
N23	187.5	-11.0	0.2	1.3
N24	148.6	-12.6	0.2	3.4
N25	196.8	-11.4	0.2	2.9
N26	122.4	-12.2	0.2	2.0
N27	248.0	-16.0	0.2	1.3
N28	117.8	-14.6	0.2	2.7
N29	257.1	-15.3	0.2	1.4
N30	151.1	-13.1	0.2	2.7
N31	121.6	-14.0	0.2	-
N32	322.7	28.5	0.2	-
N33	261.9	36.9	0.2	-
N34	234.9	30.3	0.3	-
N35	229.1	33.3	0.3	-
N36	-	2.1	-	-
N37	334.2	10.1	0.3	-
N38	159.4	15.6	0.2	-
N39	130.4	-11.2	0.2	-
N40	86.8	12.2	0.3	-
N41	-	-0.7	-	-
N42	-	2.2	-	-
N43	93.7	13.8	0.4	-
N44	78.4	16.7	0.4	-
N31	123.4	-14.8	0.2	2.5
N32	320.0	26.0	0.3	1.0
N33	303.6	34.6	0.2	0.7
N34	206.0	25.0	0.2	1.7
N35	200.6	31.2	0.2	1.3
N36	-	-1.0	-	3.4
N37	347.2	7.3	0.3	2.7
N38	174.6	12.5	0.2	3.2
N39	153.6	-10.8	0.2	3.6
N40	92.0	10.5	0.3	3.4
N41	609.3	-5.6	0.3	2.6
N42	-	-3.6	-	3.1
N43	75.1	11.6	0.3	3.0
N44	65.1	12.0	0.3	3.3

USC UNIVERSIDADE DE SANTIAGO DE COMPOSTELA

Table S2. Rules generated by FormRules® (Model A) for the parameters size, surface charge (ZP), and drug loading (DL) (membership degrees in parentheses). In blue and red, the combinations of variables that lead the highest and lowest value of the parameter studied.

Rules for Particle size (nm)			
	SubModel:1		
1	IF Ratio (LL/SL) is LOW AND Tween 80 (%) is LOW	THEN Size (nm) is	HIGH (1.00)
2	IF Ratio (LL/SL) is LOW AND Tween 80 (%) is HIGH	THEN Size (nm) is	HIGH (0.56)
3	IF Ratio (LL/SL) is HIGH AND Tween 80 (%) is LOW	THEN Size (nm) is	LOW (0.61)
4	IF Ratio (LL/SL) is HIGH AND Tween 80 (%) is HIGH	THEN Size (nm) is	LOW (0.55)
	SubModel:2		
5	IF Tween 80 (%) is LOW AND IND is LOW	THEN Size (nm) is	LOW (0.93)
6	IF Tween 80 (%) is LOW AND IND is HIGH	THEN Size (nm) is	HIGH (1.00)
7	IF Tween 80 (%) is MID AND IND is LOW	THEN Size (nm) is	LOW (1.00)
8	IF Tween 80 (%) is MID AND IND is HIGH	THEN Size (nm) is	LOW (0.70)
9	IF Tween 80 (%) is HIGH AND IND is LOW	THEN Size (nm) is	HIGH (0.74)
10	IF Tween 80 (%) is HIGH AND IND is HIGH	THEN Size (nm) is	LOW (0.72)
Rules for Zeta potential (ZP) (mV)			
	SubModel:1		
11	IF Tween 80 (%) is LOW AND Ratio (LL/SL) is LOW	THEN ZP (mV) is	LOW (1.00)
12	IF Tween 80 (%) is LOW AND Ratio (LL/SL) is HIGH	THEN ZP (mV) is	LOW (1.00)
13	IF Tween 80 (%) is HIGH AND Ratio (LL/SL) is LOW	THEN ZP (mV) is	HIGH (1.00)
14	IF Tween 80 (%) is HIGH AND Ratio (LL/SL) is HIGH	THEN ZP (mV) is	HIGH (1.00)
	SubModel:2		
15	IF IND (mg) is LOW	THEN ZP (mV) is	HIGH (1.00)
16	IF IND (mg) is HIGH	THEN ZP (mV) is	LOW (1.00)
	SubModel:3		
17	IF Lecithin (mg) is LOW	THEN ZP (mV) is	LOW (0.86)
18	IF Lecithin (mg) is HIGH	THEN ZP (mV) is	HIGH (0.67)
	SubModel:4		
19	IF Dialysis (h) is LOW	THEN ZP (mV) is	HIGH (0.70)
20	IF Dialysis (h) is HIGH	THEN ZP (mV) is	LOW (0.89)
Rules for Drug Loading (DL) (%)			
	SubModel:1		
21	IF IND (mg) is LOW	THEN DL (%) is	LOW (0.89)
22	IF IND (mg) is MID	THEN DL (%) is	HIGH (0.84)
23	IF IND (mg) is HIGH	THEN DL (%) is	HIGH (0.74)

USC UNIVERSIDADE DE SANTIAGO DE COMPOSTELA

Table S3. Rules generated by FormRules® (Model B) for the parameters size, surface charge (ZP), and drug loading (DL) (membership degrees in parentheses). In blue and red, the combinations of variables that lead the highest and lowest value of the parameter studied.

Rules for Particle size (nm)			
	SubModel:1		
1	IF Tween % is LOW AND SA (mg) is LOW	THEN Size (nm) is	LOW (1.00)
2	IF Tween % is LOW AND SA (mg) is MID	THEN Size (nm) is	LOW (1.00)
3	IF Tween % is LOW AND SA (mg) is MID	THEN Size (nm) is	LOW (1.00)
4	IF Tween % is LOW AND SA (mg) is HIGH	THEN Size (nm) is	LOW (1.00)
5	IF Tween % is MID AND SA (mg) is LOW	THEN Size (nm) is	LOW (1.00)
6	IF Tween % is MID AND SA (mg) is MID	THEN Size (nm) is	HIGH (1.00)
7	IF Tween % is MID AND SA (mg) is MID	THEN Size (nm) is	HIGH (1.00)
8	IF Tween % is MID AND SA (mg) is HIGH	THEN Size (nm) is	LOW (1.00)
9	IF Tween % is HIGH AND SA (mg) is LOW	THEN Size (nm) is	LOW (1.00)
10	IF Tween % is HIGH AND SA (mg) is MID	THEN Size (nm) is	HIGH (1.00)
11	IF Tween % is HIGH AND SA (mg) is MID	THEN Size (nm) is	LOW (1.00)
12	IF Tween % is HIGH AND SA (mg) is HIGH	THEN Size (nm) is	LOW (1.00)
	SubModel:2		
13	IF Ratio (LL/SL) is LOW	THEN Size (nm) is	HIGH (1.00)
14	IF Ratio (LL/SL) is HIGH	THEN Size (nm) is	HIGH (1.00)
Rules for Zeta potential (ZP) (mV)			
	SubModel:1		
15	IF SA (mg) is LOW AND Tween 80 (%) is LOW	THEN ZP (mV) is	LOW (1.00)
16	IF SA (mg) is LOW AND Tween 80 (%) is HIGH	THEN ZP (mV) is	LOW (1.00)
17	IF SA (mg) is MID AND Tween 80 (%) is LOW	THEN ZP (mV) is	HIGH (1.00)
18	IF SA (mg) is MID AND Tween 80 (%) is HIGH	THEN ZP (mV) is	LOW (0.73)
19	IF SA (mg) is HIGH AND Tween 80 (%) is LOW	THEN ZP (mV) is	HIGH (1.00)
20	IF SA (mg) is HIGH AND Tween 80 (%) is HIGH	THEN ZP (mV) is	LOW (0.73)
	SubModel:2		
21	IF IND (mg) is LOW	THEN ZP (mV) is	HIGH (0.69)
22	IF IND (mg) is HIGH	THEN ZP (mV) is	HIGH (0.50)
	SubModel:3		
23	IF Dialysis (h) is LOW	THEN ZP (mV) is	HIGH (0.66)
24	IF Dialysis (h) is HIGH	THEN ZP (mV) is	HIGH (0.53)
Rules for Drug Loading (DL) (%)			
SubModel:1			
25	IF IND (mg) is LOW AND Tween 80 (%) is LOW	THEN DL (%) is	LOW (1.00)
26	IF IND (mg) is LOW AND Tween 80 (%) is HIGH	THEN DL (%) is	LOW (0.99)
27	IF IND (mg) is MID AND Tween 80 (%) is LOW	THEN DL (%) is	HIGH (0.87)
28	IF IND (mg) is MID AND Tween 80 (%) is HIGH	THEN DL (%) is	HIGH (0.98)
29	IF IND (mg) is HIGH AND Tween 80 (%) is LOW	THEN DL (%) is	HIGH (0.62)
30	IF IND (mg) is HIGH AND Tween 80 (%) is HIGH	THEN DL (%) is	HIGH (0.69)

USC UNIVERSIDADE DE SANTIAGO DE COMPOSTELA

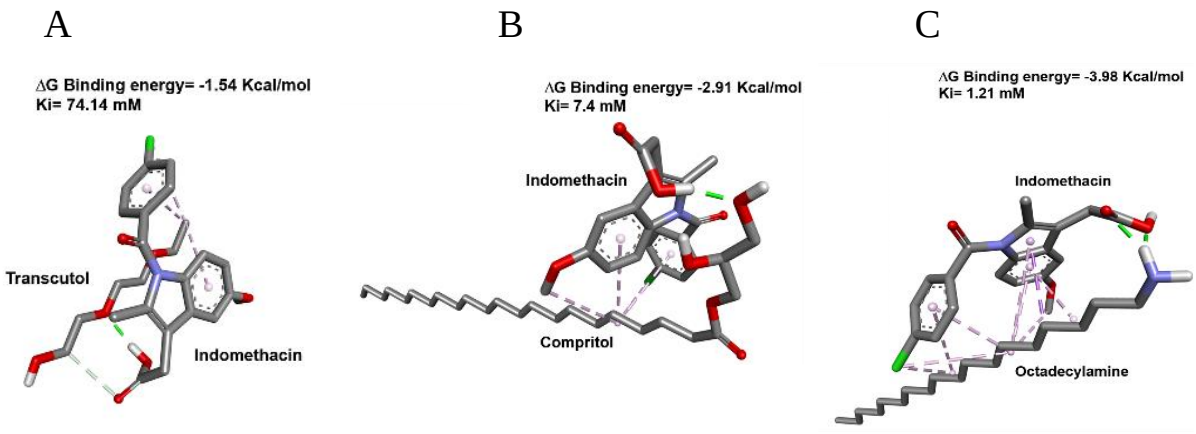


Figure S1. Binding pose of indomethacin with (A) Transcutol, (B) Compritol, and (C) Stearylamine and the respective estimated ΔG binding energy and affinity constant (K_i). In the structures, carbon atoms are shown in grey, oxygen atoms in red, nitrogen atoms are shown in blue, while chlorine atoms are shown in green. Excipients were set as rigid receptor, while the indomethacin was set as flexible ligand.

USC UNIVERSIDADE DE SANTIAGO DE COMPOSTELA

ANNEX 2

Table S1. Rules generated by FormRules® for the parameters particle size, polydispersity index (PDI), surface charge (ZP), and association efficiency (AE) (membership degrees in parentheses). The combinations of variables that lead the highest and lowest value of the parameter studied are in blue and red, respectively.

Rules for Particle size (nm)			
	SubModel:1		
1	IF BSA (%) is LOW AND PLGA (mg) is LOW	THEN Size (nm) is	LOW (0.63)
2	IF BSA (%) is LOW AND PLGA (mg) is HIGH	THEN Size (nm) is	LOW (1.00)
3	IF BSA (%) is MID AND PLGA (mg) is LOW	THEN Size (nm) is	HIGH (0.68)
4	IF BSA (%) is MID AND PLGA (mg) is HIGH	THEN Size (nm) is	LOW (1.00)
5	IF BSA (%) is HIGH AND PLGA (mg) is LOW	THEN Size (nm) is	LOW (0.95)
6	IF BSA (%) is HIGH AND PLGA (mg) is HIGH	THEN Size (nm) is	HIGH (0.99)
Rules for Polydispersity index (PDI)			
	SubModel:1		
7	IF PLGA (mg) is LOW	THEN PDI is	HIGH (1.00)
8	IF PLGA (mg) is HIGH	THEN PDI is	LOW (1.00)
	SubModel:2		
9	IF BSA (%) is LOW	THEN PDI is	LOW (0.69)
10	IF BSA (%) is HIGH	THEN PDI is	HIGH (0.97)
Rules for Surface Charge (ZP) (mV)			
	SubModel:1		
11	IF PLGA (mg) is LOW	THEN ZP (mV) is	HIGH (0.78)
12	IF PLGA (mg) is HIGH	THEN ZP (mV) is	LOW (0.94)
Rules for Association Efficiency (AE) (%)			
	SubModel:1		
13	IF BSA (%) is LOW	THEN AE (%) is	HIGH (1.00)
14	IF BSA (%) is HIGH	THEN AE (%) is	LOW (1.00)
	SubModel:2		
15	IF PLGA (mg) is LOW	THEN AE (%) is	HIGH (1.00)
16	IF PLGA (mg) is HIGH	THEN AE (%) is	LOW (0.76)

USC UNIVERSIDADE DE SANTIAGO DE COMPOSTELA

ANNEX 3

Table S1: Set of rules from FormRules® for microspheres particle size (membership degrees in parentheses). The combinations of variables that lead the highest and lowest value of the parameter studied are in blue and red, respectively.

Rules for Particle size (nm)			
	SubModel:1		
1	IF Speed is LOW AND [Polymer] is LOW	THEN Particle size is	LOW (0.69)
2	IF Speed is LOW AND [Polymer] is MEDIUM	THEN Particle size is	LOW (0.76)
3	IF Speed is LOW AND [Polymer]is HIGH	THEN Particle size is	HIGH (1.00)
4	IF Speed is MEDIUM AND [Polymer] is LOW	THEN Particle size is	LOW (0.99)
5	IF Speed is MEDIUM AND [Polymer] is MEDIUM	THEN Particle size is	LOW (1.00)
6	IF Speed is MEDIUM AND [Polymer] is HIGH	THEN Particle size is	LOW (0.98)
7	IF Speed is HIGH AND [Polymer] is LOW	THEN Particle size is	LOW (0.99)
8	IF Speed is HIGH AND [Polymer] is MEDIUM	THEN Particle size is	LOW (0.99)
9	IF Speed is HIGH AND [Polymer] is HIGH	THEN Particle size is	LOW (0.99)

USC UNIVERSIDADE DE SANTIAGO DE COMPOSTELA

Table S2: Set of rules from FormRules® for microspheres size distribution. Membership degree in parentheses. Rule in blue means the largest positive contribution, while rule in red make the largest negative contribution. The combinations of variables that lead the highest and lowest value of the parameter studied are in blue and red, respectively.

Rules for size distribution			
	SubModel:1		
1	IF Speed is LOW AND [Drug] is LOW	THEN Size distribution is	LOW (1.00)
2	IF Speed is LOW AND [Drug] is HIGH	THEN Size distribution is	HIGH (1.00)
3	IF Speed is MEDIUM AND [Drug] is LOW	THEN Size distribution is	LOW (1.00)
4	IF Speed is MEDIUM AND [Drug] is HIGH	THEN Size distribution is	LOW (1.00)
5	IF Speed is HIGH AND [Drug] is LOW	THEN Size distribution is	HIGH (0.68)
6	IF Speed is HIGH AND [Drug] is HIGH	THEN Size distribution is	LOW (0.62)
	SubModel:2		
7	IF [PVA] is LOW	THEN Size distribution is	LOW (1.00)
8	IF [PVA] is HIGH	THEN Size distribution is	HIGH (1.00)
	SubModel:3		
9	IF O/W ratio is LOW AND Time is LOW	THEN Size distribution is	LOW (1.00)
10	IF O/W ratio is LOW AND Time is MEDIUM	THEN Size distribution is	LOW (1.00)
11	IF O/W ratio is LOW AND Time is HIGH	THEN Size distribution is	LOW (1.00)
12	IF O/W ratio is HIGH AND Time is LOW	THEN Size distribution is	LOW (0.52)
13	IF O/W ratio is HIGH AND Time is MEDIUM	THEN Size distribution is	LOW (1.00)
14	IF O/W ratio is HIGH AND Time is HIGH	THEN Size distribution is	HIGH (1.00)
	SubModel:4		
15	IF Dilution ratio is LOW	THEN Size distribution is	LOW (1.00)
16	IF Dilution ratio is HIGH	THEN Size distribution is	HIGH (0.88)

USC UNIVERSIDADE DE SANTIAGO DE COMPOSTELA

Table S3: Set of rules from FormRules® for microparticles encapsulation efficiency. Membership degree in parentheses. The combinations of variables that lead the highest and lowest value of the parameter studied are in blue and red, respectively.

Rules for Encapsulation Efficiency (EE) (%)			
	SubModel:1		
1	IF [Polymer] is LOW AND O/W ratio is LOW	THEN EE is	LOW (1.00)
2	IF [Polymer] is LOW AND O/W ratio is MEDIUM	THEN EE is	HIGH (1.00)
3	IF [Polymer] is LOW AND O/W ratio is HIGH	THEN EE is	LOW (0.93)
4	IF [Polymer] is HIGH AND O/W ratio is LOW	THEN EE is	HIGH (0.92)
5	IF [Polymer] is HIGH AND O/W ratio is MEDIUM	THEN EE is	HIGH (0.45)
6	IF [Polymer] is HIGH AND O/W ratio is HIGH	THEN EE is	HIGH (0.66)
	SubModel:2		
7	IF Time is LOW AND [Drug] is LOW	THEN EE is	HIGH (1.00)
8	IF Time is LOW AND [Drug] is HIGH	THEN EE is	HIGH (0.62)
9	IF Time is MEDIUM AND [Drug] is LOW	THEN EE is	LOW (0.53)
10	IF Time is MEDIUM AND [Drug] is HIGH	THEN EE is	HIGH (1.00)
11	IF Time is HIGH AND [Drug] is LOW	THEN EE is	LOW (1.00)
12	IF Time is HIGH AND [Drug] is HIGH	THEN EE is	HIGH (0.67)

Table S4: Set of rules from FormRules® for microparticles drug loading. Membership degree in parentheses. The combinations of variables that lead the highest and lowest value of the parameter studied are in blue and red, respectively.

Rules for Drug Loading (DL) (%)			
	SubModel:1		
1	IF [Drug] is LOW AND [Polymer]is LOW	THEN DL is	LOW (0.96)
2	IF [Drug] is LOW AND [Polymer] is HIGH	THEN DL is	LOW (1.00)
3	IF [Drug] is HIGH AND [Polymer] is LOW	THEN DL is	HIGH (0.74)
4	IF [Drug] is HIGH AND [Polymer] is HIGH	THEN DL is	HIGH (0.91)

USC UNIVERSIDADE DE SANTIAGO DE COMPOSTELA

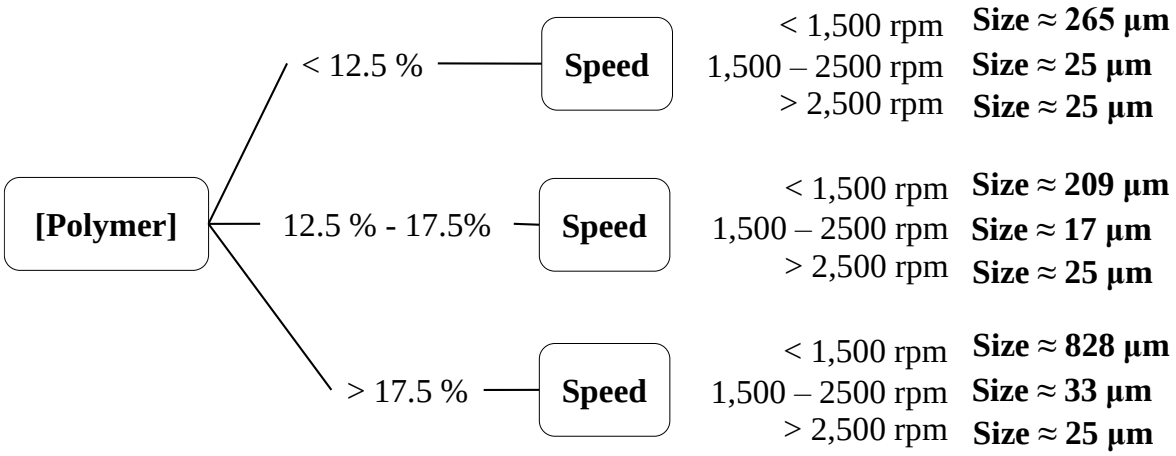


Figure S1. Particle size decision tree. (Values of sizes estimated from the rules considering categories and membership degrees).

USC
UNIVERSIDADE DE SANTIAGO DE COMPOSTELA

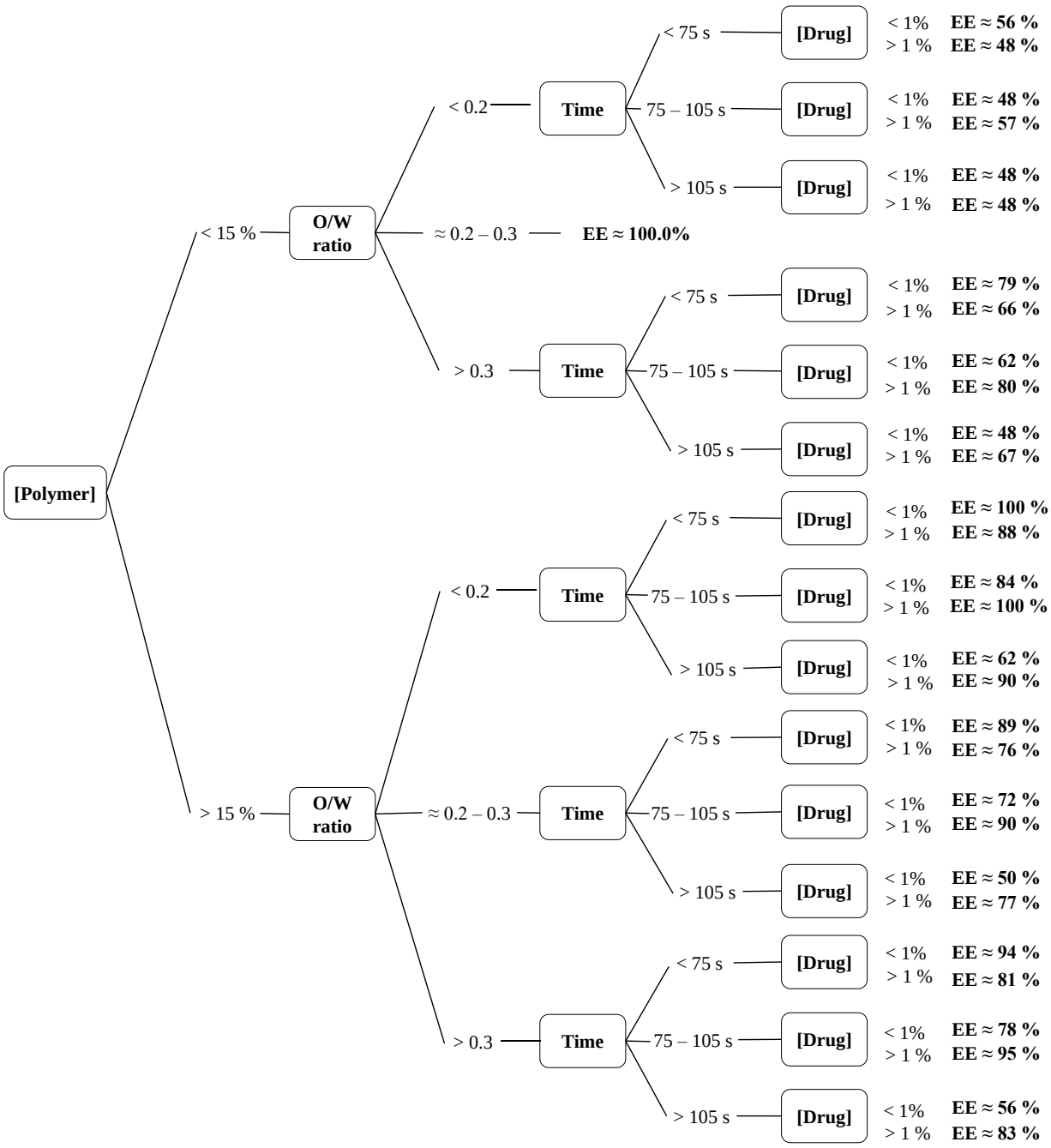


Figure S2. Encapsulation efficiency decision tree. (Values of encapsulation efficiencies estimated from the rules considering categories and membership degrees).

USC UNIVERSIDADE DE SANTIAGO DE COMPOSTELA

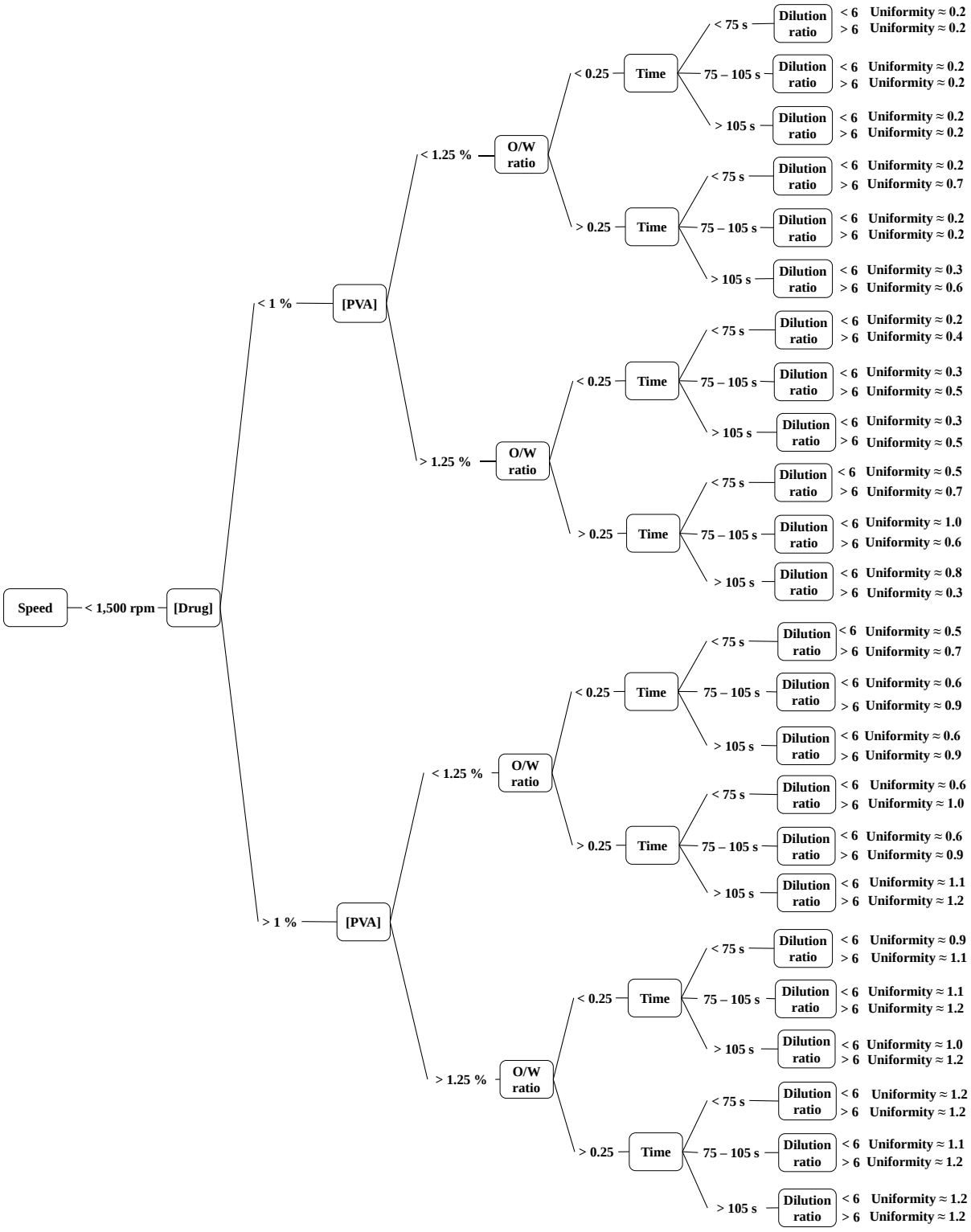


Figure S3. Uniformity decision tree when low stirring speeds are used. (Values of uniformity estimated from the rules considering categories and membership degrees).

USC UNIVERSIDADE DE SANTIAGO DE COMPOSTELA

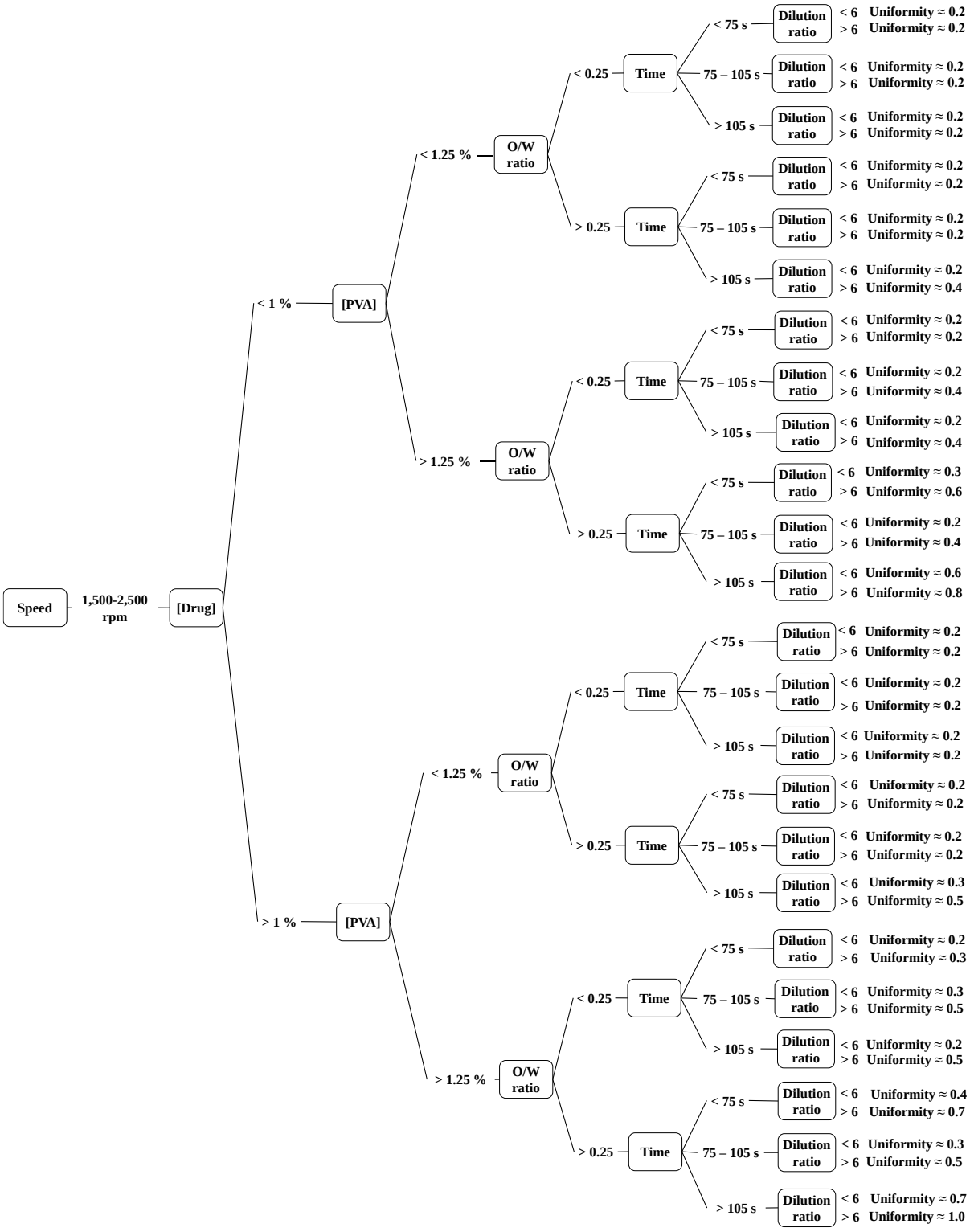


Figure S4. Uniformity decision tree when medium stirring speeds are used. (Values of uniformity estimated from the rules considering categories and membership degrees).

USC UNIVERSIDADE DE SANTIAGO DE COMPOSTELA

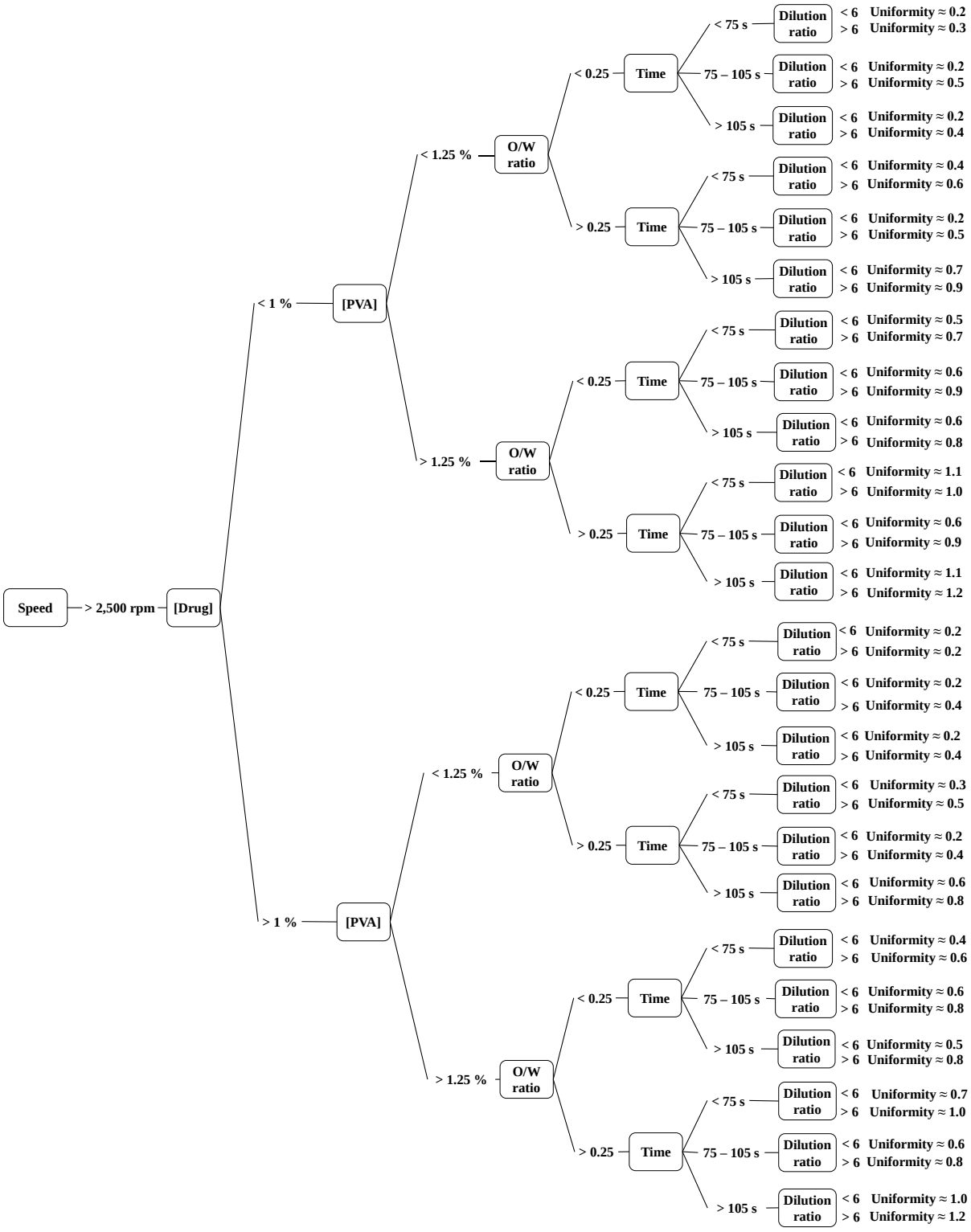


Figure S5. Uniformity decision tree when high stirring speeds are used. (Values of uniformity estimated from the rules considering categories and membership degrees).

USC UNIVERSIDADE DE SANTIAGO DE COMPOSTELA

APPENDICES. RIGHTS AND PERMISSIONS

USC
UNIVERSIDADE
DE SANTIAGO
DE COMPOSTELA

USC
UNIVERSIDADE
DE SANTIAGO
DE COMPOSTELA

APPENDIX I: CONFLICT OF INTEREST

Rebeca Martínez Borrajo, the doctoral candidate, declares there is no conflict of interest associated with this Doctoral Thesis.

USC
UNIVERSIDADE DE SANTIAGO DE COMPOSTELA

APPENDIX II: LIST OF PUBLICATIONS INCLUDED IN THIS THESIS AND PERMISSIONS

Part of the content employed in "***Functionalized indomethacin-loaded nanostructured lipid carriers"*** has been published as:

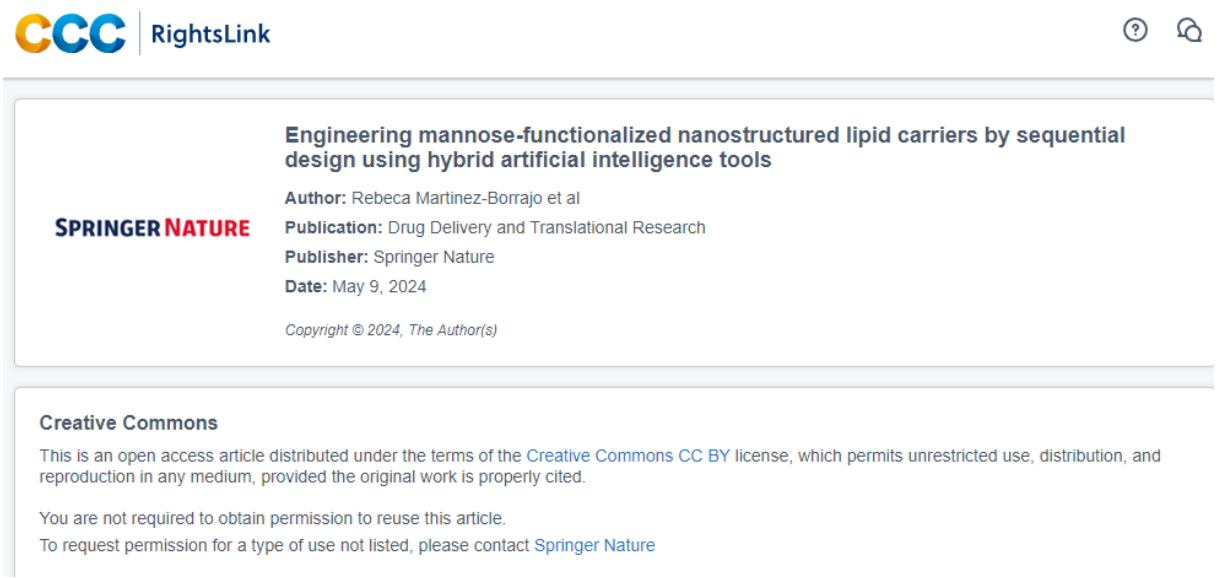
"Engineering mannose-functionalized nanostructured lipid carriers by sequential design using hybrid artificial intelligence tools". *Drug Delivery and Translational Research*, **2024**, DOI: 10.1007/s13346-024-01603-z.

Rebeca Martinez-Borrajo[1], Patricia Diaz-Rodriguez[1], and Mariana Landin[1]

[1]Departamento de Farmacología, Farmacia y Tecnología Farmacéutica, Grupo I+D Farma (GI-1645), Facultad de Farmacia; Instituto de Investigación Sanitaria de Santiago de Compostela (IDIS); Instituto de Materiais da Universidade de Santiago de Compostela (iMATUS), Universidade de Santiago de Compostela, Santiago de Compostela 15782, Spain.

Contributions: Conceptualization, data curation, investigation, methodology, visualization, and original draft writing.

Impact Factor: 5.4. Q1 in Pharmacology & Pharmacy. Copyright 2024. ISSN 2190-3948.



CCC RightsLink

SPRINGER NATURE

Engineering mannose-functionalized nanostructured lipid carriers by sequential design using hybrid artificial intelligence tools

Author: Rebeca Martinez-Borrajo et al
Publication: Drug Delivery and Translational Research
Publisher: Springer Nature
Date: May 9, 2024

Copyright © 2024, The Author(s)

Creative Commons

This is an open access article distributed under the terms of the Creative Commons CC BY license, which permits unrestricted use, distribution, and reproduction in any medium, provided the original work is properly cited.

You are not required to obtain permission to reuse this article.
To request permission for a type of use not listed, please contact Springer Nature

USC UNIVERSIDADE DE SANTIAGO DE COMPOSTELA

Part of the content employed in "***Design and evaluation of senolytic loaded microspheres"*** has been published as:

"Rationalized design to explore the full potential of PLGA microspheres as drug delivery systems". *Drug Delivery*, **2023**, VOL. 30:1, 2219864, DOI: 10.1080/10717544.2023.2219864.

Rebeca Martinez-Borrajo [a,b,c], Patricia Diaz-Rodrigue [a,b,c], and Mariana Landin[a,b,c]

[a]Departamento de Farmacología, Farmacia y Tecnología Farmacéutica, Grupo I + D Farma (GI-1645), Facultad de Farmacia, Universidade de Santiago de Compostela, Santiago de Compostela, Spain; [b]Instituto de Investigación Sanitaria de Santiago de Compostela (IDIS), IDIS Research Institute, Santiago de Compostela, Spain; [c]Instituto de Materiais da Universidade de Santiago de Compostela (iMATUS), Santiago de Compostela, Spain.

Contributions: conceptualization and design of the work, methodology, investigation, writing-drafting, revising, and visualization

Impact Factor: 6.0. Q1 in Pharmacology & Pharmacy. Copyright 2023. ISSN 1071-7544.



APPENDIX III: IMAGES, TABLES, AND FIGURES.

Rebeca Martínez Borrajo, the doctoral candidate, declares that all the other images, tables, and figures shown in this Doctoral Thesis are not previously published and created by herself

USC
UNIVERSIDADE DE SANTIAGO DE COMPOSTELA

CHECKLISTS AND PERMISSIONS

USC
UNIVERSIDADE
DE SANTIAGO
DE COMPOSTELA

USC
UNIVERSIDADE
DE SANTIAGO
DE COMPOSTELA

Checklist for Thesis that include experimental animals. **EXPERIMENTAL ANIMALS ARRIVE**

Yes/No/NA		Page
	Title	
Yes	Provide as accurate and concise a description of the content of the article as possible.	58-59
	Abstract	
Yes	Provide an accurate summary of the background, research objectives, including details of the species or strain of animal used, key methods, principal findings and conclusions of the study.	58-59 113-115
	Background	
Yes	Provide an accurate summary of the background, research objectives, including details of the species or strain of animal used, key methods, principal findings and conclusions of the study.	113-115
Yes	Explain how and why the animal species and model being used can address the scientific objectives and, where appropriate, the study's relevance to human biology.	58
	Objectives	
Yes	Clearly describe the primary and any secondary objectives of the study, or specific hypotheses being tested.	58-59
	Methods	
	Ethical statement	
Yes	Indicate the nature of the ethical review permissions, relevant licenses, and national or institutional guidelines for the care and use of animals, that cover the research.	58-59 171-172
	Study design	
Yes	Number of experimental and control groups	59
N/A	Steps taken to minimize the effects of subjective bias when allocating animals to treatment (e.g. randomization procedure) and when assessing results (e.g. if done, describe who was blinded and when).	
N/A	The experimental unit (e.g. a single animal, group or cage of animals). A time-line diagram or flow chart can be useful to illustrate how complex study designs were carried out.	
	Experimental procedures	
Yes	How (e.g. drug formulation and dose, site and route of administration, anesthesia and analgesia used [including monitoring], surgical procedure, method of euthanasia). Provide details of any specialist equipment used, including supplier(s).	59
N/A	When (e.g. time of day).	
N/A	Where (e.g. home cage, laboratory, water maze).	
Yes	Why (e.g. rationale for choice of specific anesthetic, route of administration, drug dose used).	59
	Experimental animals	
Yes	Provide details of the animals used, including species, strain, sex, developmental stage (e.g. mean or median age plus age range) and weight (e.g. mean or median weight plus weight range).	58-59
Yes	Provide further relevant information such as the source of animals, international strain nomenclature, genetic modification status (e.g. knock-out or transgenic), genotype, health/immune status, drug or test naïve, previous procedures, etc.	58-59
	Housing and husbandry	
N/A	Housing (type of facility e.g. specific pathogen free [SPF]; type of cage or housing; bedding material; number of cage companions; tank shape and material etc. for fish).	
No	Husbandry conditions (e.g. breeding program, light/dark cycle, temperature, quality of water etc for fish, type of food, access to food and water, environmental enrichment).	

USC UNIVERSIDADE DE SANTIAGO DE COMPOSTELA

N/A	Welfare-related assessments and interventions that were carried out prior to, during, or after the experiment.	
	Sample size	
Yes	Specify the total number of animals used in each experiment, and the number of animals in each experimental group.	58-59
N/A	Explain how the number of animals was arrived at. Provide details of any sample size calculation used.	
No	Indicate the number of independent replications of each experiment, if relevant.	
	Allocating animals to experimental groups	
N/A	Indicate the number of independent replications of each experiment, if relevant.	
Yes	Describe the order in which the animals in the different experimental groups were treated and assessed.	59
	Experimental outcomes	
Yes	Clearly define the primary and secondary experimental outcomes assessed (e.g. cell death, molecular markers, behavioral changes).	113-115
	Statistical methods	
Yes	Provide details of the statistical methods used for each analysis.	59
Yes	Specify the unit of analysis for each dataset (e.g. single animal, group of animals, single neuron).	58-59 113-115
N/A	Describe any methods used to assess whether the data met the assumptions of the statistical approach.	
	Results and discussion	
	Basal data	
N/A	For each experimental group, report relevant characteristics and health status of animals (e.g. weight, microbiological status, and drug or test naïve) prior to treatment or testing (this information can often be tabulated).	
	Numbers analyzed	
No	Report the number of animals in each group included in each analysis. Report absolute numbers (e.g. 10/20, not 50%).	
N/A	If any animals or data were not included in the analysis, explain why.	
	Outcomes and estimation	
Yes	Report the results for each analysis carried out, with a measure of precision (e.g. standard error or confidence interval).	113-115
	Adverse events	
N/A	Give details of all important adverse events in each experimental group.	
N/A	Describe any modifications to the experimental protocols made to reduce adverse events.	
	Interpretation/scientific implications	
Yes	Interpret the results, taking into account the study objectives and hypotheses, current theory and other relevant studies in the literature.	113-115
N/A	Comment on the study limitations including any potential sources of bias, any limitations of the animal model, and the imprecision associated with the results.	
Yes	Describe any implications of your experimental methods or findings for the replacement, refinement or reduction (the 3Rs) of the use of animals in research.	59
	Generalizability/translation	
Yes	Comment on whether, and how, the findings of this study are likely to translate to other species or systems, including any relevance to human biology.	58-59 113-115
	Funding	
N/A	List all funding sources (including grant number) and the role of the funder(s) in the study.	

Based on The ARRIVE guidelines: Animal Research: Reporting of In Vivo Experiments.

USC UNIVERSIDADE DE SANTIAGO DE COMPOSTELA

XUNTA DE GALICIA
CONSELLERÍA DO MEDIO RURAL

Xefatura Territorial
Sº de Gandaría
Edificio administrativo Monelos, 4º andar
Rúa Vicente Ferrer, Nº 2
15008 A Coruña
Tfno.: 981 184 565
Correo electrónico: servizo.gandaria.a.coruna@xunta.gal

galicia

RESOLUCIÓN DE AUTORIZACIÓN DE PROXECTO DE EXPERIMENTACIÓN ANIMAL

Expediente núm.: 15002/2021/007
Data de inicio do expediente: 23.6.2021
Persoa solicitante: Alberto Centeno Cortés
Procedemento: resolución de autorización
Forma de inicio: solicitude da persoa interesada

ANTECEDENTES

A persoa solicitante, como representante da Unidade de Cirurxía Experimental do Centro Tecnolóxico de Formación do Complexo Hospitalario Universitario da Coruña (CHUAC), presentou con data 23.6.2021 unha solicitude para a realización do proxecto de experimentación animal (entrada no Rexistro electrónico da Xunta de Galicia 2021/1538277). Posteriormente, achegou documentación complementaria o 30.6.2021 (entrada no Rexistro electrónico da Xunta de Galicia 2021/1592997). Os datos son os seguintes:

Denominación do proxecto: Determinación da eficacia terapéutica da administración intraarticular de fibratos nun modelo murino de artrose experimental
Nome do centro usuario: Centro Tecnolóxico de Formación do CHUAC
Persoa responsable do proxecto: Beatriz Caramés Pérez
Establecemento onde se realizarán os procedementos do proxecto (ou lugar xeográfico no caso de traballos de campo): Unidade de Cirurxía Experimental do Centro Tecnolóxico de Formación do CHUAC

Clasificación do proxecto : Tipo I [ ] Tipo II [ ] Tipo III [X]

CONSIDERACIÓNS LEGAIS E TÉCNICAS

1 O Real decreto 53/2013, de 1 de febreiro (BOE 34, do 8 de febreiro), polo que se establecen as normas básicas aplicables para a protección dos animais utilizados en experimentación e outros fins científicos, incluíndo a docencia, establece no seu artigo 33 as condicións de autorizacións dos proxectos con animais de experimentación.

2 O artigo 88 da Lei 39/2015, de 1 de outubro, do procedemento administrativo común das administracións públicas (BOE 236, do 2 de outubro de 2015) establece que a resolución que poña fin o procedemento decidirá todas as cuestións expostas polos interesados e aquelas outras derivadas deste.

USC UNIVERSIDADE DE SANTIAGO DE COMPOSTELA

Xacobeo 21·22

CVE: pajjE6jfU1
Verificación: https://sede.xunta.gal/cve

XUNTA DE GALICIA
CONSELLERÍA DO MEDIO RURAL

Xefatura Territorial
Sº de Gandaría
Edificio administrativo Monelos, 4º andar
Rúa Vicente Ferrer, Nº 2
15008 A Coruña
Tfno.: 981 184 565
Correo electrónico: servizo.gandaria.a.coruna@xunta.gal

galicia

3 O Servizo de Gandaría da Coruña revisou a documentación achegada na solicitude e o resultado favorable da avaliación do proxecto realizada polo órgano habilitado, a Xerencia de Xestión Integrada da Coruña.

Esta xefatura territorial é competente para ditar unha resolución, de conformidade co Decreto 149/2018, do 5 de decembro, polo que se establece a estrutura orgánica da Consellería do Medio Rural e se modifica parcialmente o Decreto 177/2016, do 15 de decembro, polo que se fixa a estrutura orgánica da Vicepresidencia e das consellerías da Xunta de Galicia (DOG 235, do 11 de novembro).

De acordo con todo o indicado, RESOLVO:

1 Autorizar o proxecto solicitado.

2 O proxecto precisa someterse a unha avaliación retrospectiva aos tres meses da súa finalización.

3 A autorización deste proxecto terá unha duración de tres meses e unha vez transcorrido este tempo, esta autorización deberá ser renovada.

A citada autorización é unicamente válida nas condicións que figuran no expediente. Ante calquera cambio significativo no proxecto que poida ter efectos negativos sobre o benestar dos animais, deberá solicitar a confirmación da autorización ao Servizo Provincial de Gandaría.

Esta autorización poderá ser suspendida no caso de que o proxecto non se leve a cabo de acordo coas condicións de autorización e retirala, previo expediente tramitado ao que se lle dará audiencia.

Contra a presente resolución, que non pon fin á vía administrativa, poderá interpoñer un recurso de alzada ante o conselleiro de Medio Rural. O prazo comezará a contar dende o día seguinte ao da recepción desta resolución. Todo isto, segundo o disposto nos artigos 121 e 122 da citada Lei 39/2015.

Mediante este escrito notifícaselle a Alberto Centeno Cortés esta resolución segundo o esixido no artigo 40.1 da antedita Lei 39/2015.

USC UNIVERSIDADE DE SANTIAGO DE COMPOSTELA

Xacobeo 21·22

Asinado por: SANTOS MANEIRO, JOSE MANUEL
Cargo: Xefe Territorial
Data e hora: 07/07/2021 14:35:04

CVE: pajjE6jfU1
Verificación: https://sede.xunta.gal/cve

XUNTA DE GALICIA
CONSELLERÍA DE SANIDADE
Secretaría Xeral Técnica

Secretaria Técnica
Comité Autonómico de Ética da Investigación de Galicia
Secretaria Xeral. Consellería de Sanidade
Edificio Administrativo San Lázaro
15703 SANTIAGO DE COMPOSTELA
Tel: 881 546425; ceic@sergas.es

DICTAMEN DEL COMITÉ DE ÉTICA DE LA INVESTIGACIÓN DE A CORUÑA-FERROL

Carlos Rodríguez Moreno, Secretario del Comité de Ética de la Investigación de A Coruña-Ferrol

CERTIFICA:

Que este Comité evaluó en su reunión del día 21/01/2015 el estudio:

Título: Colección de muestras para el desarrollo de la línea de investigación traslacional en comunicación y señalización celular
Promotor: María Dolores Mayán Santos
Tipo de estudio: Outros
Version:
Código del Promotor:
Código de Registro: 2015/029

Y, tomando en consideración las siguientes cuestiones:

- La pertinencia del estudio, teniendo en cuenta el conocimiento disponible, así como los requisitos legales aplicables, y en particular la Ley 14/2007, de investigación biomédica, el Real Decreto 1716/2011, de 18 de noviembre, por el que se establecen los requisitos básicos de autorización y funcionamiento de los biobancos con fines de investigación biomédica y del tratamiento de las muestras biológicas de origen humano, y se regula el funcionamiento y organización del Registro Nacional de Biobancos para investigación biomédica, la ORDEN SAS/3470/2009, de 16 de diciembre, por la que se publican las Directrices sobre estudios Posautorización de Tipo Observacional para medicamentos de uso humano, y el la Circular nº 07 / 2004, investigaciones clínicas con productos sanitarios.
- La idoneidad del protocolo en relación con los objetivos del estudio, justificación de los riesgos y molestias previsibles para el sujeto, así como los beneficios esperados.
- Los principios éticos de la Declaración de Helsinki vigente.
- Los Procedimientos Normalizados de Trabajo del Comité.

Emite un **INFORME FAVORABLE** para la realización del estudio **por el/la investigador/a del centro**:

Centros	Investigadores Principales
C.H. Universitario de A Coruña	María Dolores Mayán Santos

En Santiago de Compostela, a
El secretario

carlos.rodriguez.moreno@sergas.es
Firmado digitalmente por carlos.rodriguez.moreno@sergas.es
Nombre de reconocimiento (DN): cn=carlos.rodriguez.moreno@sergas.es
Fecha: 2015.01.26 09:17:27 +01'00'

DE: *Dña. María Dolores Mayan Santos. Grupo Investigación CellCOM. INIBIC - Xerencia Xestión Integrada A Coruña (XXIAC).*

A*: Red de Comités de Ética de Investigación de Galicia.*

Asunto: Notificación de adaptación al Reglamento General de Protección de Datos (RGPD) del consentimiento informado de la Línea de Investigación Traslacional en Comunicación y Señalización Celular.

Mediante la presente ponemos en su conocimiento que hemos procedido a adaptar al RGPD el documento de consentimiento informado de la Colección de Muestras y Datos para el desarrollo de la Línea de Investigación Traslacional en Comunicación y Señalización Celular, evaluada favorablemente por el CEI de Galicia con Código Registro: 2015/029 e inscrita en la Sección de Colecciones del Registro Nacional de Biobancos del ISC III con Código: C.0003333.

El modelo adjunto a esta notificación será el que se utilizará a partir de esta notificación.

Por todo ello, ruego tengan en consideración lo aquí indicado y procedan a incluir la información en el expediente que nos corresponda.

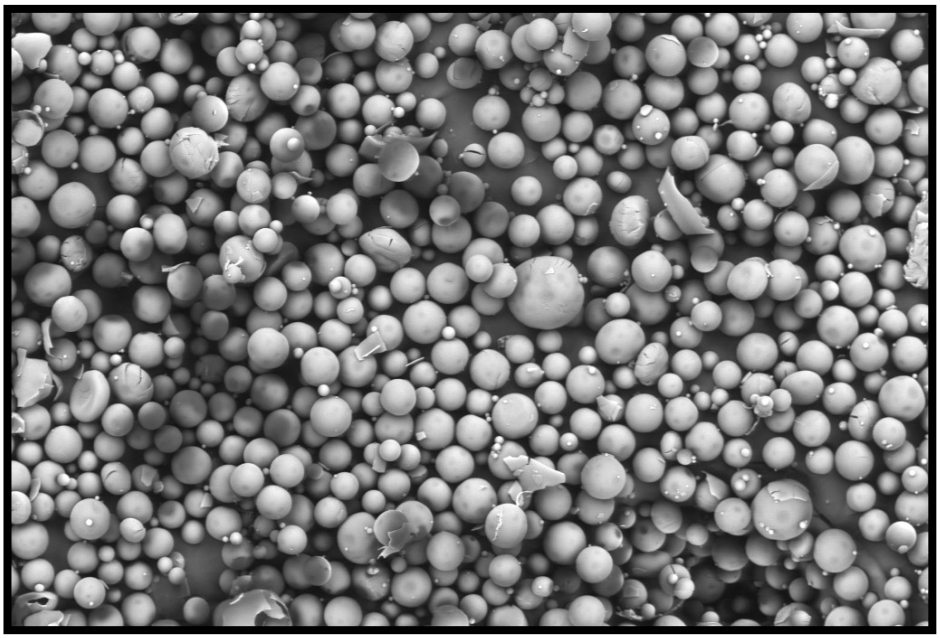
En A Coruña, a 14 de Enero de 2019

Maria D. Mayán Santos
Digitally signed by Maria D. Mayán Santos
Date: 2019.01.17 14:54:52 +01'00'

Dña. María Dolores Mayan Santos
Responsable colección
Grupo Investigación CellCOM
INIBIC - Xerencia Xestión Integrada A Coruña (XXIAC).

USC UNIVERSIDADE DE SANTIAGO DE COMPOSTELA

USC
UNIVERSIDADE
DE SANTIAGO
DE COMPOSTELA



This thesis highlights the crucial role of Artificial Intelligence (AI) tools in designing, developing, and optimizing novel formulations with potential as disease modifying osteoarthritis drugs (DMOADs). In this regard, AI tools enabled the establishment of robust protocols to prepare nanoparticles and microspheres of specific desired characteristics. The drug delivery systems developed in this thesis demonstrated its potential as DMOADs by targeting the two main hallmarks of OA: inflammation and cartilage degradation. This approach is achieved by following three independent but closely related strategies; inflammation control, macrophage phenotype modulation and reversing disease progression by modulating chondrocyte senescence. The use of AI tools was pivotal in achieving these advancements, offering innovative methodologies that surpassed traditional approaches in drug delivery systems design.